INNOVATIVE DESIGN FOR FERROFLUIDS BASED PARABOLIC TROUGH SOLAR COLLECTOR

Mustafa Mohammed H. Alsaady, MSC

Thesis submitted to the University of Nottingham for the degree of Doctor of Philosophy

November 2017

ABSTRACT

The demand for modern energy services is increasing rapidly. Solar energy has the potential to meet a significant share of the world's energy request. Solar energy is one of the cleanest renewable forms with little or no effect on the environment. The concentrating solar power is one of the methods to harvest sun's energy. Concentrating solar power has the advantage of easier energy storage compared to photovoltaic systems. However, the cost of energy generated by those systems is higher than conventional energy sources. It is necessary to improve the performance of concentrating solar power to make them cost competitive. Moreover, few countries such as Saudi Arabia are moving from energy based on fossil fuel to renewable energy, therefore, improving the performance of concentrating solar systems and reducing their cost is considered to emulate photovoltaic systems.

This research aims to develop an innovative design of parabolic trough solar collector that uses magnetic nanofluids as a heat transfer fluid to enhance the thermal efficiency compared to conventional parabolic trough. Based on past researches, new parabolic trough design is then proposed and investigated. Ferromagnetic nanoparticles dispersed in common heat transfer fluids (ferrofluids) exhibit better thermos-physical properties compared to the base fluids. By applying the right magnetic intensity and magnetic field direction, the thermal conductivity of the fluid increased higher than typical nanofluids. Moreover, the ferrofluids exhibit excellent optical properties. The external magnetic source is installed to alter the thermo-physical properties of the fluid. This thesis is comprised of four studies including two experimental studies, one heat transfer analysis, and one economic and environmental study. A small scale parabolic trough collector was manufactured and assembled at the laboratory based on the British Standards. A steady-state method was used to measure the performance of the parabolic trough collector in corresponding

studies. The performance of the ferrofluids as a heat transfer fluid was compared to the base fluid. The two experimental studies differ in the absorber used. The two absorbers used were a conventional non-direct absorber and a direct absorber without a selective surface that allows ferrofluids to absorb the incoming solar irradiation directly. The effects of nanoparticle concentration, anti-foaming, external magnetic field intensity were investigated. The volume fraction of nanoparticles was 0.05%, 0.25%, and 0.75%. Three different magnetic field intensities were investigated, 3.14 mT, 6.28 mT, and 10.47 mT. Using ferrofluids to enhance the heat transfer performance the efficiency of the ferrofluids solar collector was compared to the based fluid (water). The results show that the parabolic trough solar collector in the experiment has similar performance of flat-plate solar collectors. The efficiency of the collector improved when ferrofluids water used compared to water. Ferrofluids with low concentration improved the performance of the solar collector. The ferrofluids showed much better performance at higher reduced temperature with lower overall heat loss coefficient. Due to the non-Newtonian behaviour of the fluid, increasing the volume fraction of particles will suppress the enhancement. The pH of ferrofluids influences the behaviour of the fluid. pH values higher than 5 showed a Newtonian behaviour of the fluid. In the presence of magnetic field, the performance of the solar collector enhanced further. By increasing the magnetic field intensity, the absorbed energy parameter increased, and at higher magnetic field intensity, the rate of enhancement decreases due to the magnetic saturation of ferrofluids. In this study, the performance of non-direct absorption receiver was better than the direct absorption receiver. However, the performance of the collector with a direct absorption receiver and using ferrofluids in the presence of the external magnetic field in some cases was higher than the performance of non-direct receiver with water as heat transfer medium.

The performance of ferrofluids based parabolic trough collector was theoretically investigated. The correlation, equations, and specifications used in the model were discussed in detail. The model was used to study two different parabolic trough designs. First, the parabolic trough was validated with the experimental results of AZTRAK platform. The results of the model show a good agreement with the experimental data. Thereafter, nanoparticles were added to the heat transfer fluid, and the performance of the collector with and without the presence of external magnetic field was determined. The performance of the collector did not change a lot unless the external magnetic field was present. Moreover, the effect of the glass envelope on the performance was observed. A glass cover with vacuum in the annulus has higher performance and less thermal loss. Second, the model was used to study the performance of the test rig ferrofluids based parabolic trough. The performance of the parabolic trough was first considered as concentrating collector and then as a non-concentrating collector. With the lack of an external magnetic field, the efficiency changed slightly, wherein the presence of the external magnetic field the performances of the collector enhanced and showed higher performances. In General, the presence of the magnetic field showed promising enhancement. Economic and environmental effects of using ferrofluids based solar collector compared to a flat-plate collector for household water heating systems. Results show that the ferrofluids based parabolic trough has lower payback period and higher economic saving at its useful life end than a flat-plate solar collector. The ferrofluids based collector has higher embodied energy and pollution offsets tan flat-plate collector. Moreover, if 50% insertion of ferrofluids based parabolic trough for domestic hot water could be achieved in Tabuk over 83,750 metric Ton of CO_2 could be eliminated.

PUBLICATIONS ARISING FROM THIS WORK

- Alsaady, M., Fu, R., Li, B., Boukhanouf, R. and Yan, Y., 2015. Thermo-physical properties and thermo-magnetic convection of ferrofluid. *Applied Thermal Engineering*, *88*, pp.14-21.

- Alsaady, M., Yan, Y., and Boukhanouf, R., 2015. Heat transfer analysis of ferrofluids based solar parabolic trough collectors. *14th International Conference on Sustainable Energy Technologies*. Aug 25-27, Nottingham, U.K.

- Alsaady, M., Fu, R., LIU, Z., Yan, Y, Wu. S., and Boukhanouf, R., 2016. An experimental investigation on the effect of ferrofluids on the efficiency of novel parabolic trough solar collector under laminar flow conditions. *5th International Conference on Micro and Nano Flows*. Sep 11-14, Politecnico, Italy.

- Alsaady, M., Yan, Y., and Boukhanouf, R., 2016. The use of ferrofluids in a direct absorption solar collector. *International Heat Transfer Symposium and Heat Powered Cycles Conference 2016*. Jun 26-28, Nottingham, U.K.

ACKNOWLEDGMENT

Firstly, I would like to express my sincere gratitude to supervisor, Prof. Yuying Yan for the continuous support, patience, motivation and guidance throughout my PhD study and related research. His guidance helped me all time in my study and my personal life. I could not have imagined a better supervisor and mentor than him.

Special thanks to my colleagues and all technical staff of the Built Environment department. Thanks to Dr. Rabah Boukhanouf who guided me from the beginning of my study. I would also like to thank, Mr. David Oliver, Mr. Andrew Matthews, and Mr. James Hazzledine for their generous assistance in the laboratory.

I'm grateful to my family and friends, who have provided me with moral and emotional support in my life. Thank you, father and mother, for your encouragement, love, and trust. Thank you, Jassim, Ahmed, and Souheb for your unwavering support. Thank you Isra and Abdelaziz, I'm so grateful and thankful for all you have done. Thank you, Haya and Lujain for bringing happiness to my life. Thank you, my dear wife, Mayan, for everything. Thank you, for your unconditional love, support, and advice. Thank you, Kareem and Yousef, you are every reason to me to work hard.

NOMENCLATURE

α_{56}	= thermal diffusivity of glass envelope outer surface (m^2/s)
α_{env}	= glass envelope absorptance
β	= coefficient of volumetric thermal expansion (K^{-1})
γ	= ratio of specific heats for air (1.39)
δ	= molecular diameter of air (3.53e-8 cm).
η	= thermal efficiency
η_0	= zero-loss thermal efficiency
η_{optic}	= optical efficiency
ε_3	= emissivity of absorber selective coating
ε_4	= emissivity of glass envelope
ε_5	= emissivity of glass envelope outer surface,
ε_i'	= optical efficiency terms
κ_1	= thermal conductivity of the heat transfer fluid at T_1 (W/m K)
κ_{23}	= absorber thermal conductivity at the average temperature $(T_2 + T_3)/2$ (W/m K)
κ_B	= Boltzmann constant (1.38×10^{-23} J/K)
κ_{bf}	= base fluid thermal conductivity (W/m K)
κ_{eff}	= effective thermal conductivity of ferrofluids (W/m K)
κ_{std}	= thermal conductivity of air at standard temperature and pressure (0.025 W/m K)
λ	= wave-length (m)
μ	= permeability of vacuum which is $4\times\pi\times10^{-7}$ H/m
μ_{eff}	= effective viscosity of ferrofluids (kg/m s^{-1})

μ_{bf} = base fluid viscosities (kg/m s^{-1})

v_{56} = kinematic viscosity for air at T_{56} (m^2/s)

ξ = mean free path between collisions of particles

ρ_{bf} = density of the base fluid (kg/m^3)

ρ_{eff} = effective density of ferrofluids (kg/m^3)

$\rho_{Fe_3O_4}$ = nanoparticle density (5810 kg/m^3)

σ = Stefan-Boltzmann constant (5.67 × 10^{-8} W/m^2 K^{-4})

$(\tau\alpha)$ = transmittance-absorptance product

φ = volume fraction, specular reflectance of the mirror

ψ = intercept factor, the fraction of reflected energy that is directed towards the receiver

a = accommodation coefficient

a_1 = first order heat loss coefficient

a_2 = second order heat loss coefficient

A = amount of pollutant in kg/MJ

A_a = cross sectional area of the aperture (m^2)

A_C = cross sectional area of the collector (m^2)

$A_{f,n}$ = ratio of ineffective area

b = interact coefficient of air (1.571),

B = magnetic field intensity (Tesla), percentage of energy produced from a particular fuel type

c = lightspeed in a vacuum (299792258 m/s)

C_a = area dependent costs (£)

C_f = area independent costs (£)

C_m = maintenance costs (£)

C_s = capital costs (£)

C_t = total costs (£)

C = concentration ratio, correlation for Nu

Cp_{bf} = base fluid heat capacity (kJ/kg K^{-1})

Cp_{eff} = effective specific heat capacity (kJ/kg K^{-1})

$Cp_{Fe_3O_4}$ = heat capacity of nanoparticles (kJ/kg K^{-1})

D = Diameter of the radiation source (m)

D_2 = absorber inner diameter (m)

D_3 = absorber outer diameter (m)

D_4 = inner glass envelope surface diameter (m)

D_5 = outer glass envelope surface diameter (m)

F_R = collector heat removal factor

f_2 = factor for the inner surface fraction of the absorber tube,

g = constant of gravity m/s^2

h = Planck constant

h_1 = convection heat transfer coefficient at T_1,

h_{34} = convection heat transfer coefficient for the air in the annulus at a temperature T_{34},

I = electric current (A)

I_0 = radiation density [$W/m^2(\mu m)$ or W/cm^3]

I_D = direct solar radiation (W/m^2)

K = incident angel modifier

L_S = length of the solenoid (m)

m = correlation for Nu

$\dot{m}$ = mass flow rate of the heat transfer fluid in the collector (kg/s)

n = number of wire turns required for the electromagnet

Nu_{D2} = Nusselt number based on D_2

Nu_{D5} = average Nusselt number evaluated on D_5

p_a = air pressure (Pa)

Pr_1 = Prandtl number based on the heat transfer fluid temperature T_1

Pr_2 = Prandtl number based on the absorber inner surface temperature T_2

Pr_{56} = Prandtl number for air at T_{56}

q_0 = radiation intensity W/m

$\dot{q}'_{12,Conv}$ = energy transferred to the fluid by convection (W/m)

$\dot{q}'_{23,Cond}$ = energy conducted through the absorber (W/m)

$\dot{q}'_{3,SolAbs}$ = energy absorbed by the absorber (W/m)

$\dot{q}'_{34,Conv}$ = energy transferred from absorber to glass envelope by convection (W/m)

$\dot{q}'_{34,rad}$ = energy transferred from absorber to glass envelope by radiation (W/m)

$\dot{q}'_{45,Cond}$ = energy transferred through the glass envelope (W/m)

$\dot{q}'_{5,SolAbs}$ = energy absorbed by the glass envelope (W/m)

$\dot{q}'_{56,Conv}$ = energy lost to the environment by convection (W/m)

$\dot{q}'_{57,rad}$ = energy lost to the environment by radiation (W/m)

$\dot{q}'_{bracket,Cond}$ = energy lost through support brackets by conduction (W/m)

$\dot{q}'_{si}$ = solar irradiation per receiver length (W/m)

$\dot{q}_D$ = intensity of direct radiation (W/m^2)

$\dot{q}_G$ = intensity of global radiation (W/m^2)

$\dot{q}_S$ = intensity of (scattered) diffuse radiation (W/m^2)

$\dot{Q}$ = total energy coming from the sun, which is intercepted by the solar collector (W)

$\dot{Q}_{abs}$ = rate of solar energy absorbed by the heat transfer fluid (W)

$\dot{Q}_{aux}$ = the auxiliary energy (W)

$\dot{Q}_L$ = heat loss to the ambient (W)

$\dot{Q}_{Load}$ = the energy needed by the daily load of hot water (W)

Ra_{56} = Rayleigh number of air evaluated on the outer diameter of glass envelope D_5

$\dot{S}_{gen}$ = entropy generation rate (W/K)

T = temperature of the black body (K)

T_1 = mean (bulk) temperature of the heat transfer fluid (K)

T_2 = inner surface temperature of absorber tube (K)

T_2 = absorber inner surface temperature (K)

T_3 = absorber outer surface temperature (K)

T_{34} = average temperature $(T_3 + T_4)/2$ (K)

T_4 = inner glass envelope surface temperature (K)

T_5 = outer glass envelope surface temperature (K)

T_6 = ambient temperature (K)

T_7 = effective sky temperature (K)

T_{in} = mean fluid inlet tempreature (K)

T_{out} = mean fluid outlet temperature (K)

T_{m}^* = reduced temperature difference as defined (K)

T_{sun} = sun temperature (K)

U_L	= heat loss coefficient (W/m^2)
U_η	= uncertainty
V_{in}	= volume of prepared ferrofluids (m^3)
V_{out}	= desired volume of ferrofluids (m^3)
V_{water}	= volume of distilled water (m^3)
x	= distance (m)
X_{in}	= initial volume fraction of 15%
X_{out}	= desired volume fraction of nanoparticles
X_{water}	= volume fraction of nanoparticles in water which is 0

CONTENTS

LIST OF TABLES

LIST OF FIGURES

Chapter 1. Introduction

1.1 Background of energy in Saudi Arabia

The request for modern energy services is increasing rapidly. The global energy consumption is expected to rise by about 35 percent from 2010 to 2040. Energy demand is defined as consumer requirements for heat, electricity, and fuels. Consumers cover domestics and industries as well as public and private sector. The requirement drivers consist of population, economic development, demographics and income levels. As showing in Figure 1-1 half of the increase in global energy demand is expected to account to China and India. The progressively substantial share of the global energy market represented by a group of 10 key growth countries. The increase in the proportion associated with the growing populations and lifestyle. This geographically various group consist of Brazil and Mexico in the Americans, South Africa and Nigeria in Africa, Egypt, and Turkey in Mediterranean, Saudi Arabia and Iran in the Middle East, as well as Thailand and Indonesia in Asia. The Organisation for Economic Co-operation and Development (OECD) represents the developed countries [1]. Therefore, there is a prevailing need for efficient generation and use of energy. Saudi Arabia has an exceptional position in the international energy market, the escalating demand for power and water in Saudi Arabia has created diverse challenges to the environment. Saudi Arabia is the second world's largest producer of oil and the second largest owner of crude oil reserves.

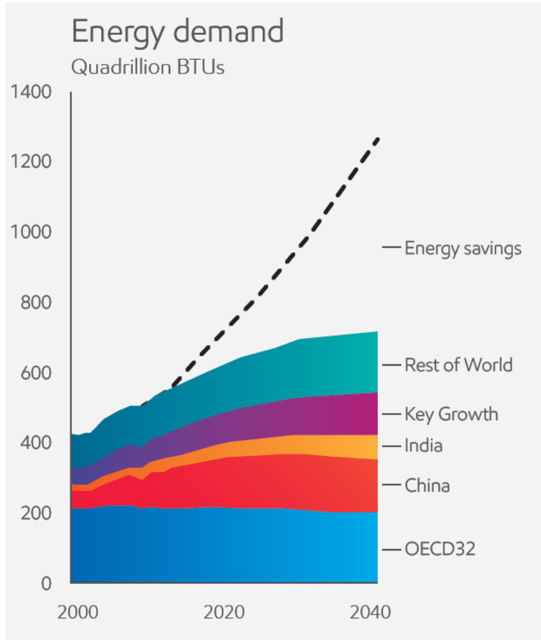

Figure 1-1: Global expected energy demand by 2040 [1].

The economy of Saudi Arabia is heavily reliant on fossil fuels. Oil accounts for 90% of the country exports and nearly 75% government revenue. Saudi Arabia's GDP ranks twentieth in the world [2]. The GDP per unit of energy use in Saudi Arabia was about PPP US$ 7.695 per kg of oil equivalent in 2013. Energy use per capita was 6363 kg of oil equivalent in 2013, which ranked thirteen in the world and considerably above the global average (1894 kg of oil equivalent in 2013). The non-targeted subsidies (i.e. the entire population is provided subsidies regardless of their earnings and status) encouraging the high current utilization of oil in transportation, utilities, and other sectors substantially. In 2010, Saudi Arabia was the largest subsidy government worth US$ 43 billion. Such a subsidy system preserve energy prices low, stimulate increased consumption, and restrains energy efficiency as well as research and development in sustainable energy, which includes both renewable energy and efficient energy [2]. Moreover, Saudi Arabia is the world's largest exporter of oil. Energy exports represent the major component of Saudi Arabia's GDP. Total natural resource rents represented 41.12% of GDP in 2013, in which 38.7% of oil and 2.36%

from natural gas [3]. Renewable energy sources can be promoted using these rents. Energy consumption depends completely on fossil fuel, generating large CO_2 emissions that lead to global climate change. Saudi Arabia has the most concentration of industries in the Gulf Cooperation Council region, and therefore, the highest level of CO_2 emissions from industrial activities is probably to witness raised environmental pollution as Saudi Arabia persists to emerge from developing country status. Figure 1-2 shows the increase in environmental pollution from greenhouse gas (GHG) emissions and waste in Saudi Arabia alongside the energy production. According to [3], CO_2 emissions per capita were close to 17.9 metric tons in 20a13 (4.9 metric tons in the world; 16.4 metric tons in the USA; 7.1 metric tons in the United Kingdom). Saudi Arabia is one of the biggest global polluters; reducing CO_2 emissions is thus necessary. Avoiding fossil fuel through cost-effective and potentially transformative technologies, Saudi Arabia could potentially reduce NO_x, SO_2, and CO_2 emissions.

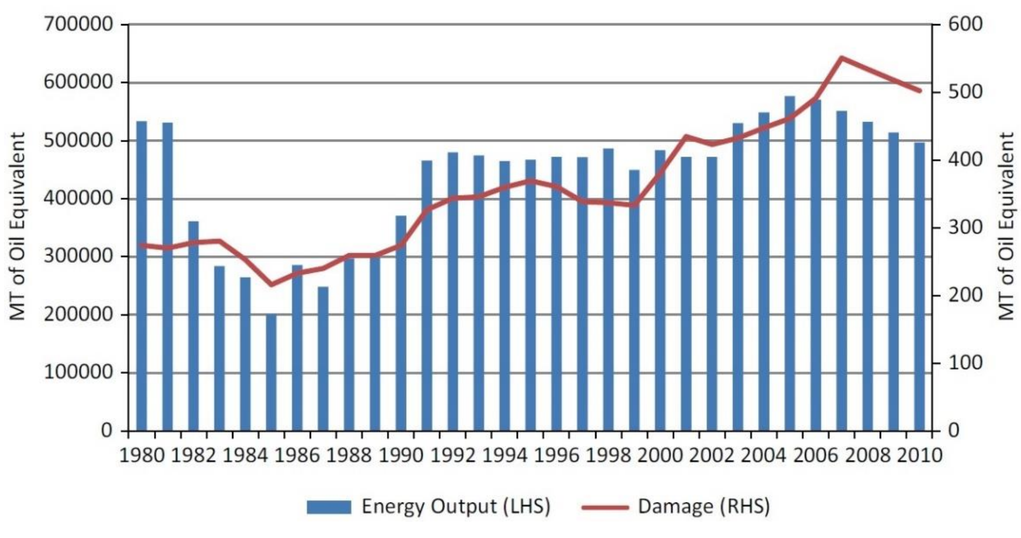

Figure 1-2: Energy generation and air pollution in Saudi Arabia [3].

While most of the oil is exported, household use is rapidly elevating, primarily for electricity production. In the last ten years, the energy consumption rose by 60%, and it is expected to increase by three folds by 2030. The growth of desalination capacity and power plants which depend extremely on burning fossil fuel is led by the growing demand of water for domestic, industrial and agriculture. Saudi Arabia generates 24 million m^3 of distilled water daily. An enormous amount of energy is used in water desalination activities, equivalent to 1.5 mmboe per day. The largest solar-powered water desalination plant in the world in the city of Al-Khafji, Saudi Arabia [4].

Policymakers in Saudi Arabia are recognizing the threat happening from this high utilization of oil to meet the requirement. The low price of oil and the high oil consumption had a genuine consequence for government revenue and GDP in 2016, where the GDP is 15% lower, causing the government to borrow to plug the kingdom's soaring fiscal deficit. This, in turn, is sending interbank rates to multi-annual highs, extract liquidity and, eventually, harming business activity. Therefore, a new vision was recently introduced "Vision 2030". Saudi Arabia is planning to move from energy based on fusil fuel to sustainable energy. The shift will include using renewable energy technology, energy efficiency projects, and change in policies (i.e. subsidies for energy, food, and water will be better used by providing them towards underprivileged.) The King Abdullah City for Atomic and Renewable Energy was established, as a first act for realizing the economic and crucial change. An initial goal of 9.5 gigawatts of renewable energy should be reached by 2023. By 2032, 50% of Saudi energy will be from renewable sources. 41 GW of solar capacity, 9 GW wind and 4 GW of other renewable energy (Figure 1-3). Solar energy has a very high potential in Saudi Arabia due to the high direct solar radiation and the large surface area of the kingdom. According to the European Commission, Saudi Arabia has the highest future potential of generating solar energy compared to today's leading solar markets Figure 1-4. The government will localize a significant share of the market including research and development, manufacturing, and production. For the first time, a framework will authorize the private sector to buy and invest in the renewable energy sector. To encourage local investors to enter renewable energy market the kingdom will encourage public-private partnerships. However, still, Saudi Arabia needs major policy movements on various aspects including encouragement of energy efficiency and employing renewable energy technology, through a mix of incentives such as feed-in-tariffs, capital grants, investment, investment credits, public investment, loans or financings as carried out in many countries in the world. For all these reasons, it is reasonable to investigate in of solar energy and make them competitive with other energy sources.

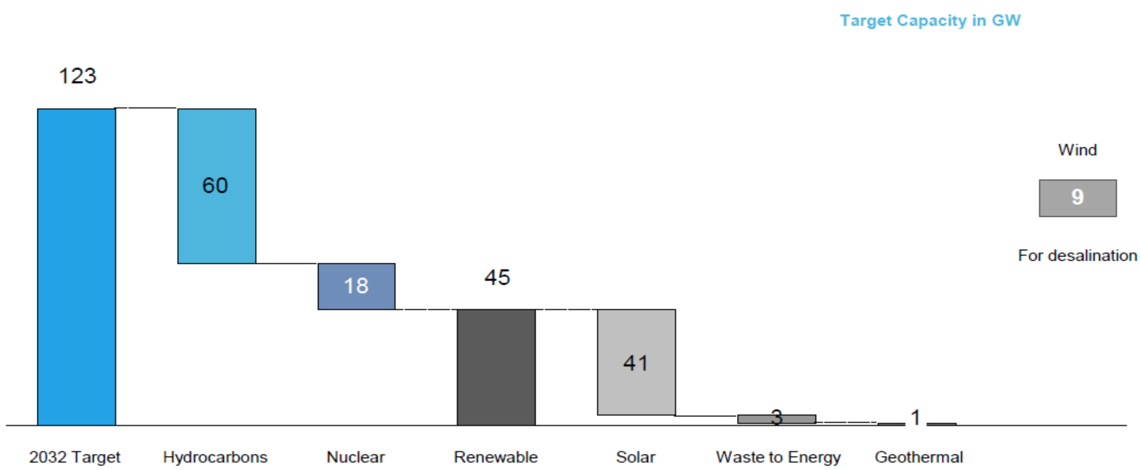

Figure 1-3: Energy consumption sources in Saudi Arabia by 2032 [2].

Country	Surface area [thousand km²]	Yield [annual kWh/installed kWp]	Generation costs [€ per kWh]	Installed capacity by 2007 [MW]
Saudi Arabia	2,240	1,400-2,100	<0.20	<5
France	672	850-1,450	0.39	75
Spain	504	1,000-1,550	0.28	632
California	424	1,400-1,800	0.22	280
Germany	357	825-1,100	0.44	3,800

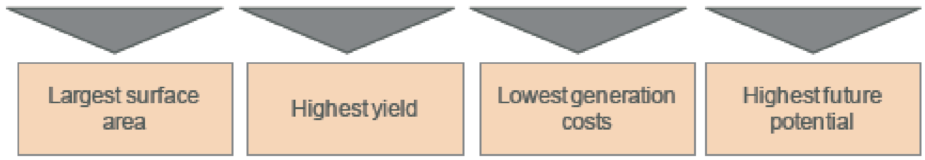

Figure 1-4: Energy potential of generating solar energy compared to today's leading solar markets [5].

1.2 Renewable energy and sustainable development

Producing, consuming and living in a way that reaches the necessity of the present without jeopardizing the ability to accommodate their own needs is known as sustainable development. Since the seminal report of the World Commission was on Environment and Development (1987), the sustainable development became generally recognised. United Nations created the commission because the exceptional pressures made by the imbalanced economic development and population growth menace the very existence of some societies, which can lead to global catastrophes in the long term. The ecological and economic pressures will force populations to change their lifestyles, especially regarding production and consumption. However, with progressive planning, political will, and foresight, the changes of lifestyles can be moderated. Energy source represents these challenges. The reliable energy source is crucial in all economics for light, heat, communications, CPU, industrial processes, transportation, etc.

World energy use is mostly from fossil fuels (i.e. coal, oil and natural gas). Fossil fuels are regenerated at an infinitesimal rate, and thus present reserves are eventually limited. The lifetime of a resource can be defined as "the known accessible amount divided by the rate of present use [6]". By using this description, the lifetime of oil and natural gas resources is limited to several decades; whereas lifetime for coal is several centuries. Moreover, the essential limitations of using fossil fuel are determined by the harmful emissions from a fossil. Increasing of CO_2 in the atmosphere is such an example. CO_2 and other gases in the atmosphere trap the heat and keep the earth warm. This phenomenon is known as greenhouse effect. Increasing the CO_2 in the atmosphere will enhance the greenhouse effect and lead to serious climate change. Climate change is not the only issue fossil fuel and nuclear energy, but also to such environmental considerations as environmental pollution, acid precipitation, ozone reduction, forest demolition and emission of radioactive materials. Accordingly, it is fundamental to spread renewable energy and utilize energy efficiently. From an economic standpoint, using renewable energy is beneficial if the full costs of paying for the damage and acquiring fuel is incorporated into the price. A promising energy future with minimal environmental influence can be achieved when all these problems are considered simultaneously.

Renewable energy is commonly defined as energy that is formed by a natural source that is naturally recovered within a span of a few years such as sunlight, wind waves, tides, and geothermal heat. [7]. Figure 1-5 illustrates an overview of renewable energy sources. Renewable energy sources have the capacity to supply over 3000 times the current global energy requirements [8]. Renewable energy contains the technologies that convert natural sources into valuable energy services:

- Solar power (including photovoltaics, solar thermal, and geothermal)
- The wind, wave, hydropower and tidal including (micro- and river-off hydropower)
- Biofuel and biomass technologies (including biogas)
- Renewable fraction of waste (household and industrial waste)

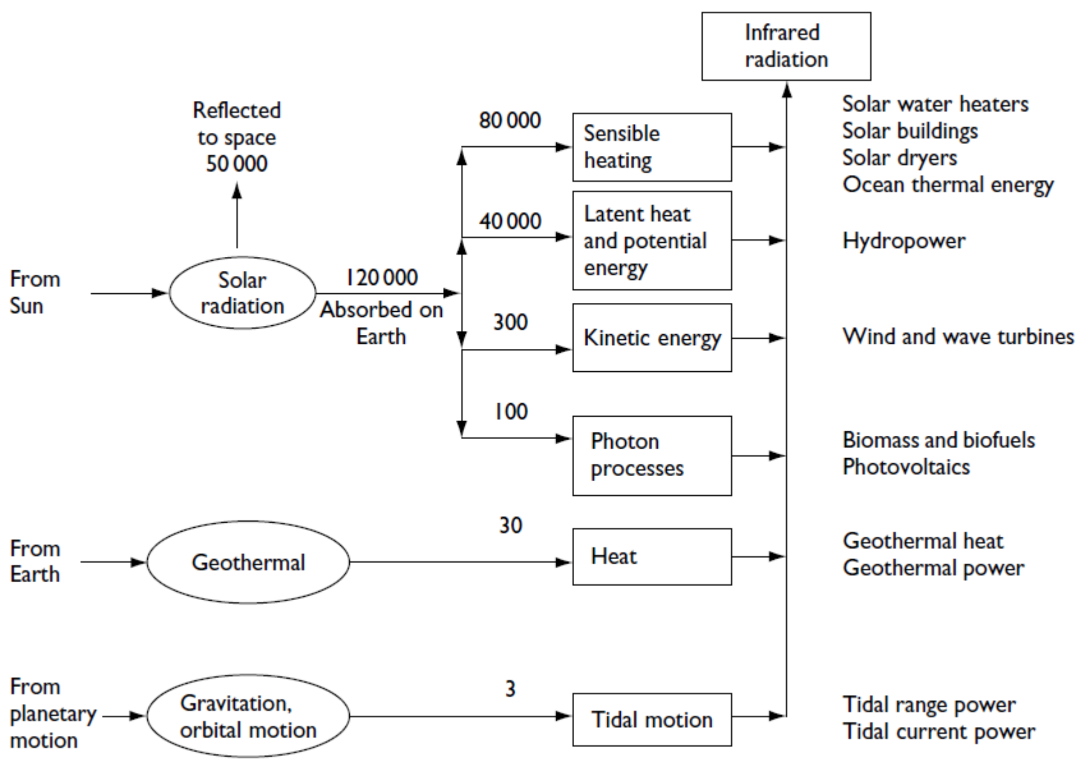

Figure 1-5: Overview of sources of renewable energy [9].

Renewable energy systems are defined as comprehensive energy supply and demand systems stand on renewable energy. The transformation from nuclear and fossil fuel-based systems to renewable energy systems associated compensation of changes in the following:

- Efficiency development in the supply system, such as combined heat and power CHP
- Demand technologies related to energy saving and conversation
- Combination of alternative renewable energy sources

Changes such as insulations and efficiency improvements of electric devices lead to changes in the energy demand. In addition to the preceding renewable energy technologies, renewable energy systems.

Over the last seven years, renewable energy markets – heating, electricity and transportation – have been increasing significantly. The creation of well-established technologies has given certainty in the technologies, reduced costs, and created new opportunities [6]. Between 2010 and 2035, the global electricity production from renewables expected to increase 2.7 times. Utilising of biofuels is predicted to increase more than double in the next few years to reach 4.3 million barrels of oil equivalent per day, up from 1.6 in 2013. Most of the biofuels are used in transportation, but the utilisation of biofuels in different sectors will be done by 2035. The use of renewable sources to reduce heat will nearly double, from 33t Mtoe to 604 Mtoe in 2035. Electricity production from renewable sources is higher than in heat generation or transportation [10]. Solar thermal energy is sufficient renewable source and is available in both directions as well as indirect forms. The research focuses on solar thermal and more specific on concentrated solar systems.

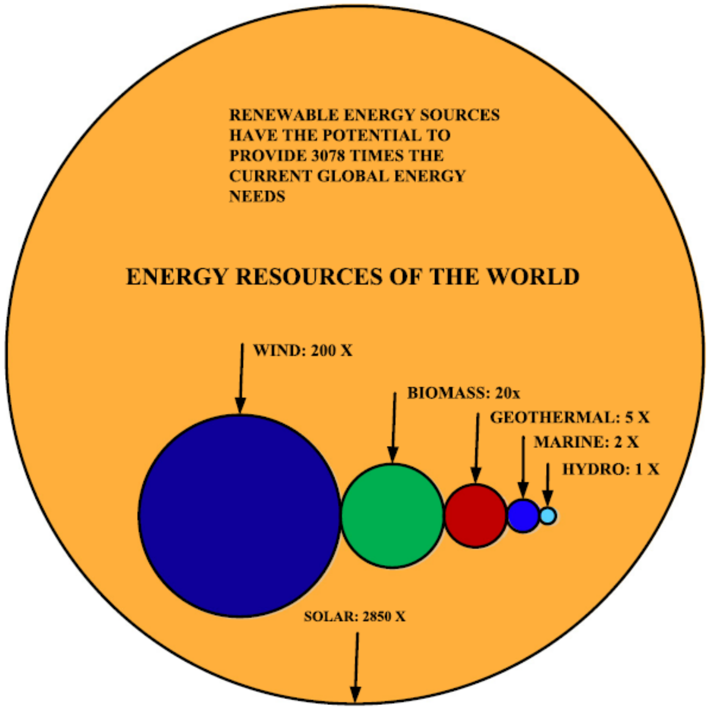

Figure 1-6: Energy sources of the world [8].

1.3 Background of solar energy

Electromagnetic radiation transfers the energy of the sun's high temperature of roughly 6000°C to the earth. Material radiation is very small therefore it is neglected. The radiation intensity of the sun is 63.5×10^6 W/m^2. The radiation of the sun decreases with the square of the distance and with absorption, reflection, and emission of materials. The solar radiation arrives at the earth atmosphere with a radiation intensity of approximately 1360 W/m^2 which is known as solar constant.

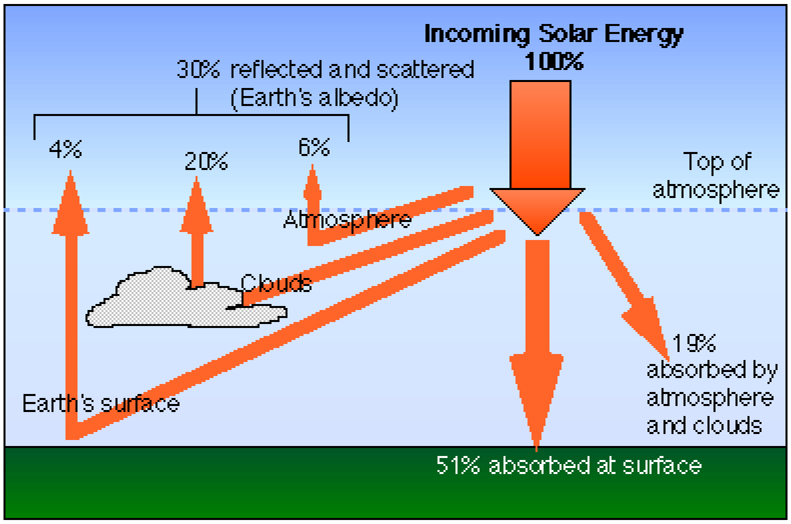

Figure 1-7: Reflecting and scattering the solar radiation when passing through the atmosphere.

As shown in Figure 1-7, 30% of the solar radiation is reflected and scattered when passing through the atmosphere. Mostly water drips (clouds) reflect the radiation into space. Another proportion is scattered by microparticles such as molecules, lumps, and aerosols. The microparticles affect the uniform radiation towards the earth, which is known as diffuse radiation. A small portion is absorbed and emitted by the ozone layer and CO_2. The portion of the radiation that reaches the earth surface is called "direct radiation." The incident solar radiation called the global radiation, which impacts the earth surface, results consequently of the total of the direct and the diffuse radiation:

$$\dot{q}_G = \dot{q}_D + \dot{q}_S \qquad \text{Eq 1-1}$$

where, $\dot{q}_G$ is the intensity of global radiation W/m^2, $\dot{q}_D$ is the intensity of direct radiation W/m^2, and $\dot{q}_S$ is the intensity of (scattered) diffuse radiation W/m^2.

Only The direct solar radiation may concentrate by lenses or mirrors in high-temperature applications. However, diffuse radiation (affecting the daylight) plays a significant role in low-temperature applications, e.g. in providing hot water and photovoltaics (PV). On a clear day, the radiation reaches the earth directly, therefore, $\dot{q}_D$ will be high. The opposite would be the case in a cloudy day. The direct and diffuse radiation are functions of the day-time and of the seasonal parameters (Table 1-1).

Table 1-1: direct and diffuse radiation [11].

	Global radiation W/m^2	Fraction of diffuse radiation %
Clear sky	800 -1000	10
Misty weather	600 - 900	50
Foggy autumn day	100 -300	100
Cloudy winter day	30 -50	100
Average	600	50 - 60

The earth is circling the sun with its polar axis tilted towards the plane of rotation. In June, the earth sits with the north pole facing the sun. The sun's rays strike the northern hemisphere more perpendicularly, and the sun appears higher in the sky. In December, the north pole is tilted aside from the sun, and its rays strike more obliquely, giving a lower radiation intensity. Another important aspect is that the lower the sun in the sky, the further it rays must pass through the atmosphere, giving them more opportunity to be scattered back into space. When the sun is at 60° to the vertical, its peak energy density on the ground will be dropped to one-quarter of that when it is vertically overhead. To plan utilization of solar energy, two values have been measured to characterize the availability of solar energy:

- The period of sunshine, expressed by radiation in hours per month or per year.
- The radiation incident on a horizontal surface expressed by the sum of monthly or annual radiation rate (kWh/m^2a).

The sun's electromagnetic wavelengths cover the entire wavelength area from 10^{-2} m up to some kilometres. However, the earth atmosphere is permeable mainly in the range of optical radiation and low-frequency waves 10^{-2} -10^{2} m. The optical radiation covers the range between 0.3-2.5 μm (100%) including mid- and long-wave ultraviolet radiation, 0.3-0.38 μm (3%) the area of visible light 0.38-0.78 μm (44%) and the shortwave infrared radiation 0.78-25 μm (53%).

The radiation parameters can be calculated using well-known radiation laws. For the radiation of a black body responds the radiation density [W/m^2(μm) or W/cm^3]to the Planck's law:

$$I_0(\lambda) = \frac{2\pi hc^2}{\lambda^5\left[exp\left(\frac{ch}{\kappa_B \lambda T}\right)-1\right]} \qquad \text{Eq 1-2}$$

where λ is the wave-length, h is the Planck constant, c is the lightspeed in a vacuum, κ_B is the Boltzmann constant, and T temperature of the black body.

$I_0(\lambda)$ varies with the wave length. The range of includes, depending on temperature, also the area of visible light, the maximum of $I_0(\lambda)$ can be calculated by the Wien's displacement law:

$$\lambda_{max} = \frac{2898}{T}\ \mu\text{m} \qquad \text{Eq. 1-3}$$

The sun surface temperature around 6000K which give us a wavelength of 0.48 μm. by integrating Eq. 1-2 over the whole wavelength spectrum, the radiation intensity (W/m^2).

$$q_0 = \int_0^\infty I_0(\lambda)d\lambda \qquad \text{Eq. 1-4}$$

where, q_0 is the radiation intensity. The solution leads to Stephan-Boltzmann law:

$$q_0 = \sigma T^4 \qquad \text{Eq. 1-5}$$

where, σ is the radiation constant of the black body = 5.67 x10-8 W/(m^{2}K^4), Sun's radiation corresponds to a black body with an average temperature of T = 5762K which gives a solar radiation of 62.5x10^6 W/m^2.

The radiation intensity decreases with the square of the distance.

$$\dot{q}_{(x)} = \dot{q}_0 \left(\frac{D}{2x}\right)^2 \qquad \text{Eq. 1-6}$$

where x is the distance, D is the diameter of the radiation source. The sun's diameter = 1.39x109 m, and the distance between the sun and the earth atmosphere is 1.5x1011m gives a radiation intensity at the earth atmosphere of:

$\dot{q}_c$ =1341 W/m^2

which is known as solar constant. However, due to seasonal fluctuations and variation of the distance between the sun and the earth, the solar constant varies in the range of 1293 – 1412 W/m^2. After passing the atmosphere, the radiation intensity decreases to the values of global radiation given by the curve underneath the curve of the solar constant. In Saudi Arabia, the average value of global radiation intensity is 1200 kWh/m^{2}a.

There are two main systems to harvest the solar radiation which is solar thermal and photovoltaics. Solar photovoltaics (PV) systems directly convert solar energy into electricity. PV system is a semiconductor device that converts solar radiation into direct current electricity. The solar thermal system is harvesting the sun's energy in the form of heat. This can be used directly as a heat source in domestic applications, and industrial thermal processes or it can be used in power generation. Solar thermal is divided into two ranges depending on the required temperature (low-, and high-temperature). The low-temperature range usually covers domestic water and space heating, in some cases also thermal processing e.g. drying (of wood) and evaporation (seawater desalination). To receive solar radiation at lower temperatures, solar collectors of different type are applied. In the high-temperature range (400-1000°C) the radiation is concentrated by means of the optical device e.g. mirrors (reflectors) or lenses. Concentrating the radiation decreases the area which heat losses exist; consequently, relatively small absorbers are used with the larger optical device. The heat produced at higher temperature can be utilized either to drive a power plant or to carry out a thermal process e.g. melting, heat treatment, unit operations, etc. Just as solar energy systems can have many variants, so can solar collectors too. The low-temperature collectors include the following:

- Unglazed collectors: they are most applicable for swimming pool heating, where the water temperature is only raised by a few degrees above ambient air temperature, so heat losses are almost unnecessary.
- Flat plate collectors: Worldwide, these are the most used in domestic solar water heating. Commonly, they have on single glazing layer, but they may have an extra second glazing layer, occasionally of plastic. The higher temperature difference between the absorber and ambient could be reached by more complicated glazing system. A black surface with a high absorptivity is commonly used on the flat plate. Most standard black paints used in the collectors reflect approximately 10% of the solar irradiation. Some collectors use a selective surface that has both high absorptivity in the visible region and low emissivity in the long-wave infrared, to reduce heat losses. Many designs of absorber plate have been tried with success in recent years, including pressed steel central heating radiators, specially made pressed aluminium panels and small-bore copper pipes soldered to thick copper or steel sheet. Mainly, an absorber plate must have high thermal conductivity, to transfer the absorbed energy to the water with minimum heat loss.
- Flat plate air collectors: These are less common as water collectors and are generally applied in space heating only. An interesting variant is to combine this type of collector with a photovoltaic, generating both heat and electricity.

- Evacuated tube collectors: they take the form of a set of standard tubes similar to fluorescent lamps. At the centre of each tube, an absorber plate is found. Heat losses are reduced by a vacuum in the tube. The absorber plate has a heat pipe that transfers the absorbed energy to the water, which flows along a header pipe at the top of the array. A heat pipe is a device with the advantage of higher thermal properties of boiling fluid. A hollow tube is filled with a liquid at a desired pressure that makes it boil at the hot end, then the vapour will condense at the other end. These tubes have a higher thermal conductivity compared to tubes made of solid metal and can transfer large amounts of heat for a small temperature rise.

For the medium and high temperature, solar collectors have also known as concentrated solar collectors the various types of collectors are:

- Line focus collectors: they focus the solar irradiances onto a tube found at the centre of a trough. Those collectors include a parabolic trough and linear Fresnel lens collector. They are mainly used for generating steam for electricity generation. The trough can be rotated to track the sun up. A line focus collector can be oriented with its axis in either a horizontal or a vertical plane. Those collectors include parabolic trough collector and linear Fresnel collector.
- Point focus collectors: These are also used for a steam generation but need to track the sun in two dimensions. Those collectors include parabolic dish and solar towers.

High-temperature solar collectors are mostly used in concentrating solar power CSP or in industrial processes

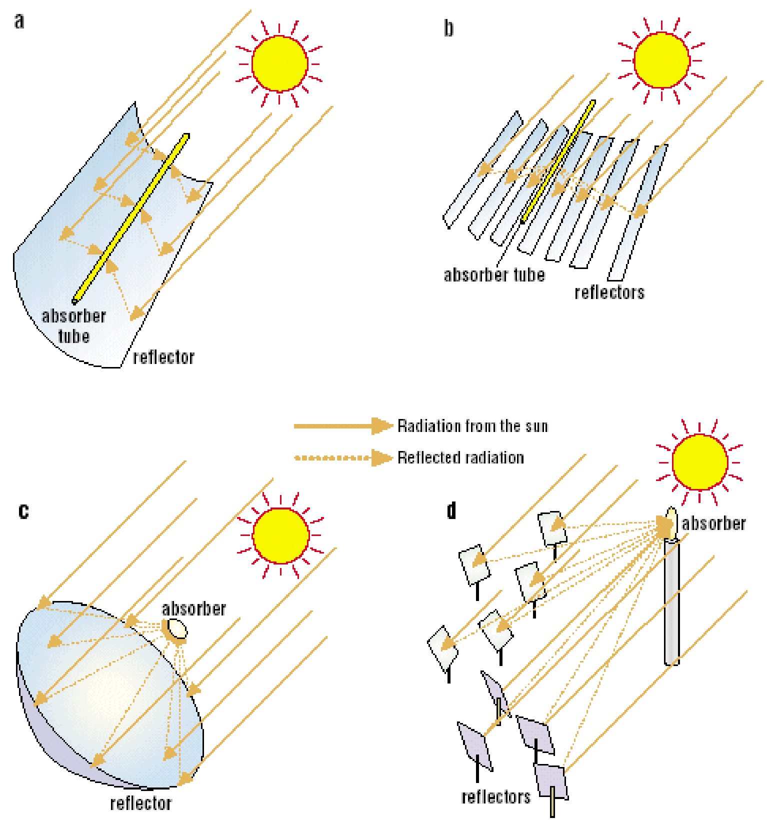

Figure 1-8: Concentration of sunlight using (a) parabolic trough collector (b) linear Fresnel collector (c) central receiver system with dish collector and (d) central receiver system with distributed reflectors [12].

1.3.1 Concentrated solar power

Concentrating Solar Power (CSP) plants utilise reflectors to concentrate solar irradiance onto an absorber, which absorbs and convert the solar irradiance to a heat transfer fluid that can be used to provide heat for industrial process applications or to produce electricity through steam turbines. One of the advantages of CSP is the heat storage system of CSP plants that allow for heat supply or electric production at night or when the sky is cloudy. The four CSP plant versions are Fresnel Reflector, Parabolic Trough, Solar Tower and Solar Dish, which vary based on the design, configuration of reflectors and absorbers, heat transfer fluid used and if heat storage is included or not. The first three types are utilized mainly for power plants. The most commercially mature technology of the three types is the parabolic trough solar collectors. Solar dishes are more applicable for distributed generation. Installing CSP in the Sun Belt region between 40° north and south of the equator is very interesting due to the high direct solar irradiance in this region. This region consists of North Africa, the Middle East, India, South Africa, Mexico, the Southwest of the United States, Chile, Peru, Australia, Western China, Turkey and southern Europe. The technological future of CSP-based energy production in nearly all of this countries is normally larger than their energy requirements, emerging in the potential for energy export. However, the application of concentrated solar power is at an early phase with roughly 4 GW installed worldwide wide in 2016, albeit the projected installation of extra 12 GW of capacity by 2019. Compared to photovoltaics (PV) farms with roughly 70 GW already in use worldwide, current CSP installed capacity is very small. In only 2015, new PV installations completed to generate 30 GW. PV total installation cost is generally lower than CSP without storage. However, it is projected that the cost of CSP will decline by approximately 15% by 2018 due to development in manufacturing and performance, scale economies, and new technology, thus lowering the Levelized cost of electricity from CSP plants to approximately USD 0.15-0.24/kWh. By 2020, projections are that the cost of capital will fall even further by 30% or 50%.

1.3.2 Industrial process

Saudi Arabia industrial sector uses heat for a wide variety of applications, including water desalination, food processing, sterilizing, drying, preheating of boiler feed water, and much more. The industrial sector uses roughly one-third of the nation's energy consumption. Process heating applications by itself count for approximately 40% of total energy consumption within the industrial sector. The large size and scale of industrial heating energy use show a unique opportunity for renewable energy. Figure 1-9 illustrate the temperature ranges for various industrial heating. The existing heating technologies could be cost-effective if used as pre-heating before an existing conventional heating source. Major considerations for industrial solar heating applications include resource intermittency, cost, storage options, and process integration.

Industrial Sector	Unit operation	Temperature range (°C)
Textile Industry	Bleaching	60-100
	Dyeing	70-90
	Drying, De-greasing	100-130
	Washing	40-80
	Fixing	160-180
	Pressing	80-100
Chemical Industry	Soaps	200-260
	Synthetic rubber	150-200
	Processing heat	120-180
	Pre-heating water	60-90
Plastic Industry	Preparation	120-140
	Distillation	140-150
	Separation	200-220
	Extension	140-160
	Drying	180-200
	Blending	120-140
Flour By-products	Sterilising	60-90
All Industrial Sectors	Pre-heating of boiler feed water	30-100
	Industrial solar cooling	55-180
	Heating of factory buildings	30-80

Kalogirou, 2003

Figure 1-9: Temperature range for different industrial processes [13].

1.4 Background of ferrofluids

Depending on their application, solar collector uses different heat transfer fluids. In low-temperature range, usually, water is used. In high-temperature range thermal oil or Phase Changing Material (PCM) is used. In this research, we use ferrofluids as a heat transfer medium. Ferrofluids (also Known as magnetic nanofluids, MNF) are stable liquid dispersed colloidal magnetic nanoparticles such as Fe_3O_4, γ-Fe_2O_3, $CoFe_2O_4$, Co, Fe or Fe-C. The substantial magnetic properties of the nanoparticles and their effect on the thermophysical nature such as thermal conductivity and viscosity distinguish ferrofluids from other nanofluids. The thermophysical properties of ferrofluids can be controlled and adjusted by an electromagnetic field. Depending on their applications, the ferromagnetic particles are dispersed in a wide range of base fluids. In theory, it is possible to disperse the magnetic particles in any base fluids to fit the application requirements (e.g. surface tension, boiling temperature, viscosity, vapour pressure, stability in a harsh environment, etc.). For example, it is necessary that base fluid has a very low vapour pressure in a rotary vacuum. Each nanoparticle (metal or ferrite made of single magnetic domain) in ferrofluids is consistently in a state of magnetic saturation in the presence of external magnetic field and/or gravitational field. Therefore, a particle diameter of roughly 10 nm is essential to keep the colloidal suspension stable. The high magnetostatic force between single particles attracts them to each other causing Agglomeration and sedimentation of particles. This issue can be resolved by modifying the particles surface with specific surface treatment to produce entropic repulsion (i.e., a coating with stabilizer layer) such as oleic acid.

Ferrofluids are widely employed in versatile applications like in sealing, as loudspeaker coolant, lubricants, in pressure sensors, in display devices, in biomedical applications like targeted drug delivery, hyperthermia, as a low side effect MRI contrasting agent, as magnetically tunable optical filters as tunable diffraction gratings, as magnetic field and moment sensor. New designs in a wide range of technical application could benefit from the magnetic control such as the utilisation of magnetic forces in fluid dynamics research.

In heat transfer applications, the usage of ferrofluids as a heat transfer medium has the main advantage of higher thermal conductivity compared to the base fluids. The thermal conductivity of nanoparticles is much higher than the base fluids. Therefore, by adding nanoparticles to the base fluid, the thermal conductivity of the mixture will increase, which leads to heat transfer enhancement. The particles distribution in the base fluid contribute to the enhancement of the thermos-physical properties of the mixture while causing issues related to sedimentation, clogging, and erosion that can be observed with the suspension of micron size particles. The use of ferrofluids as a heat transfer medium has several advantages compared to conventional non-magnetic nanofluids:

- The properties of the nanoparticles (e.g. density, viscosity, and thermal conductivity) can be changed by the external magnetic field to reach explicit design requirements.
- The thermomagnetic convection in ferrofluids is controlled and enhanced by controlling the external magnetic field.
- The size and the cost of components in heat transfer device can be reduced by using ferrofluids.

One of the most challenging aspects of ferrofluid research in the interdisciplinarity of the field. Besides chemistry for the preparation of ferrofluids, the basic theoretical physics for the description of their properties and behaviour, fluid physics, and Rheology for the investigation of lows and rheological properties under the influence of external magnetic fields are needed to cover the basic research interests, in addition, engineering and medical application contribute to the importance of ferrofluids research for everyday life. In this research, the focus is mainly on the application of ferrofluids in parabolic trough solar collector.

1.5 Outline of the research

Improving the efficiency of solar collector will make it more economical. Enhancing the heat transfer performance of the solar collector is one of the methods used to increase the efficiency of solar collectors. Nanofluids showed an improvement in the heat transfer performance of solar collectors. Moreover, magnetic nanofluids when used in heat transfer applications and in the presence of the external magnetic field, ferrofluids showed a significant increase of heat transfer performance compared to nanofluids. Therefore, the research aims to develop a small-scale ferrofluid based concentrated parabolic collector. The research objectives are: -

- Both theoretically and experimental investigation of the innovative idea of using ferrofluids to improve the efficiency of the concentrated parabolic collector.
- Investigation of the parameters affecting the performance of the solar collector such as Thermal Conductivity, Viscosity, and magnetic intensity.
- Investigation of the economic and environmental impact of using ferrofluids in concentrating solar collectors.

Ferrofluids can be used in different solar collector designs. Parabolic trough design was chosen due to their small absorber area, hence, less thermal loss and higher efficiency. Moreover, applying external magnetic field is simple compared to non-concentrating collectors, where the heat transfer fluids flow in the singular pipe in the collector. In addition, parabolic trough collectors can be very interesting in Saudi Arabia. The country has the high direct solar irradiance needed for parabolic trough systems. Moreover, the desalination of seawater can benefit from the waste heat of parabolic trough systems, supplying Saudi Arabia, currently the world's top desalinated water producer, with a remarkably economical solution for achieving its human water requirements. A comprehensive literature review related to the ferrofluids, parabolic trough collectors and nanofluids based solar collector is performed in Chapter Two. In-depth understanding of factors that could affect the performance of ferrofluids based parabolic trough is gained via a literature review. The methodologies and experiment set-up of the ferrofluids based collector is given in Chapter Three. The experimental results of the use of ferrofluids in parabolic trough collector with two different absorber types, and the effect of nanoparticles concentration, magnetic field intensity, and direction are presented in Chapter Four. A heat transfer Analysis of the ferrofluids solar absorber is carried on in Chapter Five. The results of the analysis are compared with the experimental results. Furthermore, the economic and environmental impact of ferrofluids based solar collector is available in Chapter Six. The study is concluded by the summary and future work presented in Chapter Seven.

Chapter 2. Literature Review

2.1 Ferrofluids

Enhancing the thermal performance of heat transfer processes by modifying materials properties at the nanoscale have been attempted by many researchers. This has led to the finding of distinctive engineered fluids widely known as nanofluids. Nanofluids are used in thermal devices to boost the heat transfer performance, for example, in electronic devices. A unique branch of nanofluids is ferrofluids (also known as magnetic nanofluids, MNF). Ferrofluids are a stable liquid which contains dispersed colloidal magnetic nanoparticles.

Ferrofluids can be distinct from conventional nanofluids by the particular magnetic property of the nanoparticles which affects their thermophysical properties such as density, thermal conductivity, and viscosity that can be regulated to specific values by controlling the intensity of external magnetic field [14]. Maintaining a stable dispersion with adjusting the magnetic nanoparticles requirements viscosity, surface tension, temperature, thermal conductivity, vapour pressure, etc. can be achieved to fit the desired application [15, 16]. Furthermore, in the presence of external magnetic field the individual particles (metal or ferrite made of a single magnetic domain) are consistently in a state of magnetic saturation, and for the colloidal suspension to remain stable, the particles need to have a diameter of approximately 10 nm. Additionally, the strong magnetostatic attraction forces between particular nanoparticles that causing the issue of agglomeration and sedimentation of particles needs to be solved, for example by modifying the particles with specific surface treatment (i.e. a coating with a stabilizer layer) such as oleic acid for suspending in an oil phase or depending on the type of base liquid [17, 18].

The use of ferrofluids as a heat transfer medium has several advantages compared to conventional non-magnetic nanofluids [19]. The properties of the nanoparticles (e.g. density, viscosity, and thermal conductivity) can be changed by the external magnetic field to reach explicit design requirements. The thermomagnetic convection in ferrofluids is controlled and enhanced by controlling the external magnetic field. The size and the cost of components in heat transfer device can be reduced by using ferrofluids.

In this section, the subject of thermophysical, optical properties and thermomagnetic convection of ferrofluids are examined, and the potential for the use of ferrofluids in thermal energy transfer processes and their directions are discussed. The density, thermal conductivity, heat capacity, surface tension and viscosity are the essential properties of heat transfer fluids. The change in thermophysical properties of ferrofluids in the presence of external magnetic field needs to be realized. Precisely, the change in thermal conductivity, surface tension, and viscosity are complicated and more work needs to be done while the density and specific heat capacity of ferrofluids can be determined according to the mixture model, which is applicable to conventional mixtures [20].

2.1.1 Ferrofluids preparation procedure

For most of the applications, stable ferrofluids are necessary under the operating range of temperatures and under the influence of external magnetic field. Therefore, a high degree of consistency is required when preparing ferrofluids to enhance the uniformity of nanoparticles suspended in the fluid [17]. This generally relies upon the characteristics of base liquid and stabilizer [21]. Two essential steps are used in the preparation of magnetic nanofluids. At the beginning, formation of nano-sized particles and next, stabilization/dispersion of the nanoparticles in various nonpolar or polar carrier liquids [18].

Magnetic nanoparticles are generally ferrite and metals particles. Mainly there are four different methods to prepare the ferrite (iron oxide) nanoparticles which include wet grinding, co-precipitation, microemulsion, and substituted ferrite particles.

The first method used to make ferrofluids based on ferrites was wet-grinding [22]. The method elaborated wet-grinding ferrites in a ball-mill with an appropriate surfactant till the ferrite is in a colloidal state. Cyclone separation was employed to remove bigger particles. However, the process takes a very long time (1000 hours.) "Co-precipitation" of metallic ions is the most and simplest used method to create the ferrite nanoparticles. High productivity resulted from this procedure [17]. Figure 2-1 illustrates the main steps of this procedure for co-precipitation synthesis of magnetite nanoparticles.

The polarity of the base fluid and the surfactant affects the dispersion condition of magnetic nanoparticles in the based fluids [23]. Oleic acid is the most used surface coating of the nanoparticles stabilizer in the hydrophobic modification. The stabilizer enhances the stability of suspension and keeps the magnetic nanoparticles repulsive to each other in a fluid. The procedure for dispersion of magnetic nanoparticles in the nonpolar fluid is shown in Figure 2-2a. The non-polar fluids consist of hydrocarbons (kerosene, toluene, and cyclohexane) and oils such as thermal oil, etc. Furthermore, the preparation procedure of ferrofluids with a polar organic fluid such as diesters, alcohols, ketones, amines, and mixtures of various mineral and synthetic oils (e.g. high vacuum oils) is shown in Figure 2-2b.

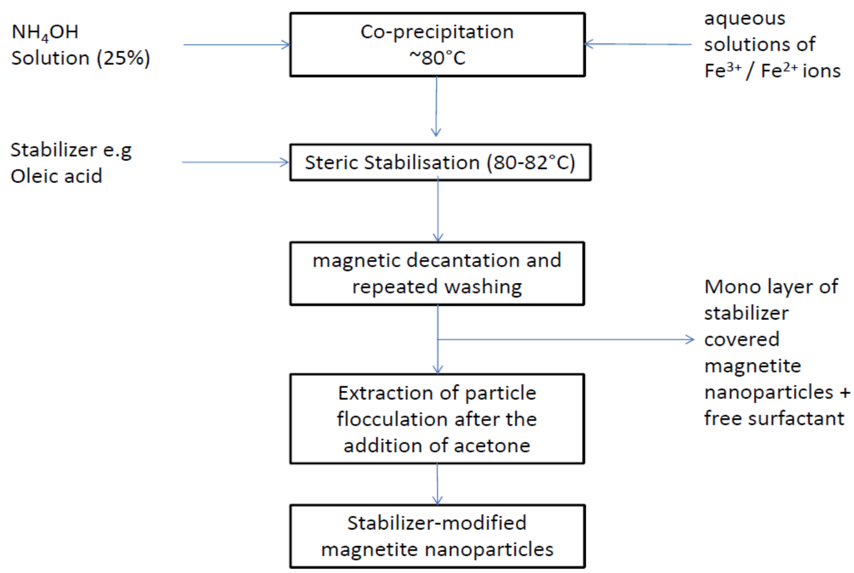

Figure 2-1: The procedure of magnetite nanoparticles formation by chemical co-precipitation [5].

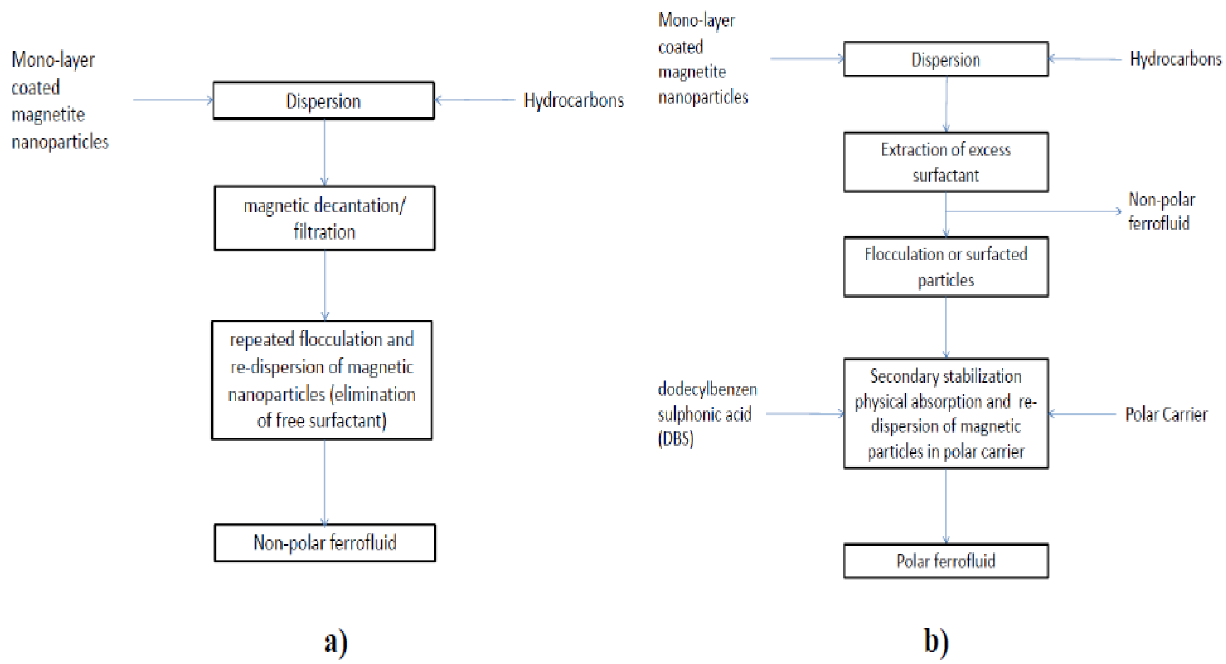

Figure 2-2: The procedure of dispersion of magnetite nanoparticle a) into non-polar base liquid b) into polar organic base liquids [10, 11].

Converting hydrophobically treated magnetic nanoparticle into hydrophilic nanoparticle by adsorption of the water-soluble surfactant is used to prepare water-based ferrofluids, as illustrated in Figure 2-3. The previous procedures are commonly used to prepare a variety of ferrofluids in terms of the type of base fluid. Ferrofluids can be prepared for a wide range of application because the properties of the chemical synthesis can be carefully selected to suit the application [18].

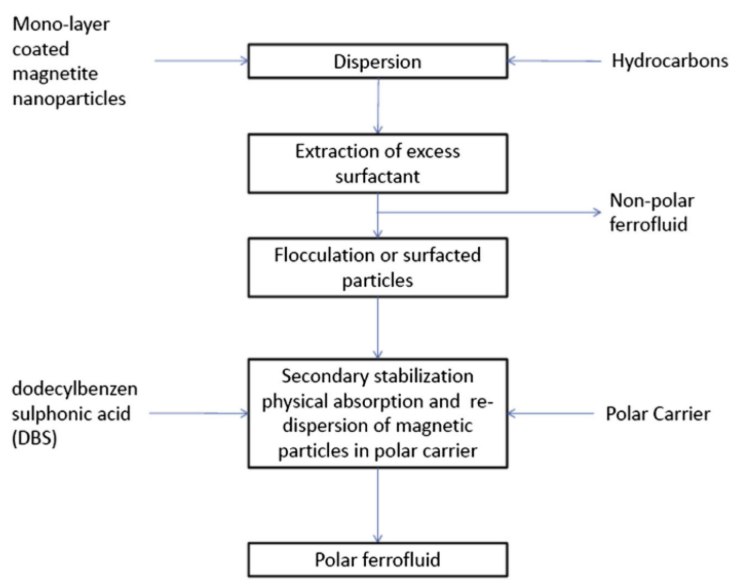

Figure 2-3: Basic procedure for preparation of water-based ferrofluids [11].

In addition to simple precipitation, micro-emulsion technique could be possibly used to produce ferrite particles. Reverse micelles are used in the preparation of ferri- or ferromagnetic nanoparticles which are considered as water-in-oil micro-emulsion with a surfactant as a stabilizer of two immiscible liquids. A triangular phase diagram of the three-component system is utilised to define the different structures that may be formed other than micro-emulsions. A detailed review study on the micelles and particle formation is available [24]. The method of particles preparation includes the formation of two macroemulsions one including an aqueous solution of one or combination of metal salts and the other an aqueous solution of an alkali and blending the two in the suitable ratio. By applying a pure surfactant, the aggregate size distribution is very small, and the particles have small particle size distribution. The disadvantage of this procedure is that the surfactant utilized in the formation may not be appropriate with the base fluid needed for an application. The problem can be solved either by replacing the surfactant from the particles with one suited with the base fluid or use multiple surfactant layers, i.e., coat the first surfactant with additional surfactant suited with the base fluid. Substituted ferrite particles are another possibility to produce nano-sized particles. In this method, the Fe^{2+} ion is simply replaced with another or combination of metal ions such as Co^{2+}, Mn^{2+}, Ni^{2+}, Zn^{2+}, etc. Ions to prepare substituted ferrites. This method is interesting due to the magnetic properties of the substituted materials that satisfy various applications. Other metals, such as cobalt and iron particles, are also used in ferrofluids, and those metals are prepared either by decomposition of organometallic compounds or Inverse microemulsion techniques. Using ferrofluids based on metallic nanoparticles has two main advantages. First, the higher saturation magnetizations of these metals compared to ferrites. Second, they can be easily formed with very small size distributions. Nevertheless, the main disadvantage of metallic nanoparticles is the limitation of their utilization in most commercial applications, and their weak resistance to oxidation and consequent loss of magnetic properties. These fluids can have long lifetime only if kept in a closed atmosphere system.

2.1.2 Thermophysical and optical properties of ferrofluids

Thermal conductivity, density, heat capacity, dynamic viscosity and specific volume are the characteristics that define the thermophysical properties of a heat transfer fluid. In nanofluids, these properties can be modified to suit the required specification for example by means of the employment of an external force. Many researchers all over the world are currently focusing on modifying these properties of nanofluids [25].

2.1.2.1 Thermal conductivity

Generally, the expected enhancement of thermal conductivity in nanofluids is compared to a base fluid [26]. The particle size, and distribution of magnetic nanoparticles, the volume fraction, chemical composition of particles, a coating layer, and bulk temperature affecting the thermal conductivity of ferrofluids in the absence of an external magnetic fluid [27]. The effect of volume fraction on the thermal conductivity of Fe_3O_4 nanofluids with a particle size of 6 nm in different base fluids was studied and the results showed that the improvement could reach 25%, as shown in Figure 2-4 [28]. Other studies reported that rapid clustering of the nanoparticles in a high concentration fluid causes the thermal conductivity to increase nonlinearly and that iron-based nanofluids showed higher thermal conductivities than copper-based nanofluid with the same volume fraction [29].

Up to 300% enhancement in the thermal conductivity of ferrofluids can be reached in the presence of an external magnetic field. as reported by to Philip et al. [30] and 200% reported by Gavili et al. [31]. The development of chain-like particle structure in the presence of external magnetic field along the thermal gradient orientation is the reason for the increase in thermal conductivity of ferrofluids. It was also noticed that the orientation of the magnetic field has a strong impact on the thermal conductivity, with the highest enhancement achieved when the field was parallel to the orientation of the thermal gradient. The thermal conductivity of hybrid nanoparticles based ferrofluids was investigated [32]. The hybrid nanoparticles consist of magnetic nanoparticles Fe_3O_4 and carbon nanotubes CNT. The carbon nanotube present excellent mechanical, electrical, thermal, and chemical properties. According to the authors, adding CNT to magnetic nanoparticles could benefit from the properties of both. The results showed enhancements of 34-44% in the temperature range of 25-55°C. The thermal conductivity of magnetic graphite nanoflake suspended in synthetic oil is reported [33]. Graphite nano flakes have higher thermal conductivity compared to Fe_3O_4 particles. The results showed that thermal conductivity enhanced up to 325% with 0.8% concentration. Moreover, the study showed that the thermal conductivity will return to the initial value after removing the magnetic field. Table 2-1 summarizes recent studies on ferrofluids thermal conductivity enhancement of in the presence and absence the presence of an external magnetic field.

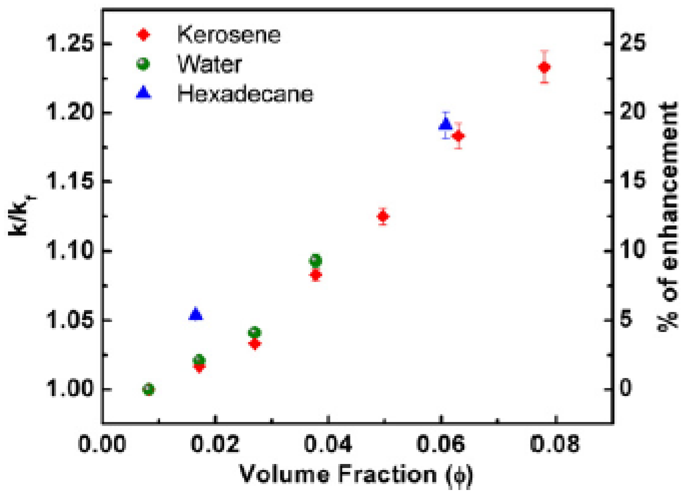

Figure 2-4: Thermal conductivity enhancement as a function of volume fraction for Fe_3O_4 ferrofluids with particle size of 6 nm in different base fluid [28].

Table 2-1 Recent studies on ferrofluids thermal conductivity enhancement in the absence and the presence of external magnetic field.

Author	Based-Fluid	Average Particle Size (nm)	Volume Fraction %	Enhancement (no magnetic field)	Enhancement with magnetic field
Philip et al. [30]	Kerosene	6.7	0.03-7.8	23% @ 7.8 %	300% @ 6.3% (80 Gauss)
Parkeh and Lee [34]	Kerosene	10	1-10	17% @ 4.7 %, 38% @ 10 %	30% @ 4.7%
Gavali [31]	Water	10	5	-	200%
Yu et al. [35]	Kerosene	15	0.1-1	34% @ 1 %	-
Li et al [36]	Water	26	1-5	14% @ 5%	13% @ 1%, 44% @ 5% (250 Gauss)
Hong et al. [29]	Ethylene glycol	10	0.2-0.55	18% @ 0.55 %	-
Zhu et al. [37]	Water	10	-	38% @ 4%	-
Abareshi et al [38]	Water	10	0.25-3	11.5% @ 3%	-
Altan et al. [39]	Water & heptane	10	1-7	-	5.2% in water & 2.8% in heptane
Sundar et al. [40]	Water	13	0.2-2	25% @ 2%	-
Pastoriza-Galeego et al. [41]	Ethylene glycol	15	0-6.9	15% @ 6.9%	-
Shahsavar et al. [32]	Water	10	0.1-0.9	44.6%	-
Sun et al. [33]	Synthetic oil	10	0.2-0.8	15%	325% (800 Gauss)

The major explanation for the improvement of thermal conductivity in ferrofluids in the presence of external magnetic field is generally due to the chain-like structure of the nanoparticle that can produce and form lengthened and highly conductive currents for heat flow since the heat is transferred faster in metal nanoparticles than in the base fluid [42]. The confirmation that the enchantment is governed by the aggregation of nanoparticles was presented in several studies. The individual nanoparticles start to form doublets, triplets, and short chains along the orientation of the magnetic field and once the magnetic field intensity increases the length of the chain also increases [42]. The impact of clustering and Brownian motion were investigated [43]. The Brownian motion defined as the random motion of nanoparticles suspended in a fluid generated by collisions with base fluid molecules [44]. The distribution of nanoparticles of nanoparticles and their motion which aids the transfer of heat among the different parts of the fluid; and generates convection paths around the nanoparticles was thought to affect the thermal conductivity of nanofluids [45]. However, researchers proposed that aggregation dominates the thermal conductivity enhancement in ferrofluids in the presence of external magnetic field and Brownian motion in case of their absent [44].

Various theoretical models have been proposed in relation to investigating the thermal conductivity of ferrofluids. Maxwell-Gannet model was modified by including an anisotropic structure specification which characterizes the non-uniform diffusion of particles suspended in the presence of magnetic field [46]. Their results showed the formation of nanoparticles chain-like structure along the orientation of the external magnetic field in the presence of a magnetic once the magnetic field was present. The homogenization method was studied, by taking into consideration the magnetic field effect and the physical anisotropy [47]. The thermal conductivity of the chain-like structure was determined by applying the differential effective medium theory.

The theory used self-consistent anisotropic effective medium theory to determine the effective thermal conductivity of ferrofluids in the presence of magnetic field. The numerical results showed that the physical anisotropy and the shape of aggregated chain-like clusters are responsible for the enhancement of the effective thermal conductivity. The thermal conductivity ratio of ferrofluids produced by the chain-like magnetic nanoparticles clusters in the presence of magnetic field was predicted by Nkurikiyimfura et al. [48].

2.1.2.2 Viscosity

Various research studies reported that in the absence of a magnetic field, the viscosity of magnetic nanofluids is no contrast from conventional of nanofluids and the viscosity enhances correspondingly with the volume fraction [40, 49]. The effect of viscosity of base fluid on the effective thermal conductivity of the ferrofluids was investigated [50]. Base fluids with high viscosity tend to weaken Brownian motion of suspended nanoparticles, inducing a reduction in thermal conductivity. The viscosity and effective thermal conductivity of water-based ferrofluids with Fe_3O_4 nanoparticles at different volume fraction and temperature were measured [40]. The enhancement ratio of viscosity was much higher than that of the thermal conductivity under the same temperature and volume fraction. Experimental study on the effect of the surfactant on the viscosity and thermal conductivity of ferrofluids in the presence of a magnetic field was carried on [36]. The experiment results showed the viscosity of ferrofluids raised considerably with the concentration of the added surfactant. The explanation for the increase is that the surfactant layer leads to a difference between the actual diameter of the nanoparticles and their hydrodynamic diameter [16]. The additional surfactant will remarkably affect the interactions between the nanoparticles and the flow of the ferrofluids is decreased so that the viscosity of the ferrofluids is increased.

In a high magnetic field intensity, the flowability of the fluid is reduced due to the zippering and clumping of particles chain-like assemblies that block the motion of the nanoparticles, therefore, the viscosity of ferrofluids increased [51]. The increase of viscosity of magnetic nanofluids in the presence of magnetic field is supported by many studies [52-54]. The effect of external magnetic field orientation on the effective viscosity was experimentally studied by using a horizontal viscometer was studied. The orientations of the magnetic field were parallel, perpendicular, and in other angular directions to the flow. It was concluded that the orientation of the external magnetic field influences the viscosity of ferrofluids greatly [54]. The viscosity was increased to a maximum of 200% when the external magnetic field was switched from perpendicular to parallel to the flow direction. The reliance of viscosity of ferrofluids on the intensity of external magnetic field and the volume fraction of a particle was also investigated. The results showed that either applying a high-intensity magnetic field or increasing the volume fraction produced the increase of viscosity. The rheological properties of ferrofluid by utilising a conventional rotating rheometer with the various external magnetic field was investigated [52]. The results showed that the ferrofluids have a non-Newtonian behaviour where the viscosity is depending on the shear rate. The viscosity of the ferrofluids is much higher at a low shear rate also known as the magneto-viscous effect. The increase in viscosity is caused by the magnetic force along the suspensions which attempts to align the nanoparticles magnetic moments with the magnetic field orientation.

Nevertheless, at higher shear rates, the magnetic nanofluids showed the shear thinning behaviour, as shown in Figure 2-5. The behaviour of the ferrofluids should be taken into consideration for any applications of ferrofluids, e.g. magnetically controlled drug targeting, as they can greatly impact the rheological characteristics of the blood flow [53]. A Recent study investigated the viscosity of water-based manganese ferrite nanofluid with and without magnetic field [55]. The results showed a maximum increase of 14% at 3% volume fraction of nanoparticles under no magnetic field, whereas the maximum viscosity of 75% was observed under 400 G magnetic field as shown in Figure 2-6.

The viscosity and thermal conductivity and as a function of magnetic field intensity, volume fraction and shear rate were measured and reported [56]. The results exhibit that the enhancement of ferrofluids viscosity was larger than the enhancement of thermal conductivity. However, by alternating the external magnetic field intensity (controlling magnetic field), the proportion of thermal conductivity to the viscosity was regulated from 0.725 to 2.35. The rheological properties of concentrated ferrofluids with 6% volume fraction was theoretically studied [57]. The assumption made for the model was that the nanoparticles in ferrofluids create a linear chain-like structure in the presence of magnetic field. The results showed the chains caused the strong magneto-viscous effect.

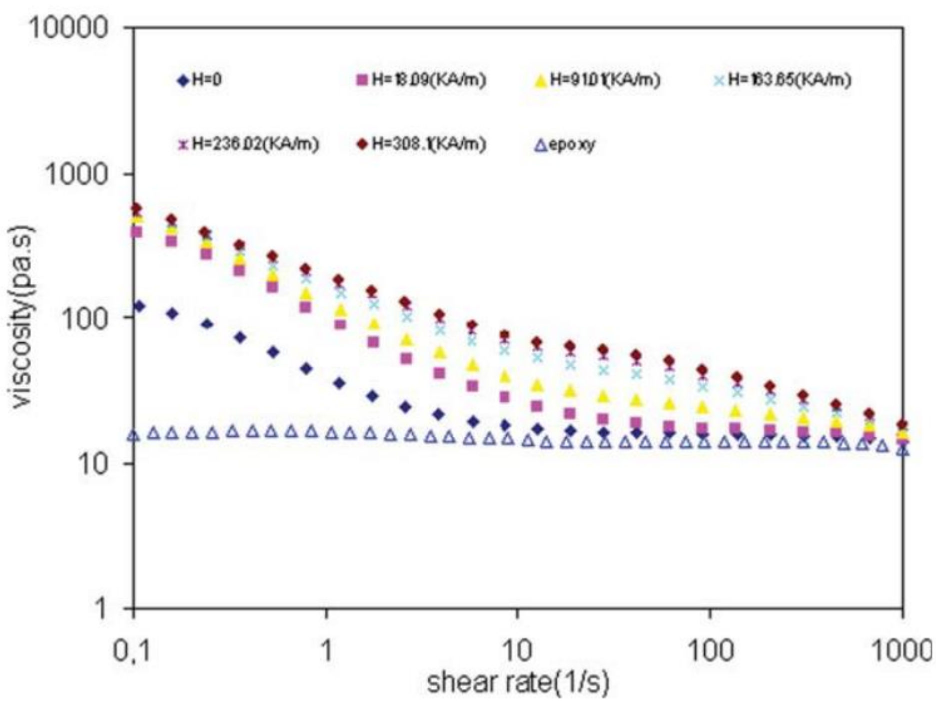

Figure 2-5: Viscosity of ferrofluids and base fluid as a function of shear rate in the presence of magnetic field [52].

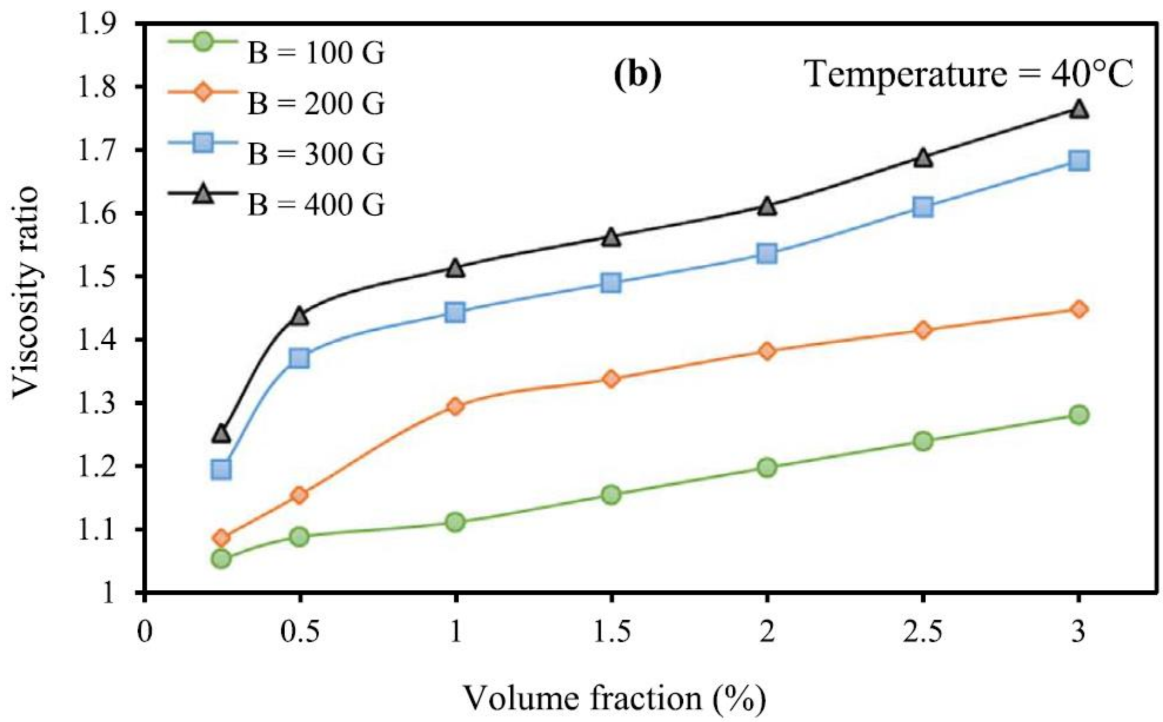

Figure 2-6: Variation of viscosity ratio versus solid volume fraction under magnetic fields at the temperature of 40°C [55].

2.1.2.3 Optical Properties

The optical properties of ferrofluids usually studied because of their use of optical filters. However, the optical properties of ferrofluids could be beneficial in solar absorption. Therefore, in this section, we include the general optical properties of ferrofluids in the presence and the absence of magnetic field. Recently many studies showed a change in the optical properties of fluids when nanoparticles were added [58-62]. The optical properties that were investigated are the transmission and extension coefficient. The nanoparticles shape, size, concentration, the optical properties of the base fluid, and the optical properties (absorption & scattering) of the nanoparticles themselves affect the optical properties of nanofluids. The effect of the nanoparticles material is reflected by the complex refractive index of the bulk material. Different materials exhibit diverse optical properties, because of their different complex refractive index. An experimental study was conducted to investigate the optical properties of multi-walled carbon nanotubes (MWCNTs) nanofluids with various concentration and base fluid [60]. The study also investigated the stability of nanofluids after 8 months from synthesis and high-temperature application. As shown in Figure 2-7, long-term stability at ambient temperature and pressure (tested up to 8 months) has been observed for the glycol-based nanofluids, on the other hand, a slow aggregation of MWCNT was demonstrated with the water-based nanofluids. Moreover, a considerable amount of aggregation was observed in nonpolar Therminol VP-1 based nanofluids due to the polar nature of the oxygen characteristics bonded to the surface of the nanoparticles. No aggregation was observed at high temperatures after heating the ferrofluids to 85 and 170 °C for the water and glycol-based nanofluids, respectively. The results also demonstrate that low concentration MWCNTs nanofluids are absorbing most the solar spectrum. The optical properties of ferrofluids in the presence of external magnetic field was investigated [63]. As shown in Figure 2-8, results showed once a magnetic field was applied the optical transmittance decreased to a minimum then gradually increased, until it becomes steady. The microscopic images showed that this behaviour is due to the formation of the chain-like structure of the magnetic nanoparticles in the presence of the external magnetic field, causing the optical transmittance to decrease. When the chain-like structure was formed by the applied magnetic field, the optical transmittance was decreasing. As shown in Figure 2-9, the transmittance increased due to the increase of the distance between the chains of particles as they became longer and bigger. Moreover, the experiment result showed that the transmittance is affected by the magnetic field intensity, nanoparticles concentration, and the base fluid.

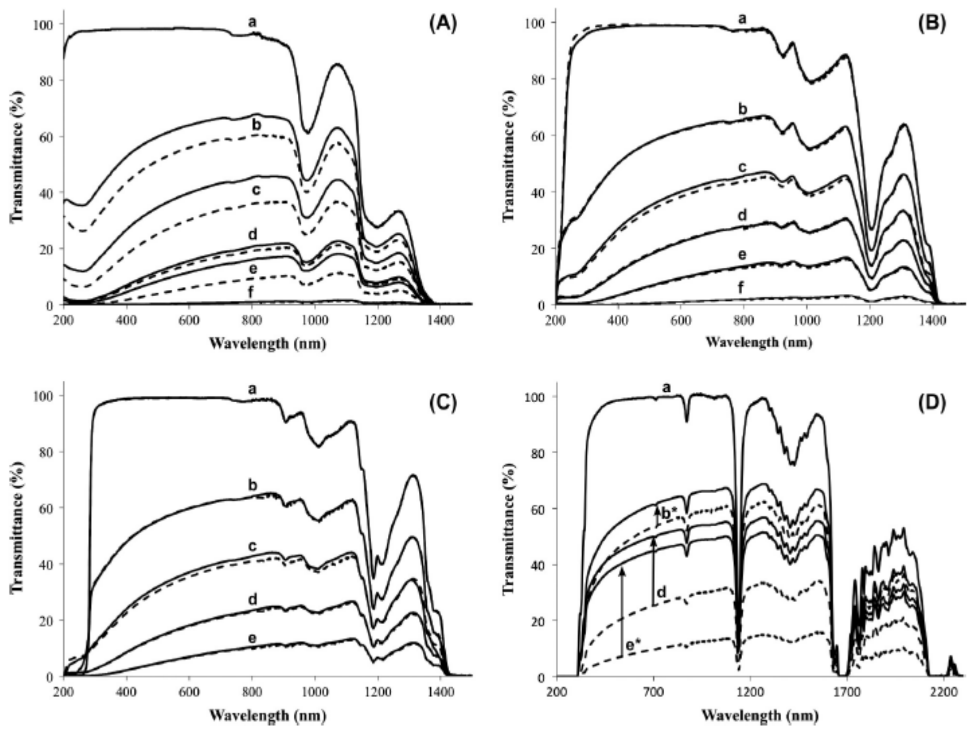

Figure 2-7: Transmission spectra for various concentrations of nanofluids, immediately after synthesis (dash) and after 3 months (solid). (A) Water, (B) ethylene glycol, (C) propylene glycol, and (D) Therminol VP-1. Absorption path length was 1 cm. The concentration of nanofluids in mg/L a) 0, b) 5.6, b*) 6.5, c) 11.0, d) 17.0, e) 27.0, e*) 33.0, f) 53.0 [60].

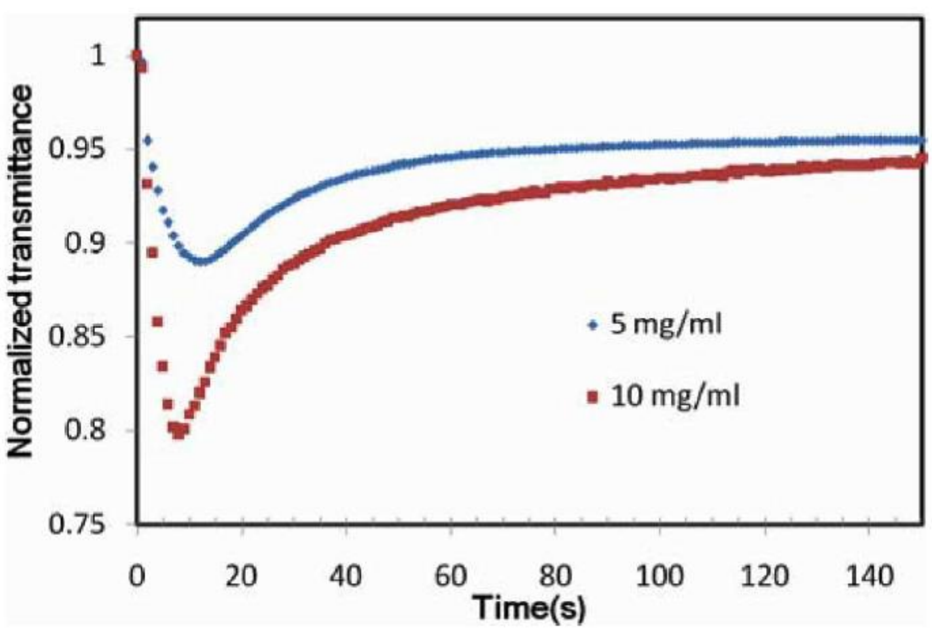

Figure 2-8: Normalized transmittance as a function of time with an applied magnetic field 500 Oe with different concentrations [63].

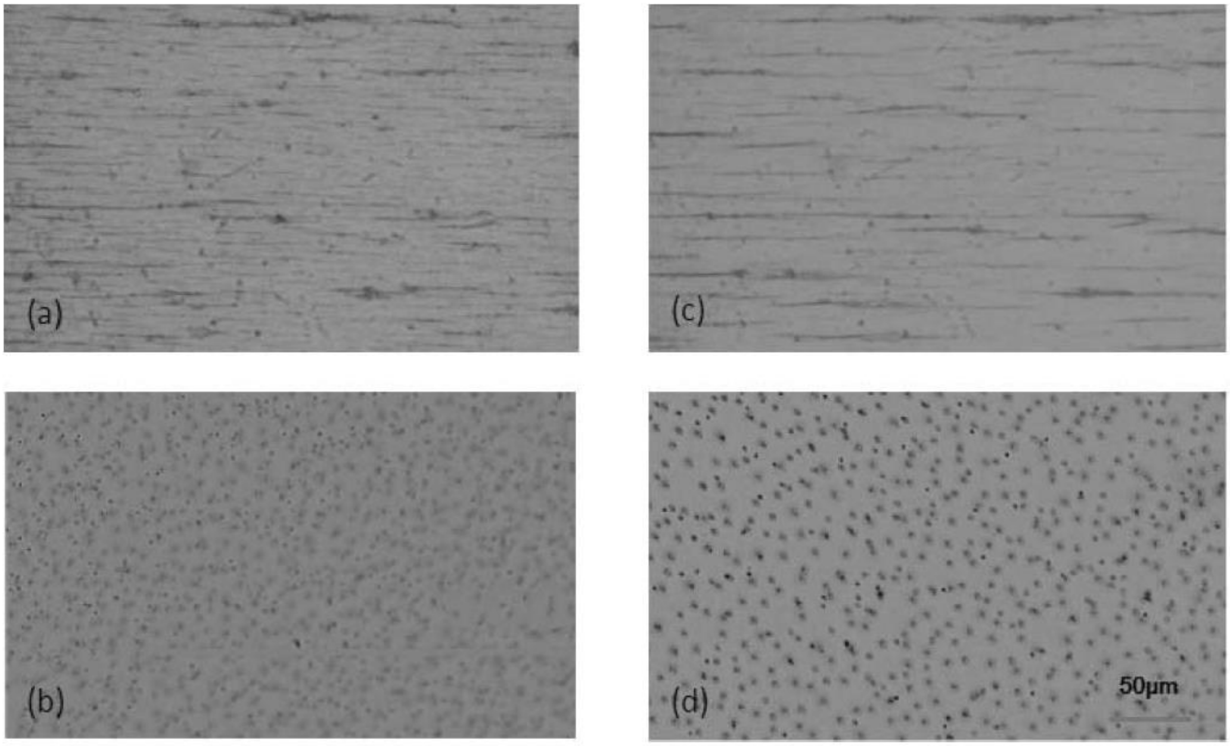

Figure 2-9: Optical microscope images of ferrofluids under a magnetic field. The direction of both the chains and the magnetic field were horizontal (a), (c) and normal (b), (d) to this picture. (a) In the beginning, many small chain structures of ferrofluids were formed. (c) In the stability state, the chain structure and the distance between two chains became larger [63].

Theoretical and experimental investigations were conducted to study the optical properties of ionic liquid-based nanofluids. Ionic liquid was used due to their beneficial thermophysical properties such as high boiling point, physical and chemical stability and low vapour pressure [62]. A double-beam UV–vis-NIR spectrophotometer (PerkinElmer Lambda950) using a differential measurement technique was used to determine the optical properties of the ionic based nanofluids. The results show that the transmittance of the ionic liquid-based decreases with the increase in the optical path length as shown in Figure 2-10a. The experimental and calculated extinction coefficients of Ion-based nanofluids are shown in Figure 2-10b. As illustrated in the graph the extinction coefficient of the ion based is very low in the visible-light range. All ion based nanofluids extinction coefficients are higher than the ion based fluid. The experimental extinction coefficients do not match well with the model predictions.

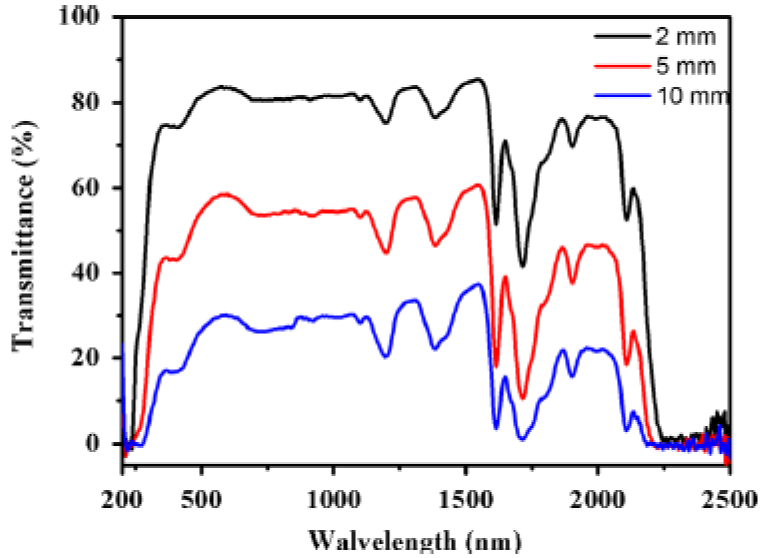

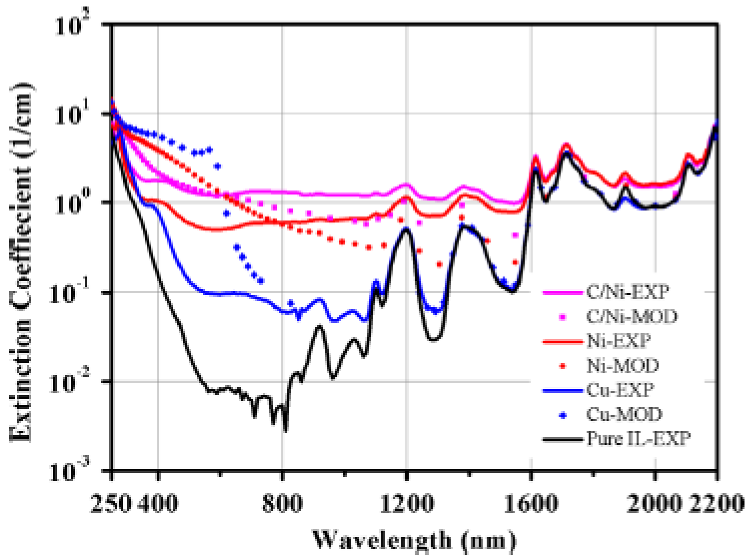

Figure 2-10: a) Room temperature transmission spectra of the ionic nanofluids containing 10 ppm of the Ni/C nanoparticles passing through different optical path lengths. b) Room temperature transmission spectra of the ionic nanofluids containing different kinds of nanoparticles with the same average sizes of ca.40nm at the same volume fraction of 10ppm [62].

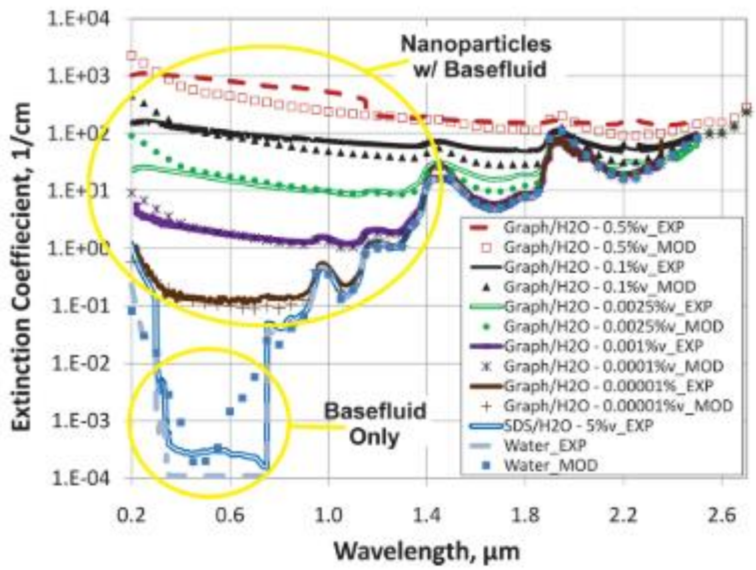

Figure 2-11: Modeled and experimental extinction coefficients for several concentrations of aqueous graphite nanofluids. [64].

2.1.3 Thermomagnetic convection

Studies on thermomagnetic convection of the ferrofluids in the presence of an external magnetic field have been carried out by many researchers. Table 2-2 shows a list of recent studies in this area. Compared to base fluid and in the absence of an external magnetic field, utilising ferrofluids as a heat transfer fluid in the presence of external magnetic field showed considerable improvement in heat transfer performances [65-67]. The convective heat transfer performance of Fe_3O_4 water-based ferrofluid with a particle diameter of 10 nm in a heated copper tube were experimentally investigated [65]. As shown in Figure 2-12 in the absence of magnetic field, the use of Fe_3O_4 magnetic nanofluids does not improve the heat transfer performance under the laminar flow conditions. In the other hand, in the presence of the external magnetic field, the enhancement of heat transfer performance is exceptionally significant and got affected by nanoparticle volume fraction. Due to the increase of the intensity of the magnetic field and ferrofluids volume fraction, a considerable enhancement in heat transfer could be recognised. The effect of an external magnetic field on the heat transfer performance and pressure drop of magnetic nanofluids in the laminar flow regime was examined [68]. Specifically, the effect of magnetic field intensity on the heat transfer coefficient was experimentally investigated. As shown in Figure 2-13, the results show a huge improvement in the local heat transfer coefficient can be reached by raising magnetic field intensity. The improvement of heat transfer can be four times higher than the case of the absence of magnetic field. At higher Reynolds number, the heat transfer enhancement becomes more evident. The pressure drop increases insignificantly in the presence of magnetic field. The aggregation of nanoparticles close to the heat flow which leads to higher thermal conductivity is the main reason that contributed to the enhancement of heat transfer.

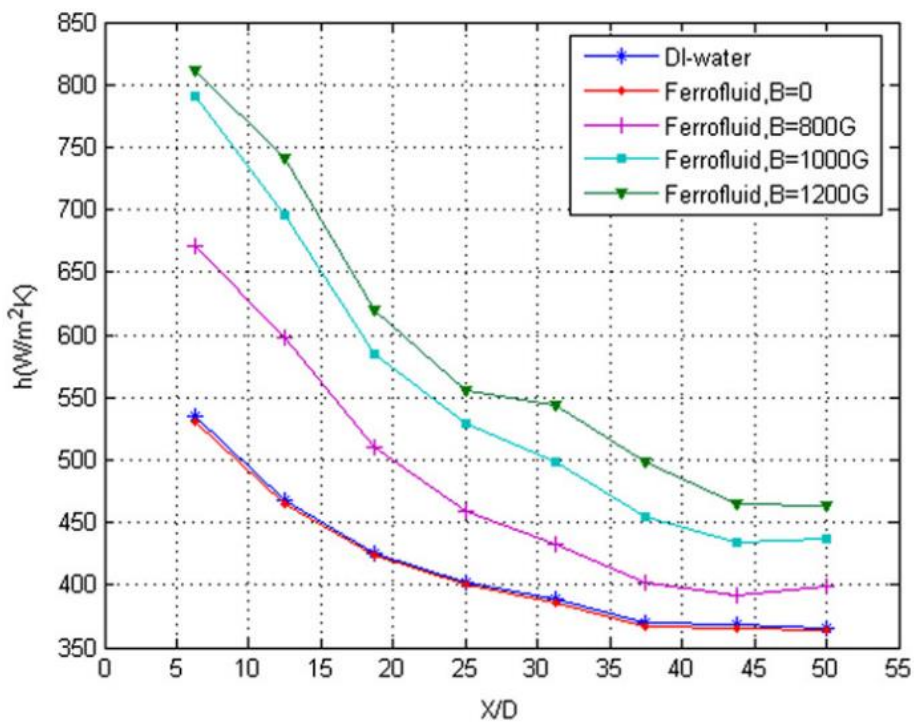

Figure 2-12: Axial profile of local heat transfer coefficient for the different magnetic field [65].

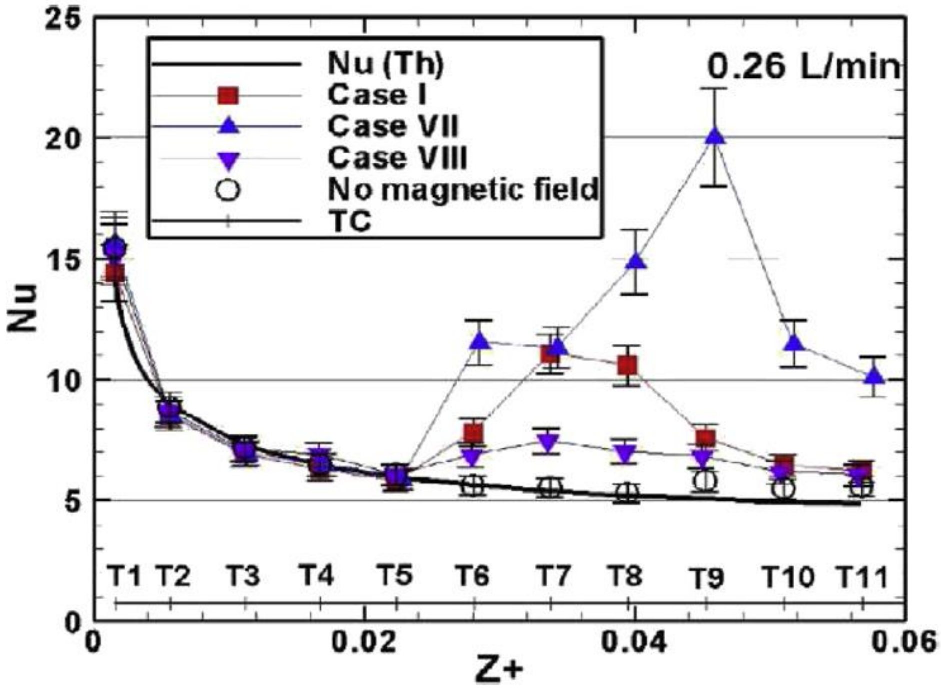

Figure 2-13: Nusselt number (Nu) vs. dimensionless distance (zþ) at three different locations and strength Case I, Case VII, and Case VIII [68].

Simulation of heat transfer process and flow of ferrofluids with both single and multiphase fluid models were developed. Many factors are considered in multiphase modelling due to their complex nature of each phase and their effect on the heat transfer. Those factors include friction between nanoparticles and the base fluid, dispersion, Brownian diffusion, and sedimentation. The impact of ferrofluids under the influence of external magnetic field on the natural convection heat transfer in a cavity using Lattice Boltzmann Method (LBM) were reported [69-72]. This issue is of significant interest when considering cooling of microelectronic devices, where forced convection is not feasible due to the complication related to pumping ferrofluids, and natural convection does not reach the cooling needed. The results determined from those LBM studies show good agreement compared to the experimental study performed by Calcagni et al. [71]. This shows that Lattice Boltzmann method is a suitable method to use for ferrofluids heat transfer and flow. The natural convection of a cavity filled with kerosene-based ferrofluids heated from bottom in the presence of an external magnetic field using LBM was numerically investigated [69]. The effects of magnetic coefficient, Rayleigh number, volume fraction, and heat source length on heat transfer performance were examined. The results showed that larger volume fraction and small particle size could transfer heat better and leads to enhancement in the temperature profile. The Nusselt number decreases with the increase of the particle size but increases with the increase of heat source length and Rayleigh number. In another study, the effect of kerosene-based magnetic nanofluids on free convection flow in a sloped cavity in the presence of an external magnetic field using LBM were analysed [70]. The study studied the impact of the inclined angle, Rayleigh number, and volume fraction. The results showed a reduction in heat transfer performance with increasing the concentration of nanoparticles. The heat transfer performance improved when Rayleigh number increased. The heat transfer performance in a distinctively heated cavity with an extremely long third dimension was numerically simulated utilising the single relaxation time lattice Boltzmann method (LBM) [73]. At the bottom of the cavity, a dipole was placed to generate a magnetic field. The modelling for thermomagnetic convection were determined for a range of magnetic field intensity and Rayleigh numbers under the laminar conditions. The impact of these factors on the heat transfer performance was analysed; the simulation results showed that in the presence of an external magnetic field, the velocity and temperature fields were reasonably altered. Even at low magnetic field intensities, both magnetic force and buoyancy force have an impact on the heat transfer performance. However, at adequately high magnetic field intensities, the heat transfer performance was reduced for all tested Rayleigh numbers. This study shows that even for relatively low magnetic field intensities, the enhancement in heat transfer for heat transfer devices is considerable. The heat transfer performance can be controlled by tuning an external magnetic field, and ferrofluids show great potential for heat transfer applications.

Table 2-2: List of recent studies on thermomagnetic convection.

Author	Features	Comment
Thermomagnetic free convection		
Sheikholeslami & Bandpy [69]	Numerical Analysis using Lattice Boltzmann method to investigate free convection of ferrofluid in a cavity heated from below in the presence of external magnetic field	Results show that particles with a smaller size have better ability to dissipate heat, and a larger volume fraction would provide a stronger driving force which leads to increase in the temperature profile.
Kefayati [70]	Heat dissipation effect of a ferrofluid on natural convection flow in a cavity at the presence of an external magnetic source has been analysed with Lattice Boltzmann method (LBM).	Indicates that the Nusselt number increases with the increase of the Rayleigh number and heat source length, but it decreases with the increase of the size of the nanoparticle.
Nemati et al. [72]	Experimental study on thermo-magnetic convection inside cavities. They examine the flow induced by convective currents inside a cavity with aspect ratio near the unity and the heat transfer rates measurements.	The experiments reveal that magnetic field enhances the instability in the convective flow leading to a more effective mixing and consequently to a more statistically homogeneous temperature distribution inside the test cell.
Hadavand & Sousa [73]	Simulations for thermomagnetic convection were conducted for a range of Rayleigh numbers and magnetic field strengths in the laminar regime.	This study shows that even for relatively weak magnetic fields, the increase in heat transfer for small-scale devices is considerable.

Author	Features	Comment
Thermomagnetic forced convection		
Lajvardi et al. [65]	Experimental investigation of thermomagnetic convection of ferrofluid flowing throw heated copper tube in the laminar regime	Significant enhancement of heat transfer observed under the presence of magnetic field. The enhancement is attributed to the ferrofluid thermo-physical properties.
Goharkhah & Ashjaee [66]	Forced convective heat transfer of water-based Fe_3O_4 nanofluids (ferrofluid) in the presence of an alternating non-uniform magnetic field is investigated numerically. The geometry is a two-dimensional channel which is subjected to a uniform heat flux at the top and bottom surfaces. The non uniform magnetic field produced by eight-line source dipoles is imposed on several parts of the channel.	A maximum of 13.9% enhancement in heat transfer has been obtained at Re = 2000 and frequency of 20 Hz. The alternating magnetic field causes the increase of the pressure drop up to a maximum of 6% at Re =2000 and frequency of 5 Hz. However, it is not as significant as the heat transfer enhancement.
Azizian et al. [68]	Experimental Investigation on Convective heat transfer coefficient of magnetite nanofluids in laminar flow regime was investigated under applied external magnetic field	It was demonstrated that the local heat transfer coefficient of magnetite nanofluids could be increased significantly (up to 300%) when a magnetic field was applied. The observed enhancements were found to be a function of flow rate (Re number), magnetic field strength and gradient.
Aminfar et al. [74]	3D numerical investigation of mixed convection in a tube using two-phase model. Positive and negative magnetic field gradients have been examined.	Negative gradient enhances the Nusselt number, while the positive gradient decreases it.

Author	Features	Comment
Bahiraei & Hangi [67]	The two-phase model used to examine the effect of magnetic field on the performance of counter-flow double-pipe heat exchanger using ferrofluid as heat transfer medium.	Significant enhancement of heat transfer under the presence of magnetic field. The magnetic field enhanced the heat transfer and increased the pressure drop. The enhancement of heat transfer is more considerable in low Reynolds number.
Aminfar et al. [75]	Investigated numerically the hydro-thermal features of ferrofluid flowing in a vertical rectangular duct under the influence of non-uniform transverse magnetic field resulting from a current of wire.	The increase of Nusslet number is considerable in all length along the duct, and the Reynolds number have more effect than an axial magnetic field. The average heat transfer coefficient enhancement is 22%
Shahsavar et al. [76]	Experimental study on the effect of magnetic field of hybrid nanofluid on laminar forced convective heat transfer.	Application of a magnetic field led to an improved convective heat transfer. Effect of a constant field on the heat transfer was higher than that of an alternating field.
Sadeghinezhad et.al [77]	Hybrid magnetite nanofluids under forced laminar flow were experimentally investigated.	A maximum enchantment of 82% in the convective heat transfer coefficient.
Sheikholeslami et al. [78]	Investigated numerically the ferrohydrodynamic features of ferrofluid flowing in a semi-annulus lid under the influence of magnetic field. Control Volume based Finite Element Method (CVFEM) was used to solve the equations.	Thermal boundary layer thickness decreases with an increase the Kelvin forces. Heat transfer enhancement has a direct relationship with the Reynolds number and the magnetic number.

2.1.4 Applications

A wide range of applications is using ferrofluids including hydraulic damping, dynamic sealing, heat transfer applications, biomedical technology and doping materials [79]. Improving the efficiency of conventional energy equipment, thermal conduction based on smart cooling, and thermomagnetic convection are recent interests on ferrofluids application. The efficiency of a parallel duct-type energy conversion device in the presence of nonuniform magnetic field was investigated [80]. A numerical model for the prediction of heat transfer and flow of the energy conversion device developed based on the thermomagnetic effect was examined [81]. Small-scale cooling devices like microscale electronic devices can benefit from the great potential of thermomagnetic cooling [82]. The ferrofluids used for heat transfer application should maintain a low Curie point, a high paramagnetic coefficient, higher boiling point, a lower viscosity and a high saturation magnetization, moreover, the magnetic field orientation should be applied in parallel to the flow direction and heat direction. A design based on thermomagnetic convection for a liquid cooling device with a permanent magnet placed close to the heat source was experimentally investigated [83]. Better cooling performance and balanced start-up procedure were observed.

2.1.5 Conclusion

This section overviewed recent work on thermophysical and optical properties and thermomagnetic convection of ferrofluids. The impact of thermomagnetic effect on heat transfer performance was the focus of recent studies, however, few researchers studied the heat transfer through the improvement of thermal conductivity. Enhancing the heat transfer performance by utilising ferrofluids has evident potential. Still, more studies and investigations are needed to use ferrofluids in heat transfer applications. Those studies are needed to fully understand the mechanism behind the heat transfer enhancement. To form an optimal design of heat transfer device that utilises ferrofluids, a comprehensive study of the mechanism and physical phenomena are required.

Many papers studying the application of ferrofluids in heat transfer fluid did not concentrate on the preparation of ferrofluids. Ferrofluids mainly prepared using co-precipitation method and researchers focused more on the nature of the base fluid and magnetic nanoparticles. Future work on the preparation of ferrofluids should concentrate on preparing ferrofluids with very high stability and it should create chain-like structures in the presence of low magnetic field intensity. Moreover, further work to study the impact of the surfactant is required. Magnetic properties of ferrofluids such as magnetization, chain length, and susceptibility are affected by the concentration and thickness of surfactant. Forthcoming works should focus on understanding the diffusion of magnetic nanoparticles in the presence of magnetic field.

There are many contradicting reports on the improvement of thermal conductivity despite the significant amount of work about thermo-physical properties. This is due to the unsatisfactory description of ferrofluids and errors in the measurement techniques. Many works did not fully characterise the type of ferrofluids used in their study (surfactant thickness, particle distribution, etc.). Huge errors could occur due to small temperature gradient during thermal conductivity measurement.

A few papers have shown that increasing nanoparticles volume fraction enhances the thermal conductivity in the absence of an external magnetic field. The examination of the impact of other factors is needed (such as temperature, surfactant layer, etc.) The notable improvement of thermal conductivity of ferrofluids in the presence of external magnetic field is attributed to the chain-like structure. The improvement is acceptable when the magnetic field gradient is parallel with the temperature gradient. Forthcoming studies should focus on modifying and understanding the chain-like structure behaviour in various magnetic field intensity, surfactant concentration and thickness and their impact on the effective thermal conductivity. Additionally, recent thermal conductivity model based on aggregation should consider the hydrodynamic particle size (nanoparticle and surfactant). The viscosity o high concentrated ferrofluids are mostly reported in the literature due to their use in sealing and damping. Future studies should include the viscosity of low volume fraction ferrofluids and their behaviour under different shear rates. The magneto-viscous impact on heat transfer performance should be examined and linked to thermal conductivity enhancement. Much attention was raised for the thermomagnetic convection, and the result of thermomagnetic convection simulation was raised in the literature. Future studies should include experimental validation of the existing models.

2.2 Nanofluid-based solar collector

In recent years, solar thermal energy has shown exceptional growth integrating many new technologies into new operations [84]. Researchers are encouraged to find alternative sources of energy due to the lack of fossil fuels along with environmental consideration. One year of the world energy consumption is less than the energy received by the earth in less than an hour. Most small equipment for individual use just a few kilowatts of energy. Therefore, the application of solar energy is financially feasible [84, 85]. The employment of solar energy to a wide range of applications to supply a substantial solution is important. This can be carried on through enhancing energy stability, the alteration of the energy proportion, improving system efficiency, and increasing energy sustainability [86].

The application of nanofluids in solar energy generally is relevant to their utilization in solar collectors. Researchers investigated the impact of nanofluids on the efficiency enhancement of solar collectors along with their economic and environmental effect when used in solar collectors. The solar collector can be defined as a type of heat exchanger that convert solar radiation energy into heat energy carried out by the heat transfer medium. The solar collector absorbs the arriving solar irradiance, convert into heat, and transfer the heat to a heat transfer fluid (commonly water, oil, or air) passing through the device. The heat transfer fluid carries the collected energy to water heating system, space conditioning system, industrial heat processes, or to a thermal energy storage tank that can save the energy to be used on cloudy days or at night [87]. The efficiency of the solar collector is determined by the following equation: -

$$\eta = \frac{Useful\ Gain}{Available\ Energy} = \frac{\dot{Q}_{abs}}{\dot{Q}} = \frac{\dot{m}C_p(T_{out}-T_{in})}{A_c\, I_D} \qquad \text{Eq. 2-1}$$

where $\dot{Q}_{abs}$ is the rate of solar energy absorbed by the heat transfer fluid; $\dot{Q}$ is the total energy coming from the sun, which is intercepted by the solar collector; $\dot{m}$ is the mass flow rate of the fluid passing through the solar collector; C_p is the specific heat capacity; T_{in} and T_{out} are the mean fluid inlet and the outlet temperatures, respectively. A_c is the cover area of the collector, and I_D is the solar intensity of the sun.

Using nanofluids in solar thermal energy collectors have several advantages. First, the enhancement of the efficiency can be observed with very low concentration of nanoparticles. Second, the nanoparticles could be efficient absorber due to their exceptional optical properties [88]. Moreover, the Nano-sized particles allow them to flow through common pumps and plumbing [89]. Additionally, the significant improvement in a wide range of optical, and thermal properties of the nanofluids properties. However, very well-designed collectors are needed to benefit from these advantages. Also, the thermal improvement must be balanced with the economic impact and complexity linked to manufacturing nanofluids. Studies have shown the possibility to make significant efficiency enhancement in solar collectors with nanofluids as heat transfer medium. The previous works on the utilisation of nanofluids in solar collectors are summarized in Table 2-3.

2.2.1 Non-direct absorption nanofluids collectors

Replacing the working fluid of solar collectors with nanofluids is an effective method to increase the efficiency. In the past few years, researchers focused on increasing the thermal efficiency by applying nanofluids on flat-plate solar collectors [90-97]. Yousefi et al. [96] conducted an experimental study on the influence of Al_2O_3 based nanofluid shown an increase of 28.3% efficiency of the flat-plate collector with 0.2 wt% (wt% weight fractions) compared to water. The experimental setup is shown in Figure 2-14. Two weight fractions were examined 0.2% and 0.4%, where the diameter of particles was 15 nm. As shown in Figure 2-15, the solar collector efficiency with 0.2 wt% is larger than 0.4 wt% ferrofluids for a various range of reduced temperature parameter. The effect of surfactant (Triton X-100) on the efficiency was studied. The surfactant causes a 15.63% increase of the efficiency. The influence of MWCNT nanofluids on the performance of the flat plate collector by using the same experimental setup in the previous study was investigated [95]. The effects of multi-wall carbon nanotubes nanofluids on the efficiency of the flat plate collector was investigated. The results showed that using 0.4 wt% MWCNT nanofluids without surfactant enhanced the efficiency of the collector, while with 0.2 wt% the efficiency decreases compared to water as a heat transfer fluid. By using a surfactant, the collector efficiency of 0.2 wt% nanofluids is higher compared to water. Moreover, Yousefi et al. [95] examined the impact of PH of the 0.2 wt% MWCNT nanofluid on the performance of the flat plate collector. pH values of 3.5, 6.5 and 9.5 and Trito X-100 was used as an additive. They found that higher efficiency can be achieved when the difference between the pH of nanofluids and pH of the isoelectric point is bigger. The isoelectric point is defined as the point at which a particular molecule carries no electric charge. The pH for MWCNT of the isoelectric point is 7.5.

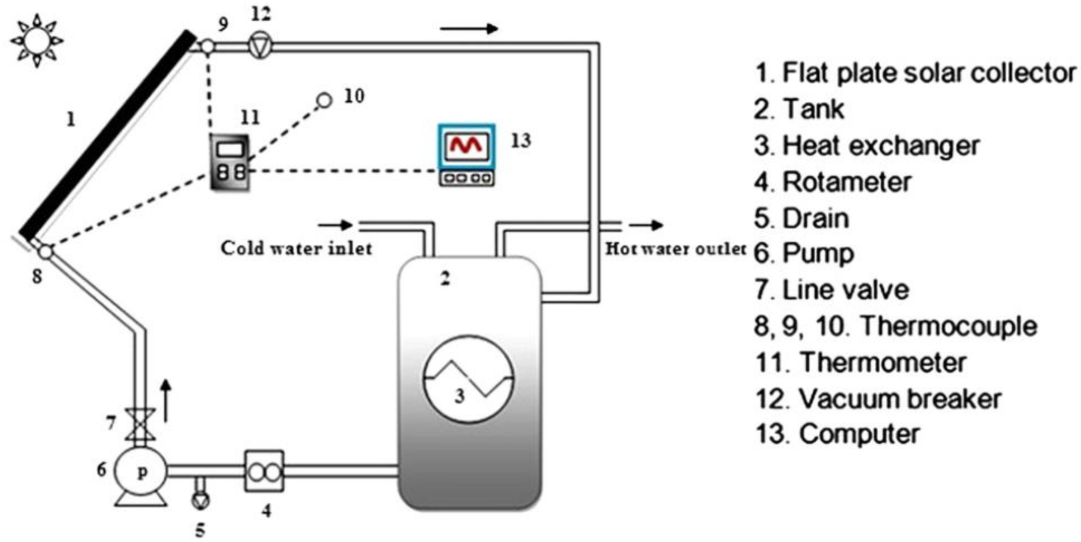

Figure 2-14: The experimental setup used by Yousefi et al. [96].

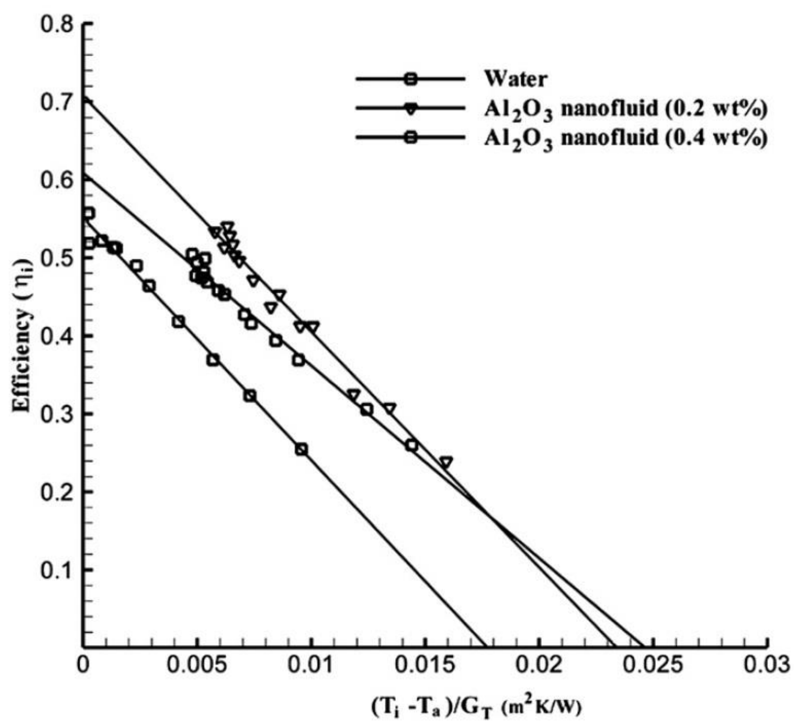

Figure 2-15: The performance of solar collectors for water and Al_2O_3 nanofluids without surfactant [96].

Thermal performance analysis using various nanofluids as a heat transfer medium in a flat plate solar collector was carried on. The performance was investigated by using the second law of thermodynamics [94]. Oxide nanofluids and singled wall carbon nanotube (SWCNT) nanofluids performance in the solar collector was compared to each other. Furthermore, the pressure drops and pumping power were numerically investigated using thermo-physical properties obtained from the experimental measurement. The results show that the performance of solar collectors can be enhanced by using nanofluids as heat transfer medium. As shown in Figure 2-16 SWNCT nanofluids have greater heat transfer enhancement 15.33 % and lower entropy generation compared to the other oxide nanofluids. The entropy generation was calculated using Eq. 2-2. Higher heat transfer can be achieved with the higher volume fraction of nanoparticles dispersed in a fluid.

$$\dot{S}_{gen} = \dot{m}C_p ln\frac{T_{out}}{T_{in}} - \frac{I_D}{T_{sun}} + \frac{\dot{Q}_L}{T_a} \qquad \text{Eq. 2-2}$$

where $\dot{S}_{gen}$ is the entropy generated; $T_{sun}$is the sun temperature; $Q_L$is the heat loss; and $T_a$is the ambient temperature. As shown in Figure 2-17 the effect of various volume fractions and various flow rate of few nanofluids on the pressure drop and pumping power was observed. It was observed the change between nanofluids and base fluids is very small and negligible.

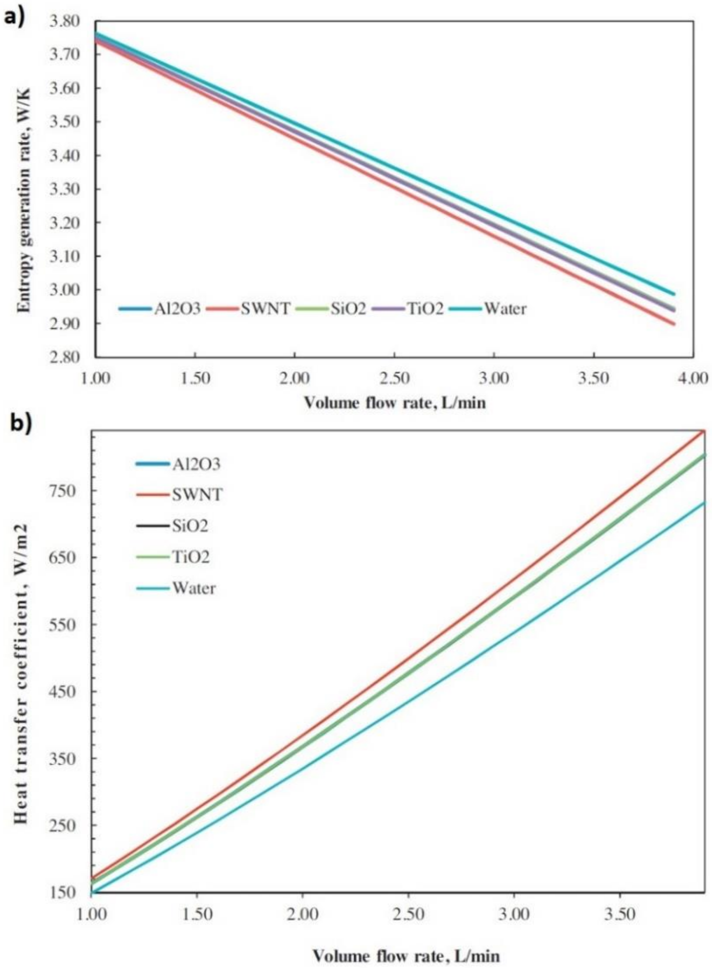

Figure 2-16: Effect of volume flow rate on a) entropy generation b) heat transfer coefficient [94].

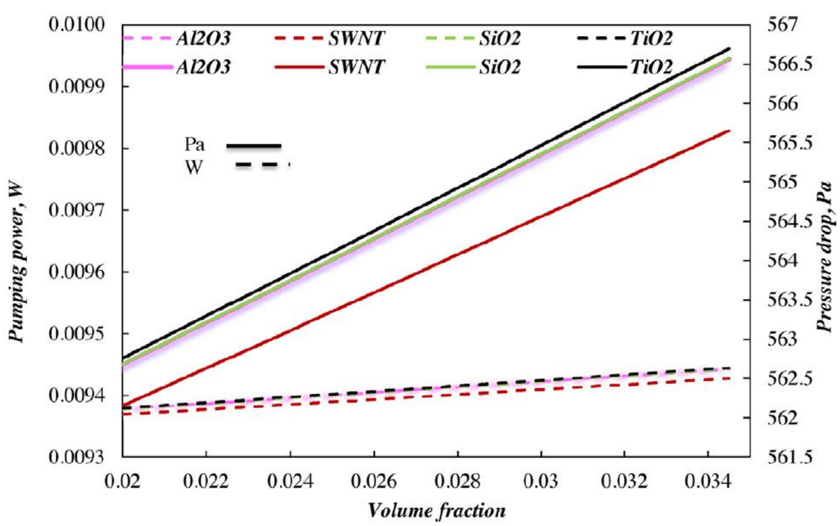

Figure 2-17: Effect of volume fraction on pumping power [94].

An experimental investigation conducted to study the influence of Cu nanoparticle on the performance of a flat plate solar collector [97]. The copper nanofluids were prepared using one-step method, which gives an average particle size of 10 nm. The experiments were conducted with weight fractions of 0.2% and 0.3% and volume flow rate from 0.15 L/min to 1.5 L/min. The standard ASHRAE 93 was used to analyse the performance of the flat plate solar collector. The results showed improvement in the thermal efficiency of the collector via increasing the nanoparticles concentration. The nanofluid increased the absorbed energy parameter of the solar collector compared to base fluid. The optimal operating point for the efficiency of a solar collector could be achieved for 0.3 wt% Cu/EG nanofluids at 1.5 Lit/min.

Another experimental study was performed to investigate the thermal efficiency of helical pipe solar collector using water-based Cu nanofluids as a heat transfer fluid [91]. The experiment setup is shown in Figure 2-18. The effect of flow rate, nanoparticles concentration, and surfactant on the efficiency was considered. Compared to water the maximum thermal efficiency of the solar collector increased to 25.6% through the use of 0.1wt% CuO nanofluids and 0.0083 kg/s. The results show an increase in thermal efficiency by increasing the nanoparticles concentration from 0.1 wt% to 0.2wt%. However, with increasing the nanoparticles concentration further to 0.4wt%, the efficiency decreased. As shown in Figure 2-19 The efficiency enhanced by increasing the flow rate of nanofluids for low temperature ranges. In the other hand, the efficiency decreased by increasing the mass flow for higher reduced temperature differences. This can be explained that the thermal conductivity improvement has a substantial reliance on the bulk temperature of the nanofluids. In addition, by using a surfactant, the stability of CuO particles in the nanofluid was about one day which was higher than the previous case. The highest enhancement in the efficiency for nanofluids with surfactant was 24.2%. This is due to the increase of nanoparticles stability by adding a surfactant.

The efficiency of mini-channel based solar collector utilising four different nanofluids was theoretically investigated [92]. The four different nanofluids are Cu/water, Al_2O_3/water, TiO_2/water, and SiO_2/water. A constant mass flow rate of nanofluids was conducted for the analysis of first and second laws of thermodynamics. The characteristics of nanofluids are up to 4% volume fractions, and 25 nm nanoparticle size, where the inner diameter of the flat plate collector tube is estimated to be 2 mm. The results of the first law of thermodynamics showed that Al_2O_3/water nanofluids had the largest heat transfer coefficient whereas the lowest value recorded was for SiO_2/water nanofluids. Cu/water nanofluids generated the maximum outlet temperature, and after that TiO_2/water, Al_2O_3/water, and SiO_2/ water nanofluids respectively. Analysis of the second law showed that Cu/ water nanofluid generated the minimum entropy generation compared to other nanofluids. It is concluded that despite the effective thermal conductivity of Al_2O_3/water nanofluids is higher than TiO_2/water nanofluids, the entropy generation of Al_2O_3/water is higher than TiO_2/water nanofluids. This research displayed that the density and heat capacity control the change of the parameters when the mass flow rate is constant, opposite to most of the studies that suggested that the thermal conductivity and viscosity are the governing properties. The use of nanofluids in parabolic trough collector was also considered [98]. A new shape of the reflector was developed with four kinds of receivers were studied. 0.2% and 0.3% carbon nanotube with oil as a base fluid was prepared. The results showed an increase in the efficiency about 5-7% compared to pure oil. Colangelo et al. [99] experimentally investigated the effect of sedimentation on conventional flat plate collector and modified one. The modified solar collector has tapered lower and top header to keep the fluid axial velocity constant. The modification of collector enabled a negligible deposit. The results of using water-Al_2O_3 nanofluids in the modified collector showed an enhancement up to 25%.

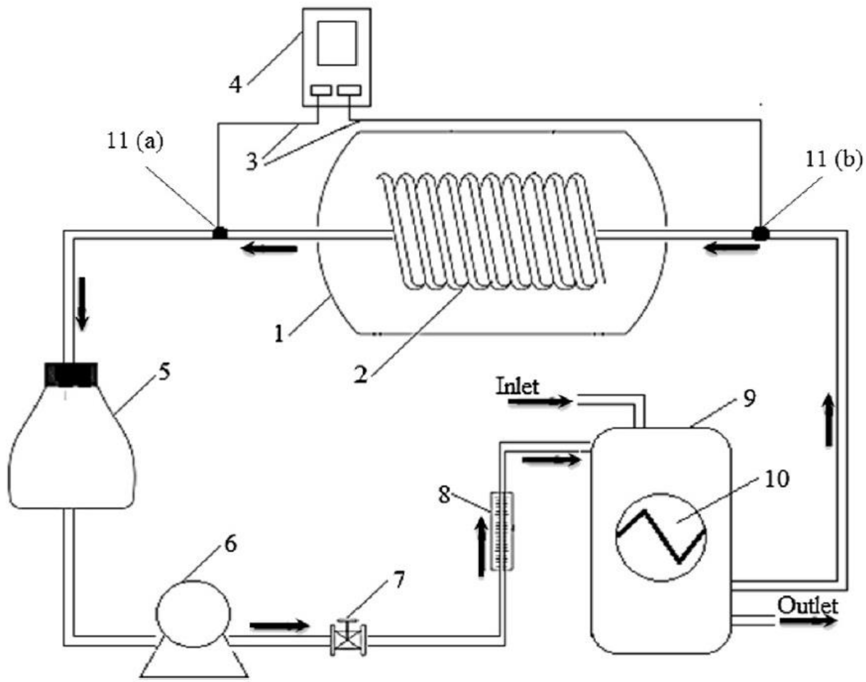

Figure 2-18: Schematic of the experimental device. (1) Cylindrical glass, (2) copper coil, (3) thermocouple wires, (4) data logger, (5) water supply and drainer, (6) pump, (7) line valve, (8) rotameter, (9) reservoir tank, (10) heat exchanger, and (11a) and (11b) thermocouples (C 5).

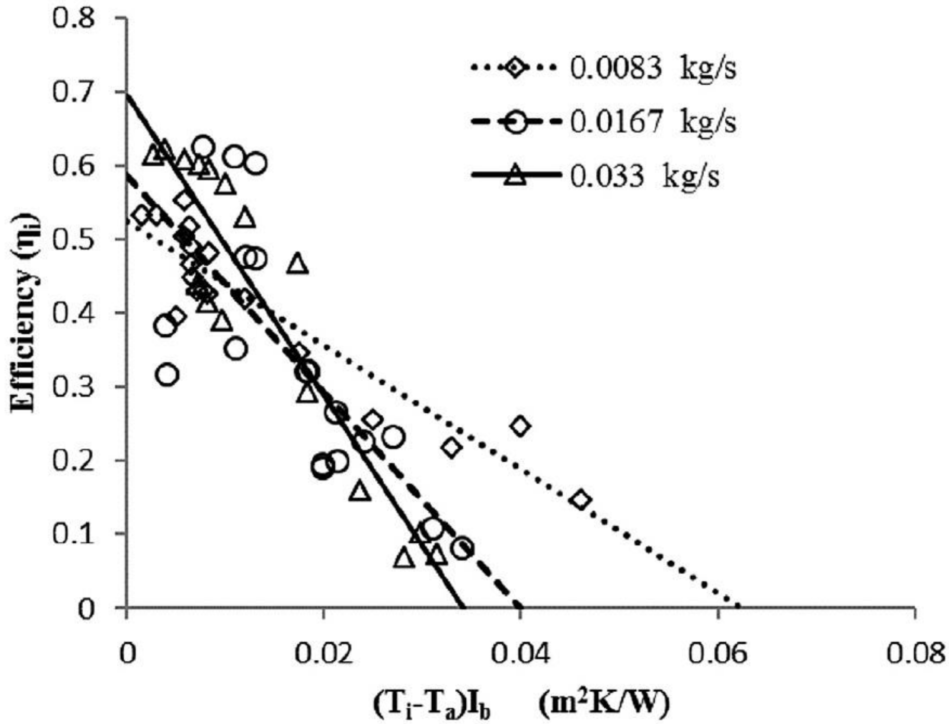

Figure 2-19: The efficiency of the solar collector with various mass flow rates of nanofluids [91].

Few studies investigated the economic and environmental effect of using nanofluids in flat plate collectors [90, 93]. Life cycle assessment was used to investigate the economic and environmental effects of nanofluid-based solar collector and compare it to common flat plate solar collector[93]. The economic analysis shows that the nanofluid based solar collector has higher capital and maintenance costs $120 and $20 respectively compared to conventional one. However, the fuel cost saving per year of the nano-based solar collector, for both natural gas and electricity, is higher than that of the common solar collector. The reason for this is the higher performance of nanofluid-based solar collectors. Furthermore, in the case of the nanofluid-based solar collector, the payback period is longer than common solar collector due to the higher cost of nanofluids compared to common. However, the nanofluid based solar collector has the same life cycle saving as a common collector at the end of its useful life. The embodied energy for the nanofluid based collectors are 9% lower than the embodied energy of common solar collector. Compared to common solar collectors, 34 kg less CO_2 emissions is achieved by manufacturing the nanofluid-based solar collector, and it saves 50 kg year during its operation. The values of other emissions such as SOx and NOx are very little, so the variations are not significant. Over the expected time of solar collector which is 15 years, 740 kg of CO_2 can be saved by using nanofluids based solar collectors instead of common solar collectors. The study concluded that more than one million metric tons of CO_2 could be compensated per year if the nanofluid-based solar collector is utilised. A similar study used numerical methods and data from the literature to calculate efficiency, size reduction, cost and embodied energy savings of nanofluids based solar collector for various nanofluids [90]. The possibility of reduction of the solar collector size by utilising various nanofluids is shown in Figure 2-20. Compared to water; solar collector's area can be decreased up to 25.6%, 21.6%, 22.1% and 21.5% for CuO, SiO_2, TiO_2, and Al_2O_3 respectively. The average saved embodied the energy of nanofluids based solar collectors is 220 MJ. The payback average of nanofluids based solar collectors is 2.4 years compared to 2.49 years for conventional one. The average CO_2 emissions from the nanofluids based solar collector are 170 kg less than a conventional collector.

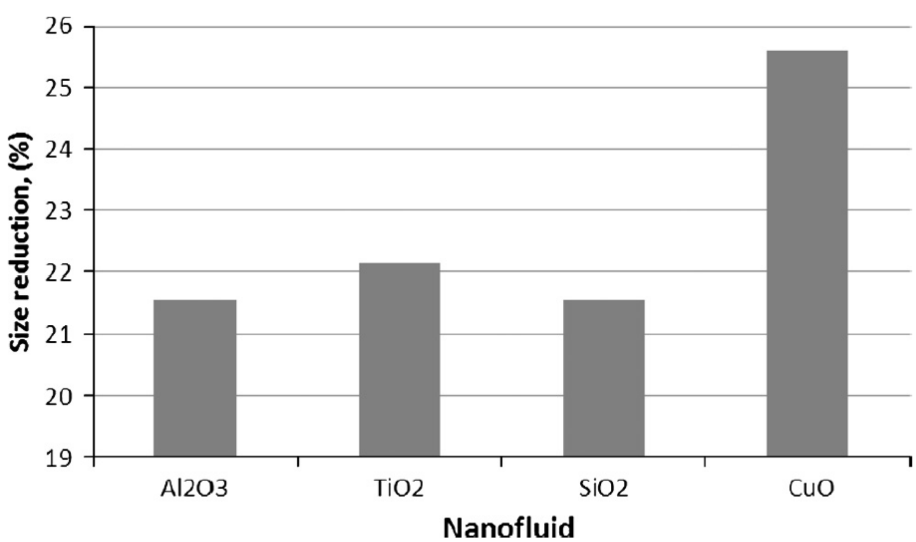

Figure 2-20: Percentage of size reduction for the solar collector by applying different nanofluids [90].

2.2.2 Direct absorption collectors

Nanofluids have shown potential to make significant direct absorption collector. Direct Solar absorption collector using small particles has been investigated since the late 70s [100]. As discussed previously, unlike common heat transfer fluids for solar collector applications, nanofluids have high optical properties, they absorb and scatter adequately the solar radiation going through it [58, 88]. Therefore, an innovative non-concentrating type solar collector using nanofluids as the heat transfer fluid has been proposed by few types of research [101-103]. The high optical property of nanofluids reveal that it may be beneficial to provide a solar collector design which could decrease the number of energy transfer stages as shown in Figure 2-21, and thus reduce losses in converting solar energy to heat energy. In the common solar collector absorber, the solar irradiance is first absorbed by the absorber tube and then transferred to the heat transfer fluid by conduction and convection heat transfer. The heat transfer fluid does not directly contact the approaching solar irradiance. In the other hand, in the case of direct absorption collector, the heat transfer fluid can interact with the approaching solar irradiance immediately, and accordingly, volumetric energy absorption occurs through absorption and scattering process. This develops more efficient heat transfer and better uniform energy distribution inside the heat transfer fluid.

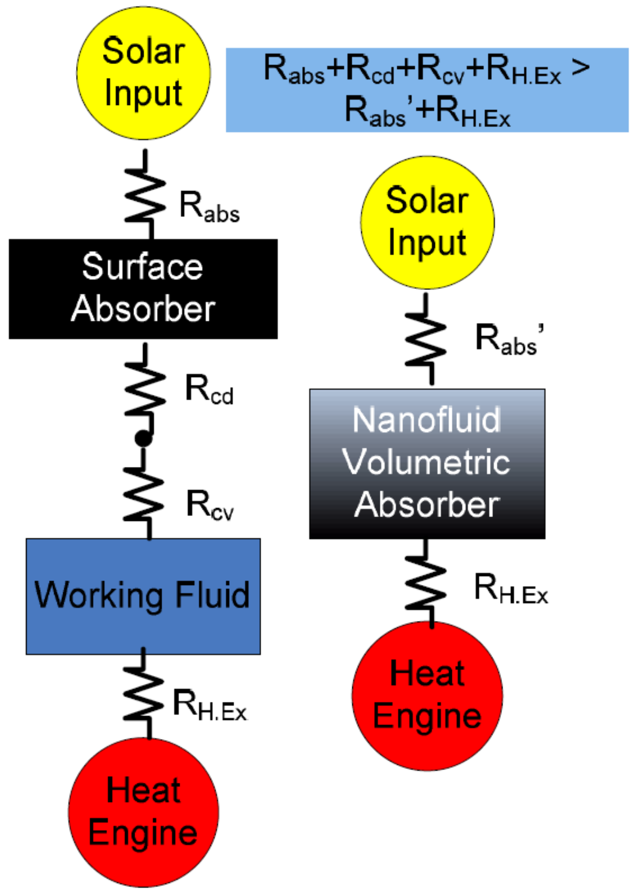

Figure 2-21: Thermal resistance network - comparison between a conventional solar thermal plant and a nanofluid solar thermal plant. R_{abs}, R_{cd}, R_{cv}, $R_{H.Ex}$, and $R_{abs'}$ refer to the thermal resistance present during the solar solid surface absorption, conduction, convection, fluid to fluid heat exchange and volumetric solar absorption heat transfer steps, respectively [103].

Hunt [104] explained how a dispersion of small absorbing particles creates an ideal medium to collect radiant energy, transform it into heat, and effectively transfer the heat to the surrounding fluid. Furthermore, he explained how the particles could be used to heat a compressed gas in an engine using a Brayton cycle. Abdelrahman et al.[100] investigated suspensions of solid particles for direct absorption concentrated radiation. The results showed the dependence of absorption on the size of the particle and the imaginary part of the complex index of refraction of the particle. A detailed mathematical model of coupled radiative and convective transfer in an emitting, absorbing, and scattering falling film has been presented by Kumar and Tien [105]. The model was evaluated for a solar receiver with nitrate salt, as the base fluid, and cobalt oxide particles. The results showed the possibility of absorbing the entire incident flux and reaching high film temperature by increasing the film width, particles diameter, and the particle volume fraction. Lenert and Wang [106] presented the experimental and numerical study to optimize the performance of volumetric solar receiver with thermal oil-based nanofluids. The effect of receiver height, solar concentration and optical thickness on the efficiency was investigated by developing one-dimensional heat transfer model. The results showed that increasing the solar concentration and the receiver height improved the efficiency of the solar collector.

Theoretical investigation on the impacts of various parameters on the performance of low-temperature nanofluids based direct absorption solar collector [102]. The nanofluids consist of aluminium nanoparticles and water. A schematic of the direct absorption collector is shown in figure 2-22. Glass covers the top side of this absorber whereas the bottom side is properly insulated. The volume fraction of nanoparticles was between 0.1% and 5%. As shown in Figure 2-23 the results showed that the performance of the collector remarkably increased by adding a small amount of nanoparticles to the heat transfer fluid. The increase in the performance was associated with the increase in debilitation of solar irradiance passing through the collector due to the nanoparticles suspended in the fluid which absorb the solar irradiance and leads to increase in the performance of the collector. Moreover, it was observed that no change in the performance at nanoparticles concentration higher than 2% volume fraction.

Experimental and numerical investigation on the influence of diverse nanofluids (silver, graphite, and carbon nanotubes) on the efficiency of a microscale direct absorption solar collector was conducted [101]. The results were compared to a common solar collector system where the solar irradiance is absorbed by a selective surface. As shown in Figure 2-24, the addition of a small number of nanoparticles (up to approximately 0.5% volume fraction) induces the extraordinary improvement of the performance. A concentration higher than 0.5% volume fraction, the efficiency of the collector starts to decline. The authors explained this decline to the location of solar absorption inside the nanofluid. At higher volume fraction, the absorption occurs near to the surface similar to common collectors.

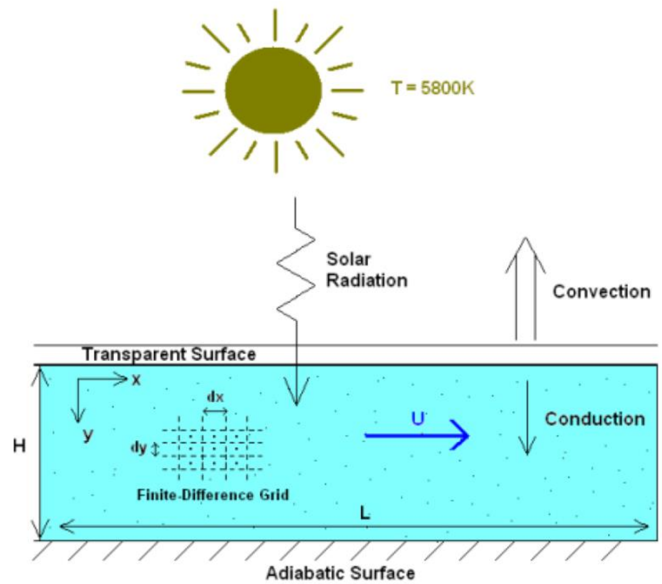

Figure 2-22: Schematic of the nanofluid-based direct absorption solar collector (DAC) [102].

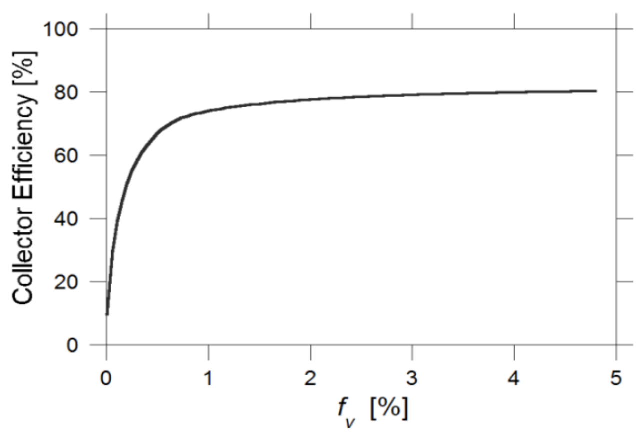

Figure 2-23: Impact of nanoparticle volume fraction on solar collector efficiency [102].

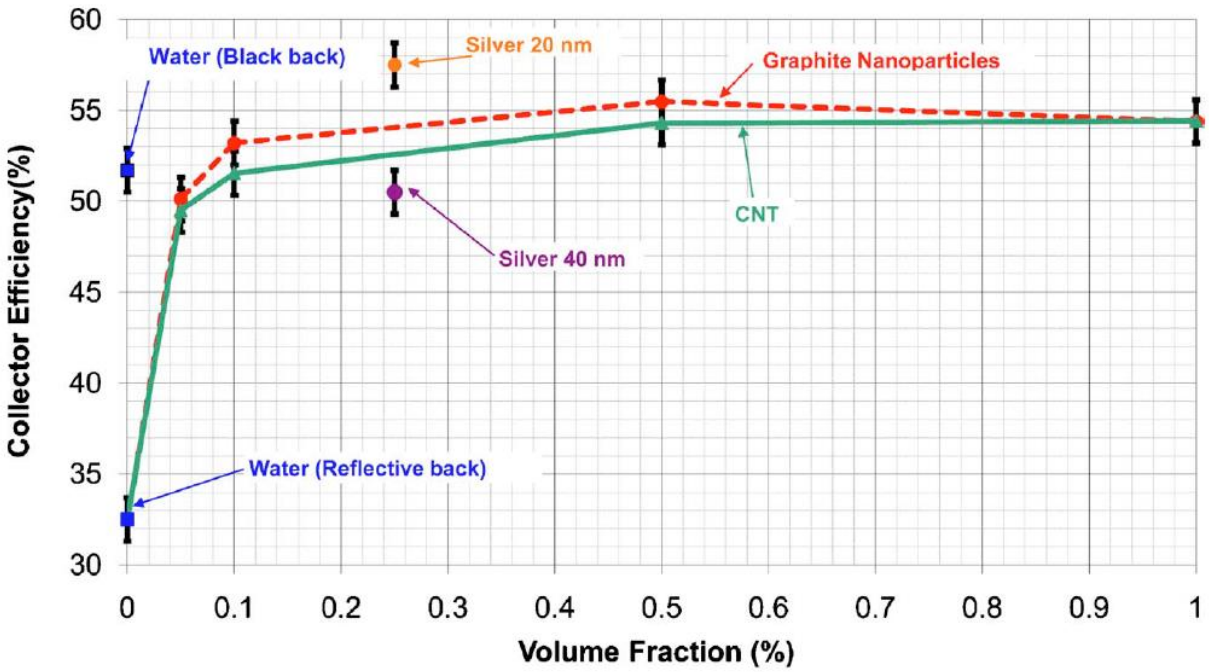

Figure 2-24: Steady-state collector efficiency of Experimental micro solar thermal collector testing results [101].

As shown in Figure 2-25 Khullar et al. [107] introduced the idea of using nanofluids in transparent concentrating parabolic solar collectors. The numerical model was compared to conventional concentrating parabolic trough. The heat transfer in the nanofluids has been assumed as coupled radiative and conduction heat transfer in scattering, emitting and absorbing fluid. They also investigated a nanofluid-based concentrating parabolic solar collector theoretically and compared the results determined with the experimental results of common concentrating parabolic solar collectors working under the same conditions [108]. Aluminium nanoparticles with 0.05% volume fraction suspended in Therminol VP-1 as the base fluid for the investigation were used. Figure 2-26 shows the computed collector efficiencies as a function of normalized fluid inlet temperatures for the nanofluids based solar collector and conventional flat plate collectors. This clearly indicates that the proposed water heating system has relatively better performance characteristics as compared to the conventional flat plate collectors. De Risi et al. [59] numerically examined the utilization of gas-phase nanofluids in direct absorption parabolic trough collector. A mixture of CuO and Ni nanoparticles was used. The model used discretized in space model to simplify the behaviour of the physical system. For nanofluids with 0.03% volume fraction and an outlet temperature of 650°C, the maximum efficiency obtained was 62.5%.

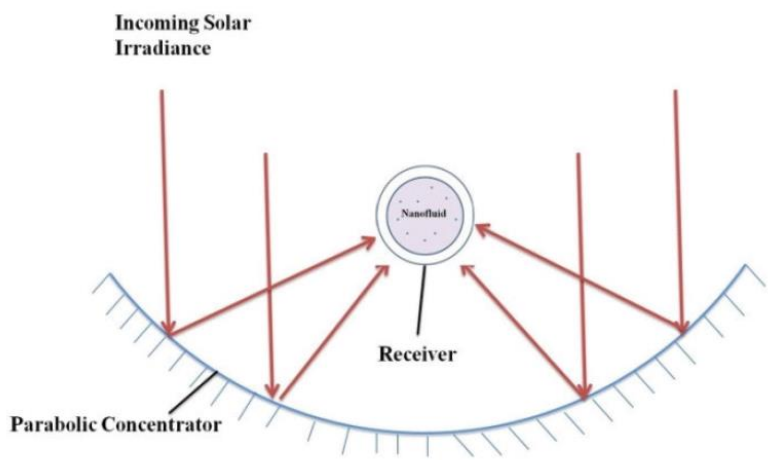

Figure 2-25: drawing of nanofluid-based parabolic trough solar collector [108].

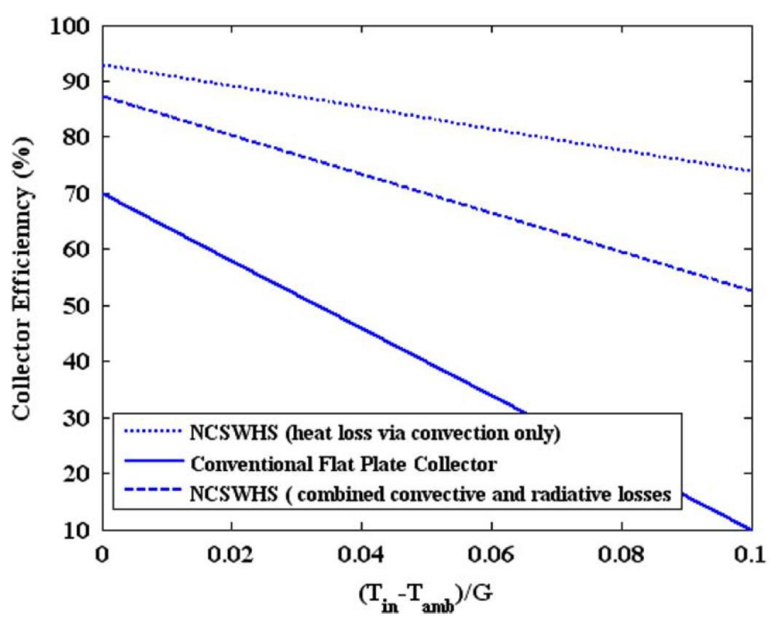

Figure 2-26: The performance of nanofluid-based concentrating parabolic solar collector compared to conventional flat plate collector [108].

A nanofluid-based concentrating solar collector was compared with a common concentrating solar collector [109]. The results showed that the efficiency can enhance by 10% by using nanofluids in the collector. They also found that 10-100 MWe power plants can improve their performance by using nanofluids with nanoparticles concentration of 0.001% or less. The authors assumed that integrating a direct nanofluids absorber with a solar thermal power tower with the capacity of 100 MWe operating in a solar resource like Tucson, Arizona, could produce $3.5 million more per year. They studied two designs for possible direct nanofluids absorber, labelled as A and B, as shown in Figure 2-27.

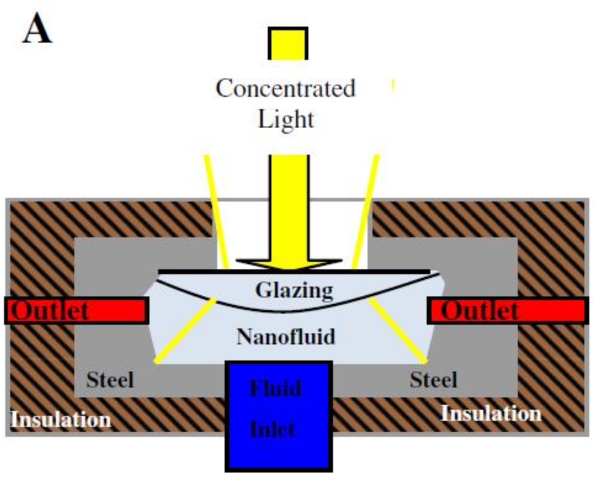

Figure 2-27: (A) potential design of a nanofluid concentrating collector with glazing. (B) potential design of a nanofluid concentrating collector without glazing [109].

A numerical study on a direct absorption nanofluid based solar collector was conducted by solving radiative transfer and integrating convection and conduction heat transfer equations [61]. The solar collector efficiency and temperature profile are evaluated by investigating the absorption and scattering of nanoparticles and the absorption of the mixture. The results of the simulation were in good agreement with the experiments. The efficiency and outlet temperature of nanofluids enhanced by 2–25% and by 30–100 K compared to the base fluid. The thermal efficiency of a graphite nanofluid with 0.01% volume fraction is 122.7% higher than a solar collector with a selective surface absorber (non-direct absorber). The study pointed out that even at a very low concentration of nanoparticles, the nanofluids showed good absorption of solar radiation, and it improves the outlet temperatures and collector efficiency. The radiative heat ‘‘source’’ and temperature distributions in the solar collector are shown in Figure 2-28 (a2) and (b2) illustrate that the solar irradiation could be fully absorbed in the top layer of the fluid inside collector due to the presence of nanoparticles. The absorption distributions varied for various nanofluids, e.g. Figure 2-28 (b2) versus (c2). The temperature profile remarkably affected by the radiation distributions of nanofluids. Figure 2-28 (d2) illustrates that solar irradiance was completely absorbed by a selective surface coating layer attached to the surface of glass plate of the solar collector. The surface temperature of the selective surface absorber was higher compared to direct absorption as shown Figure 2-28 (b1) or (c1), therefore, more heat loss occurs in the selective surface absorber. Hence, higher temperature profile in the direct absorber. The figures also show that the nanofluids have higher absorption of solar irradiance compared to the base fluid. The temperature profile in the solar collector shows that nanofluids absorption characteristics reduce energy loss to the atmosphere considerably. The mean outlet temperature is 215 °C in Figure 2-28 (b1) and 207 °C in Figure 2-28 (c1), which are higher than the outlet temperature of the selective absorber collector, as shown in Figure 2-28 (d1). The thermal efficiencies of nanofluids with 0.01 % graphite volume fraction and 0.5 % Al_2O_3 volume fraction enhanced by 122.7% and 117.5% compared to the non-direct absorption collector, respectively.

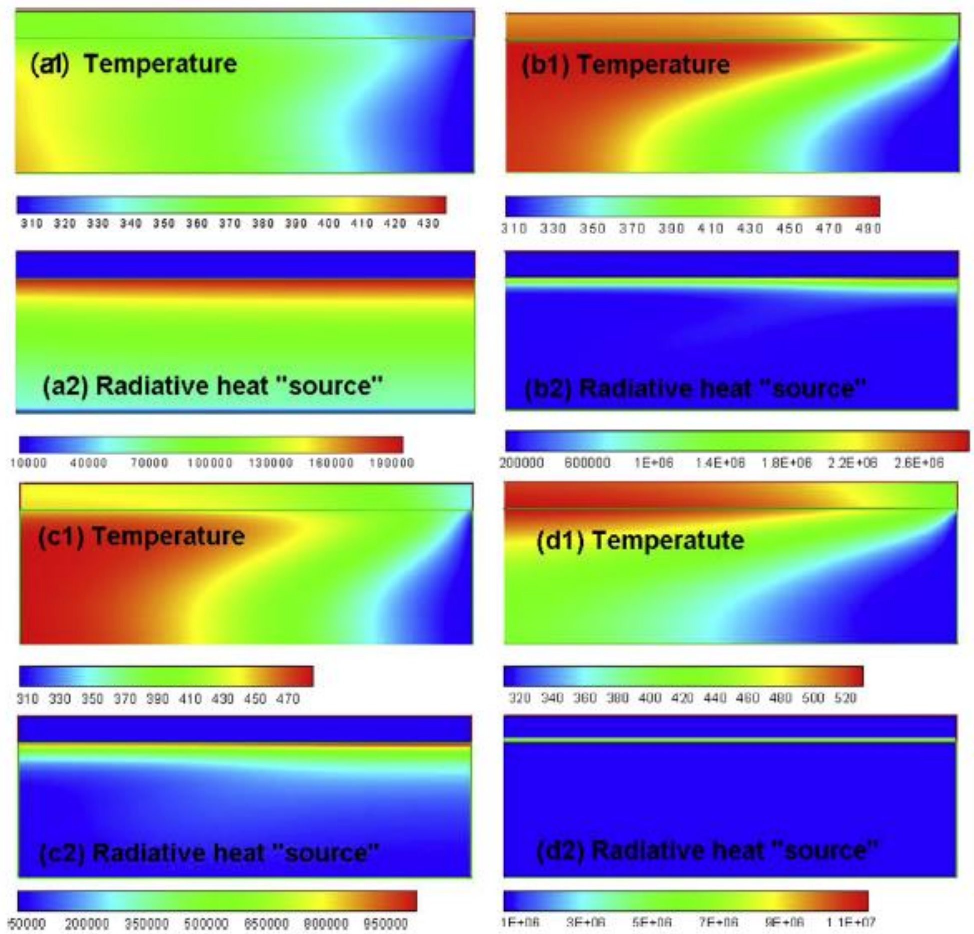

Figure 2-28: The temperature distribution and radiative heat ''source'' in the fluid layer (a1) and (a2) oil, (b1) and (b2) 0.01 vol.% graphite nanofluid, (c1) and (c2) 0.5 vol.% Al2O3 nanofluid, (d1) and (d2) oil with a black coating.

The study of Tyagi et al. [102] introduced the basis for a numerical model of a direct absorption absorber that uses nanofluids as an absorber fluid. most of the work is based on models that consider the radiative transport equation (RTE) integrated to the energy equation for small particles suspended in a gas [110]. The results were compared to the flat-plate collector under similar condition. The efficiency of direct absorber collector was up to 10% higher than that of the common solar collector. Recently, Turkylimazoglu [111] numerically investigated the effect of the bottom plate of direct absorption flat plate collector on the performance of the collector. The bottom panel heat transfer coefficient and the isothermal wall temperature was included in the model. the model utilized Al_2O_3 nanofluid as a heat transfer fluid. The results showed higher efficiency could be achieved by applying heat transferring material in the bottom panel.

Khullar and Tyagi [112] tested the future of the nanofluid based concentrating solar collector as a water heating system. Using nanofluid based concentrating solar collector can save approximately 1716 kWh/household/year of electricity and 206 kg/household/year of gas, which gives significant economic advantages.

Table 2-3 List of recent studies on the applications of nanofluids in solar collectors.

Author and type of study	Collector type	Nanofluid type and nanoparticle size	Results
Taygi et al. [102] (Theoretical)	Non-concentrating direct absorption	Aluminum/water (0–20 nm)	–Efficiency significantly improved for volume fraction below 2% –Efficiency stayed almost constant for volume fraction above 2% –Efficiency improved a little with larger nanoparticles size
Otanicar et al. [93] (Theoretical and experimental)	Non-concentrating microscale direct absorption	Graphite/water (30 nm) silver/water (20 and 40 nm) carbon nanotube/water (6–20 nm diameter, 1000–5000 nm length)	–Efficiency considerably increases for volume fractions below 0.5% –Efficiency may decrease for volume fractions above 0.5% –Efficiency enhanced by 6%, with smaller nanoparticle size in Silver/Water nanofluids
Taylor et al. [109] (Theoretical and experimental)	Concentrating direct absorption	Graphite/therminol VP-1 aluminium/therminol VP-1 silver/therminol VP-1 copper/therminol VP-1 (10–100 nm)	–Efficiency improved up to 10% by utilising a nanofluids in the absorber –Utilising graphite/therminol VP-1 nanofluids with 0.001% volume fractions is valuable for 10–100 MWe power plants
He et al. [113] (Experimental)	Vacuum tube	TiO_2/water (5–10 nm) CNT/water (10–50 nm diameter, 100–1000 nm length)	–CNT/water nanofluids is more appropriate than the TiO_2/water to be utilised in a vacuum tube solar collector
Li et al. [114] (Experimental)	Tubular	Al2O3/water ZnO/water MgO/ Water (size < 20 nm)	–ZnO/water nanofluids with 0.2% volume fractions is the better option for the solar collector

Author and type of study	Collector type	Nanofluid type and nanoparticle size	Results
Taylor et al. [88] (Theoretical and experimental)	Direct absorption	Graphite/water and graphite/VP1 Aluminium/water and aluminium/VP1	–Over 95% of incoming solar irradiance absorbed by the nanofluids with the thickness >10 cm and nanoparticle volume fraction less than 1 x 10^{-5}
Khullar et al. [107] (Theoretical)	Concentrating Parabolic	Aluminium/therminol VP-1 (5 nm)	–Thermal efficiency of nanofluids concentrating parabolic collectors compared to a common parabolic trough collector is approximately 5 – 10% higher
Yousefi et al. [96] (Experimental)	Flat plate	Al_2O_3/water (15 nm) Triton X-100 is used as a surfactant	–Efficiency of the solar collector with 0.2% weight fraction nanofluids is higher compared to water by 28.3%. –Efficiency improved by15.63% by applying the surfactant
Yousefi et al. [95] (Experimental)	Flat plate	Water-Multi wall carbon nanotubes (MWCNT)/water (10–30 nm) Triton X-100 is used as a surfactant	–Efficiency of the solar collector enhanced significantly for 0.4 wt.% nanofluids, while with 0.2 wt.% the efficiency declined compared to water
Otanicar and Golden [93] (theoretical)	Direct absorption	Graphite/water and propylene glycol	–Utilising a nanofluids-based solar collector gives less CO_2 emissions compared to the common solar collector
Vakili et al. [115] (Experimental)	Direct absorption	Graphite/water	–Efficiency of solar collector improved up to 33% by using only 0.005 wt% graphite nanoplatelets.
Said et al. [116] (Experimental)	Flat plate	PH treated Al_2O_3/water	–The thermal efficiency enhanced by 83.5% for 0.3% volume fraction and 1.5 L/min. –The exergy efficiency is improved by up to 20.3% for 0.1% volume fraction and 1 L/min.
Khullar and Tyagi [112] (Theoretical)	Concentrating direct absorption	Aluminium/water	–Using this type of solar collector produces CO_2 emissions by 2.2% 103 kg in 1 year
De Risi et al. [59] (Theoretical)	Concentrating direct absorption	Cu &Ni/ Air	–High outlet temperature 650°C with high efficiency 65% and low particle concertation
Turkylimazoglu [111] (Theoretical)	Direct absorption	Aluminium/water	–Improving the bottom panel material could enhance the efficiency further.

2.2.3 Conclusion

This section overview shows the use of nanofluids in the solar thermal system is still at early stage. Nanofluids can be applied in different fields of solar energy. Nanofluids are utilised to enhance the efficiency of various thermal engineering devices. The application of nanofluids in the solar collectors may increase the performance of the collectors. Experimental studies faced the main limitations, such as particle aggregation, stability, erosion, and corrosion of the heat transfer devices. Numerical simulations require more exact models such as two-phase mixture models need to be done for various solar collector applications. As seen before the performance of nanofluids are not well defined. The different approach in preparation and measurements led to conflicts results. It will be beneficial to study the thermos-physical properties of nanofluids with different preparation methods. Most experiments studied the performance of nanofluids in low to medium temperature range. Especially in the case of solar collectors, it will be beneficial to study the performance to nanofluids in the high-temperature range. The authors suggest studying the use of ferrofluids in solar collector system since previous work showed an increase in thermal conductivity compared to nonmagnetic nanofluids. These results present the benefit of nanofluids in heat transfer systems. However, the current data are neither sufficient nor reliable for engineering applications. The experimental results have been inconsistent from different research groups. The rationale behind that is the different preparation method of nanofluids and incomplete characterization of nanofluids. For example, whether surfactant was used or no, the kind of surfactant, the concentration of surfactant, and the size and distribution of particles. Moreover, most experimental data are obtained under inadequate application range such as low temperatures. As discussed, only theoretical studies have been carried out on parabolic trough collectors. Therefore, experimental invitations can be conducted on the impacts of nanofluids on the performance of parabolic trough systems. Future works are should include widely on the utilisation of nanofluids for high-temperature solar collectors and energy storage ranks by having experimental and theoretical studies. The nanofluids for solar collectors can be made feasible practically by conducting the study under various environment, geographical conditions testing, and thermophysical properties of the fluid on various thermal systems. Furthermore, we couldn't find any previous work on ferrofluids based solar collector.

Chapter 3 Experiment Principle and Method

3.1 Introduction

In the presence of an external magnetic field, the efficiency of ferrofluids based parabolic trough collector is greater than a conventional parabolic trough with common heat transfer medium. This hypothesis was experimentally tested by studying heat transfer performance of ferrofluids based parabolic trough collector. The performance of ferrofluids parabolic trough was experimentally tested based on the British Standard BS EN ISO 9806:2013 "Solar Energy – Solar thermal collectors – test methods."[117]. In the experimental work, indoor tests have been carried out using a solar light simulator. The ferrofluids parabolic trough performance was investigated for water and water-based Fe_3O_4 ferrofluids, and the effect of other design parameters such as inlet temperature, the concentration of nanoparticles, and magnetic field intensity was also considered. In addition to the development of solar light simulator associated with a standardized experimental method of testing, this chapter presents the experimental setup, including the system description, working principle, instruments and measurements, and testing procedures.

The ferrofluids parabolic trough test rig was designed based on concentrating solar collector concept. For this, design parameters such as concentration ratio, efficiency, mirror reflection ratio, receiver outer diameter, inlet temperature, mass flow rate, focal point, and collector length have been assumed, and its associated collector parameters such as aperture width, outlet temperature have been calculated. The parabolic trough test rig was manufactured and assembled at the laboratories. The performance of ferrofluids parabolic trough test rig was then investigated using water and water-based ferrofluids as heat transfer medium. High concentrated ferrofluids were prepared by Fluids and Thermal Engineering research group at the University of Nottingham. The ferrofluids were diluted to 4 different concentrations. Two different types of the solar receiver were investigated. Non-direct absorber and direct absorber receivers were used and compared.

3.2 Test methods

The performance and quality of solar collector test methods have a long history. The current standards were developed based on the International Organization for Standardization ISO and the American Society of Heating, Refrigerating, and Air-Conditioning Engineers ASHRAE standards created in the mid-eighties. The most common test methods of the collector thermal performance recommended by ISO and ASHRAE is determined under the stationary condition, i.e. steady-state method. The other methods used is a quasi-dynamic test method.

In a steady state method, all essential variables for the collector thermal performance held constant throughout the test period. Those variables include the ambient temperature, wind speed, solar irradiance on the collector, the inlet temperature of the heat transfer medium, and the mass flow rate. All variables have a certain limit defined by BS EN ISO 9806:2013 and ASHRAE. There are also experimental methods to obtain the collector efficiency dependence on the incidence angle, called the incidence angle modifier (IAM). The IAM is described as the efficiency at the incidence angle dived by the efficiency at zero-degree incidence. Hence, at zero degrees IAM is equal 1. In the case of concentrating solar collector, the efficiency is not necessarily at its maximum at zero-degree incidence. The steady-state method is a clear sky model with a low percentage of diffuse radiation.

In 2001 version of EN 12975 the quasi-dynamic test method was first introduced. The quasi-dynamic test method performed under natural conditions with variable radiation, wind speed, and ambient temperature. The method is based on the original steady-state mathematical model with modification and additional extension of terms. The major correction is that solar radiation is considered both direct and diffuse with corresponding IAM s. The effect of wind speed on heat loss and optical performance is added to the method. No specific test methods for concentrating collectors were developed within those standards. However, good results were reported by applying quasi-dynamic to parabolic trough [118]. One-third of the laborites in Europe use the Quasi-dynamic test method.

The steady-state method has been used for a long time, and substantial experience gained making it well defend method. The steady-state method is easier to apply in a sunny climate. Performance testing includes the assessment of the heat power delivered by the collector under various operating conditions as well as the assessment of additional collector parameters (pressure drop, heat capacity) required for the calculation of the collector heat output. As described by the British standard there are different methods to test the performance of a solar collector which is steady-state and quasi-dynamic thermal performance of glazed and unglazed liquid heating solar collectors and steady-state thermal performance of glazed and unglazed air heating solar collectors (open to ambient as well as a closed loop). In this research, the steady state method was used to determine the efficiency of the solar collector. ASHRAE and the British standard suggest performing the test in various inlet temperature.

3.3 Experimental setup

A novel ferrofluids parabolic trough solar collector small-scale test rig was developed and investigated at the Fluids and Thermal Engineering Research Group laboratories at the University of Nottingham. The small-scale is an initial phase to recognise the potential of ferrofluids in CSP systems. This system employs the concept of enhancing thermo-physical properties of ferrofluids by adding external magnetic field source to parabolic trough collector to improve heat transfer performance of the parabolic trough. Figure 3-1 shows a schematic diagram of the proposed parabolic trough test rig and its component. This small-scale test rig includes the parabolic trough collector unit, solar simulator, circulation pumps, DC power supply, chiller, heat exchanger, and fluid tank. The parabolic trough collector unit (PTC) used in the experiment consisted of a sheet of the reflective mirror with a parabolic shape, receiver tube, and electromagnets as shown in Figure 3-1. The key innovation of this test rig is the electromagnets installed in the parabolic trough to generate an external magnetic field that improves the heat transfer performance when ferrofluids are used. The enhancement of heat transfer performance, hence the collector efficiency, makes the required collector area and manufacturing materials much lower than conventional solar collector that uses conventional heat transfer medium. In both receivers, the objective is the same which is improving the heat transfer performance. In the non-direct receiver, the external magnetic field will increase the thermal properties of the fluid allowing heat to transfer faster from the receiver surface to the fluids making the surface temperature lower. In a direct absorption, the external magnetic field increases the optical properties of the fluids where nanoparticles absorb the solar radiation due to the structure and alignment of nanoparticles when external magnetic field is present will increase the absorption of solar radiation of nanoparticles and increase the efficiency of the solar collector.

3.3.1 Experimental setup and system components

The test rig of the ferrofluids parabolic trough collector has been assembled as shown in Figure 3-1. A photo of the test rig is shown in Figure 3-2. Table 3-1 shows the geometries of the collector. The components of the test rig are described below:

- Circulating pumps
- Storage tank
- Solar simulator
- Concentrating mirror
- Solar receiver
- Electromagnets
- DC power supply
- Heat exchanger
- Chiller

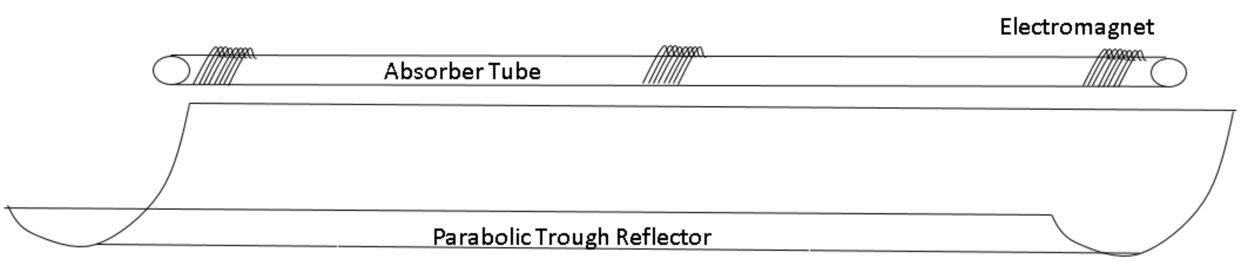

Figure 3-1: Schematic of proposed parabolic trough Collector.

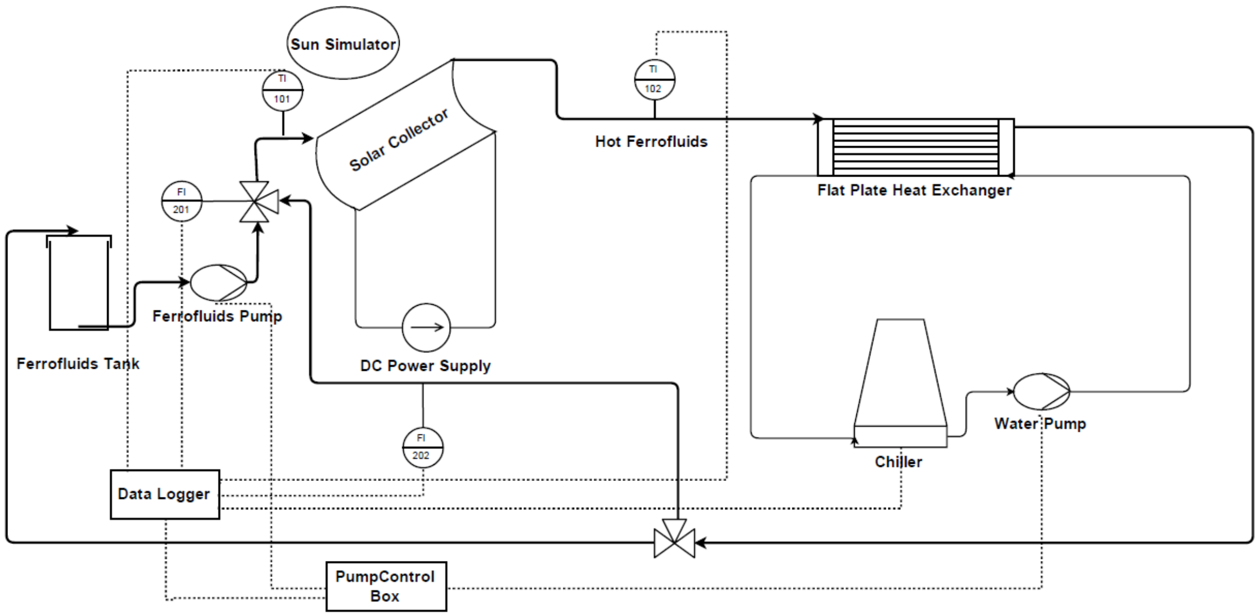

Figure 3-2: Schematic and photograph of the experimental setup.

Table 3-1: Geometries and dimensions of the solar collector components.

Component	Dimensions
Aperture Width (mm)	250
Aperture length (mm)	450
Absorber outer diameter (mm)	15
Absorber inner diameter (mm)	14
Absorber length (mm)	450
Focal distance (mm)	50
Rim angle (°)	90
Electromagnet length (cm)	50
Number of copper wire turns	84
Electromagnet inner diameter	15.1

3.3.1.1 Solar simulator

The light irradiance of solar collector varies depending on the lamp type and operation time. The spectral irradiance of these lamps slightly differs from natural sunlight which can lead to measurement error. Solar simulators using a various source of lights have been intensively investigated by many researchers. However, such simulators have the disadvantage of low performance due to the disproportionate in solar irradiance distribution. A small simulator utilising LED lamps has been developed and studied by Kohraku and Kuokawa [119]. The solar simulator was developed for solar cells experiment with an area of 100 x 100 mm^2, and it had 3% unevenness. In another study, a solar simulator was developed by combining metal halide and quartz halogen light sources. The study focused on the quality and optimal operational points for maximum electrical output for an area of 8 inches in diameter. To achieve a uniform distribution of solar irradiance with minimum unevenness, most of the studies developed the small-scale solar simulator. Using LED and halogen lamps as light sources in solar simulators gain a lot of interest due to their spectral output, low cost, high energy efficiency, and long operating life [120]. A solar simulator utilizing 30 halogen lamps with an area of $2.32 m^2$ was assembled and tested [121]. The results showed that the unevenness is a function of the distance between the simulator and the measurement points. At 23 cm distance, the maximum unevenness measured was 9.1% which is within the acceptable limits of 15% suggested by the British Standards for testing solar simulator.

The solar simulator used in this research consists of 3 tungsten halogen floodlights, each with a maximum of 400 W, covering an area of $0.165 m^2$ was assembled and tested for unevenness. Due to their stability and smooth spectral output, tungsten halogen lamp is extensively used in solar beam experiments for solar simulator applications. In terms of thermal radiation, like the sunlight, the wavelength of tungsten halogen ranges between 360-2500 nm. They require simple power supply units, and they are considered inexpensive. Natural sunlight has a colour temperature of approximately 5600K, whole halogen lamps produce a radiation at a block body temperature about 3200K.

A pyranometer with a sensitivity of 17.99×10^{-6} Volts/W/m^2 was used to measure the intensity of solar radiation from solar simulator at uniformly spaced points that resemble the reflector mirror parabolic surface. As shown in Figure 3-3, nine measuring points of solar irradiance were considered. The solar irradiance was measured to determine the unevenness and optimize the lamps of the solar simulator and the distance between the solar simulator and the solar collector.

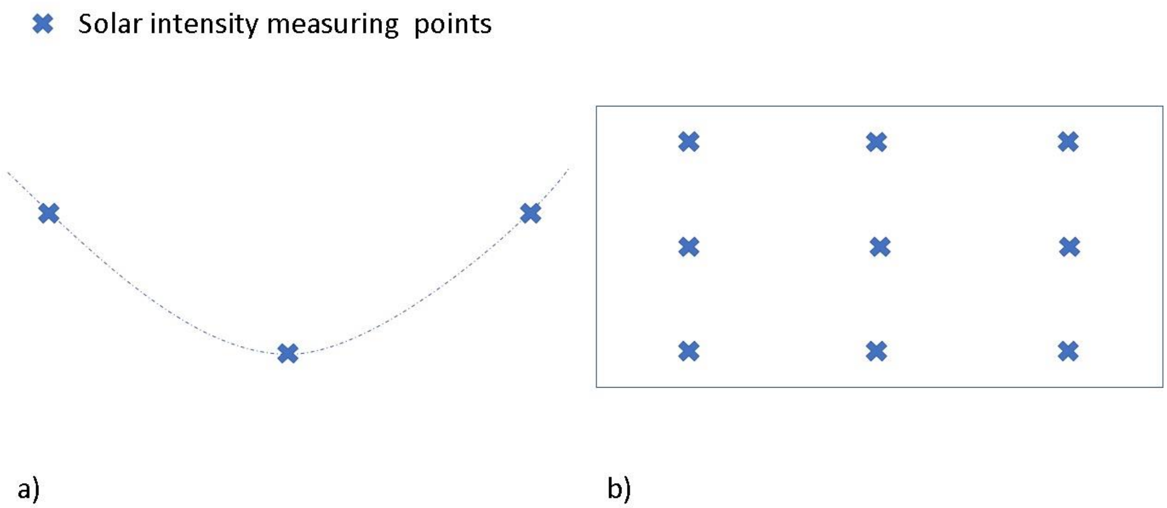

Figure 3-3: Measuring points of solar irradiance to determine their unevenness.

As shown in Figure 3-4, both distances affected the unevenness of the radiation. The closer the lamps to each other the higher the unevenness. A maximum unevenness of 27.7% was observed when the distance between the lamps is 10 cm, and the height between lamps and the solar collector receiver is 57 cm. The high unevenness is contributed to the overlap of lamps light irradiance and the low irradiance at the edge of the reflector. Shorter distance between the lamps and the solar collector receiver makes the solar irradiance more even around the reflector area. When the distance is 35 cm, and the distance between the lamps is 20 cm we have unevenness of 12%. We fixed the solar simulator to this position during the testing of ferrofluids parabolic trough performance. The unevenness of 12% is within the acceptable limits of 15% suggested by the British Standards for testing solar simulator. The average solar irradiance over the collector gross area at this height was 1011.89 W/m^2 which is higher than the minimum value specified by the British Standard of 700 W/m^2. As shown in Figure 3-5, the solar radiation change by changing the height of the lamps to the solar collector receiver. At the height of 57 cm, the solar irradiance measured was 571.43 W/m^2, after that the solar irradiance augmented by shortening the distance between the lamps and the solar collector absorber to 749.55 W/m^2, 1011.89 W/m^2 for 40 cm, 35 cm, respectively. However, during this research, the position of the lamps and their height was not changed to maintain constant solar irradiance and keep the unevenness below 15%.

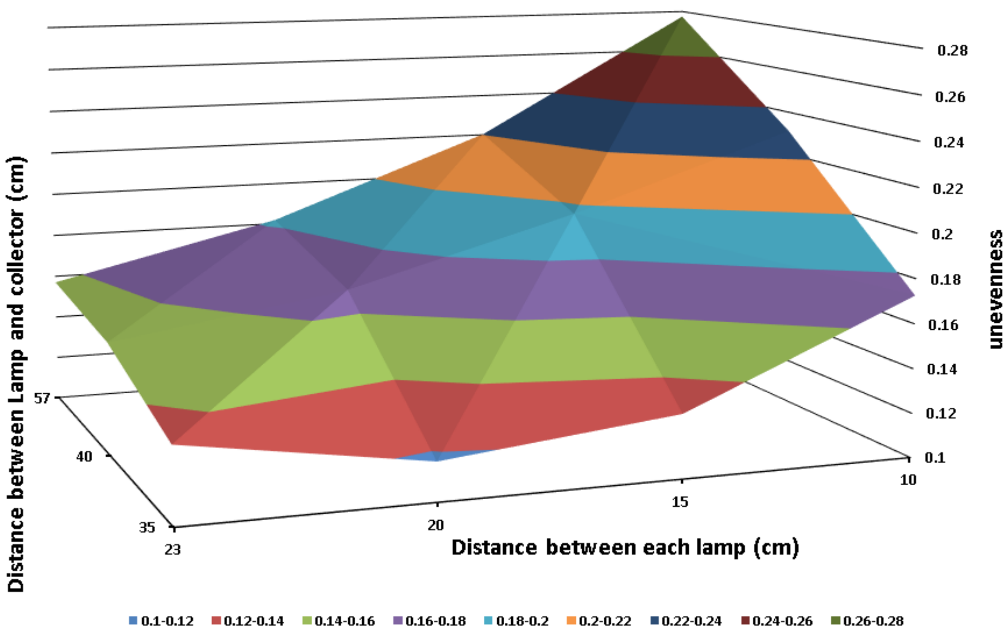

Figure 3-4: The unevenness of Solar simulator is a function of height and distance between lamps.

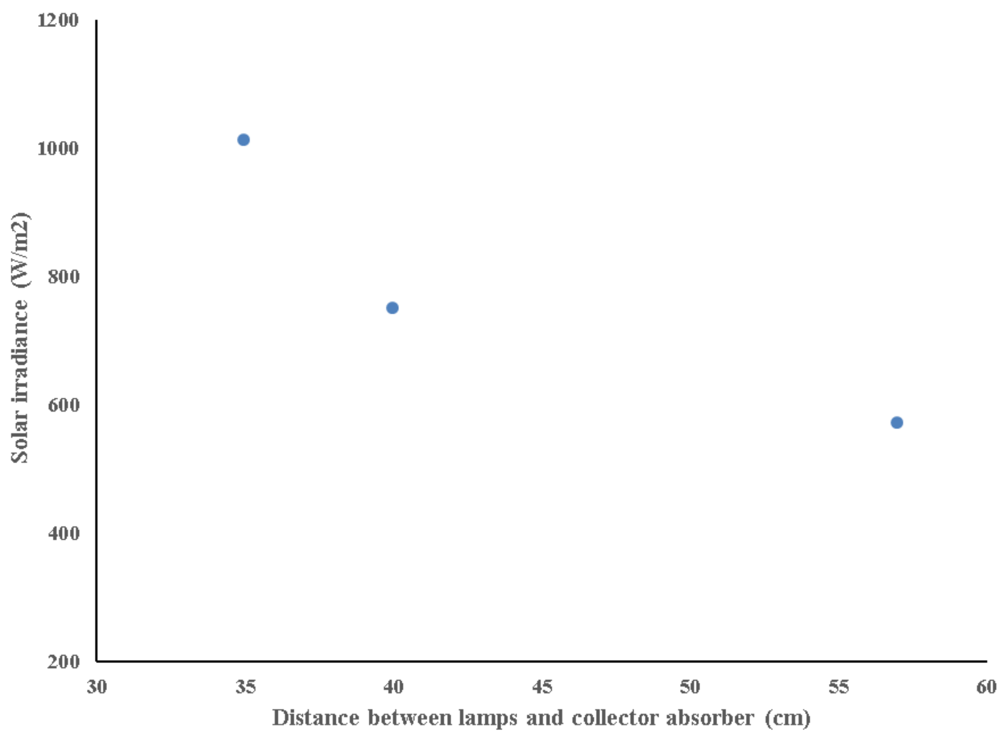

Figure 3-5: Solar irradiance as a function of the distance between lamps and solar collector receiver.

3.3.1.2 Concentrating mirror

Reflective surfaces used to concentrate solar irradiance to a focus point. In the parabolic trough, as the name suggests a reflective surface is shaped to a parabola to concentrate the solar irradiance to the receiver tube. Figure 3-6 illustrates the parameters affect the parabolic profile. The geometric design of parabolic trough collector is explained in detailed by Kalogirou. The parabolic reflector was designed with the length of 500 mm, and an aperture width of 250 mm. The rim angle of the test rig collector was selected as 90°, and a focal distance of 50 mm. There are several reflective surfaces that can be used for small-scale parabolic trough such as MIRO IV, galvanized steel, aluminium flashing, reflective film, acrylic mirror, high impact polystyrene silver mirror. Most of those surfaces are coated with aluminium or silver due to their high reflectivity. MIRO IV is optically clear electropolished anodized aluminium sheet usually used in light fixtures. The reflection of light in ideal condition is over 95%. The thickness of MIRO IV is 0.5 mm which makes it perfect mirror that can be bent. Another possibility is to use mirror film which is laminated to substrate material with the shape of the reflector. The mirror film consists of multiple layers of polymer films with a layer of pure silver that provides reflectance of 94%. However, to apply such a film it needs to be laminated evenly and straight onto the substrate to avoid any wrinkles. Some manufacturers recommend a special machine for lamination of mirror films. The Acrylic mirror is a clear plastic mirror with a good reflectivity and low cost. The thickness of the mirror varies from 3 to 1 mm. However, the acrylic mirror is difficult to bend by hand and mostly needs to be heated in an oven to get it in the required shape; moreover, the heat might destroy the surface of the mirror. Therefore, another type of plastic mirror was considered which is the high impact polystyrene silver mirror (HIPS) which is polystyrene sheet laminated with metalized polyester foil in silver or gold. They are usually used in toys, or as safety mirrors because they are easily bent.

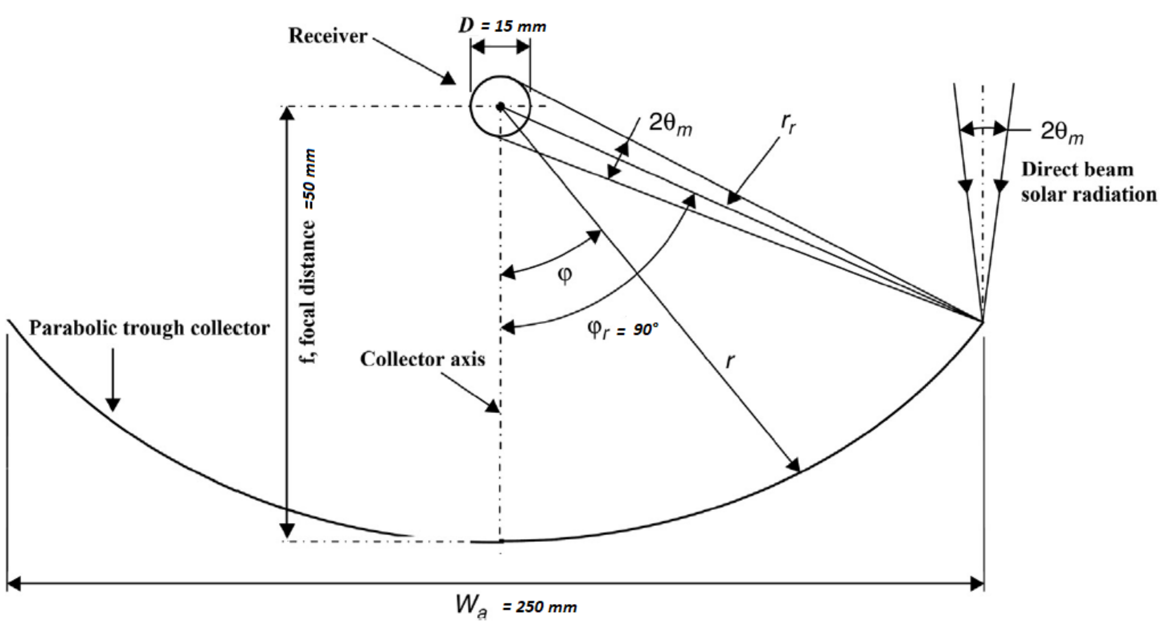

Figure 3-6: Parameters of the parabolic profile [87].

The reflective mirror used in this research was 1 mm thick high impact polystyrene sheet with white painting on the back. White painting is recommended to avoid any thermal radiation that can deform the surface. The parabolic trough shape is created by a number of ribs underneath the reflective sheet. The reflective sheet is held firmly against the parabolically shaped edge of the ribs by metal clamps.

As described before the efficiency of solar collector is defined as the usable thermal energy divided by the direct solar irradiance, it's also known as thermal efficiency. Besides the thermal loss, there is an optical loss. Optical loss always exists, and it establishes the maximum limit of collector efficiency. Optical efficiency in concentrating solar collector is defined as the ratio of solar radiation reaching the absorber to the energy collected from the aperture area. In commercial concentrating solar collector, the optical loss is between 10 and 20%. There is no specific method to check the optical efficiency of a parabolic trough collector or any concentrating solar collector. However, a basic method can be used to check the precision of the optical efficiency of the collector. The reflected solar irradiance by the mirror is observed on the receiver from all positions and angles. In the ideal concentrating parabolic mirror, no reflected solar irradiance should leak from the receiver, from any observation position and angle. A paper strip was used to check the leaking, as the leaking will illuminate positions of the strip. The leaking of solar irradiance identifies defocusing and causes a loss of collector efficiency. There are different types of leaking, and each has its nature and causes. The different type of leaking includes biased, sided, end, joint, curvature leaking. In this research, a curvature leaking was observed when the paper strip moved from the begging of the collector to further to the middle a leaking appears; then it disappears only to appear once again a bit further. This means that the curvature of the reflective surface is not parabolic along the length of the collector. A 10% of the leak was observed and considered in our calculation. Improving the curvature is necessary to reach higher collector efficiency.

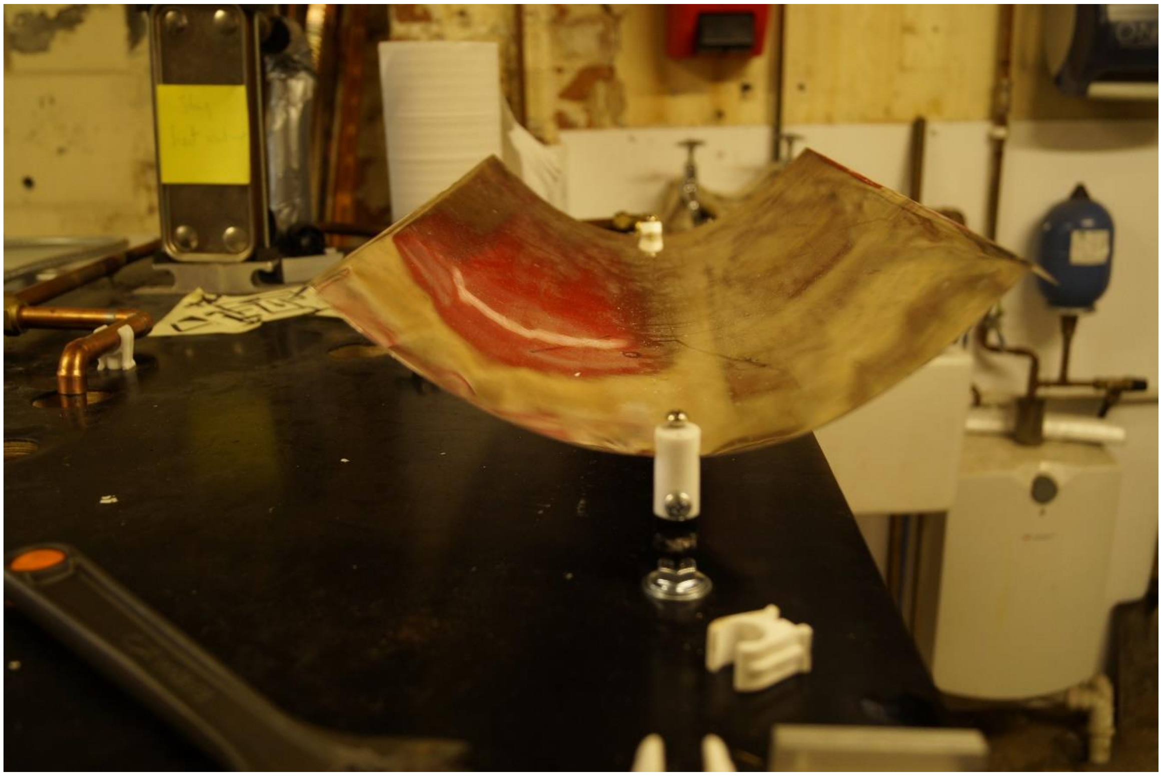

Figure 3-7: Parabolic mirror used in the experiment.

3.3.1.3 Solar collector receiver

Conventional parabolic trough receivers are usually consisting of borosilicate glass tube with anti-reflective coating, stainless steel tube with a selective coating, getters to absorb gases, bellows, and glass to metal seal. The glass tube which also known as envelope decrease the thermal loss of the collector and allows the collector to operate at high temperatures. In this experiment, we use two different kinds of receivers and both they don’t have an envelope. An envelope wasn’t used for two reasons. First, we are operating at low temperature, second, we are installing temporary electromagnets into the receiver, and we change their location and direction. Both tubes have the same dimensions with 15 mm outer diameter and 14 mm inner diameter. The two receivers used were the following:

1) Direct solar absorber: - Copper tube with selective coating
2) Non-direct solar absorber: - transparent borosilicate glass tube

To compare the performance of both absorbers, both have the same inner, outer diameter, and length. Few selective coatings are used in parabolic trough collectors, due to the effect of the high operating temperature of the parabolic trough on the solar absorptance and thermal emittance of the selective coating. The most common selective materials used are Black Chrome, Luz Cermet, and Al_2O_3-based cermet with anti-reflective coating. The copper tube was coated by SOLKOTE HI/SORB-II^{TM} selective solar coating with emissivity range of 0.2 to0.49 and absorptivity range from 0.88 to 0.94. The coating thickness was 0.025 mm. The copper tube was cleaned by Acetone before spraying the coating surface. The electromagnet is firmly attached to the copper tube and removing it will cause the degradation.

The non-direct absorber was a simple, transparent glass tube that widely used in chemistry labs. The glass tube allows the solar irradiance to transmit through it and absorption occurs inside the ferrofluids. It was difficult to attach the glass tube to the system due to the fragile of the tube, and it was necessary to make sure no leaking acquired during operation. During initial tests, many glass tubes were broken on the joint. Ideally, a glass to metal seal should be used on both ends of the glass tube.

Figure 3-8: Coated copper tube used in the experiment.

3.3.1.4 Electromagnet

The electromagnet was used to generate an external magnetic field to alter the thermophysical properties of ferrofluids inside the receiver. As shown in Figure 3-9, three electromagnets were used to make sure the nanoparticles are magnetized along the length of the collector. The electromagnets were located at the beginning, middle and the end of the absorber. Ferroparticles are reversible and will go back to their initial state after the external magnetic field disappear. In this research, we didn’t investigate the reversibility of the particles to determine the exact distance between electromagnets needed. We assume that the particles are magnetized and do not return to their initial state until they leave the collector. Moreover, Altan [122] showed that reversibility of the enhanced thermal conductivity is very slow once the electromagnet was switched off.

The electromagnets are air core solenoids with an inner diameter close to the outer diameter of the absorber tube 15.1 mm, allowing the absorber tube to enter into the electromagnet. The electromagnet has a length of 50 mm and 4 layers, approximately 84 turns, of polyurethane enamelled copper wire. The external magnetic field intensity was similar to the study of Nkurikiyimfura et al. [123]. The magnetic field intensity was calculated as follow:

$$B = \frac{n\,\mu\,I}{L_S} \qquad \text{Eq. 3-1}$$

where B is the magnetic field intensity in Tesla, L_S is the length of the solenoid in meter, μ is the permeability of vacuum which is $4\times\pi\times10^{-7}$ H/m, and I is the current in Amber. The electromagnet generates a uniform magnetic field when a current is passing through the coils. Adjustable DC power supply is used to control the current applied to the electromagnet with a maximum current of 5A. Three different currents were used 1.5, 3, 5 A. Using a gauss meter, the external magnetic field intensity of the electromagnets was measured. The wires connecting the electromagnet affect the reflection of the mirror, but due to their small size, it was neglected. The electromagnet itself covers a good amount of area of the collector 5 cm. we excluded this length to the absorber area.

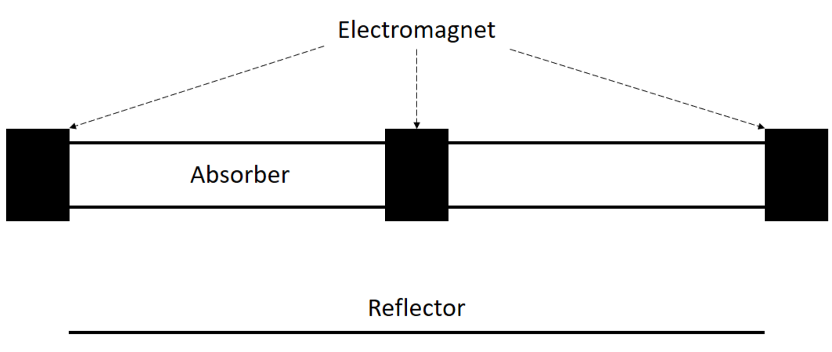

Figure 3-9: Electromagnet location at the ferrofluids based solar collector.

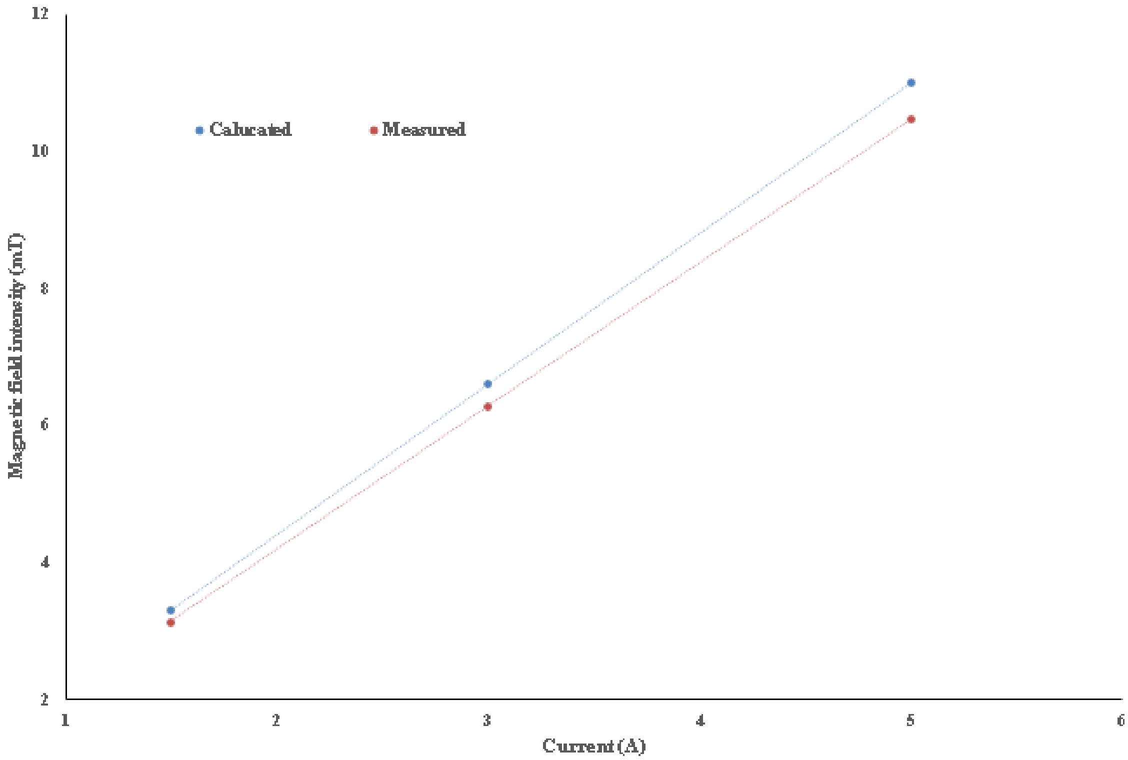

Figure 3-10: Measured and calculated magnetic field at the centre of the electromagnet.

3.3.1.5 Heat Exchanger

The heat exchanger was configured to keep the inlet temperature of the collector constant throughout the measurement of the performance of the solar collector. This can be achieved by keeping the mass flow and the inlet temperature of the cooling water constant throughout the measurement. The mass flow of the cooling water was set to 0.015 kg/s. The inlet temperature of the cooling water is adjusted according to the desired inlet temperature of the solar collector. The cooling water temperature was controlled by the chiller. The cooling water temperature was set to be 0.6°C to 0.2°C below the inlet temperature of the solar collectors. Once the measurement is completed the temperature of the chiller is changed according to the next desired collector inlet temperature. The next measurement will be recorded once the system reaches steady state condition. The heat exchanger used in this experiment is brazed plate exchanger (Alfa Laval AC10-14).

3.3.1.6 Water Chiller

A chiller is used to cool down the heat transfer fluids coming out of the solar collector. The chiller uses water as a cooling medium. The Chiller used in the research is Hailea Water-Chiller HC250A with 250 Litre water cooling capacity. The chiller uses refrigerant R134a and operates down to temperatures of 4°C. The chiller has an electronic control that controls the temperature of the water to 0.1°C increments, and with temperature setting in 1°C steps.

Figure 3-11: Hailea Water-Chiller used in the research.

3.3.2.7 Circulation Pumps

Two pumps are used to circulate the heat transfer medium and the cooling water through the system. The pumps are usually used in chemical industry, water treatment, pharmaceuticals industry, food industry, etc. Since the solar collector operates at low temperatures and low pressure, a domestic central heating pump is sufficient. The pump used in the research for the solar collector cycle is Grundfos UPA15-90. A basic variable speed drive was used to control and adjust the speed of the pump. for the water cooling cycle, a Lowara TLC25 is used.

3.3.2.8 Ferrofluids preparation

The magnetite nanoparticles Fe_3O_4 were prepared by Fluids and Thermal Engineering Research Group at the University of Nottingham using co-precipitation methods. The average diameter of nanoparticles was 10 nm. Sodium dodecyl SDS absorbed onto the surface of the nanoparticle, and then the nanoparticles were suspended in water. SDS increase the stability of the suspension and avoid sedimentation of particles. The ferrofluids had a high concentration of magnetic nanoparticles with the volume fraction of 15%. The ferrofluids were diluted in distilled water to the required volume fractions. The following mass balance was used to determine the required water.

$$V_{out}X_{out} = V_{in}X_{in} + V_{water}X_{water}$$

where V_{out} is the desired volume of ferrolfuids, X_{out} is the desired volume fraction of nanoparticles, V_{in} is the volume of prepared ferrofluids, X_{in} is the inital volume fraction of 15%, V_{water} is the volume of distilled water, $X_{water}$is the volume fraction of nanooparticles in water which is 0. First, the volume of prepared ferrofluids is determined, and then the volume of distilled water is calculated. To prepare 1 litre of ferrofluids with volume fractions of 0.05%, 0.25%, and 075%, the volume of distilled water is 996.66 ml, 983.33 ml, 950 ml respectively. Using a static position method, the stability of ferrofluids was investigated. The ferrofluids were left standing in a container for four months. The distance or color difference in sedimentation within ferrofluids was observed by naked eye. The change of concentration is barely noticed. SDS produced a lot of bubbles when used in the solar collector. Therefore, a defoamer (DF, Antifoam B Silicone Emulsion) was added to suppress the bubble formation DF concentration was 15% of the weight of the added SDS. There are no changes observed to the sedimentation phenomena was noticed after adding defoamer.

3.3.2 Measurement instruments and calibration

3.3.2.1 Measurement of flow rate

An ultrasonic transmit time inline flow meter of type Flownetix 100 series was used to measure the flow rate of the heat transfer medium in the collector cycle. This type of flow meters has two transducers and it measures the time difference when an ultrasonic signal is transmitted from the first transducer until it crosses the tube and received by the second transducer. The flow meter has a flow range of 0.2 to 25 L/min with an accuracy of 3%, and a resolution better than 0.001 L/min with operating temperature range of fluid -10°C to 85°C, and Ambient 10°C to 55°C.

The standing-start-and-finish method was used to calibrate the flow meter. This procedure is usually favoured for flow meters that are utilised for measuring the fluid load, especially flow meters for batch loads. As shown in Figure 3-12, the needed flow rate is settled into a container. Then a fast-acting solenoid valve stopped the flow, the tank drained, and the drain valve closed. The flow is re-established, the container filled, and the flow stopped. The filling time for the tank, the weight of the fluid and the reading of the flow meter is noted. Pressure and temperature of the fluid at the flow meter are also noted during the fill. To have an efficient permanent start and stop calibration technique, few criteria should be met. First, the flow loop system has to be designed and assembled to allow the flow to pass through the meter and stopped without harming to the pump and the system; a pump bypass is commonly equipped. Second, no air must be trapped in corners or T parts as this will lead to a spring effect producing fluctuation when stopped quickly, causing an error in meter readings. The flow should be turned on and off as quickly as possible to decreases the rise and fall time errors. Figure 3-13 shows the results of the calibration and the coefficient was added to the data acquisition to show a volume flow in L/s.

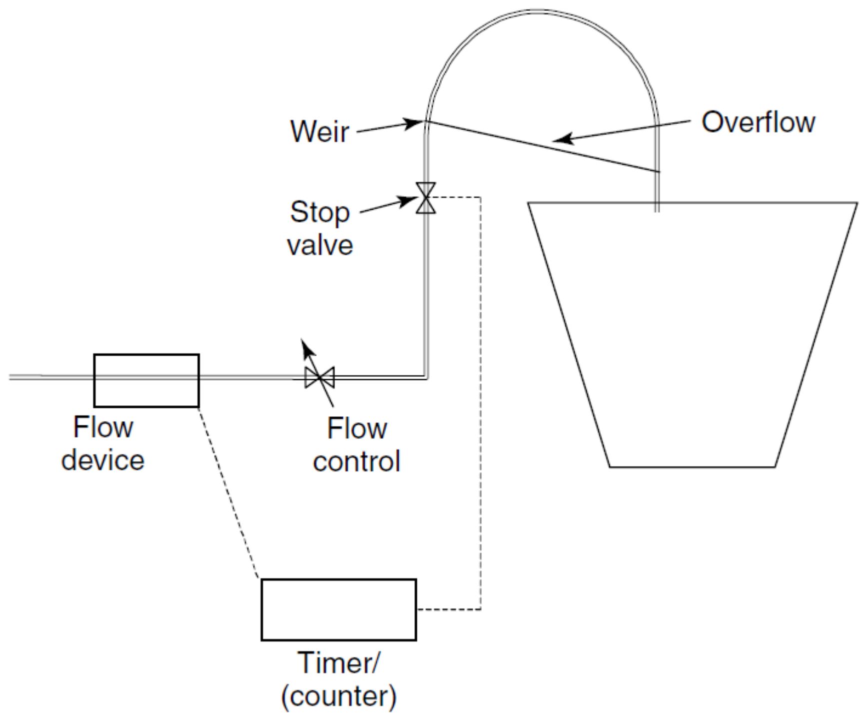

Figure 3-12: Standing-start-and-finish method for the gravimetric calibration of liquid flowmeters.

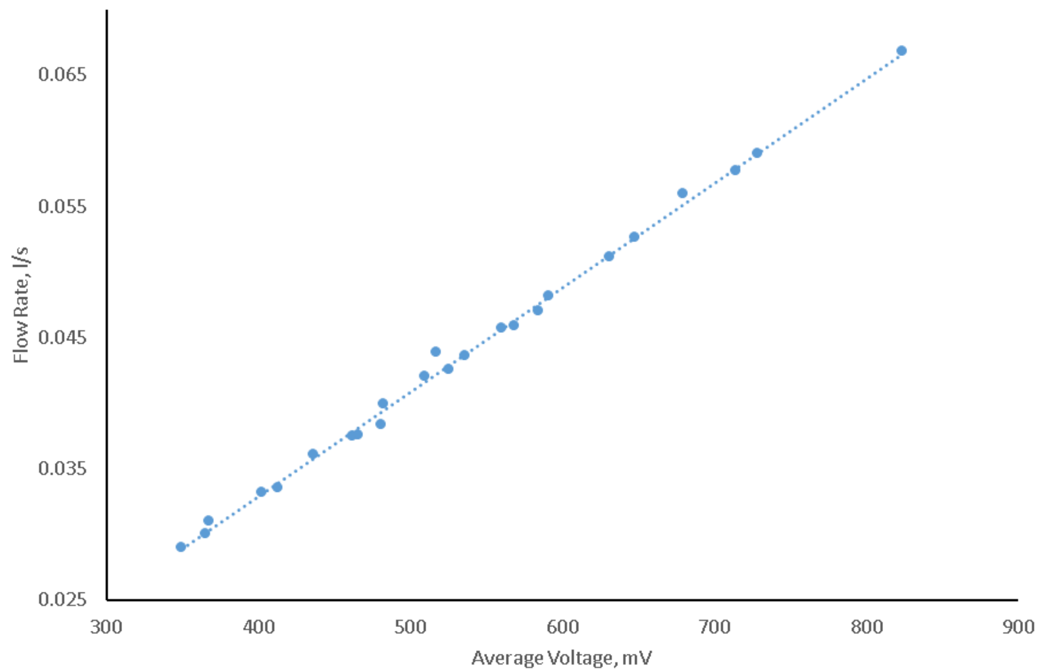

Figure 3-13: Calibration of flow meter.

3.3.2.2 Measurement of temperatures

The temperatures were measured using T-type thermocouples as shown in Figure 3-14. All the thermocouples are connected to a digital data taker DT500 with a computer acquisition system. T-type thermocouples consist of two conductors copper and constantan. Both materials are non-magnetic, and therefore they are not affects by external magnetic field. The effect of magnetic field on the thermocouple was investigated [124]. The results showed that ferromagnetic thermocouples (J-type and K-type) are sensitive to the magnetic field where T-type thermocouple was not magnetically affected. Five thermocouples were used to measure the inlet and outlet temperature of the fluid, inlet and outlet surface temperature of the absorber, and the ambient temperature.

The thermocouples used in this project were calibrated by comparison with a standard platinum resistance thermometer. All the thermocouples and standard platinum resistance were firstly connected with data acquisition system (DT800). So, thermocouples and data acquisition system were all calibrated at the same time. The thermocouples and standard platinum resistance were put into a water bath where water was heated from 0°C to 75°C. A temperature increment of 5°C was set at each calibration data captured. All the temperature data were captured when they reached steady state temperature.

Figure 3-14: T-type thermocouples.

3.3.2.3 Measurement of fluid pressure

The fluid's pressure was measured using PTX 14 DRUCK with an accuracy of 0.15% and pressure gauge. PTX 14 DRUCK is connected to digital data taker DT500 with a computer acquisition system. The pressure gauge was used to make sure we have an accurate reading from the pressure sensor. The pressure was used to investigate the increase of total pressure due to increasing the concentration of the nanoparticles, and to see the effect of the magnetic field on the pressure. The pressure transmitter was calibrated by comparing it to a calibrated pressure gauge. The results showed a good agreement and very small error in the reading.

3.3.3 Operation

In this experiment, the solar simulator produces a constant solar radiation that hit the mirror and reflected the receiver tube selective surface. The selective surface absorbs the incoming solar radiation and converts it to thermal energy which passes to the ferrofluids. The electromagnet at the entrance, middle, and at the end of the receiver, alter the thermophysical properties of the ferrofluids. In this way, the cold ferrofluids in the receiver raise the temperature by solar radiation.

Ferrofluids found in the tank was pumped into the ferrofluids parabolic trough solar collector where ferrofluids thermo-physical properties is altered due to the electromagnet found in the entrance of the collector. Then ferrofluids temperature increase due to the hot receiver surface. The heated ferrofluids bring useful heat energy to the heat exchanger and the ferrofluids temperature decrease to the same temperature as the inlet collector temperature. At first measurement point, the inlet temperature of the parabolic trough should remain approximately equal to the ambient temperature (steady-state). The useful heat in the heat exchanger transferred to the cold water coming from the chiller. The hot water exiting the heat exchanger is brought back to the chiller and cooled down. In a real application, the useful heat is transferred to thermal storage such as water storage tank or molten salt storage tank.

The parabolic trough collector cycle has four stages.

1. The heat transfer medium is pumped from the tank to the parabolic trough.
2. Concentrating solar collector in the focal point where the solar radiation will be focused at one point. A receiver found in the focal point to convert the solar radiation into thermal energy. The thermal energy is transferred from the receiver surface to the heat transfer fluid.
3. The heat transfer medium brings the thermal energy to the heat exchanger and leaves the heat exchanger at a temperature equals the inlet temperature of the collector.
4. The heat transfer medium is brought back to the tank.

At the beginning of the experiment, the parabolic trough was shielded from the solar radiation by means of solar reflecting cover until the solar simulator reaches constant radiation intensity. Then the cover was removed, and the inlet temperature was kept approximately equal to ambient temperature (first steady-state point). The first steady-state point is when the difference between the inlet temperature and the ambient temperature remains constant. When the first steady-state reached, the measurement was taken when the outlet temperature of the collector varies by less than 0.5°C (second steady-state point). The second steady-state condition is reached when the difference between the outlet temperature and the ambient temperature remains constant. As mentioned by the British standard two minimum data points are recorded at the second steady-state point (data period) before going to the next step. The next step is to increase the inlet temperature of the collector around 2°C. Increasing the inlet temperature of the solar collector is done by increasing the temperature of the chiller. The next data points were recorded once the inlet temperature reaches the required value and the second steady-state condition is reached. This step was repeated at least 5 times for each experiment.

All the experiments are conducted in low pressure and low flow (LPLF) conditions. The pressure was at the atmospheric pressure of 1.01 bar. Water-based ferrofluid and was used as the working fluid with the variations of nanoparticles concentration from 0 to 0.75% volume fraction. The working fluid flows through the solar receiver with the constant mass flow of 0.02 kg/s. The mass flow rate was chosen based on the British Standard, and it was close to those used in previous studies on nanofluids based solar collector [99, 125]. From the mass flow and the fluid property, the Reynolds number in the receiver can be calculated.

$$Re = \frac{\rho_{eff}\, v\, D_2}{\mu_{eff}} \qquad \text{Eq. 3-1}$$

where ρ_{eff} is the effective density of ferrofluids calculated by Eq. 5-33, v is the velocity of the fluid, D_2 is the inner diameter of the absorber rube (14 mm), and μ_{eff} is the effective viscosity of ferrofluids calculated by Eq. 5-36. Reynolds number distinguish the flow pattern. It is recommended to operate at Turbulent flow due to higher convention heat transfer at turbulent flow compared to laminar flow. Ferrofluids have higher viscosity than the base fluid and might change the flow pattern. Therefore, Reynolds number was determined during the experiments. All experiments were conducted at the atmospheric pressure 1.01 bar. Two types of absorber systems were used. Black coated copper absorber as a direct absorber and a transparent glass tube as direct absorber were used. The magnetic intensity near the centre of the absorber tube was varied between 0 to 10.47 mT. The magnetic field orientation was studied in two different directions. Since the temperature gradient and the magnetic field gradient are two vital factors of affecting the flow and thermal behaviour of the ferrofluid, two possible combination cases of these gradients were applied to investigate their effects.

The control variables are the following: -

1. Two types of absorbers (direct and indirect)
2. Volume fraction of nanoparticles (0.05% - 0.75%)
3. Magnetic Intensity (0 – 10.47 mT)
4. Magnetic field orientation (→←)

The response variables are the following: -

1. Temperature of ferrofluids at the inlet of the collector
2. Temperature of ferrofluids at the outlet of the collector

3.4 Calculation of efficiency

A steady–state method was used to calculate the parabolic trough efficiency, according to BS EN ISO 9806:2013 standard. The test condition is shown in Table 3-1.

The usable heat extracted by the parabolic tough, $\dot{Q}_U$, is calculated by Eq. 3-2:

$$\dot{Q}_U = \dot{m}_f C_{p,f}(T_{out} - T_{in}) \quad \text{Eq. 3-2}$$

where $\dot{m}_f$ is the mass flow of ferrofluids $C_{p,f}$ is the specific heat capacity of ferrofluids which is calculated by Eq.3-3:

$$C_{p,f} = (1 - \varphi)C_{p,w} + \varphi C_{p,np} \quad \text{Eq. 3-3}$$

where φ is the volume fraction, and $C_{p,w}$ and $C_{p,np}$ are specific heat capacity of water and nanoparticles, respectively. The heat capacity is effected by the temperature. Therefore, the heat capacity calculated at the mean temperature T_m which calculated by Eq.3-4:

$$T_m = \frac{T_{in} + T_{out}}{2} \quad \text{Eq. 3-4}$$

The $C_{p,w}$and $C_{p,np}$ are specific heat capacity of water and nanoparticles are calculated as follow:

$$C_{p,w} = 1.857 \times 10^{-9}T^4 - 4.519 \times 10^{-7}T^3$$

$$+4.991 \times 10^{-5}\,T^2 - 2.286 \times 10^{-3}T + 4.214 \qquad \text{Eq. 3-5}$$

$$C_{p,np} = -6 \times 10^{-6}T^2 + 0.0048\,T - 0.2804 \qquad \text{Eq. 3-6}$$

The thermal efficiency of solar collector can be calculated by Eq. 3-6:

$$\eta = \frac{\dot{Q}_U}{I_D A_C} \qquad \text{Eq. 3-7}$$

where η is the efficiency of the parabolic trough, I_D is the direct solar radiation and A_C is the area of the collector. in the case of Concentrating solar collector, the concentrating ratio is added to Eq. 3-7,

$$\eta = \frac{\dot{Q}_U}{I_D\,C\,A_C} \qquad \text{Eq. 3-8}$$

where the concentration ratio is defined as the ratio of the aperture area over the surface area of the receiver.

$$C = \frac{A_a}{A_C} \qquad \text{Eq. 3-9}$$

where A_a is the aperture area. The concentration ratio of the test rig collector is 5.

The solar radiation uncertainty $U_{I_D}$is less than 2%. The uncertainty of mass flow $U_{\dot{m}}$ is less than 1%. Uncertainties for inlet $U_{T_{in}}$and outlet temperatures$U_{T_{out}}$ were less than 0.1 °C. Complex uncertainty U_η was calculated by Eq. 3-8 and was between 1% and 5.2%:

$$U_\eta = \sqrt{\left(\frac{\partial\eta}{\partial\dot{m}_f}U_{\dot{m}}\right)^2 + \left(\frac{\partial\eta}{\partial I_D}U_{I_D}\right)^2 + \left(\frac{\partial\eta}{\partial T_{out}}U_{T_{out}}\right)^2 + \left(\frac{\partial\eta}{\partial T_{in}}U_{T_{in}}\right)^2} \qquad \text{Eq. 3-8}$$

Table 3-2: Parameters of the parabolic trough and test condition

Parameters	Values
Length of the receiver	500 mm
Width of the aperture	250 mm
outer Diameter of the absorber	15 mm
Solar irradiance	1000 W/m^2
Mass flow	0.02 kg/s
Magnetic field intensity	3.14, 6.28 ,10.47mT

Chapter 4. Experimental Study on Ferrofluids Based Parabolic Trough

4.1 Introduction

In this chapter, the ferrofluids based parabolic trough collector with the selective surface absorber (non-direct absorption) and transparent glass tube (direct absorption) has been experimentally studied. The performance of the collector has been carried out under laminar flow conditions. The performance of the collector includes the effect of volume fraction of nanoparticles, magnetic field intensity, Reynolds number, and thermal loss of the collector. The enhancement of heat transfer performance of the ferrofluids based solar collector by using ferrofluids was compared to the performance of the collector using the base fluid (water) as heat transfer medium. Furthermore, the comparison between the selective surface and transparent glass receivers are carried on.

4.2 Background

One of the methods to reduce cost is increasing the heat transfer performance of parabolic trough systems. In case of constant heat flux, increasing the heat transfer performance will decrease the absorber surface temperature and subsequently reduce the receiver's thermal loss particularly at the high operating temperatures [126, 127]. This improvement could be achieved by enhancing the convective heat transfer in the absorber tube. Researchers have tried modifying the surface and the design of the absorber tube to enhance the convective heat transfer [128-132]. Others have used a different kind of heat transfer fluids such as molten salt or nanofluids to improve the performance of heat transfer [133].

Heat transfer can be enhanced by increasing the thermal properties of heat transfer fluid (nanofluids). Nanofluids are illustrating excellent thermo-physical properties are appropriate to enhance the efficiency of any thermal management systems by selecting base fluids with suitable nanoparticle materials, dispersion agents, nanoparticle sizes, and particle volume fraction [134, 135]. Moreover, magnetic nanoparticles in the presence of external magnetic field enhanced heat transfer further compared to nanofluids.

Harvesting the solar energy using nanofluids has been the focus of few researchers. There are two methods to harvest the solar energy when nanofluids are used, which are direct absorber collectors and non-direct absorber collectors. Non-direct absorber collectors are the conventional solar collector with an absorber that has a selective surface to absorb the solar radiation. Direct solar collectors use a transparent receiver to allow nanofluids to absorb the solar radiation. Due to the additional enhancement in the thermophysical properties of ferrofluids in the presence of magnetic field, the author tested the performance of ferrofluids as a heat transfer medium in the innovative parabolic trough solar collector.

4.3 Objectives

The aim of this work is to modify parabolic trough collector design to increase the heat transfer performance by using ferrofluids. In particular, a modified small-scale parabolic trough collector using water-based Fe_3O_4 nanofluids was built, and its efficiency was measured under the different working condition, according to BS EN ISO 9806:2013. The comparison between the heat transfer fluids has been performed in controlled and standard conditions, reducing the possibility of error.

4.4 Thermal performance of parabolic trough

The genialized thermal analyses of a concentrating collector are similar to that of a flat-plate collector. There are two popular methods to analyse the performance of solar collectors. The first is the method used in BS EN ISO 9806:2013 and the second is the method used by ASHRAE standard. Both methods determine the instantaneous efficiency by statistical curve fitting, using the least square method.

ASHRAE standard expresses the useful energy in terms of the energy absorbed by the absorber and the energy loss from the absorber as given by Eq. 4-1:

$$Q_u = A_a F_R \left[I_D \, \eta_{optic} - \frac{U_L}{C} (T_{in} - T_a) \right] \qquad \text{Eq. 4-1}$$

where F_R is the collector heat removal factor, $I_D \, \eta_{optic}$ is the absorbed solar radiation, $\mathrm{U_L}$ is the loss coefficient, C is the concentration ratio and T_a is ambient temperature. The heat removal factor is similar to heat exchanger effectiveness defined as the ratio of the actual heat transfer to the maximum possible heat transfer. The optical efficiency η_{optic} is related to the optical properties of materials used in the parabolic trough, and it is defined as the ratio of solar radiation reaching the absorber to the energy collected from the aperture area. It can be expressed as

$$\eta_{optic} = \left[(\tau\alpha) \varphi \psi \right] \left(1 - A_{f,n} \right) \qquad \text{Eq. 4-2}$$

where $(\tau\alpha)$ is the transmittance-absorptance product, φ is the specular reflectance of the mirror, ψ is the intercept factor [136], the fraction of reflected energy that is directed towards the receiver, $A_{f,n}$ is the ratio of ineffective area due to geometrical effects (e.g., shading to blockages and the receiver, and solar rays reflected from the mirror past the end of the receiver) to the whole aperture of the collector. The heat removal, loss coefficient, and the optical efficiency are used to characterize the collector. Eq. 4-3 is written in terms of an instantaneous efficiency as [87]

$$\eta = \frac{\dot{Q}_U}{I_D A_C} = F_R \eta_{optic} - \frac{F_R U_L}{C} \frac{(T_{in} - T_a)}{I_D} \qquad \text{Eq. 4-3}$$

With a variety of inlet temperature conditions are made for tests, U_L F_R, C and $(\tau\alpha)$ are all constant, a straight line will result from plotting η versus $(T_{in} - T_a)/I_D$ with intercept $F_R \eta_{optic}$. At this point, the inlet temperature of the collector equals the ambient temperature and the collector efficiency at its maximum. The slope $-F_R\,U_L/C$ represents how energy has removed from the collector that nominated as removed energy parameter.

The British standard determines the performance of the collector at different at various heat transfer fluid mean temperature. The instantaneous efficiency is determined as follow:

$$\eta = \eta_0 - a_1 T_m^* - a_2 (T_m^*)^2 \qquad \text{Eq. 4-4}$$

where η_0 is the zero-loss thermal efficiency and T_m^* is the reduced temperature difference as defined in Eq. 4-5:

$$T_m^* = \frac{T_m - T_a}{I_D} \qquad \text{Eq. 4-5}$$

A second order fit was not used if the value for a_2 is negative. If a_2 is negative, the efficiency will increase at higher reduced temperature differences which is not reasonable. Therefore, efficiency can be calculated as follow:

$$\eta = \eta_0 - a_1 T_m^* = \eta_0 - a_1\left(\frac{T_m - T_a}{I_D}\right) \qquad \text{Eq. 4-6}$$

In this section, we used both methods to determine the performance of the parabolic trough. However, to decrease the length of this chapter, we used the ASHRAE method because it is mostly used for parabolic trough collectors. The results from using the British Standard is presented in Appendix A.

4.5 Results and discussion

The thermal performance of the parabolic trough was experimentally investigated. The performance of the parabolic trough collector has been carried out in the University of Nottingham laboratory. The experimental results are introduced in the form of diagrams and equations that describe the collector efficiency versus the inlet temperature parameter $(T_{in} - T_a)/I_D$. The performance of the collector was recorded once the collector reached the second steady state condition (constant outlet temperature).

4.5.1 Ferrofluids based parabolic trough with selective surface receiver

At the steady state condition five data points were recorded. The time between each reading is 1 minute. The average number was used to calculate the efficiency of the collector. The regime of the flow affects the performance of the parabolic trough collector. Therefore, the author pays special attention to the flow, and we make sure we include only the performance of collector in laminar flow. Increasing the water temperature will cause the viscosity to decrease, hence increasing the Reynolds number. The results of Reynolds number above 2000 were neglected.
The performance of ferrofluids as a heat transfer fluid was compared to the performance of water. Moreover, the performance of the collector is compared to the flat-plate solar collector. The comparison to the flat-plate collector and not to parabolic trough collector is due to the low concentration ratio and unglazed receiver used in the experiment. According to both standards, unglazed receivers in concentrating solar collectors with a concentration ratio lower than 10 are considered as a non-concentrated collector.

4.5.1.1 Water and ferrofluids in the absence of external magnetic field

During the test of water as a heat transfer fluid in the ferrofluids parabolic trough collector, the electromagnetic was kept in their location. Hence, the optical efficiency and receiver area for all tests are the same. As shown in Figure 4-1 and Figure 4-2 shows the efficiency of ferrofluids parabolic trough with water. Figure 4-1 shows the performance of the parabolic trough collector with laminar flow using water as a heat transfer fluid with respect to the water mean temperature. The efficiency of the parabolic trough with selective surface tube is 49.4% when water is used, and the mean temperature is very close to the environment T_m^* is 0.00041 °C m^2/W, and with average ambient temperature of 18.84°C. The efficiency declines with increasing the mean temperature. The lowest efficiency obtained was 34% at T_m^* is 0.00957 °C m^2/W. Using Eq. 4-6 the zero-loss collector efficiency, η_0 (η at T_m^*= 0), has been obtained 0.473, as well as a_1 14.289 W/m^2 °C. Compared to the experiment from Colangleo et al. [125] the zero-loss efficiency is close to the present experiment. However, the present experiment has higher thermal loss at higher fluid mean temperature due to the glazed collector used by Colangleo et al. Figure 4-2 illustrate the performance of the parabolic tough collector using water as a heat transfer fluid and corresponding to the water inlet temperature. The efficiency of the parabolic trough with selective surface tube is 49.4% at $(T_{in} - T_a)/I_D$ 0.00006 °C m^2/W. Higher inlet temperature of the water lead to lower efficiency, the lowest efficiency recorded was 34% at $(T_{in} - T_a)/I_D$ 0.00934 °C m^2/W. Based on Eq. 4-3 the value of $F_R\eta_{optic}$ for water is 0.469 and the removed energy parameter $F_R U_L$ is 14.139 W/m^2 °C. The concentrating ratio is equal 1 since the collector is considered as non-concentrated collector. The heat removal factor F_R can be determined since the optical efficiency η_{optic} is known (0.81), $F_R$is equal 0.578. Applying the heat removal factor to the removed energy parameter, the overall heat loss coefficient U_L is 24.47 W/m^2 °C. Compared to the work of Yousefi et al. [96] the present work has lower heat removal factor and lower heat loss coefficient. In general, the performance of the parabolic trough collector in laminar flow conditions is similar to unglazed non-concentrated solar collectors. As showing in Figure 4-2, the performance of conventional parabolic trough collector is usually much better with higher heat removal factors and lower heat loss due to the higher concentration ratio and the envelope cover [137, 138]. Moreover, all the studies on parabolic trough was carried on with turbulent flow. As discussed previously the mass flow effect the performance of the collector. Therefore, to be able to compare the present work with conventional parabolic trough the bigger concertation ratio, glazed receiver, and higher flow rate should be used. The collector reach high working temperature with minimal loss when high concentration ratio is used, but demands higher manufacturing precision [139].

As shown in Figure 4-3 By using Fe_3O_4-water ferrofluids 0.05% as a heat transfer medium with no external magnetic field applied, the highest efficiency obtained was 49.12% at $(T_{in} - T_a)/I_D$ 0.000079 °C m^2/W. The lowest efficiency has been obtained 44.7% at $(T_{in} - T_a)/I_D$ 0.0083 °C m^2/W. The lowest efficiency was determined at inlet temperature, ambient temperatures of 27.11°C and 18.76°C respectively. From linearization of data points, the values of $F_R\eta_{optic}$ and $F_R U_L$were 0.49 and 7.24 respectively. The heat removal factor $F_R$is equal 0.6, and the overall heat loss coefficient U_L is 11.989 W/m^2 °C. As shown in Figure 4-3, the efficiency of low concentrating parabolic trough collector with Fe_3O_4-water ferrofluids is higher than the efficiency of the collector with water. This can be concluded by comparing the heat removal F_R and overall loss coefficient U_L for Fe_3O_4-water ferrofluids and water in Table 4-1, which shows that the heat removal factor for Fe_3O_4-water ferrofluids 0.05% is slightly higher than the heat removal for water by 3.8%. The heat loss coefficient of Fe_3O_4-water ferrofluids 0.05% is much lower than the heat loss coefficient of water by 51%. Therefore, the thermal efficiency of the collector with Fe_3O_4-water ferrofluids 0.05% is higher than the thermal efficiency of the collector with water at higher inlet temperature parameter. The increase in the efficiency is induced by the higher thermo-physical properties of ferrofluids compered to water. In the absence of magnetic field, the major mechanism of thermal conductivity enhancement can be attribute to the stochastic motion and aggregation of the nanoparticles. This Brownian motion will be reliant on fluid temperature, hence, the rate of enhancement, with temperature is fairly explainable in this case. Accordingly, higher temperature leads to the additional speed of particles, and enhance collisions between nanoparticles and the base fluid, result in the enhancement thermal conductivity, hence, the increase in heat transfer at higher operating temperature. It has also been suggested [140] that the non-uniform shear rate of ferrofluids flow across the tube cross section induce both viscosity reduction near the tube wall and movement of particles are responsible for the enhancement in heat transfer.

Table 4-1 Values for the heat removal and overall heat loss coefficient for Fe_3O_4-water ferrofluids and water

Heat transfer fluid type	$F_R\eta_{optic}$	F_RU_L	Heat removal Factor F_R	Heat loss coefficient U_L (W/m^2 °C)
Water	0.469	14.139	0.578	24.47
Fe_3O_4-water ferrofluids 0.05%	0.497	7.24	0.6	11.99
Fe_3O_4-water ferrofluids 0.25%	0.5	40.523	0.62	65.7
Fe_3O_4-water ferrofluids 0.25% with defoamer	0.51	28.427	0.63	45.23
Fe_3O_4-water ferrofluids 0.75%	0.7438	54.197	0.91	59.12

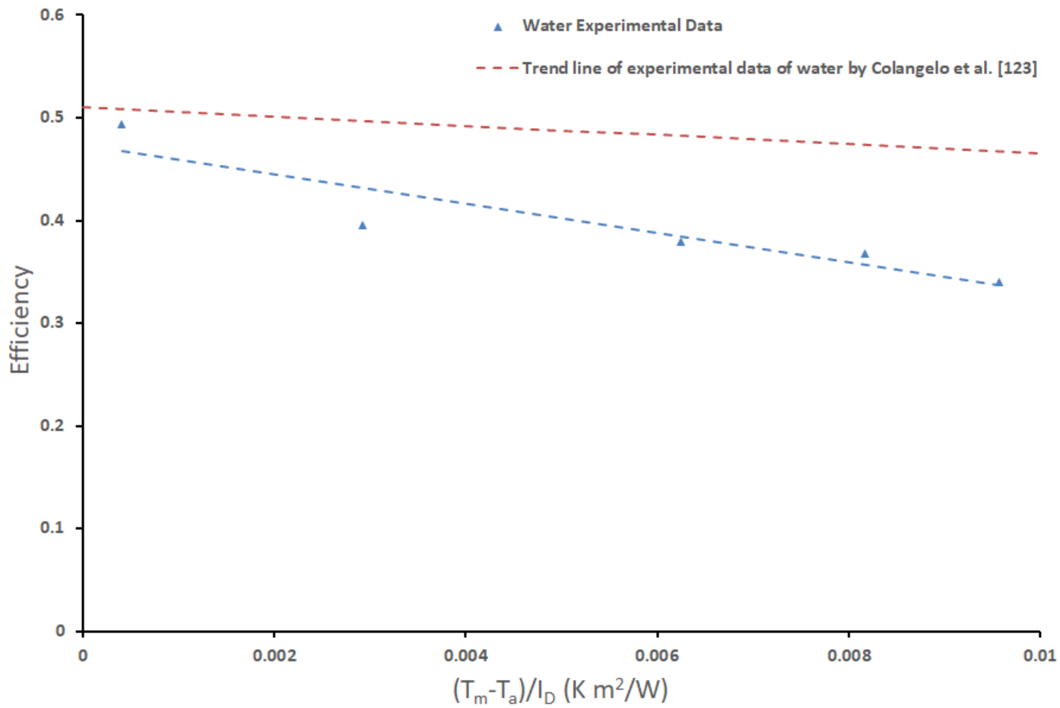

Figure 4-1: Collector efficiency with water as heat transfer fluids and different mean fluids temperature.

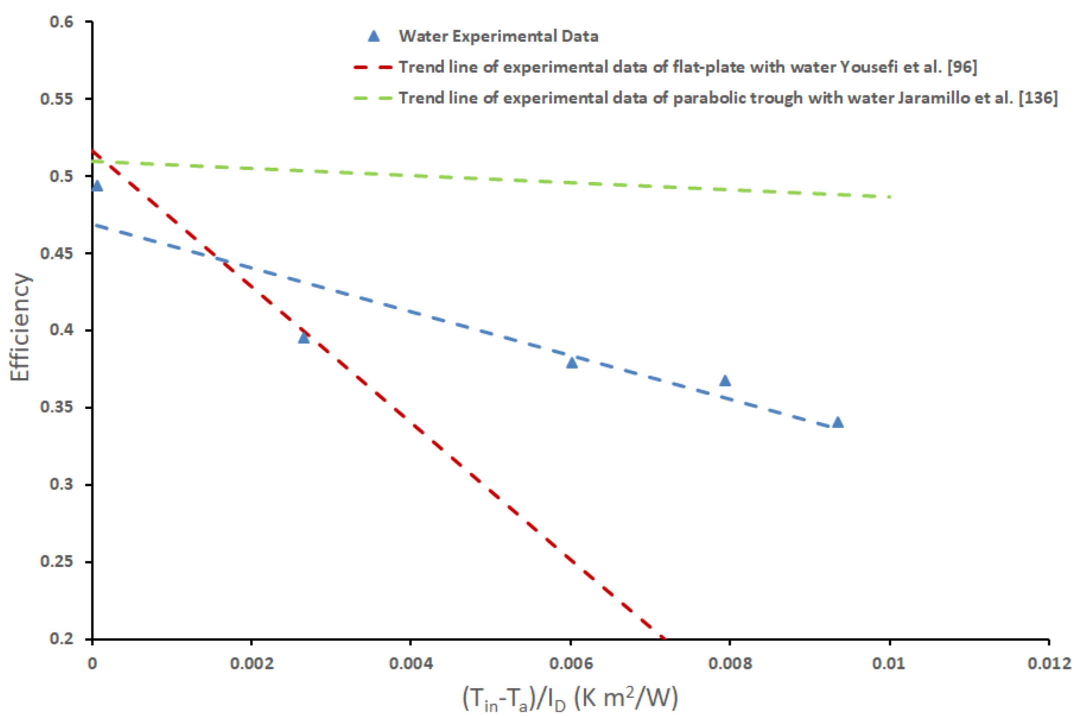

Figure 4-2: Collector efficiency with water as heat transfer fluids and different inlet fluids temperature.

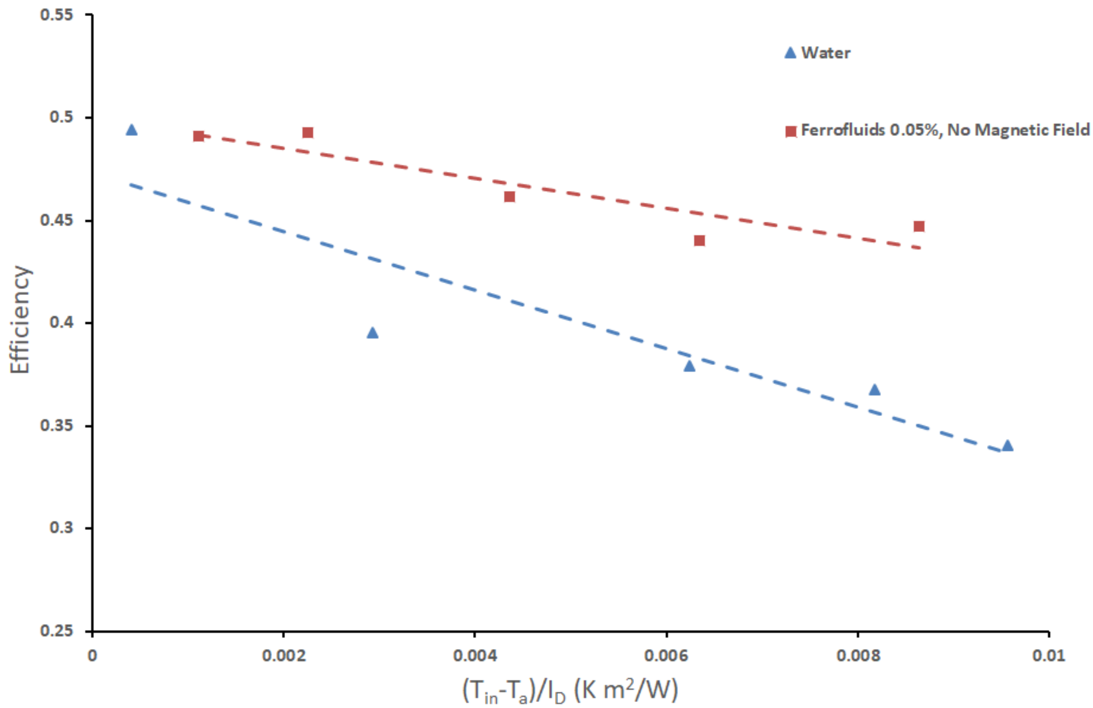

Figure 4-3: Collector efficiency with 0.05% Ferrolfuids as heat transfer fluids and different inlet fluids temperature.

4.5.1.2 Effect of anti-foaming

The effect of different concentration of particles on the collector performance was investigated. Immediately after using a volume fraction higher than 0.05%, the ferrofluids produced a huge amount of foam (bubbles) in the system. SDS is the main reason for the formation of bubbles. Figure 4-5 shows the bubbles in the ferrofluids tank. The bubbles in the receiver will affect the convection heat transfer negatively. Therefore, a defoamer (DF, Antifoam B Silicone Emulsion) was added to suppress the bubble formation. DF concentration was 15% of the weight of the added SDS. The test of ferrofluids with and without defoamer is presented in Figure 4-6. The defoamer improved the performance of the collector. For Fe_3O_4-water ferrofluids 0.25% at inlet temperature parameter $(T_{in} - T_a)/I_D$ 0.00036 °C m^2/W of the collector efficiency was 46.3%. Once the operating temperature raised the efficiency declined to a minimum of 18.3% at $(T_{in} - T_a)/I_D$

0.0067 °C m^2/W. The heat removal factor F_R for Fe_3O_4-water ferrofluids 0.25% is equal 0.62, and the overall heat loss coefficient U_L is 65.7 W/m^2 °C. By adding the defoamer to the Fe_3O_4-water ferrofluids 0.25% there was no foam observed in the tank. Moreover, the performance of the collector improved compared to Fe_3O_4-water ferrofluids 0.25% without defoamer. The efficiency marginally increased by 2% when the inlet temperature is close to the ambient temperature. In contrast, the efficiency of the collector significantly increased by 80% when the inlet temperature is 6°C above ambient temperature. For Fe_3O_4-water ferrofluids 0.25% with defoamer at inlet temperature parameter $(T_{in} - T_a)/I_D$ 0.00038 °C m^2/W of the collector efficiency was 49.7%, and with lowest efficiency of 35.7% at $(T_{in} - T_a)/I_D$ 0.0042 °C m^2/W. The heat removal factor F_R for Fe_3O_4-water ferrofluids 0.25% is equal 0.63, and the overall heat loss coefficient U_L is 45.23 W/m^2 °C. Without defoamer, the overall heat loss coefficient U_L of Fe_3O_4-water ferrofluids 0.25% is 45%higher than with ferrofluids containing defoamer. Since foam is generated by increasing the volume fraction of nanoparticles in the fluid, defoamer was added to Fe_3O_4-water ferrofluids 0.75% before using it in the solar collector experiment.

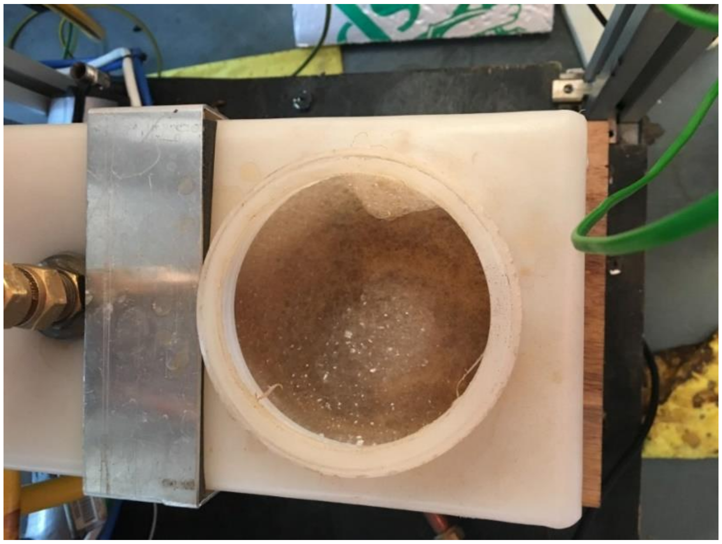

Figure 4-4: Foam formation in ferrofluids tank when Fe_3O_4-water ferrofluids 0.25% pumped through the system.

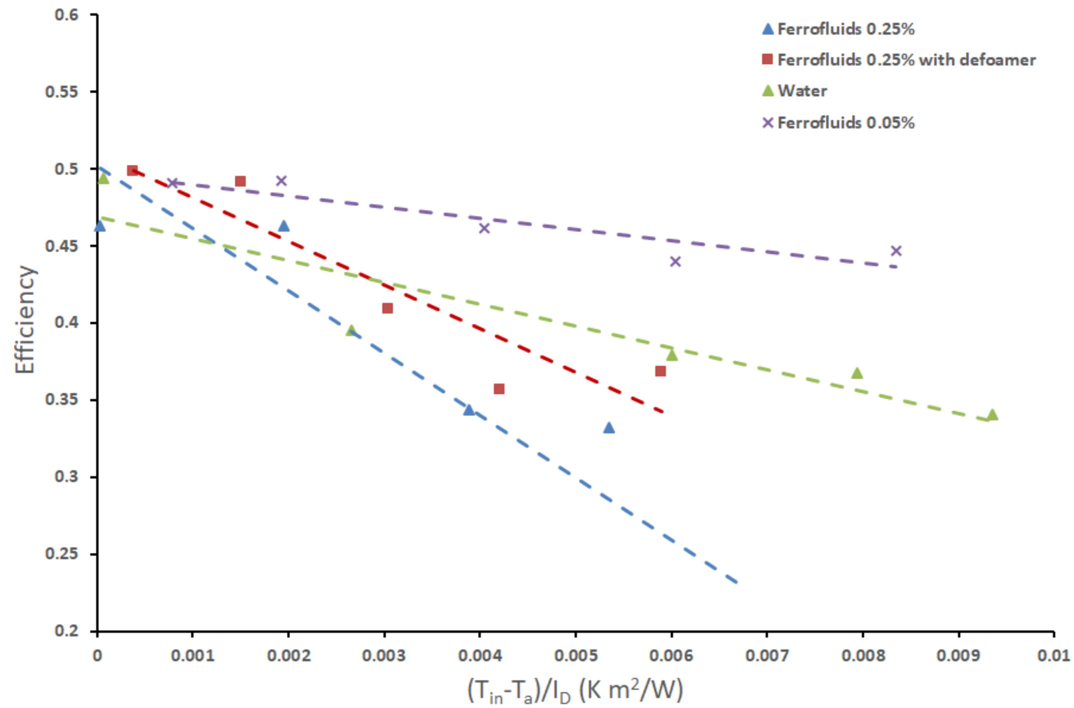

Figure 4-5: Collector efficiency with Fe_3O_4-water ferrofluids 0.25% with and without defoamer as heat transfer fluids and different mean fluids temperature.

4.5.1.3 Effect of volume concentration

By comparing the efficiencies of Fe_3O_4-water ferrofluids with three different concentration, as illustrated in Figure 4-6, the efficiency of 0.05% ferrofluids for a wide range of temperature differences is higher than that at 0.25% and 0.75%. Ferrofluids with volume fraction of 0.75% showed the highest efficiency of 72% at $(T_{in} - T_a)/I_D$ 0.0001 °C m^2/W. However, as the operating temperature increases the efficiency dropped dramatically to reach 35.29% at $(T_{in} - T_a)/I_D$ 0.0082 °C m^2/W. As shown in Table 4-1 ferrofluids with 0.75% volume fraction has the highest heat removal factor F_R of 0.91 and the worst overall heat loss coefficient U_L with the value of 59.12 W/m^2 °C. The heat removal, increased with increasing the concentration of particles. However, the overall heat loss also increases by increasing the concentration of particles as shown in Figure 4-6. This is contributed to the non-Newtonian behaviour of ferrofluids at higher concentration. At a volume fraction of 0.05% the ferrofluids behaves as newton fluid, but increasing the volume fraction, the fluid behaves as non-Newtonian fluid (volume fractions of 0.25% and 0.75%). As discussed in chapter 2, with concentration below 1% by weight, the fluids can be considered as Newtonian fluid and the viscosity dependence can be neglected. The shear rate in this experiment is 7.7 1/s, in such low shear rate the viscosity of the fluid can reach to 7 times higher than the based fluid. The variation of thermal conductivity with shear rate can be important, but it is often disregarded under the assumption that the variations of the viscosity and the effect of elasticity on the flow field, and hence on the thermal field, are much stronger and essentially determine the non-Newtonian nature of the heat transfer characteristics. In experimental studies the results are often correlations for the Nusselt number, in which the shear rate dependence of is eventually considered as an increase or decrease in heat transfer, although in a less physically meaningful way. All experimental studies on ferrofluids thermal conductivity were conducted at steady state. Furthermore, convection and conduction heat transfer are contesting. The heat transfer coefficient could be approximately demonstrated as k/dt where k and dt are the thermal conductivity of the nanofluids and thickness of thermal boundary layer, respectively. It may be explained that with increasing nanoparticles volume fraction from 0.05% to 0.75% the enchantment of thermal conductivity is smaller than the increase in the thermal boundary layer and therefore the heat transfer is reduced. This conclude that increasing the volume fraction of nanoparticles in low shear rate will lead to deterioration in heat transfer performance. Ideally a ferrofluids that behaves as Newtonian fluids at low shear rate will be more suitable to use in laminar flow heat transfer applications. The problem with higher concentration ferrofluid rheological behaviour can be solved by modifying the pH of the ferrofluids. At the University of Nottingham, we studied the effect of colloidal of pH on the viscosity of Fe_3O_4 ethylene glycol - water nanofluid. The results of our tests showed that at neutral pH, the best colloidal stability was obtained. The viscosity barely changed with the shear rate despite the variances in particle concentration and temperature. After being kept for one week, the nanofluid still exhibited Newtonian behaviour. However, the results of the heat transfer performance have not been studied yet. The viscosity of modified Fe_3O_4 nanofluids was studied at different pH. The particle volume fraction was fixed at 0.69 %; temperature was also set at 30 ºC. As shown in Figure 4-7 a, it is very clear that the nanofluids at pH of 2.5 and 3.0 were totally Non-Newtonian fluids. The viscosity decreased by 40 % as shear rate increased to 2500 s^{-1} (Figure 4-7b). After pH increased to 3.5 and 4.0, the decline of viscosity stopped at 800 s^{-1}, and the decrease percentages were both around 8% (Figure 4-7b). At pH of 5, 7 and 9, the nanofluid behaved as a Newtonian fluid. The decrease percentages were very close to 0 (Figure 4-7b). RSDs of viscosities obtained at different shear rates were all lower than 1% for these three pH values, suggesting the viscosity was independent of shear rate. From the discussion above, we have known that when pH was lower than 5, the colloidal stability of modified particles was improved with increasing the pH. Therefore, a better colloidal stability will make the nanofluid behave more like a Newtonian fluid. However, higher volume fraction of nanoparticles may still decrease the heat transfer performance due to the higher increase of thickness of thermal boundary layer compared to the thermal conductivity.

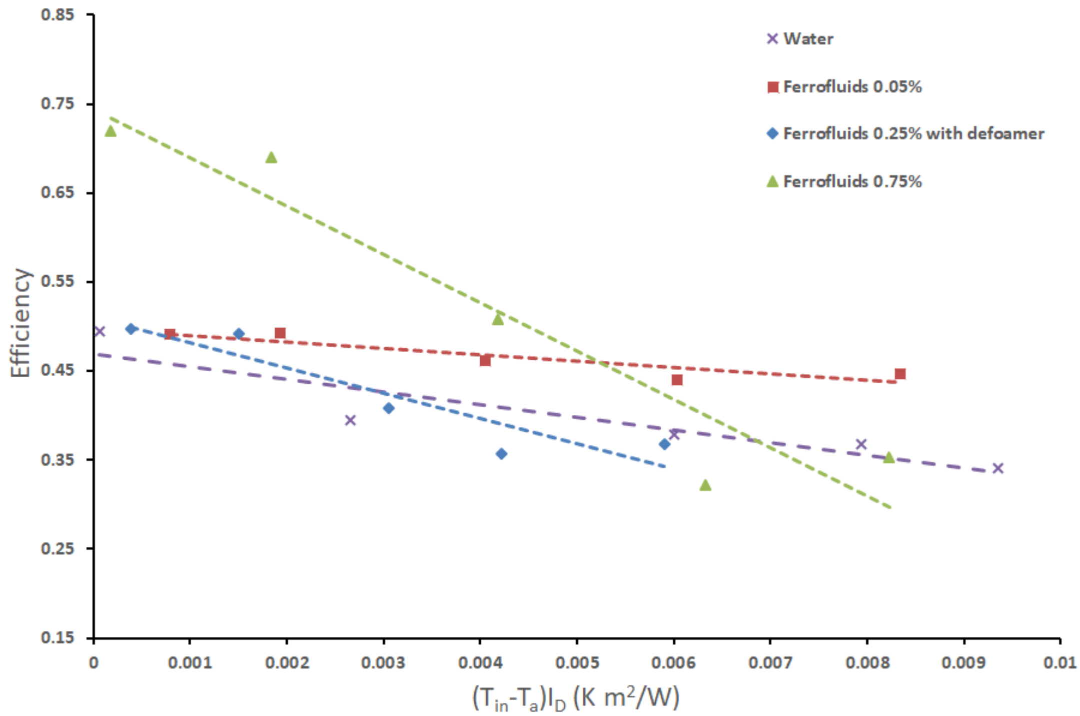

Figure 4-6: Collector efficiency with various concentration of Ferrofluids.

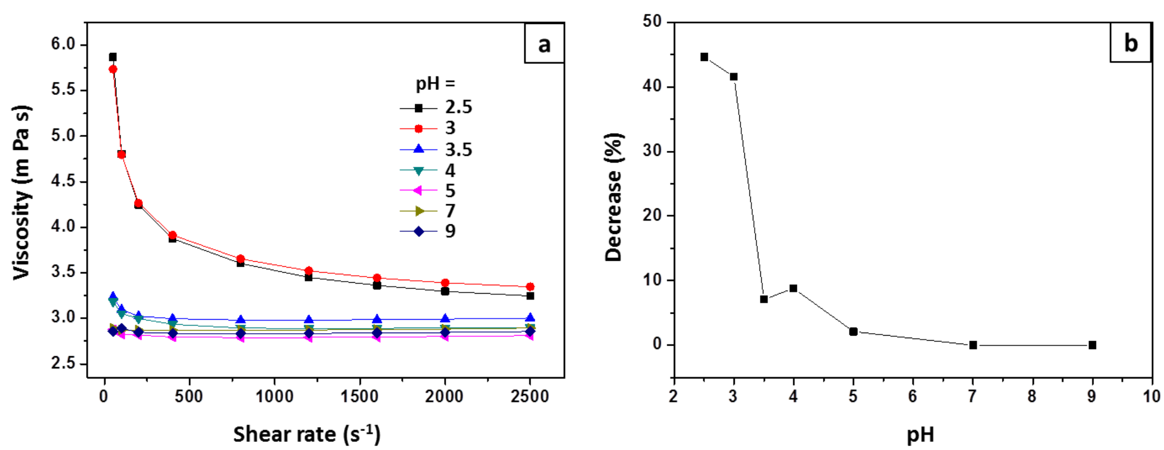

Figure 4-7 (a) Viscosity as a function of shear rate for CA modified Fe_3O_4 nanofluids at different pH. (b) Decrease percentage of viscosity at each pH.

4.5.1.4 Effect of external magnetic field on the collector efficiency

As showing the previous section, using very low concentration of Fe_3O_4 nanofluid has a positive effect on the efficiency of the parabolic trough collector. In this section, the effect of external magnetic field on the efficiency of the solar collector is investigated. The magnetic field direction is parallel to the incoming stream. The external magnetic field intensity was changed by regulating the current of the DC power supply. The external magnetic field intensities at the centre of the electromagnet were 3.14 mT, 6.28 mT, 10.47 mT. For every external magnetic field intensity, the efficiency of the collector was graphed against the temperature parameter, $(T_{in} - T_a)/I_D$. To assure the external magnetic field are not affecting the measurements, water was used as a heat transfer fluid to test the performance of the solar collector in the presence of the external magnetic field. As shown in Figure 4-8 the performance of the water has not changed in the presence of the magnetic field. Consequently, there is no effect of the external magnetic field on the measurements of temperature and the flow. The efficiencies of the collector in the presence of external magnetic fields for 0.05% ferrofluids are shown in Figure 4-9 with external magnetic intensity of 3.14 mT, the highest efficiency value, 50.7, has been obtained at $(T_{in} - T_a)/I_D$of 0.000791 °C m^2/W, which corresponds to an inlet temperature of 20.72 °C, and an ambient temperature of 19.49 °C. Moreover, at $(T_{in} - T_a)/I_D$of 0.00835 °C m^2/W the lowest efficiency value has been obtained, 44%. In this case, the inlet temperature and ambient temperature were 27.71 °C and 18.76 °C, respectively. Using Eq. 4-6 the heat removal factor F_R of 0.63 and the overall heat loss coefficient U_L with the value of 10.8 W/m^2 °C. The efficiency of the solar collector with 0.05% ferrofluids in the presence of external magnetic field intensity of 6.28 mT has the maximum value of 69.24% at $(T_{in} - T_a)/I_D$of 0.000266 °C m^2/W, with inlet temperature and ambient temperature of 22.46 °C and 22.195 °C, respectively. The lowest efficiency obtained was 60.6% at $(T_{in} - T_a)/I_D$of

0.00413 °C m^2/W, with inlet temperature and ambient temperature of 26.2 °C and 22.07 °C respectively. The heat removal factor F_R for Fe_3O_4-water ferrofluids with 6.28 mT external magnetic field is 0.85 and the overall heat loss coefficient U_L with the value of 11.23 W/m^2 °C. Finally, the efficiency of the solar collector with 0.05% ferrofluids in the presence of external magnetic field intensity of 10.47 mT showed a maximum value of 69.3 % at $(T_{in} - T_a)/I_D$ of 0.00066 °C m^2/W, with inlet temperature and ambient temperature of 20.26 °C and 19.59 °C respectively. The lowest efficiency reached was 63.7% at $(T_{in} - T_a)/I_D$of 0.0082 °C m^2/W, with inlet temperature and ambient temperature of 27.9 °C and 19.66 °C respectively. The heat removal factor F_R for Fe_3O_4-water ferrofluids with 6.28 mT external magnetic field is 0.847 and the overall heat loss, coefficient U_L with the value of 8.63 W/m^2 °C. A comparison of the results, shown in Figure 4-9, indicates the of the performance of the collector improved due to the presence of external magnetic field when Fe_3O_4-water was used as a heat transfer medium. By comparing the heat removal F_R and overall loss coefficient U_L for Fe_3O_4-water ferrofluids 0.05% at different external magnetic field intensity, Table 4-2, which shows that the heat removal factor for 3.14 mT external magnetic field intensity is slightly higher than the heat removal of Fe_3O_4-water ferrofluids 0.05% in the absence of external magnetic field by 5%. The heat loss coefficient for 3.14 mT external magnetic field intensity is slightly lower than the heat loss coefficient of Fe_3O_4-water ferrofluids 0.05% in the absence of external magnetic field by 10%. For external magnetic intensity of 6.28 mT and 10.47 mT the heat removal factor improved by 41.3%, 40%, and the overall heat loss coefficient by 6%, 38% respectively. Figure 4-10 illustrate the change of the heat removal and overall heat loss of the collector with increasing the external magnetic field intensity. Increasing external magnetic intensity enhance the performance of the collector. At low external magnetic intensity, the heat removal has little change. Thereafter, the heat removal increases and reach a maximum of 0.692 and slightly decrease afterwards. The highest heat removal factor was observed from 6,28 mT and the lowest overall heat loss coefficient was obtained from 10.46 mT. The overall heat loss decreased by increasing the external magnetic field intensity. The little to no change the heat removal factor is similar to the behaviour of thermal conductivity in the presence of the external magnetic field, were the thermal conductivity reaches a the saturation point [123]. The enhancement of the performance of the collector is due to the enhancement of thermal conductivity of ferrofluids in the presence of external magnetic field. The effective heat transport through the aggregate of nanoparticles is the main reason for the enhancement. The nanoparticles in the absence of a field are in Brownian motion as the thermal energy excels the magnetic dipolar attraction. In the presence of magnetic field, the nanoparticles start to form chain-like structure along the orientation of the magnetic field. As the magnetic field intensity increases, the chain length also extends. As the nanoparticles starts to form aggregates of larger size or chains, the convection velocity decreases extremely when the nanoparticles form large size clusters or chains, due to the cubic reliance on the nanoparticle size or the aspect ratio of the long chain. Hence, the Brownian motion is dropped as the chain length extends. Moreover, the distance between the nanoparticles inside the chain reduces with raising the magnetic field, because the magnetic attraction becomes stronger than the repulsion force. The formation of linear chain- like structure can lead to the enhancement of thermal conductivity and surpass the Maxwell due to percolation currents that favour a parallel mechanism of conduction. The distribution of chains in the fluid in the presence of external magnetic field are well organised. This leads to the enhanced conduction through the paths that favour parallel mechanism of conduction. Increasing the magnetic field intensity leads to the formation of bigger chains with larger distance between them. Therefore, the enhancement decrease at high magnetic field intensity [42].

Table 4-2 Values for the heat removal and overall heat loss coefficient for Fe_3O_4-water ferrofluids and water.

Heat transfer fluid type	$F_R\eta_{optic}$	F_RU_L	Heat removal Factor F_R	Heat loss coefficient U_L (W/m^2 °C)
Water	0.469	14.139	0.578	24.47
Fe_3O_4-water ferrofluids 0.05%	0.497	7.24	0.6	11.99
Fe_3O_4-water ferrofluids 0.05%, 3.14 mT	0.52	6.872	0.64	10.8
Fe_3O_4-water ferrofluids 0.05%, 6.28 mT	0.692	9.59	0.85	11.24
Fe_3O_4-water ferrofluids 0.05%, 10.47 mT	0.687	7.3314	0.85	8.63

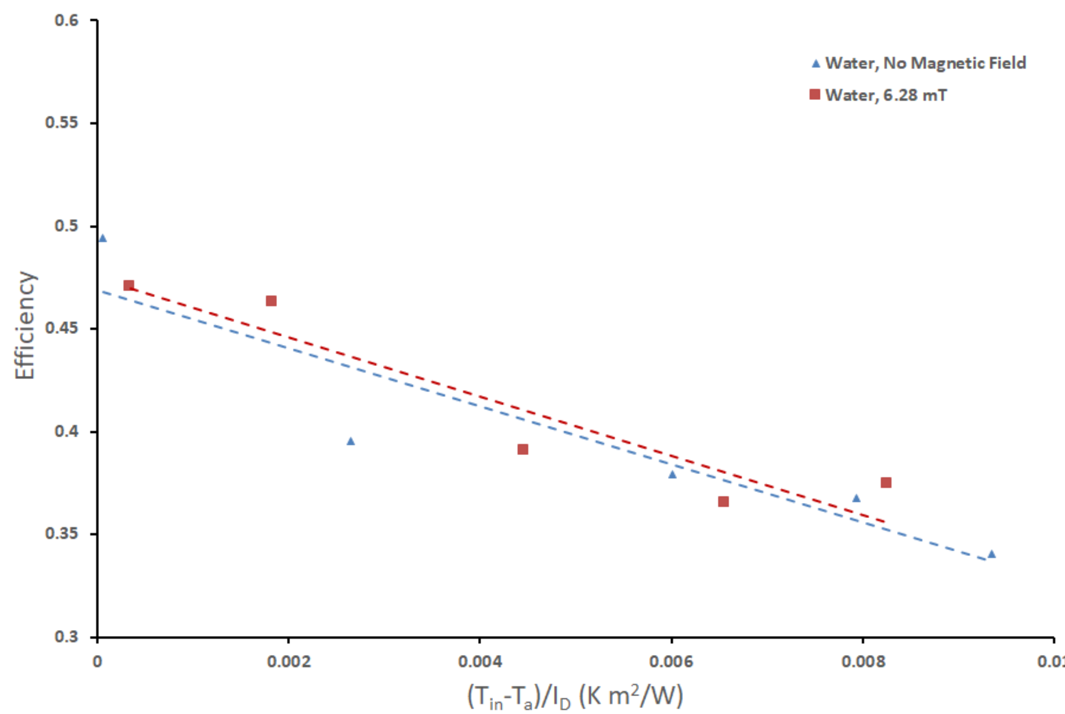

Figure 4-8: Collector efficiency with water as heat transfer fluids with and without the presence of external magnetic field.

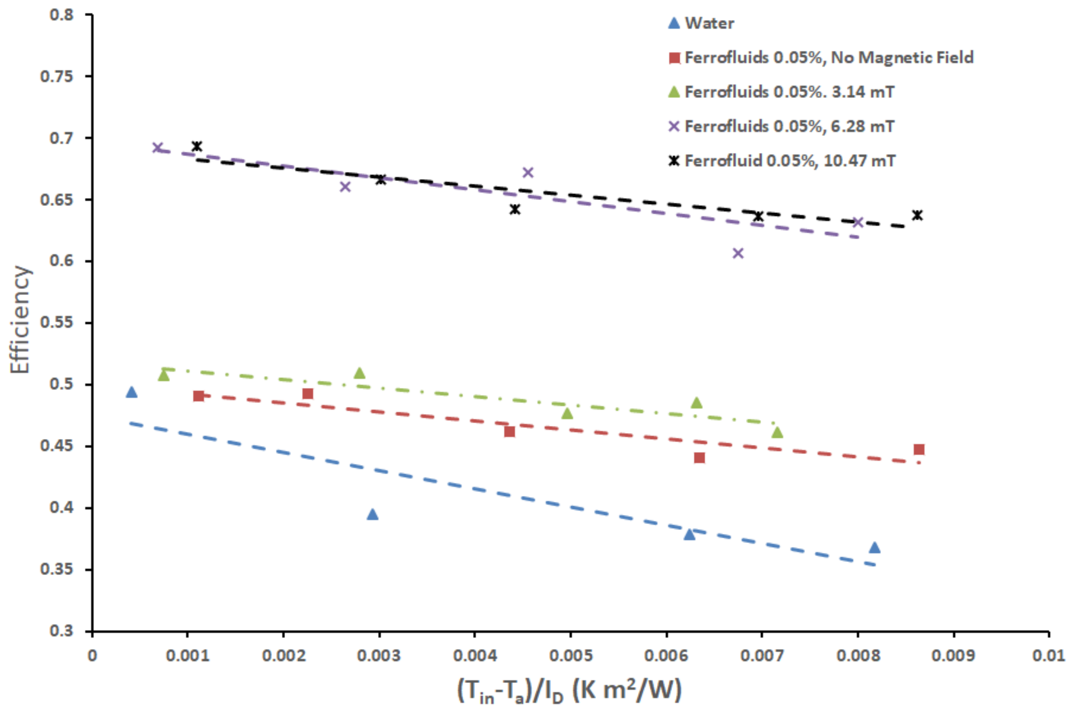

Figure 4-9: Collector efficiency with 0.05% in the presence of external magnetic field and different inlet fluids temperature.

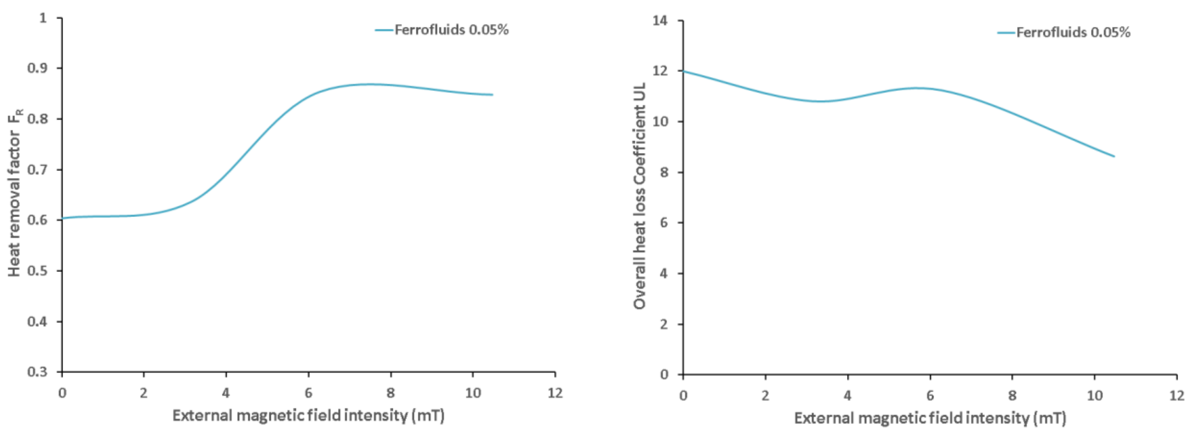

Figure 4-10: Heat removal factor and overall heat loss coefficient of a solar collector with ferrofluids 0.05% in the presence of external magnetic.

The efficiencies of the collector in the presence of external magnetic fields for 0.25% are shown in Figure 4-11 Similar to ferrofluids 0.05%, the efficiency of the collector using ferrofluids 0.25% improved in the presence of the external magnetic field in contrast to the efficiency with the absence of the external magnetic field. With the external magnetic intensity of 3.14 mT, the highest efficiency value, 52.78, has been obtained compared to 49% in the absence of an external magnetic field. The lowest efficiency value has been obtained 34.69%. The highest collector efficiency observed for the external magnetic intensity of 6.28 mT, and 10.47 mT were 64.1% and 68.86%, respectively; the lowest efficiencies recorded were 46% and 49%. From the trend line, it's clear that the fluid still behaves as a non-Newtonian fluid. The performance of solar collector using ferrofluids 0.25% with an external magnetic field intensity of 6.28 mT and 10.47 mT is higher than the base fluid at the experimental reduced temperature parameter. Using Eq. 4-3 the heat removal factor $F_R$and the overall heat loss coefficient U_L are obtained and presented in Table 4-3. With raising the intensity of external magnetic intensity, the heat removal factor increases with similar behaviour to ferrofluids with volume fraction of 0.05%, the improvement is low at low intensity and reaches a saturation at higher intensity.

Table 4-3 Values for the heat removal and overall heat loss coefficient for 0.025% Fe_3O_4-water ferrofluids and water.

Heat transfer fluid type	$F_R\eta_{optic}$	F_RU_L	Heat removal Factor F_R	Heat loss coefficient U_L (W/m^2 °C)
Water	0.469	14.139	0.578	24.47
Fe_3O_4-water ferrofluids 0.25%	0.51	28.427	0.63	45.23
Fe_3O_4-water ferrofluids 0.25%, 3.14 mT	0.56	30.612	0.69	44.4
Fe_3O_4-water ferrofluids 0.25%, 6.28 mT	0.65	25.491	0.79	31.9
Fe_3O_4-water ferrofluids 0.25%, 10.47 mT	0.66	24.03	0.80	26.69

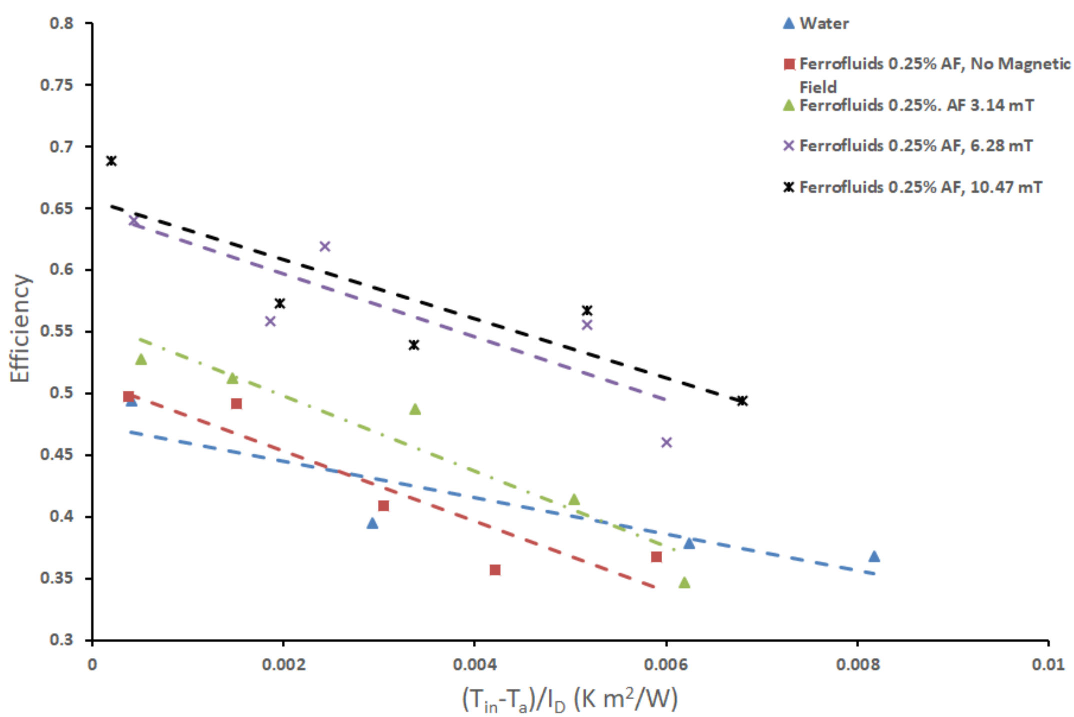

Figure 4-11: Collector efficiency with 0.25% in the presence of external magnetic field and different inlet fluids temperature.

The efficiencies of the collector in the presence of external magnetic fields for 0.75% are shown in Figure 4-12 Similar to 0.05% and 0.25% ferrofluids, the efficiency of the collector using 0.75% ferrofluids improved in the presence of the external magnetic field in contrast to the efficiency with the absence of the external magnetic field. With the external magnetic intensity of 3.14 mT, the highest efficiency value, 72.68, has been obtained compared to 49% in the absence of an external magnetic field. The lowest efficiency value has been obtained 34 %. The highest collector efficiency observed for the external magnetic intensity of 6.28 mT, and 10.47 mT were 78.5% and 78.86% respectively; the lowest efficiencies recorded were 46% and 49%. From the trend line, it's clear that the fluid still behaves as a non-Newtonian fluid. The performance of solar collector using 0.25% ferrofluids with an external magnetic field intensity of 6.28 mT and 10.47 mT is higher than the base fluid at the experimental reduced temperature parameter. Using Eq. 4-3 the heat removal factor $F_R$and the overall heat loss coefficient U_L are obtained and presented in Table 4-4. With raising the intensity of external magnetic intensity, the heat removal factor increases with similar behaviour to 0.05% ferrofluids, the improvement is low at low intensity and reaches a saturation at higher intensity.

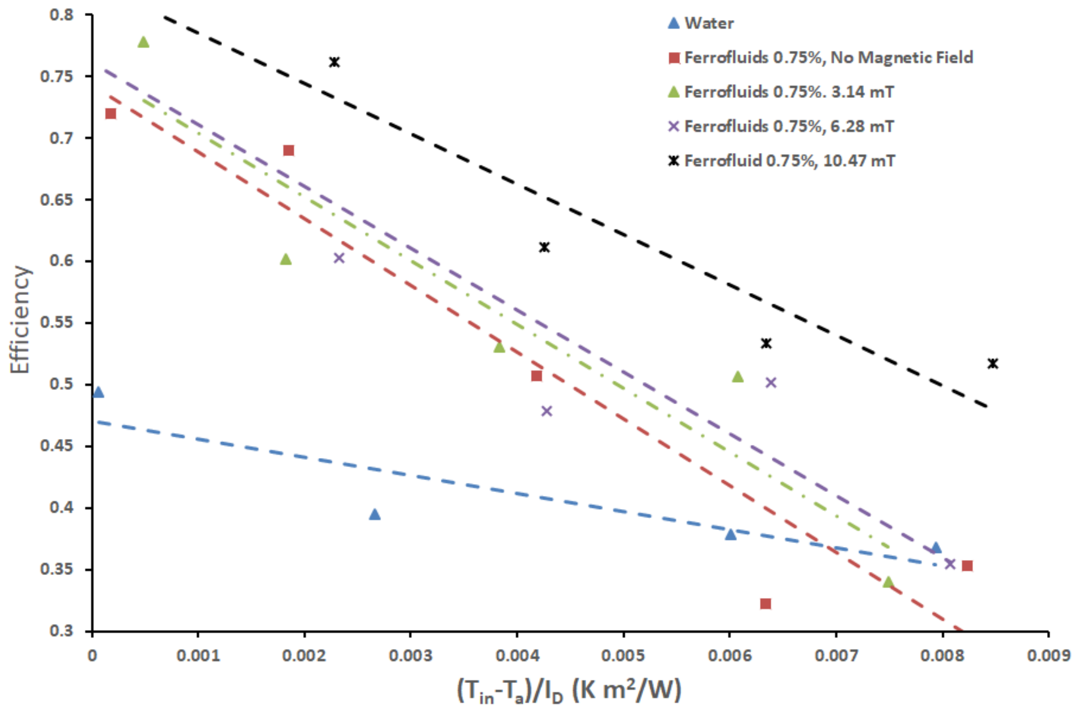

Figure 4-12: Collector efficiency with 0.75% in the presence of external magnetic field and different inlet fluids temperature.

Table 4-4 Values for the heat removal and overall heat loss coefficient for 0.75% Fe_3O_4-water ferrofluids and water.

Heat transfer fluid type	$F_R\eta_{optic}$	F_RU_L	Heat removal Factor F_R	Heat loss coefficient U_L (W/m^2 °C)
Water	0.469	14.139	0.578	24.47
Fe_3O_4-water ferrofluids 0.75%	0.743	54.197	0.63	45.23
Fe_3O_4-water ferrofluids 0.75%, 3.14 mT	0.753	51.617	0.69	44.4
Fe_3O_4-water ferrofluids 0.75%, 6.28 mT	0.761	50.193	0.79	31.9
Fe_3O_4-water ferrofluids 0.75%, 10.47 mT	0.8139	38.571	0.80	26.69

4.5.1.5 Effect of magnetic field orientation

As discussed in chapter 2 and 3 the magnetic field gradient affects the heat transfer when ferrofluids are used as a heat transfer medium. In this section, the effect of magnetic field gradient on the performance of solar collector is discussed. In the previous section showed the performance of ferrofluids in the presence of magnetic field parallel to the incoming stream direction, Figure 4-13 a). As shown in Figure 4-13 b) the other direction investigated was when the magnetic field gradient opposite to the incoming stream. The results of using ferrofluids with the volume fraction of 0.05% in the presence of external magnetic field oriented in the opposite direction of the flow are showing in Figure 4-14 the results showed that the performance of the collector decrease and became less than the base fluid. With the external magnetic intensity of 3.14 mT, the efficiency of the collector at low reduced temperature parameter is lower than water, and ferrofluids 0.05% in the absence of magnetic field by 37.6%. And 36.9% respectively. The performance aggravates with higher reduced temperate parameters to reach a maximum decay by 60% compared to water. The linearization of data produces a heat removal factor F_R of 0.41 and the overall heat loss coefficient U_L with the value of 41.8 W/m^2 °C. Raising the external magnetic intensity made the performance of the collector worst. Compared to water, the collector efficiency decreased by 45% at reduced temperature parameter close to zero. The efficiency decreased rapidly reaching a minimum of 2% at $(T_{in} - T_a)/I_D$of 0.008 °C m^2/W, where water had an efficiency of 34% around the same reduced temperature parameter. The heat removal factor F_R of 0.43 and the overall heat loss coefficient U_L with the value of 94.6 W/m^2 °C. The results clearly identify that the performance of the collector is superior with a magnetic field gradient parallel to the flow. These phenomena were explained in literature [141, 142]. In case the magnetic field oriented parallel to the flow, due to the kelvin force, the auxiliary static pressure gradient will accelerate the ferrofluids flow and enhance the heat transfer between the receiver surface and the ferrofluid. On the other hand, if the magnetic field gradient is opposite to the flow direction of the ferrofluids, the magnetic pressure difference will hinder the main flow and the flow velocity in the pipe decreases, the boundary layer thickened, and the heat transfer between the ferrofluids and the surface is descended.

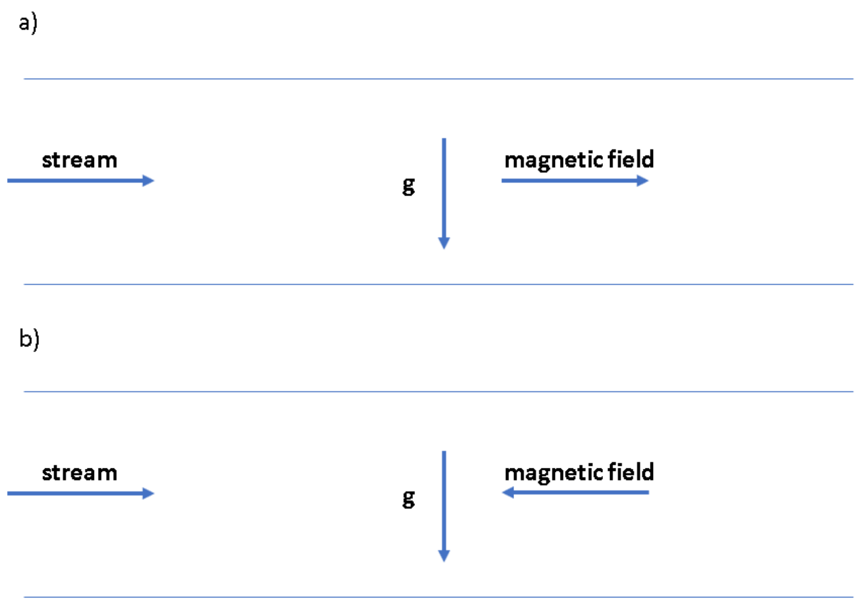

Figure 4-13: Orientation of the magnetic field gradient a) parallel to the flow b) opposite to the flow.

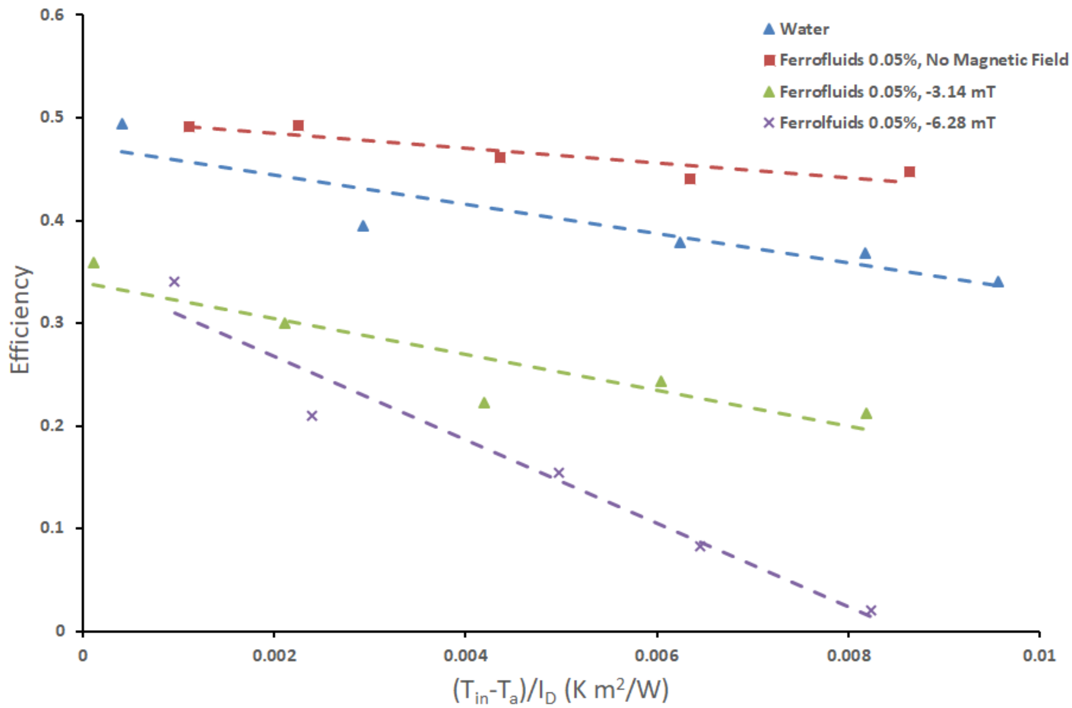

Figure 4-14: Solar collector efficiency with ferrofluids 0.05% in the presence of external magnetic field oriented opposite to the flow.

4.5.2 Ferrofluids parabolic trough with transparent glass receiver

The optical and thermos-physical properties of ferrofluids could be beneficial to design a solar collector with minimum energy losses. The direct absorption collector supports the incoming solar irradiance to be absorbed and scattered by the nanoparticles found in the heat transfer fluid. A transparent glass tube was used to allow the ferrofluids to absorb the entire solar irradiance.

4.5.2.1 Water and ferrofluids in the absence of external magnetic field

As Figure 4-15 indicates the deviations of the collector efficiency with water as a heat transfer medium versus the reduced temperature parameters, $(T_{in} - T_a)/I_D$. The characteristic parameters of the solar collector are illustrated by the fitting the experimental data with a linear equation. The efficiency of the parabolic trough with transparent glass tube is 9.47% at $(T_{in} - T_a)/I_D$ 0.00023 °C m^2/W. Higher inlet temperature of the water cause lower efficiency, the lowest efficiency recorded was 0.3% at $(T_{in} - T_a)/I_D$ 0.0059 °C m^2/W. Based on Eq. 4-3 the value of $F_R\eta_{optic}$ for water is 0.098 and the removed energy parameter $F_R U_L$ is 15.544 W/m^2 °C. The optical efficiency η_{optic} includes the absorption and transmittance factor of the fluid, which is unknown. Compared to selective surface receiver the water has low optical properties hence the low collector efficiency when water is used in direct absorption collector. $F_R\eta_{optic}$ was 376% higher when selective surface was used.

Figure 4-16 compares the efficiency of the parabolic trough collector for water and Fe_3O_4-water ferrofluids with the volume fraction of 0.05%. As shown in Table 4-5, the $F_R\eta_{optic}$ and $F_R U_L$ values for ferrofluids were 0.227 and 6.266, respectively. $F_R\eta_{optic}$ increased by 131% and $F_R U_L$ decreased by 146% compared to water. However, the parabolic trough efficiency with the transparent receiver is lower than the efficiency with selective surface receiver used in the previous section (non-direct receiver). The low efficiency is due to low optical thickness caused by the low volume fraction of nanoparticles and small diameter of the receiver (15 mm). The solar irradiance is not completely absorbed by the nanoparticles and some of the solar irradiance is transmitted through the ferrofluids. The optical thickness also known as optical depth is defined as how opaque the fluid is to the radiation passing through it. The optical thickness is function of the absorption coefficient of the nanoparticles along a path. The absorption coefficient also known as extension coefficient increases linearly with the increase of the volume fraction. To achieve the highest efficiency of the system an optimum optical thickness of the receiver should be determined. The optimum optical thickness for the receiver can be achieved by changing the diameter of the receiver or changing the volume fraction of nanoparticles. In this work, the diameter of the glass tube kept constant and changed the volume fraction.

Table 4-5: Values for the heat removal and overall heat loss coefficient for Fe_3O_4-water ferrofluids and water.

Heat transfer fluid type	Non-direct absorption		Direct absorption	
	$F_R\eta_{optic}$	F_RU_L	$F_R\eta_{optic}$	F_RU_L
Water	0.469	14.139	0.098	15.44
Fe_3O_4-water ferrofluids 0.05%	0.497	7.24	0.227	6.26
Fe_3O_4-water ferrofluids 0.25%	0.51	28.427	0.37	5.134
Fe_3O_4-water ferrofluids 0.75%	0.7438	54.197	0.63	10.537

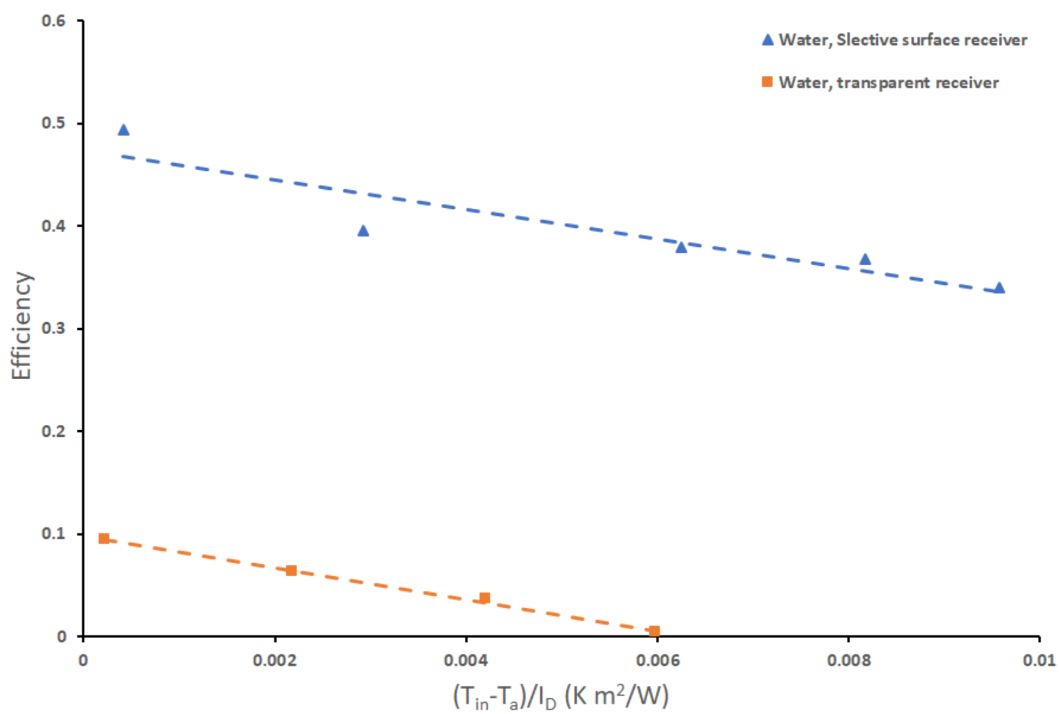

Figure 4-15: Solar collector efficiency with selective surface absorber and transparent glass absorber.

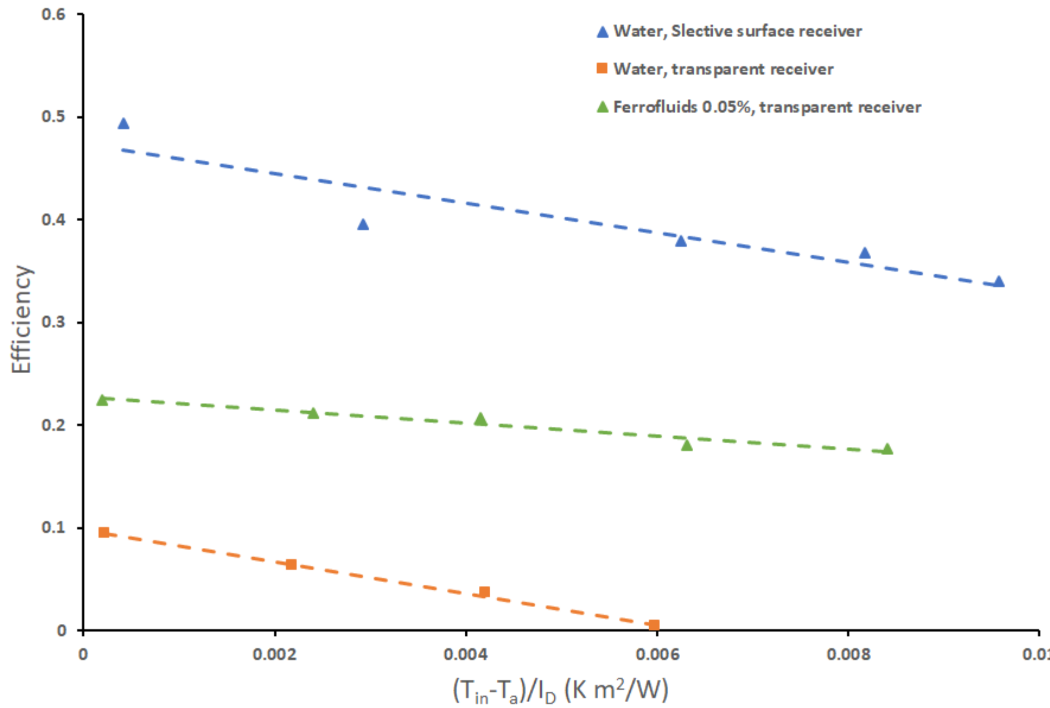

Figure 4-16: Solar collector efficiency of water and 0.05% ferrofluids with transparent glass absorber.

4.5.2.2 Effect of Volume concentration

Figure 4-17 illustrates the effect of volume fraction of ferrofluids on the efficiency of the collector versus the reduced temperature $(T_{in} - T_a)/I_D$. It is found that the of the absorbed energy parameter $F_R\eta_{optic}$ for the collector at 0.75% is higher than the other cases and the absorbed energy parameter for 0.05% is the lowest. The absorbed energy parameter increases by increasing the volume fraction of ferrofluids. As shown in Table 4-6 absorbed energy parameter of selective surface receiver in all cases is still higher than the transparent glass receiver, but compared to selective surface receiver with water, the transparent glass with ferrofluids concentration of 0.75% volume fraction is higher by 34%. Moreover, the direct absorption showed lower removed energy parameter compared to direct absorption receiver. The lowest removed energy parameter observed was for Fe_3O_4-water ferrofluids 0.25%, and the highest was for Fe_3O_4-water ferrofluids 0.75%.

The author concludes that rising the volume concentration of the ferrofluids improve the absorption coefficient and increase the optical thickness. However, increasing the optical thickness further will lead to absorption of incoming solar irradiance in a thin layer close to the surface of the receiver. This will induce the thermal energy loss to the environment. A higher collector efficiency could be achieved by increasing the receiver diameter. The heat can be generated within the receiver by bigger diameter. The solar irradiance absorbed by the suspended nanoparticles as it travels through the fluid. Hence, for solar collector with a greater diameter, the amount of incident solar radiation absorbed by the ferrofluids will be higher.

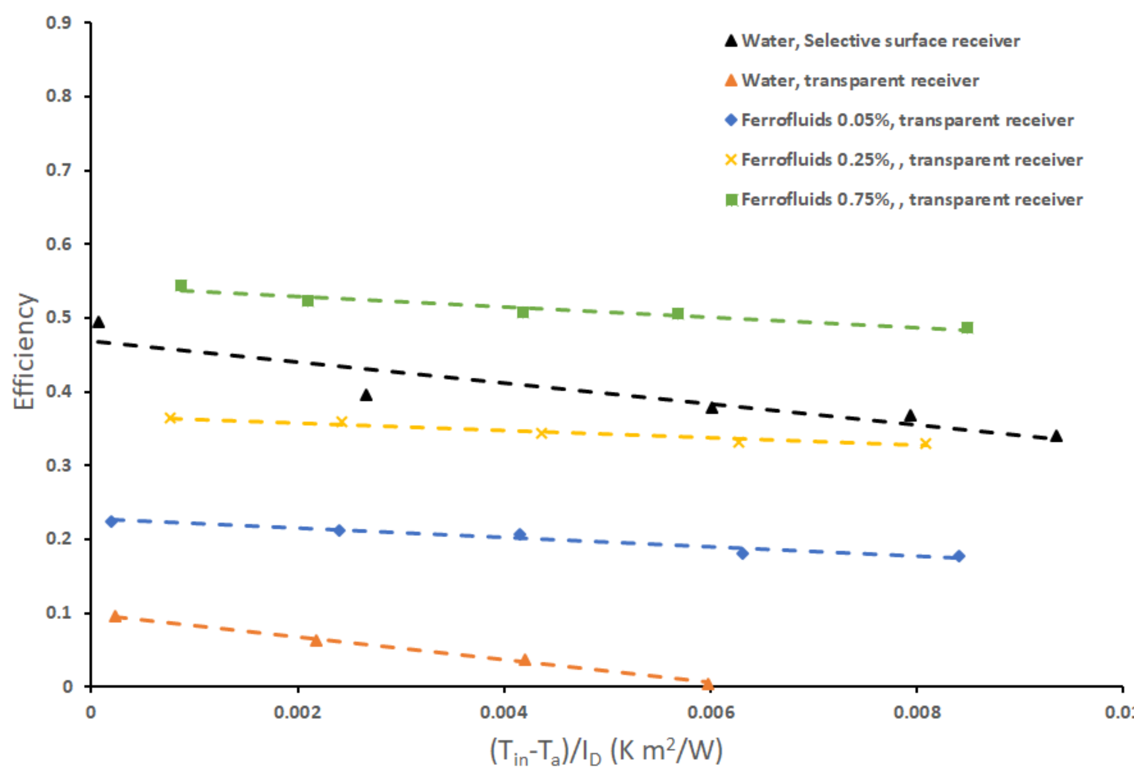

Figure 4-17: Solar collector efficiency of various concentration ferrofluids with transparent glass absorber.

4.5.2.3 Effect of external magnetic field on the performance of parabolic trough

In this section, the effect of an external magnetic field on the performance of parabolic trough with transparent glass receiver was investigated. The tests were carried out with 3.14, 6.28, 10.47 mT magnetic field intensity. Figure 4-18 illustrates the effect of external magnetic field in the efficiency of the collector versus the reduced temperature parameter $(T_{in} - T_a)/I_D$. It is found from Figure 4-18 that the efficiency of the parabolic trough at 0.05% ferrofluids improved further in the presence of external magnetic field. Table 4-6 shows all the absorbed energy parameter and removed energy parameter for direct and no-direct receiver with different volume fraction and magnetic intensity. As shown in Figure 4-19 the enhancement of absorbed energy parameter increased by increasing the magnetic intensity by 161% at 10.47 mT. On the other hand, the removed energy parameter increased in the presence of magnetic field and reached a peak at 3.14 mT and decreased thereafter. In the presence of magnetic intensity, the nanoparticles distribution changes and therefore the absorption and scattering of the incoming solar radiation also alters. The well-spaced distribution of nanoparticles could improve the absorption of incoming radiation and enhance the thermal conductivity of the bulk fluid. Figure 4-20 illustrate the efficiency of direct absorption parabolic trough collector in the presence of external magnetic field with 0.25% volume fraction ferrofluids. The performance of the parabolic trough collector improved with rising the external magnetic field intensity. The improvement is higher at lower reduced temperature difference. As shown in Figure 4-21 and Table 4-6 the absorbed removal parameter increased by increasing the magnetic intensity. At low magnetic field, the removed energy increased slightly by 6% and by 172% at higher magnetic field intensity. Moreover, compared to the selective surface absorber, the direct absorption with 0.25% ferrofluids showed higher absorbed removal parameter and lower removed energy parameter at higher magnetic field intensity. Figure 4-22 illustrate the efficiency of direct absorption parabolic trough collector in the presence of external magnetic field with 0.75% volume fraction ferrofluids. The performance of the parabolic trough collector improved with rising the external magnetic field intensity. The improvement is higher at lower reduced temperature difference. As shown in Figure 4-23 the absorbed removal parameter increased by increasing the magnetic intensity. At low magnetic field intensity, the removed energy increased slightly by 6% and by 172% at higher magnetic field intensity. In the presence of magnetic field, the optical and thermo-physical properties of the ferrofluids altered. Accordingly, the performance of the solar collector changes. At the operating temperature tested, the performance of the parabolic trough is better in the presence of the magnetic field. The author concludes that ferrofluids could be beneficial in direct absorption parabolic trough systems. The heat transfer in direct absorption is coupled radiative and convective heat transfer. The improvement in the performance could be more effective by changing the diameter of the transparent glass receiver. Moreover, low emissivity glass tube could be used to decrease the heat loss.

Table 4-6: Summary of heat removal parameter and absorbed energy parameter for ferrofluids based solar collector.

Heat transfer fluid type	Magnetic Intensity (mT)	Non-direct absorption		Direct absorption	
		$F_R\eta_{optic}$	F_RU_L	$F_R\eta_{optic}$	F_RU_L
Water	0	0.469	14.139	0.098	15.44
Fe_3O_4-water ferrofluids 0.05%	0	0.497	7.24	0.227	6.26
	3.14	0.52	6.872	0.438	13.039
	6.28	0.692	9.59	0.50	12.871
	10.47	0.687	7.3314	0.595	11.851
Fe_3O_4-water ferrofluids 0.25%	0	0.51	28.427	0.368	5.134
	3.14	0.56	30.612	0.413	5.484
	6.28	0.65	25.491	0.582	11.271
	10.47	0.66	24.03	0.694	13.99
Fe_3O_4-water ferrofluids 0.75%	0	0.743	54.197	0.543	6.94
	3.14	0.753	51.671	0.63	10.537
	6.28	0.761	50.193	0.58	11.223
	10.47	0.8139	38.573	0.6877	14.351

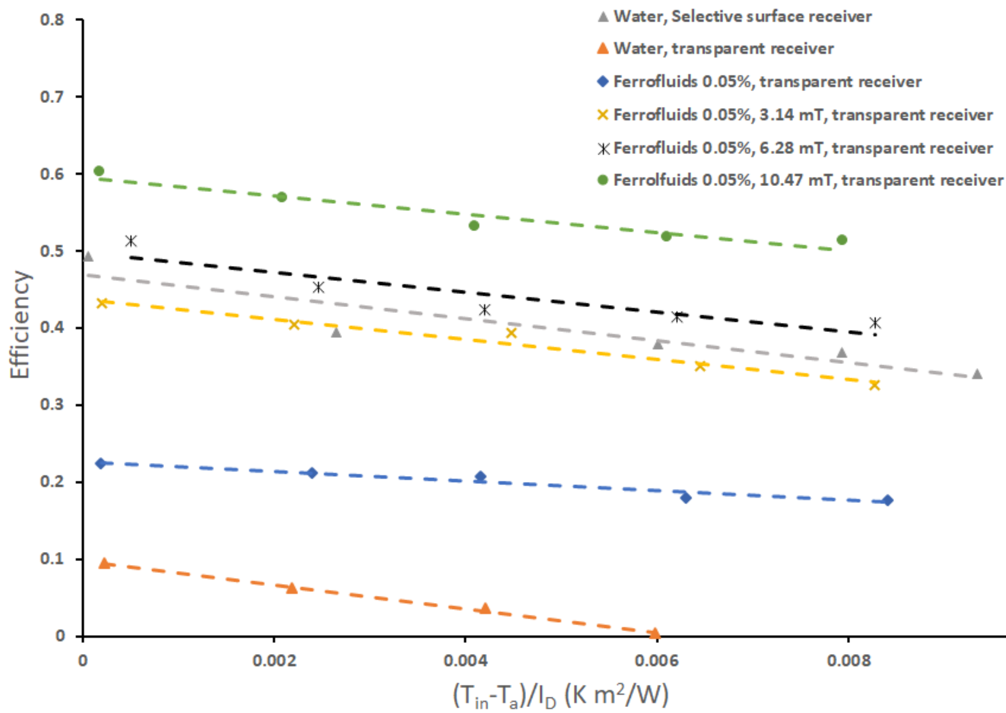

Figure 4-18: Collector efficiency of direct absorption ferrofluids based collector with 0.05% in the presence of external magnetic field and different inlet fluids temperature.

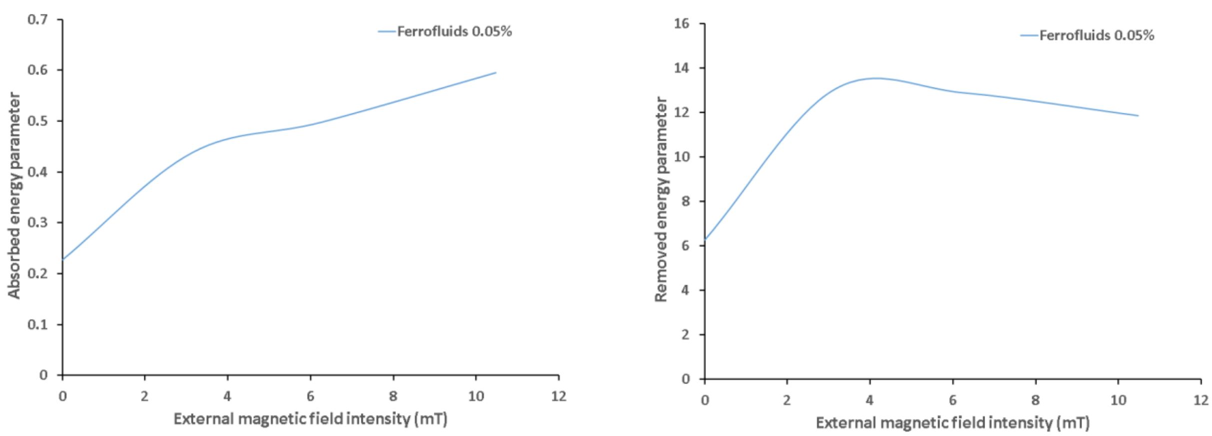

Figure 4-19: Heat removal factor and overall heat loss coefficient of a direct absorption ferrofluids based solar collector with ferrofluids 0.05% in the presence of external magnetic.

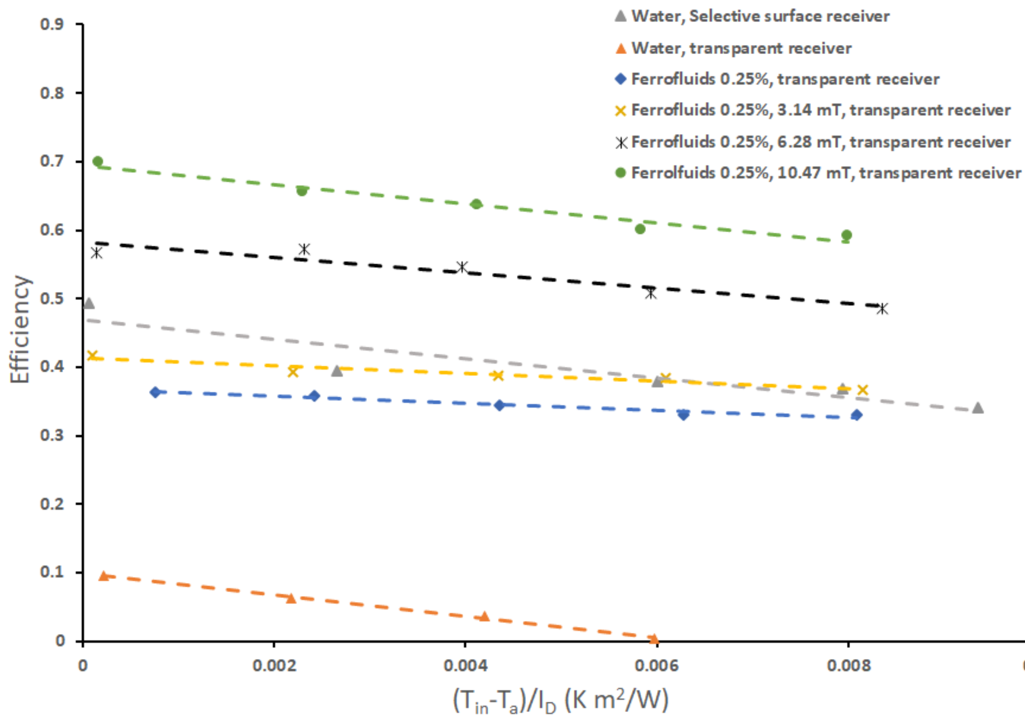

Figure 4-20: Collector efficiency of direct absorption ferrofluids based collector with 0.25% in the presence of external magnetic field and different inlet fluids temperature.

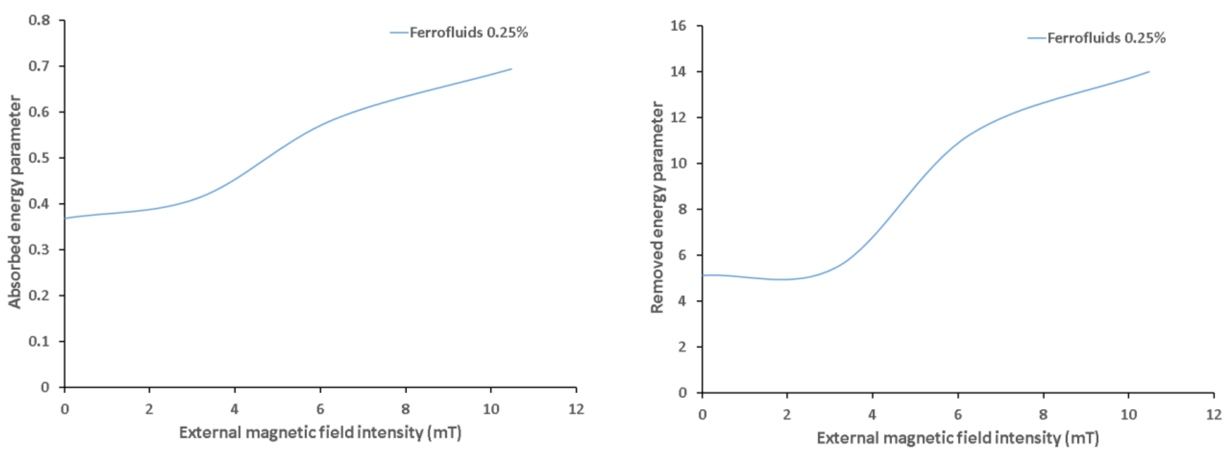

Figure 4-21: Heat removal factor and overall heat loss coefficient of a direct absorption ferrofluids based solar collector with ferrofluids 0.25% in the presence of external magnetic.

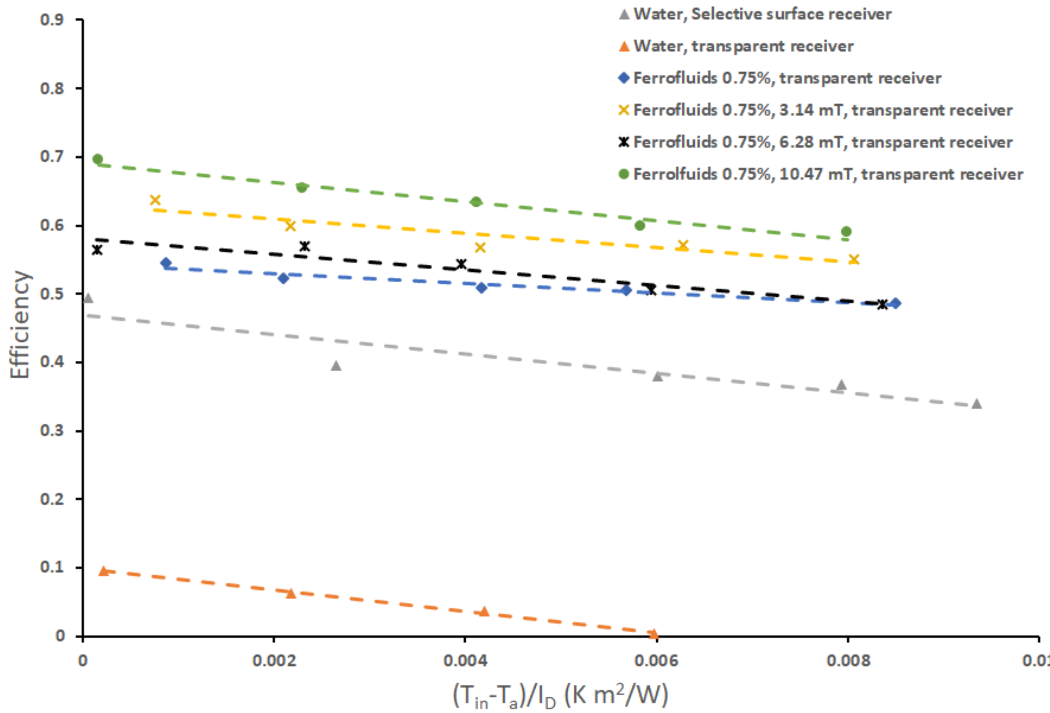

Figure 4-22: Collector efficiency of direct absorption ferrofluids based collector with 0.75% in the presence of external magnetic field and different inlet fluids temperature.

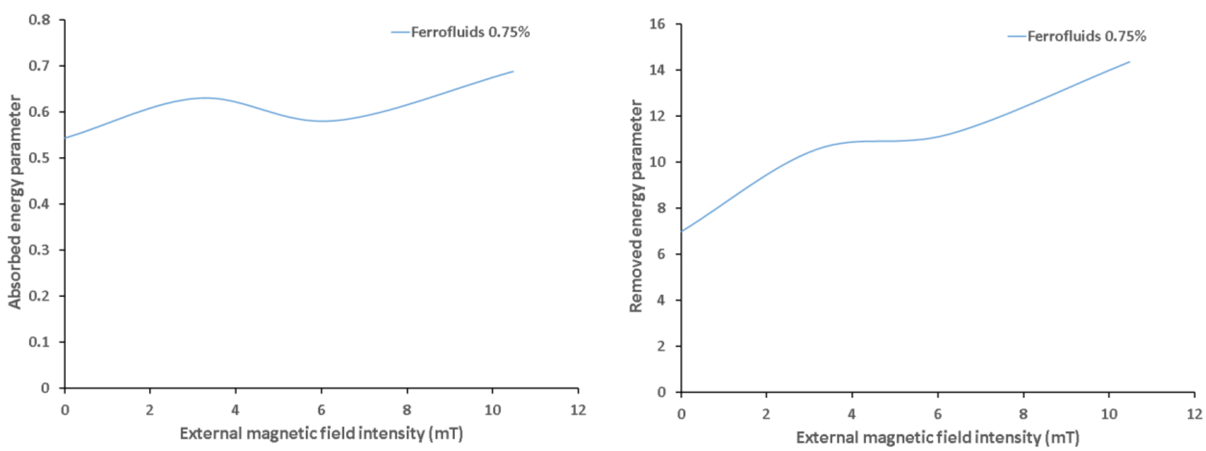

Figure 4-23: Heat removal factor and overall heat loss coefficient of a direct absorption ferrofluids based solar collector with ferrofluids 0.75% in the presence of external magnetic.

4.6 Conclusion

The ferrofluids parabolic trough collector with the selective surface has been experimentally studied. The performance of the collector with the laminar flow has been carried out. The performance of the collector includes the effect of volume fraction of nanoparticles, magnetic field intensity, Reynolds number, and thermal loss of the collector. The volume fraction of nanoparticles was 0.05%, 0.25%, and 0.75%. Three different magnetic field intensities were investigated, 3.14 mT, 6.28 mT, and 10.47 mT. Using ferrofluids to enhance the heat transfer performance the performance of the ferrofluids solar collector was compared to the based fluid (water). Main conclusions were drawn as following:

- The parabolic trough solar collector in the experiment has similar performance of flat-plate solar collectors. The low concentration ratio and the unglazed receiver are the main reason for the high thermal loss compared to conventional parabolic trough collector. The British standard considers unglazed receivers and concentration ratio lower than 10 as non-concentrated solar collectors.
- The performance of the collector improved when ferrofluids water used compared to water. Ferrofluids with low concentration improved the performance of the solar collector. The enhancement of heat transfer is due to the enhancement of thermos-physical properties of ferrofluids resulted from the Brownian motion of particles in the fluid. The ferrofluids showed much better performance at higher reduced temperature with lower overall heat loss coefficient.
- The formation of foam in ferrofluids is evident at higher concertation of nanoparticles due to SDS. The foam in the solar collector receiver affected the performance of solar

collector negatively. Adding defoamer to control the formation of foam improved the performance of the solar collector, and no foam was visible in the tank.

- Due to the non-Newtonian behaviour of the fluid increases, the volume fraction of particles will suppress the enhancement. The increase of viscosity at low shear rate affect the flow and the heat transfer. At low reduced temperature, the performances of the collector were better when ferrofluid with higher concentration was used. However, the efficiency of the collector declines at higher reduced temperature parameter. The pH of ferrofluids influences the behaviour of the fluid. pH values higher than 5 showed independence of viscosity on shear rate.
- In the presence of magnetic field, the performance of the solar collector enhanced further. By increasing the magnetic field intensity, the absorbed energy parameter increased, and at higher magnetic field intensity, the rate of enhancement decreases due to the magnetic saturation of ferrofluids.
- In this study, the performance of non-direct absorption receiver was better than the direct absorption receiver. However, the performance of the collector with a direct absorption reviver and using ferrofluids in the presence of the external magnetic field in some cases was higher than the performance of non-direct receiver with water as heat transfer medium. Moreover, the direct absorption receiver did not consider the optimum optical thickness of the receiver (i.e. bigger receiver diameter could give higher performances).
- The ferrofluids based solar collector showed higher performances when the magnetic field gradient was parallel to the direction of the flow. In the other hand, a negative effect on the performance was vivid when the magnetic field gradient was opposite to the flow direction.

Chapter 5 Heat transfer Analysis of Non-Direct Absorption Collector

5.1 Introduction

Experimental study on the performance of small-scale ferrofluids parabolic trough collector has been carried out in the last chapter. Known from the last chapter, employing magnetic nanofluids in the presence of external magnetic field has a significant improvement in the performance of parabolic trough collector. However, the small scale is much smaller than commercial parabolic trough collector, and most collector has an envelope to decrease the thermal loss. Therefore, in this chapter, heat transfer analysis model has been carried out to investigate the effect of utilizing ferrofluids as a heat transfer fluid in commercial parabolic trough design. Moreover, the model was carried out in the small-scale design, and the results were compared with the experimental results from the previous chapter. One dimensional mathematical model for ferrofluids parabolic trough collector was developed. The thermal analysis model evaluates the efficiency of a parabolic trough solar collector's linear absorber, also known as solar receiver, using ferrofluids as heat transfer fluid (HTF). Thermodynamics equations, heat transfer, and all parameters used in the model are discussed. Parameters include solar absorber geometries, nanofluids thermal and optical properties, flow rate, wind speed, ambient temperature, inlet and outlet temperatures of nanofluids, heat gain, heat losses, and optical losses. Modeling assumptions are also discussed. The model was implemented in Excel where Excel's solver was used to solve the energy balance and find the unknown surface temperatures. The solar absorber design and parameters are investigated in the two design versions. The collector design and experimental data obtained from Sandia National Laboratory (SNL) was used to verify the model. As shown by the various researcher's one-dimensional energy balance model is valid only for receivers shorter than 100 meters. Receivers with longer than 100 meters, a two-dimensional model is necessary [1-4].

5.2 Solar receiver model

The solar absorber performance analysis is based on an energy balance between the solar collector and the atmosphere. The energy balance consists of the direct thermal solar irradiation on the collector, thermal losses, optical losses, and heat gain of the solar absorber. All balances and correlations needed to predict their characteristics in the total energy balance are relying on the collector type of solar collector, optical properties, solar collector quality, and ambient conditions.

Figure 5-1 illustrates the one-dimensional energy balance for a parabolic trough solar absorber, with and without the glass envelope attached, and Figure 5-1 b shows the thermal resistance model used in the heat transfer analysis. For simplicity, the incident solar energy and optical losses have been excluded from the resistance model. Tracking errors, mirror and solar absorber cleanness, imprecations in the reflector are causing optical losses. Since most of the solar radiation is absorbed very close to the surface and the absorptance of glass is relatively small, the solar absorptance is considered as heat flux terms. The solar energy reflected by the mirror is absorbed by the glass envelope ($\dot{q}'_{5,SolAbs}$) and absorber selective surface ($\dot{q}'_{3,SolAbs}$). A part of energy absorbed by the selective surface is conducted through the absorber ($\dot{q}'_{23,Cond}$) and transferred to the heat transfer fluid by convection ($\dot{q}'_{12,Conv}$): remaining energy is transferred back to the glass envelope by radiation ($\dot{q}'_{34,rad}$) and natural convection ($\dot{q}'_{34,Conv}$) and lost through the support brackets by conduction ($\dot{q}'_{bracket,Cond}$) as well. The energy from radiation and convection then penetrates through the glass envelope by conduction ($\dot{q}'_{45,Cond}$) and radiation ($\dot{q}'_{12,Conv}$) and with the energy absorbed by the glass envelope ($\dot{q}'_{5,SolAbs}$) is lost to the environment by convection ($\dot{q}'_{56,Conv}$) and radiation ($\dot{q}'_{57,rad}$).

The energy balance equations determined at each surface of the solar absorber for both with and without glass envelope are the following:

with the glass envelope

$$\dot{q}'_{12,Conv} = \dot{q}'_{23,Cond} \qquad \text{Eq. 5-1}$$

$$\dot{q}'_{3,SolAbs} = \dot{q}'_{34,Conv} + \dot{q}'_{34,rad} + \dot{q}'_{23,Cond} + \dot{q}'_{bracket,Cond} \qquad \text{Eq. 5-2}$$

$$\dot{q}'_{34,Conv} + \dot{q}'_{34,rad} = \dot{q}'_{45,Cond} \qquad \text{Eq. 5-3}$$

$$\dot{q}'_{45,Cond} + \dot{q}'_{5,SolAbs} = \dot{q}'_{56,Conv} + \dot{q}'_{57,rad} \qquad \text{Eq. 5-4}$$

$$\dot{q}'_{HeatLoss} = \dot{q}'_{56,Conv} + \dot{q}'_{57,rad} + \dot{q}'_{bracket,Cond} \qquad \text{Eq. 5-5}$$

without the glass envelope

$$\dot{q}'_{12,Conv} = \dot{q}'_{23,Cond} \qquad \text{Eq. 5-6}$$

$$\dot{q}'_{3,SolAbs} = \dot{q}'_{36,Conv} + \dot{q}'_{37,rad} + \dot{q}'_{23,Cond} + \dot{q}'_{bracket,Cond} \qquad \text{Eq. 5-7}$$

$$\dot{q}'_{HeatLoss} = \dot{q}'_{36,Conv} + \dot{q}'_{37,rad} + \dot{q}'_{bracket,Cond} \qquad \text{Eq. 5-8}$$

In the case of no glass envelope, due to the loss of energy from the absorber surface directly to the atmosphere rather on going through the glass envelope, equations Eq.5-3 and Eq. 5-4 withdrew, and the absorber convective and radiation from the subscript 4 changes to 6 and 7 respectively.

The model estimates all heat fluxes, temperatures, and thermodynamics properties are uniform around the perimeter of the solar absorber. Temperatures properties are reliant on angular and longitudinal solar absorber orientations.

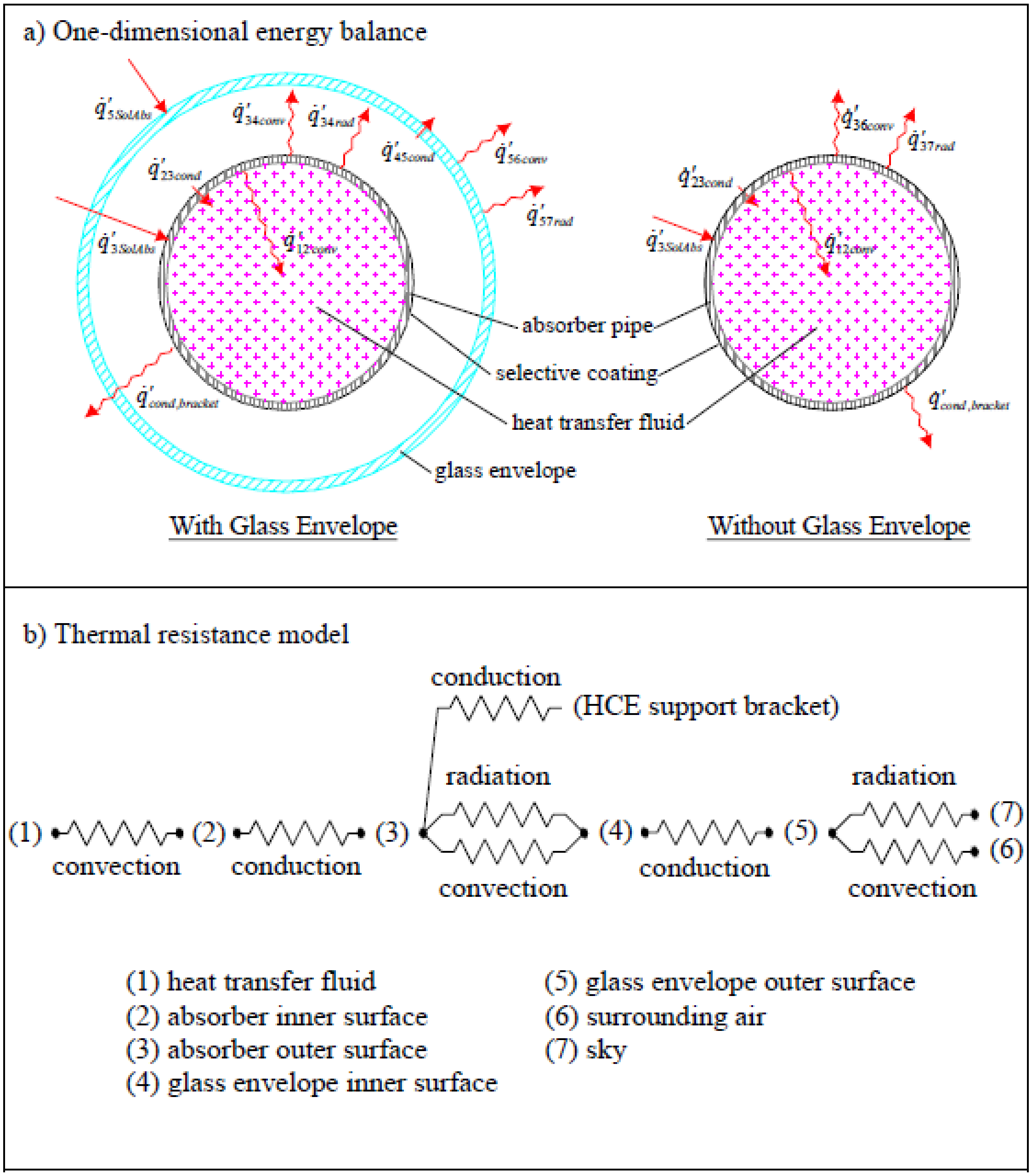

Figure 5-1: a) one-dimensional steady-state energy balance and b) thermal resistance model for a cross-section of a solar absorber.

Based on Newton's law of cooling, the convection heat transfer from the absorber inner surface to the heat transfer fluids is

$$\dot{q}'_{12,Conv} = h_1 D_2 \pi (T_2 - T_1) \quad \text{Eq. 5-9}$$

$$\text{With } h_1 = Nu_{D2} \frac{k_1}{D_2} \quad \text{Eq. 5-10}$$

where h_1 is the convection heat transfer coefficient at T_1, D_2 inner diameter of the absorber tube, T_1 mean (bulk) temperature of the heat transfer fluid, T_2 inner surface temperature of absorber tube, Nu_{D2} Nusselt number based on D_2, and $k_1$thermal conductivity of the heat transfer fluid at T_1. The type of flow through solar absorber determines Nusselt number. Turbulent flow in the solar absorber is normally used at typical operating conditions. However, when less energy output is required, the flow in the solar absorber may become transitional or laminar due to the viscosities of heat transfer fluid at lower temperatures. Moreover, the flow in the experimental test was laminar.

For the convective heat from the absorber to the heat transfer fluid, the Nusselt number for both turbulent and laminar regimes were considered. The Nusselt number correlation of Gnielinski for turbulent and transitional cases (Reynolds number > 2300) is used [143]. Furthermore, a correction factor is added to improve the accuracy of Nusselt number [144].

$$Nu_{D2} = \left(1 - 0.14 \left(\frac{D_3}{D_2}\right)^{0.6}\right) \frac{f_2/8 (Re_{D2} - 1000) Pr_1}{1 + 12.7 \sqrt{f_2/8} \left(Pr_1^{2/3} - 1\right)} \left(\frac{Pr_1}{Pr_2}\right)^{0.11} \quad \text{Eq. 5-11}$$

$$\text{With } f_2 = (1.82 \, log_{10}(Re_{D2}) - 1.64)^{-2} \quad \text{Eq. 5-12}$$

$$Pr = \frac{C_p \mu}{k} \quad \text{Eq. 5-13}$$

where f_2 is the friction factor for the inner surface of the absorber tube, Pr_1 is Prandtl number evaluated at the heat transfer fluid temperature T_1, Pr_2 is Prandtl number at the absorber inner surface temperature T_2, and D_2 is the absorber inner diameter, and D_3 is the absorber outer diameter. The correlation is valid for 0.5 < Pr_1< 2000 and 2300 <Re_{D2}<5x10^6. Other than Pr_2, all fluid properties are determined at the mean heat transfer fluid temperature, T_1. Nusselt number remains constant at laminar flow regimes. The value for Nusselt number will be 4.36 for pipe flow [145].

The conduction heat transfer through absorber wall is described by Fourier's law of conduction through a hollow cylinder:

$$\dot{q}'_{23,Cond} = 2\pi k_{23}(T_2 - T_3)/ln(D_3/D_2) \qquad \text{Eq. 5-14}$$

where k_{23} is the absorber thermal conductivity at the average temperature $(T_2 + T_3)/2$, T_2 is the absorber inner surface temperature, T_3 is the absorber outer surface temperature. The conduction coefficient relays on the absorber material. In this model, a stainless steels H321H is chosen for AZTRAK design with the following equation:

$$k_{23} = (0.0153)T_{23} + 14.775 \qquad \text{Eq. 5-15}$$

For the test rig receiver, a constant thermal conductivity of 400 W/mK was chosen due to the small range of operating temperatures. Conductive resistance by the selective coating has been ignored.

Between the glass envelope and the solar absorber, radiation and convection heat transfer take place. The annulus medium and pressure plays a huge role in convection heat transfer mechanism. In the commercial parabolic trough, the solar absorber annulus is under vacuum with pressure below 1 Torr. Therefore, the heats transfer between the glass envelope and solar absorber develop by free-molecular convection.

$$\dot{q}'_{34,Conv} = \pi D_3 h_{34}(T_3 - T_4) \qquad \text{Eq. 5-16}$$

with $h_{34} = \frac{k_{std}}{(D_2/2\ln(D_4/D_3)+b\xi(D_3/D_4+1))}$ Eq. 5-17

$$b = \frac{(2-a)(9\gamma-5)}{2a(\gamma+1)} \qquad \text{Eq. 5-18}$$

$$\xi = \frac{2.331E(-20)(T_{34}+273.15)}{(p_a\delta^2)} \qquad \text{Eq. 5-19}$$

where h_{34} is the convection heat transfer coefficient for the air in the annulus at a temperature T_{34}, T_4 is the temperature of inner surface of glass envelope, D_4 is the diameter of inner glass envelope surface, k_{std} is the thermal conductivity of the air at standard temperature and pressure (0.02551 W/m-K), b is the interact coefficient of air (1.571), ξ is the mean free path between collisions of molecule, a is the accommodation coefficient, γ is the ration of specific heats for air (1.39), T_{34} is the average temperature $(T_3 + T_4)/2$, p_a is the air pressure, and δ is the molecular diameter of air (3.53e-8 cm).

The radiation heat transfer between the glass envelope and the solar absorber $\dot{q}'_{34,rad}$ is determined with the following equation:

$$\dot{q}'_{34,rad} = \frac{\sigma\pi D_3(T_3^4 - T_4^4)}{(1/\varepsilon_3+(1-\varepsilon_4)D_3/(\varepsilon_4 D_4))} \qquad \text{Eq. 5-20}$$

where σ is the Stefan-Boltzmann constant, ε_3 is the emissivity of absorber selective coating, and ε_4 is the emissivity of glass envelope. The equation was developed by taking few assumptions: gas the gas in annulus inactive, grey surface, diffuse reflections and irradiation, and long isothermal cylinder. Moreover, it assumed that the glass envelope is opaque to infrared radiation. Some of the above-mentioned assumptions are not precise. However, the errors related with those assumptions should be relatively small.

The heat will escape from the glass envelope to the environment through radiation and convection. Relying on the wind, the heat convection is either natural or forced. The difference between the temperature of the glass envelope and the temperature of the atmosphere causing radiation heat loss to occur. The convection heat transfer from the glass to envelope to the environment $\dot{q}'_{56,Conv}$ is the biggest source of heat loss, especially if there is a wind. From Newton's law of cooling

$$\dot{q}'_{56,Conv} = h_{56}\pi D_5(T_5 - T_6) \qquad \text{Eq. 5-21}$$

$$h_{56} = \frac{k_{56}}{D_5}Nu_{D5} \qquad \text{Eq. 5-22}$$

where h_{56} is the heat transfer coefficient of air at $(T_5 - T_6)/2$, T_5 glass envelope outer surface temperature, T_6 is the ambient temperature, k_{56} is the thermal conductivity of air at, D_5 is the outer diameter of glass the envelope, Nu_{D5} average Nusselt number based on the outer diameter of glass envelope. The Nusselt number relays on if there is no wind (natural convection heat transfer) or with wind (forced convective heat transfer.) In case of no wind, the heat transfer from glass envelope to the atmosphere will be natural convection and the equation established by Churchill and Chu [146] will be used to determine Nusselt number:

$$Nu_{D5} = \left[0.6 + 0387\left\{\frac{Ra_{56}}{\left[1+(0.559/Pr_{56})^{\frac{9}{16}}\right]^{\frac{16}{9}}}\right\}\right]^2 \qquad \text{Eq. 5-23}$$

$$Ra_{56} = \frac{g\beta(T_5 - T_6)}{(\alpha_{56}v_{56})} \qquad \text{Eq. 5-24}$$

$$\beta = \frac{1}{T_{56}} \qquad \text{Eq. 5-25}$$

$$Pr_{56} = \frac{\alpha_{56}}{v_{56}} \qquad \text{Eq. 5-26}$$

where Ra_{56} is the Rayleigh number of air based on the outer diameter of glass envelope D_5, g is the gravitational constant, α_{56} is the thermal diffusivity, β is the volumetric thermal expansion coefficient, Pr_{56} is the Prandtl number for air at T_{56},and v_{56} is the kinematic viscosity for air at T_{56}. The correlation is valid for $10^5 < Ra_{56} < 10^{12}$, and assumes a long isothermal horizontal cylinder.

In the case of wind, forced convection is the type of convection heat transfer from the glass envelope to the atmosphere. The Nusselt number, for forced convection, is determined with Zhukauskus equation for external forced convection.

$$Nu_{D5} = CRe_{D5}^{m} Pr_6^{n} \left(\frac{Pr_6}{Pr_5}\right)^{1/4} \qquad \text{Eq. 5-27}$$

with

Re_D	C	M
1-40	0.75	0.4
40-1000	0.51	0.5
1000-200000	0.26	0.6
20000-1000000	0.076	0.7

and n=0.37, for Pr<=10

n= 0.36, for Pr>10

The validation for this correlation is at 0.7<Pr_6<500, and 1<Re<106. All properties of the fluid are calculated at the ambient temperature, T_6, only Pr_5, which is calculated at the outer diameter of glass envelope.

The temperature difference between the sky and the envelope causes the radiation transfer between them. To estimate the radiation transfer, the envelope is assumed to be a convex grey object in a large Blackbody Cavity. The radiation transfer between the sky and glass envelope becomes

$$\dot{q}'_{57,rad} = \sigma D_5 \pi \varepsilon_5 (T_5^4 - T_7^4) \qquad \text{Eq. 5-28}$$

where ε_5 is the emissivity of the outer surface of glass envelope, and T_7 is the effective sky temperature. The sky, especially in cloudy and dusty conditions, does not behave like a blackbody; nevertheless, it is accepted practice to model it as described and to use an effective balance for the difference [11]. The model is simplified by assuming an effective sky temperature lower than the ambient temperature by 8°C. The glass envelope emissivity and absorptance are independent of temperature and therefore constants.

Accurate modelling of solar absorption and optical losses is very difficult due to the inconsistent of solar angle, direct normal irradiation, and optical properties of the reflected mirrors and absorber. Therefore, the optical efficiency elements are determined and integrated to form effective optical efficiency. The optical efficiency is estimated to calculate the solar absorption. The equation for the solar absorption n the glass envelope becomes

$$\dot{q}'_{5,SolAbs} = \dot{q}'_{si} \eta_{optic} \alpha_{env} \qquad \text{Eq. 5-29}$$

with $\eta_{optic} = \sum \varepsilon'_i K$ Eq. 5-30 where $\dot{q}'_{si}$ is the solar radiation per absorber length, η_{optic} is the effective optical efficiency at glass envelope, α_{env} is the glass envelope absorptance, ε'_i is the optical efficiency elements, and K is the incident angel modifier. The optical effective includes the absorber shadowing, tracking error, geometry error, clean mirror reflectance, dirt on mirrors, and dirt on the absorber. The incident angle losses are estimated by adding incident angle modifier to the equation. The effective optical efficiency is estimated from the data published in a report by NREL [147]. The solar irradiation $\dot{q}'_{si}$ in Eq. 5-29 is estimated by multiplying the solar irradiation by the aperture area and dividing by the absorber length.

The solar energy absorbed by the solar absorber happens near the surface; hence, it is considered as a heat flux. The solar absorption at the surface of the absorber is

$$\dot{q}'_{3,SolAbs} = \dot{q}'_{si}\eta_{abs}\alpha_{abs} \qquad \text{Eq. 5-31}$$

with $\eta_{abs} = \eta_{env}\tau_{env}$ Eq. 5-32

where η_{abs} is the effective optical efficiency at absorber, α_{abs} is the absorptance of absorber, τ_{env} is the transmittance of the glass envelope. The solar collector efficiency is calculated as follow:

$$\eta_{Colector} = \frac{\dot{q}'_{12,Conv}}{\dot{q}'_{si}} \qquad \text{Eq. 5-33}$$

5.3 Assumption and simplifications

The modelling of the parabolic trough performance model has various assumptions and simplifications which are listed in Table 5-1. The heat transfer analysis assumes a uniform solar irradiance over the circumference along the length of the solar absorber. In reality, the solar irradiance relies on optical distortions in the mirror, tracking errors, alignment errors, and collector geometry. The typical solar irradiance profile around the circumference is like asymmetric distribution with the minimum at the side opposite to the mirror and the maximum point closest to the reflector. The real solar irradiance profile needs more study to fully understand the losses and the effectiveness of heat removal due to the distribution of ferrofluids in the solar absorber. Moreover, the non-uniform solar irradiance affects the flow and the temperature profile around the perimeter. Therefore, to accurately predict the convective heat transfer rate a computational fluid dynamics model would need to be used. Especially to determine the effect of the distribution of nanoparticles in the absorber tube and the possibility of bringing those particles closer to the maximum heated surface area.

Diffuse heat radiation from the mirror, ground, and surrounding in neglected. Those radiations can lead to error between 5%-1% of the radiation heat transfer [148]. However, due to the over prediction of radiation heat transfer, the simplification is balanced. Furthermore, the radiation loss is rather small compared to the loss of convective heat.

Notwithstanding, the heat gain per absorber length reduces the heat transfer when temperature increase, the temperatures along the length of the absorber is considered uniform. The mean temperatures are usually used in many correlations in the model. The uniform temperature may under predict the heat losses and over-predict the heat gain. However, to treat all heat fluxes as one-dimensional and significantly simplify the model, uniform temperature profiles are assumed. In reality, the wind is non-uniform and very turbulent in both directions along the parabolic trough. However, the wind is assumed to acts normal to the axis. Another simplification was to assume uniform optical properties. Tests have exhibited that some variation in optical properties over a single absorber may occur. Furthermore, the absorptance elements and glass envelope emittance and transmittance are assumed to be independent of temperature.

Several assumptions on the ferrofluids thermo-physical properties have been implemented. The thermophysical properties assumed to be constant along the length of the absorber. In practice, the magnetic nanoparticles return to their position in the absence of the external magnetic field. Therefore, the effect of the distance between the magnetic sources is not considered. Moreover, the previous chapter showed that the concentration of nanoparticle could affect the behaviour of the flow. However, the ferrofluids are assumed to be Newtown fluids. The changes of the thermophysical properties are taken from experimental data. Unfortunately, the reported thermo-physical properties of ferrofluids in the presence of magnetic field differ significantly between researchers. Further studies are required to determine the correct values of thermophysical properties with various magnetic field intensity. Furthermore, the magnetic field intensity is assumed to be independent of temperatures. Operating in high temperature causes the nanoparticles to lose their permanent magnetic properties also known as Curie temperature. The magnetization of nanoparticles decreases with increasing the temperatures where the thermal energy overcome the magnetic forces and create the randomizing effect. For Fe_3O_4 the magnetization starts to decrease at temperatures higher than 245°C, decreasing the magnetization will make the chain particles shorter and will affect the thermos-physical properties of ferrofluids, and they will lose their magnetic properties completely at Curie temperature is 585°C [149].

Table 5-1: Assumptions and simplifications of the current model.

Model element	Assumptions and simplifications
Convective heat transfer between heat transfer fluids and absorber	• Uniform flow. • Fluids bulk temperature.
Thermo-physical properties	• Constant Thermo-physical properties along the length of the absorber. • All the fluids considered as Newtonian • The change of thermophysical properties in the presence of magnetic field is independent of the base fluid. • The magnetic properties are independent of temperatures.
Conduction heat transfers through the absorber wall and glass envelope	• Uniform conductions in both directions • Linear in the radial direction. • Thermal resistance from the selective surface was neglected. • Glass envelope anti-reflection treatment was neglected. • Constant thermal conductivity.
Convection heat transfer between the absorber and glass envelope	• The heat transfer may be slightly overestimated. • Constant convection heat coefficient. • Long cylinders at uniform temperatures.
Radiation heat transfer between the absorber and glass envelope	• Gas is not affecting the heat transfer. • Both surfaces are grey. • Surfaces are long isothermal cylinders. • Glass envelope is opaque to radiation in the infrared range.
Convection heat transfer between glass envelope and atmosphere	• Wind direction has no effect • Long isothermal tube
Radiation heat transfer between the glass envelope and sky	• The mirror has a 5% effect on radiation escaping glass envelope outer surface. • Sky temperature is 8°C lower than ambient temperature.
Optical properties	• Uniform properties. • No degradation with time. • Anti-reflection treatment has no effect on glass envelope emittance. • Incident angle modifier is constant. • Optical properties are independent of temperature except for the selective coating emissivity.
Solar absorption	• Can be treated as heat fluxes.
Solar irradiance	• Uniform in both directions.

5.4 Thermo-physical properties of ferrofluids

The thermophysical properties of the base fluids (synthetic oil), water and the nanoparticles (Fe_3O_4) including density, viscosity, thermal conductivity and specific heat are highly reliant on the operational temperature. The correlations for synthetic oil are valid for temperature ranges of 0°C and 450°C, and for water the correlations are valid for temperature ranges of 0°C and 100°C. Using the following correlation the effective density of ferrofluids is determined[150].

$$\rho_{eff} = (1+\varphi)\rho_{bf} + \varphi\rho_{Fe_3O_4} \qquad \text{Eq. 5-33}$$

where ρ_{eff} is the effective density of ferrofluids, φ is the volume fraction, ρ_{bf} is the density of the base fluid, and $\rho_{Fe_3O_4}$ is the nanoparticle density ($\rho_{Fe_3O_4} = 5810$ kg/m3). The variation of density of the base fluids was extracted from Ref. [151]:

For Thermal oil

$$\rho_{bf,Oil} = -0.9985\,T + 1236 \qquad \text{Eq. 5-34}$$

for water

$$\rho_{bf,water} = -0.0035\,T^2 + 1.8142\,T + 765.33 \qquad \text{Eq. 5-35}$$

where T is the temperature of the fluid. The correlation of the effective viscosity with the influence of temperature is estimated [40].

$$\mu_{eff} = \mu_{bf}\left(1+\frac{\varphi}{12.5}\right)^{6.356} \qquad \text{Eq. 5-36}$$

where μ_{eff} is the effective viscosity of ferrofluids, and μ_{bf} is the base fluid viscosities, which are dependent on the temperature.

$$\mu_{bf,oil} = 6.67 \times 10^{-7}T^4 - 1.56 \times 10^{-3}T^3$$

$$+1.38\,T^2 - 5.541 \times 10^2 T + 8.848 \times 10^4 \quad \text{Eq. 5-37}$$

$$\mu_{bf,water} = -2.244 \times 10^{-9}T^3 + 5.062 \times 10^{-7}T^2$$

$$-4.264 \times 10^{-5}T + 1.684 \times 10^{-3} \quad \text{Eq. 5-38}$$

The effective thermal conductivity of ferrofluids k_{eff} is determined as follow

$$k_{eff} = k_{bf}(1 + 10.5\varphi)^{0.1051} \quad \text{Eq. 5-39}$$

where k_{bf} is the base fluid thermal conductivity.

$$k_{bf,oil} = -5.753496 \times 10^{-10}T^2 - 1.875266 \times 10^{-4}T + 0.1900210 \quad \text{Eq. 5-40}$$

$$k_{bf,water} = -8.151 \times 10^{-6}T^2 - 1.946 \times 10^{-3}T + 0.5636 \quad \text{Eq. 5-41}$$

The effective specific heat capacity Cp_{eff} is calculated by Eq. 5-42 which is similar to mixing theory for ideal gas mixtures. While it is simple, commonly used and experimentally validated, Eq. 5-42 has little theoretical justification in the context of nanofluids [152].

$$Cp_{eff} = (1 + \varphi)Cp_{bf} + \varphi Cp_{Fe_3O_4} \quad \text{Eq. 5-42}$$

where $Cp_{bf}$is the base fluid heat capacity, and $Cp_{Fe_3O_4}$ is the heat capacity of nanoparticles and determined from experiment data [153].

$$Cp_{bf,oil} = 0.001708\,T + 2.207798 \quad \text{Eq. 5-43}$$

$$Cp_{bf,water} = 1.857 \times 10^{-9}T^4 - 4.519 \times 10^{-7}T^3$$

$$+4.991 \times 10^{-5}\,T^2 - 2.286 \times 10^{-3}T + 4.214 \quad \text{Eq. 5-44}$$

$$Cp_{Fe_3O_4} = -6 \times 10^{-6} T^2 + 0.0048\, T - 0.2804 \qquad \text{Eq. 5-45}$$

As previously discussed in Chapter 2, the change of ferrofluids thermo-physical properties in the presence of external magnetic field was investigated by many researchers [154]. Experimental data was used in this model [56, 123]. The mechanisms proposed to explain the change in the thermos-physical properties is the formation of chain-like magnetite particles in the ferrofluids induced by an external magnetic field. As shown in Figure 5-2, the thermal conductivity increases with increasing volume fraction and magnetic intensity. When the magnetic field increase, the chain length increase, creating more bridge of thermal energy conduction along the magnetic field direction.

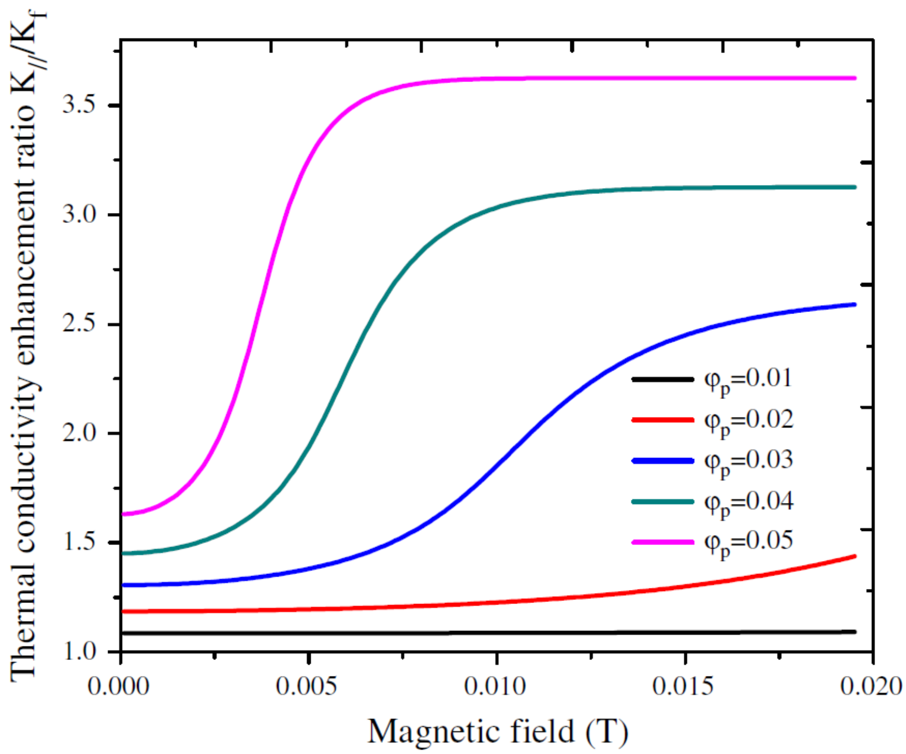

Figure 5-2: Thermal conductivity of ferrofluids with respect to magnetic field parallel to the temperature gradient [123].

As the magnetic field intensity increases, the interaction among particles increases, leading to increasing the viscosity also called the magneto-viscous effect. As shown in Figure 5-3 the lower viscosity values observed during the decay of magnetic field strength compared to rising are attributed to the fact that the structure formed during the rise magnetic field takes longer time than the measurement time for relaxation.

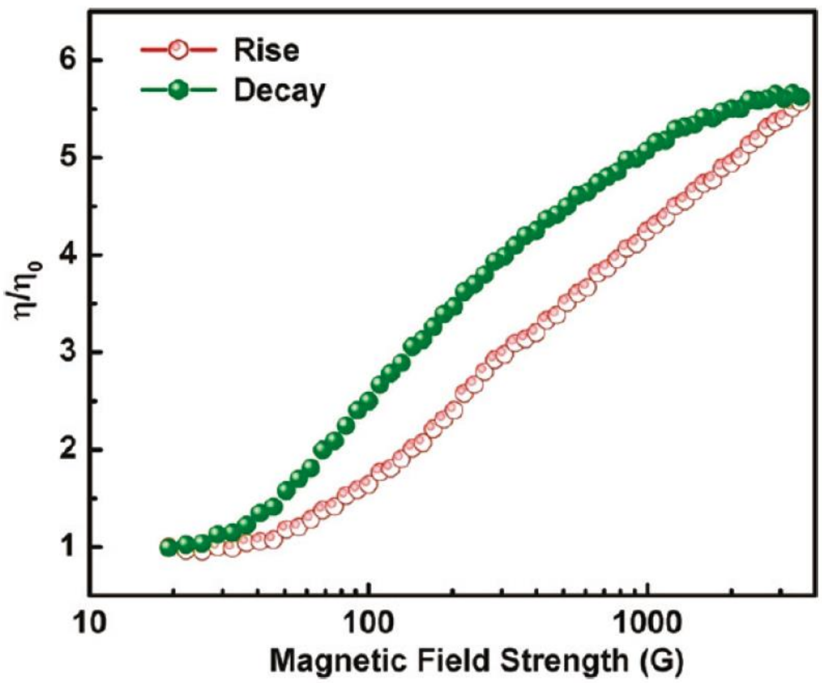

Figure 5-3: The viscosity of ferrofluids as a function of applied magnetic field strength [56].

The heat capacity is assumed to be the same in the presence of magnetic field. Many researchers consider the change of ferrofluids heat capacity in the presence of magnetic field to be slight, and it is not taken into account in calculations. From the correlations from Eq. 5-33 to Eq. 5-46 and Figure 5-2 and Figure 5-3 the properties of 0.05% water and oil-based ferrofluids in the presence of external magnetic field and shown in Figure 5-4 and Figure 5-5.

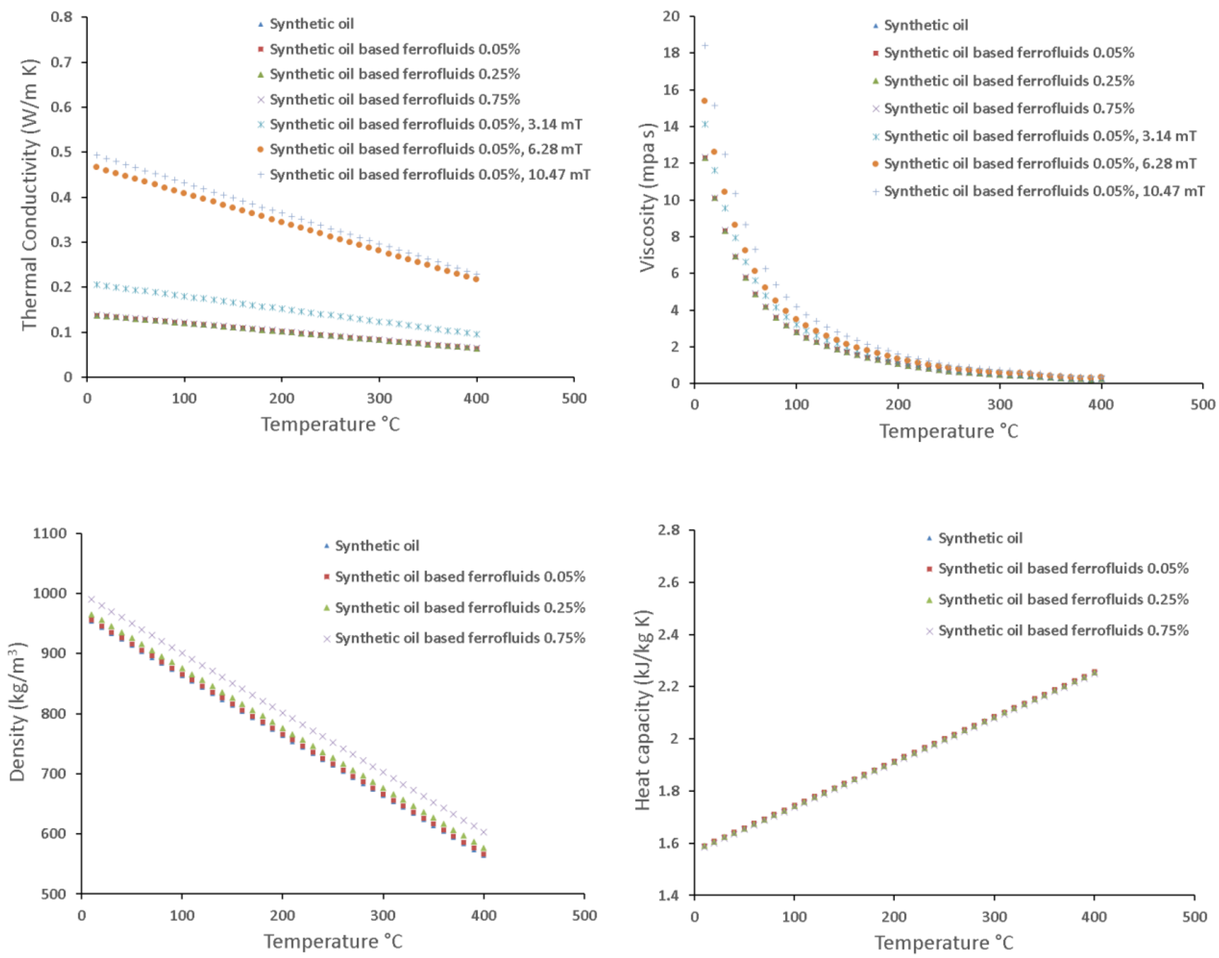

Figure 5-4: Thermophysical properties of synthetic oil based ferrofluids with three different volume fractions.

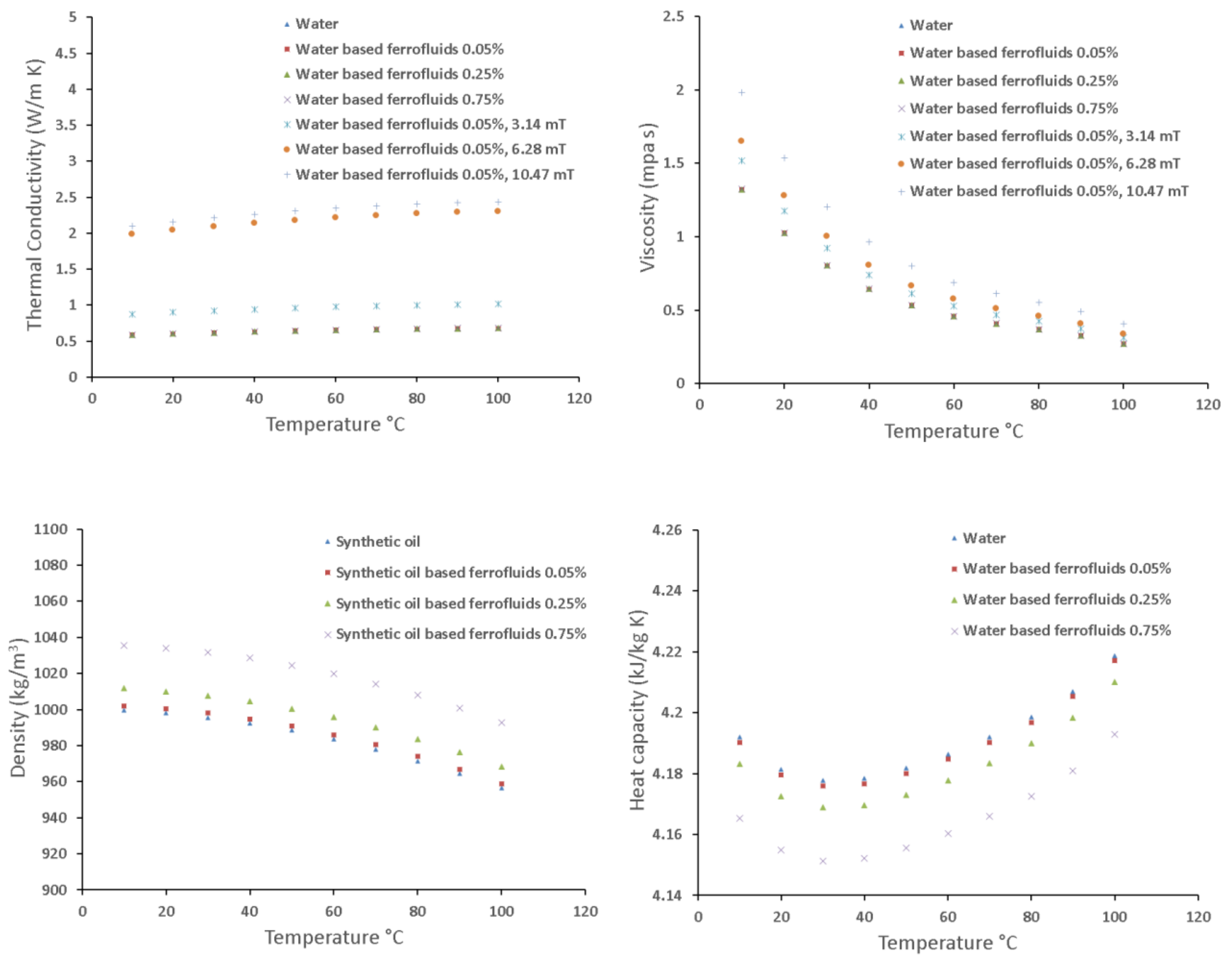

Figure 5-5: Thermophysical properties of water-based ferrofluids with three different volume fractions.

5.5 Geometries and specification of solar collector

Two different geometries and specification were used. First, the solar collector assembly (LS-2) module placed at the AZTRAK rotating platform at SNL. The second is the solar collector used in this study. Table 5-1 illustrate the specification and geometry of each solar collector.

Table 5-1: Geometries of AZTRAK platform and current solar collector.

	AZTRAK platform	Current study
Aperture Width (mm)	5000	250
Aperture length (mm)	7800	450
Glass envelope outer diameter (mm)	115	-
Glass envelope inner diameter (mm)	109	-
Absorber Outer diameter (mm)	70	15
Absorber inner diameter (mm)	66	14
Glass envelope transmittance	0.965	-
Glass envelope emissivity	0.86	-
Glass envelope absorption	0.02	-
Optical terms	0.9	0.9
Absorber absorption	0.955	0.9
Absorber emissivity	-	0.3

5.6 Results and discussion

In this section, the results of the heat transfer analysis are presented. The two different geometries of the absorber were investigated. Moreover, the effect of the glass envelope was studied.

5.6.1 AZTRAK platform

To validate the heat transfer model, it was compared with experimental data obtained from Sandia National Laboratory (SNL) [126]. The experimental results used were taken from a solar collector assembly (LS-2) module placed at the AZTRAK rotating platform at SNL. The one-dimensional model could evaluate the AZTRAK test data since the length of the platform is only about 10 m; therefore, the properties of the heat transfer fluids have a slight variation along the length of the receiver. Due to limitations in the experimental setup, a 5 cm flow restriction device (solid plug) was centred in the inside diameter of the absorber tube. Two different selective coating were used in the test: black chrome and cermet. Cermet has better radiative properties (low emissivity) at high temperatures than black chrome and does not oxidize if the vacuum is lost [5]. The test was performed in various conditions. A silicone heat transfer fluid (Syltherm 800) was used in the experimental setup. The input data for the model includes the direct normal insolation, wind speed, ambient temperature, and the heat transfer fluids inlet temperature, outlet temperature, and volume flow rate. The output data include absorber and glass surface temperatures, solar absorber heat loss per collector area, heat gain, and collector efficiency. The input data for the model are set up to replicate the experimental data presented by AZTRAK testing. The collector efficiency of AZTRAK and the current model is illustrated in Figure 5-6. The model for Syltherm follows the trends of the experimental values, and all the results are within the experimental error bars.

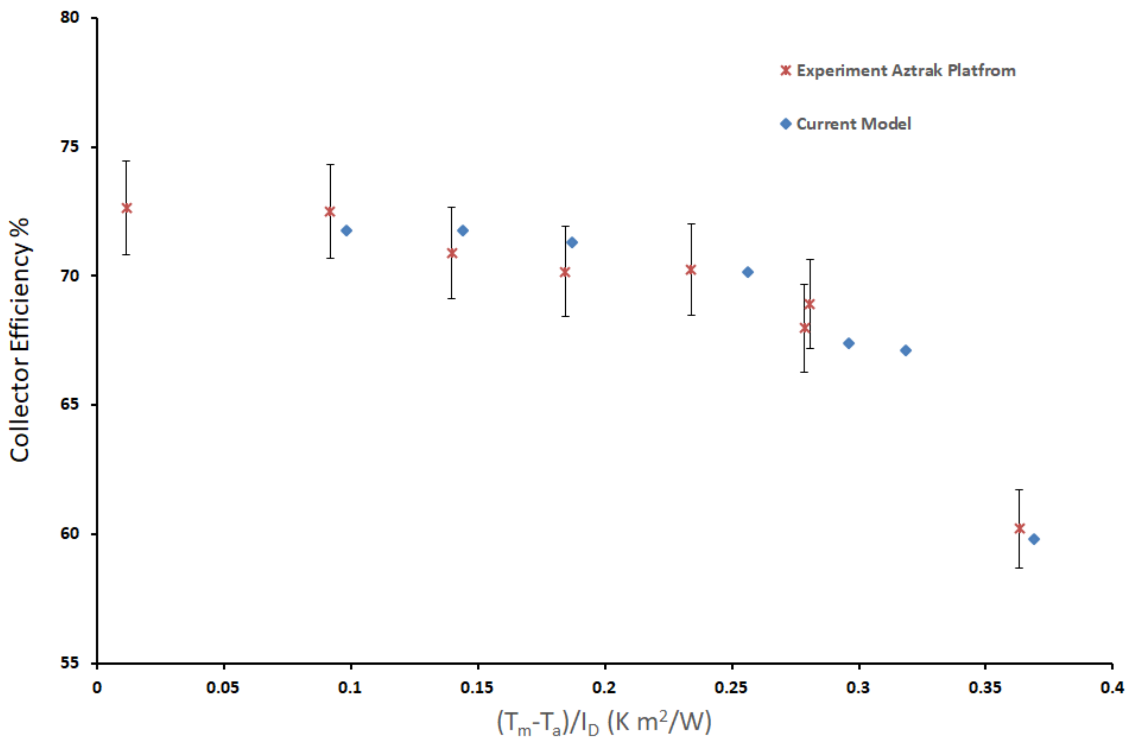

Figure 5-6: AZTRAK Parabolic trough collector efficiency from the experimental data and the current model.

5.6.1.1 Performance of ferrofluids solar collector with glass envelope

The model was used to determine the performance of the solar collector with Syltherm 800 based ferrofluids as a heat transfer medium. Five different volume fractions are considered 0.05%, 0.25%, 0.75%, 2.5% and 5% to observe the effect of the volume fractions on the performance of the solar collector. The results obtained for the collector efficiency and thermal losses are shown in Figure 5-7 and Figure 5-8. The efficiency of the collector improved with increasing the concentration of the nanoparticles in the fluid and reach the maximum improvement with 2% ferrofluids. Thereafter, with 5% ferrofluids, the performance of the solar collector was lower than the performance of the base fluid. With very low volume concentration 0.05% volume concentration, the performance is improved fractionally, where the highest improvement was around 0.1%. Ferrofluids with 2.5% volume fraction should be better performance. At low reduced temperature, the difference between the efficiency of solar collector is small around 1.8%. At high average temperature, the difference increases to reach 3.7% at a reduced temperature of 325°C. This is due to the enhancement of the convection heat transfer of ferrofluid compared to the base fluid. The improved thermal conductivity of ferrofluids is the most important factor for improving the heat transfer in parabolic trough collectors. Ferrofluids reduces the thermal resistance at interfaces and minimizes the temperature difference between the absorber surface and the heat transfer fluid. Figure 5-9 illustrate the convective heat transfer coefficient of ferrofluids at different volume concentration. The ferrofluids at high average temperature are more efficient compared to base fluid. At 325°C, the heat transfer coefficient of ferrofluids with 2.5% volume fraction is 531 W/m^2K, where at the same temperature the base fluid heat transfer coefficient is only 394 W/m^2K. The heat transfer coefficient curve has a peak, where the heat transfer coefficient decreases with increasing temperature. This is because a large fraction of the absorber surface is covered by a vapour film, which acts as an insulation due to the low thermal conductivity of the vapour. Figure 5-7 represent the thermal loss of ferrofluids based solar collector with the absence of magnetic field. The thermal losses increase with increasing the average temperature above ambient. Adding ferromagnetic particle to the base fluid decreased the thermal loss, ferrofluid with 2.5% decreased the thermal loss by 24% compared to the base fluid at an average temperature of 325°C.

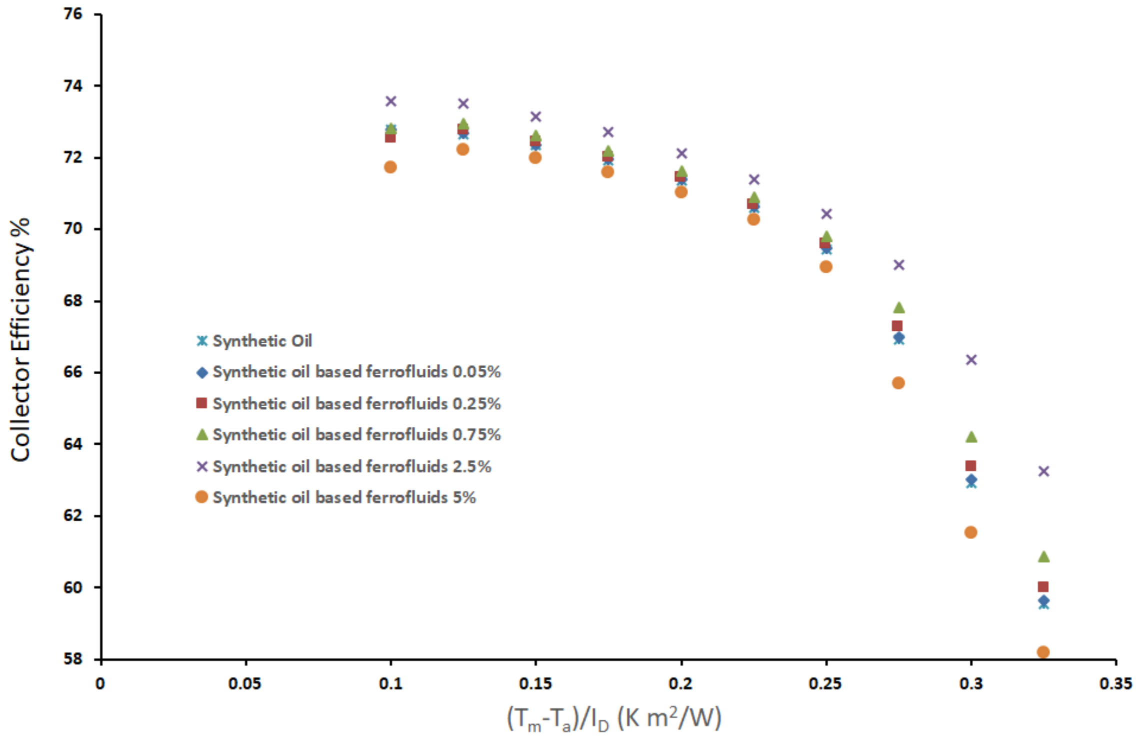

Figure 5-7: Comparison of calculated ferrofluid collector efficiency with different volume fraction and experiment data.

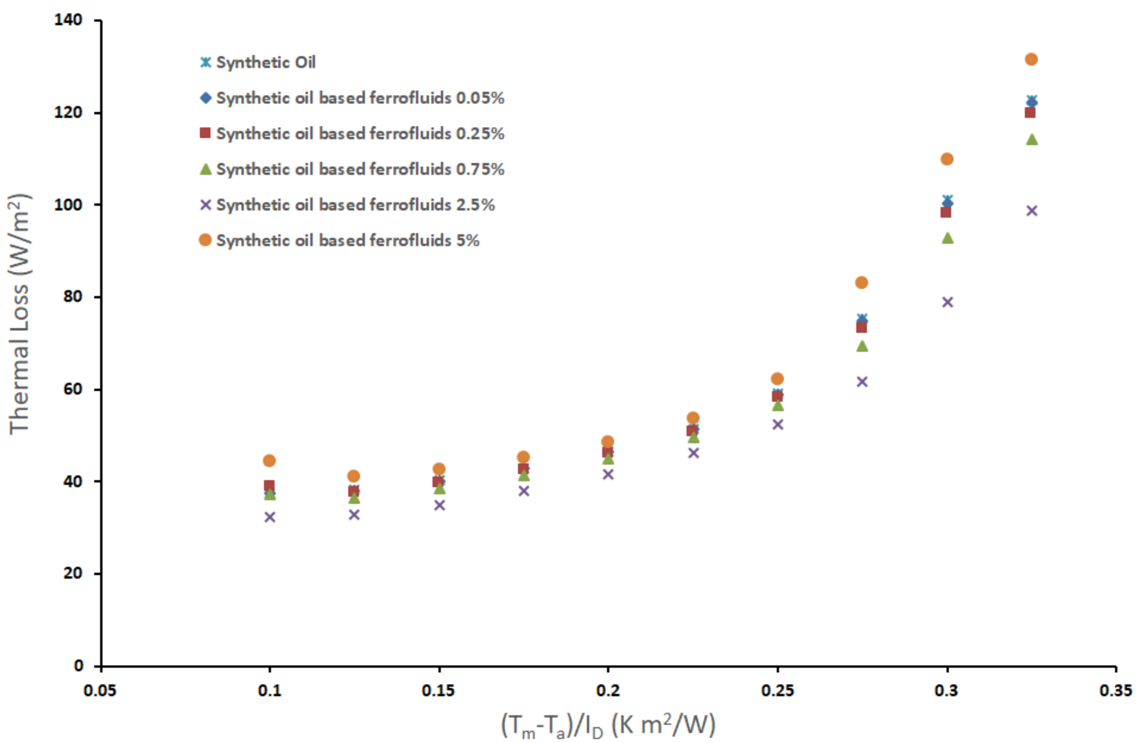

Figure 5-8: Heat loss of ferrofluids parabolic trough collector AZTRAK design.

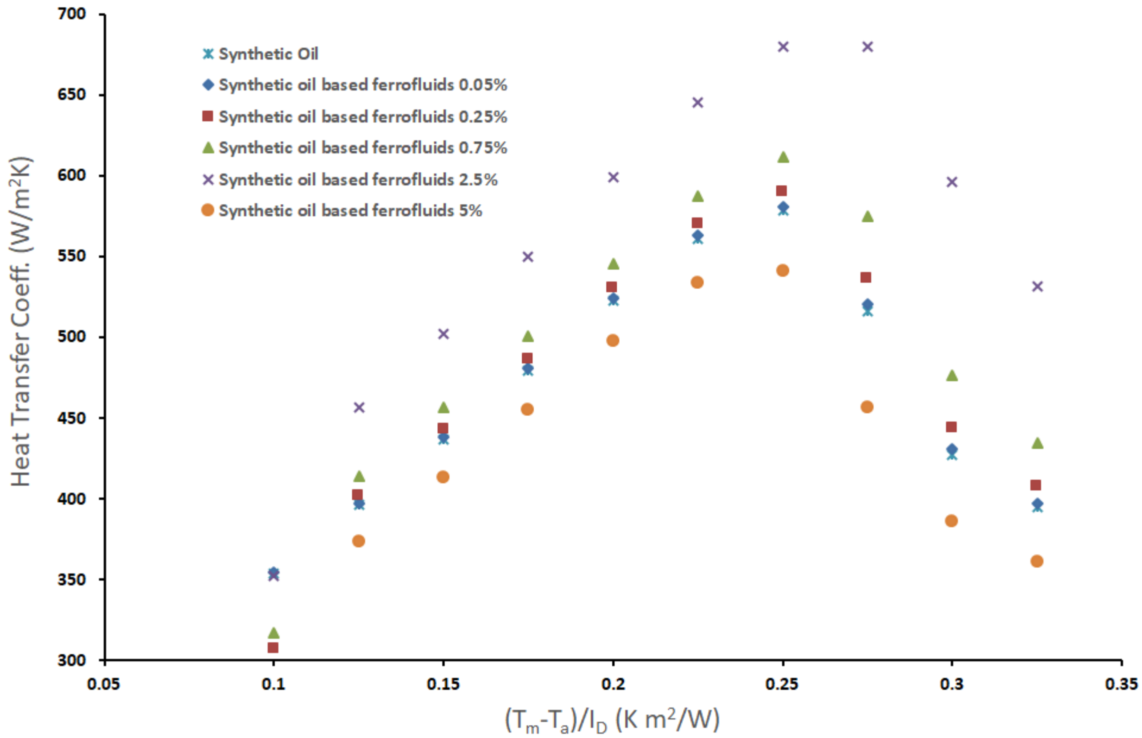

Figure 5-9: Convective heat transfer coefficient of different volume fraction vs. average temperature of ferrofluids above ambient.

5.6.1.2 Effect of external magnetic field

Figure 5-10 shows the efficiency of ferrofluids parabolic trough collector with 0.05% volume fraction ferrofluids in the presence of an external magnetic field. It is assumed that the enhancement in the properties is independent of temperature, and no effect on heat capacity in the presence of magnetic field. The enhancement of the performance of the collector is evident at low magnetic field intensity. The efficiency of the collector at a low reduced temperature increased 0.8% and at a higher reduced temperature 3.8%. Increasing the magnetic field intensity further will improve the performance of the collector and reach the peak at 6.28 mT and declines afterwards. The efficiency of the collector was minimum 2.5% and maximum 8.6% higher than the base fluid in the presence of 6.28 mT magnetic field intensity. The efficiency of the collector dropped afterwards due to the higher increase of viscosity of the ferrofluids compared to the thermal conductivity. The thermal conductivity almost reached the magnetization saturation, and a further increase in the magnetic field intensity will cause only increase in the viscosity and deteriorate the heat transfer. Figure 5-11 presents the thermal loss of the solar collector in the presence of an external magnetic field. Synthetic oil based ferrofluids with nanoparticles volume fraction of 0.05% and with a magnetic field intensity of 6.28 mT has the lowest thermal loss. Figure 5-12 illustrates the convective heat transfer coefficient of the collector in the presence of magnetic field.

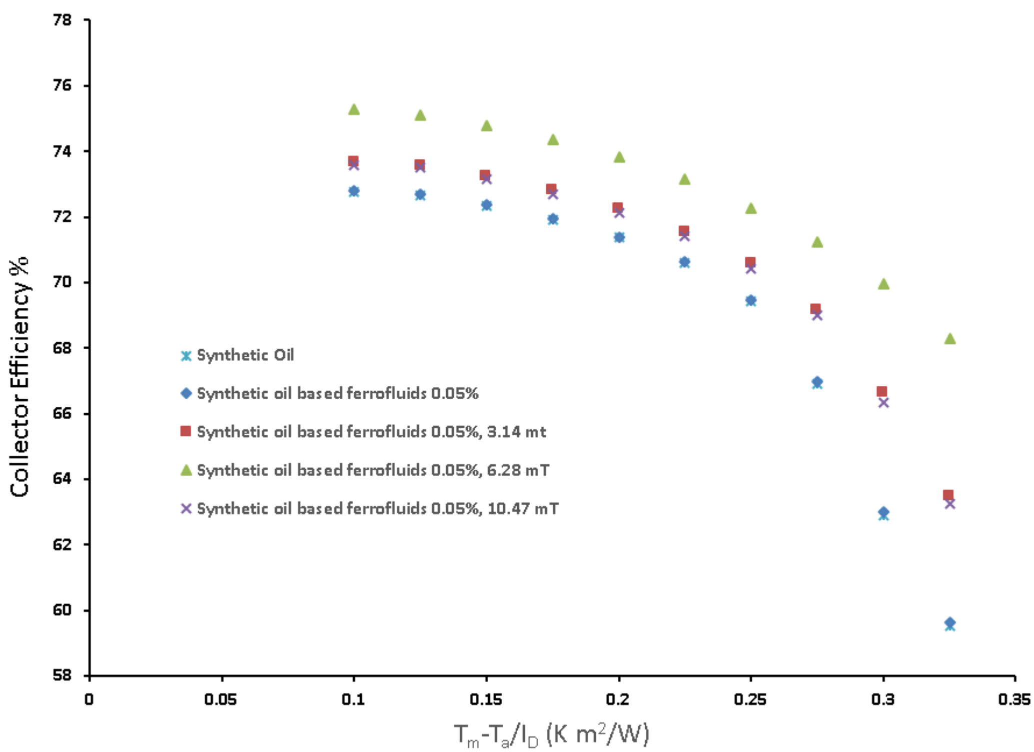

Figure 5-10: The efficiency of AZTRAK platform collector with 0.05% in the presence of magnetic field.

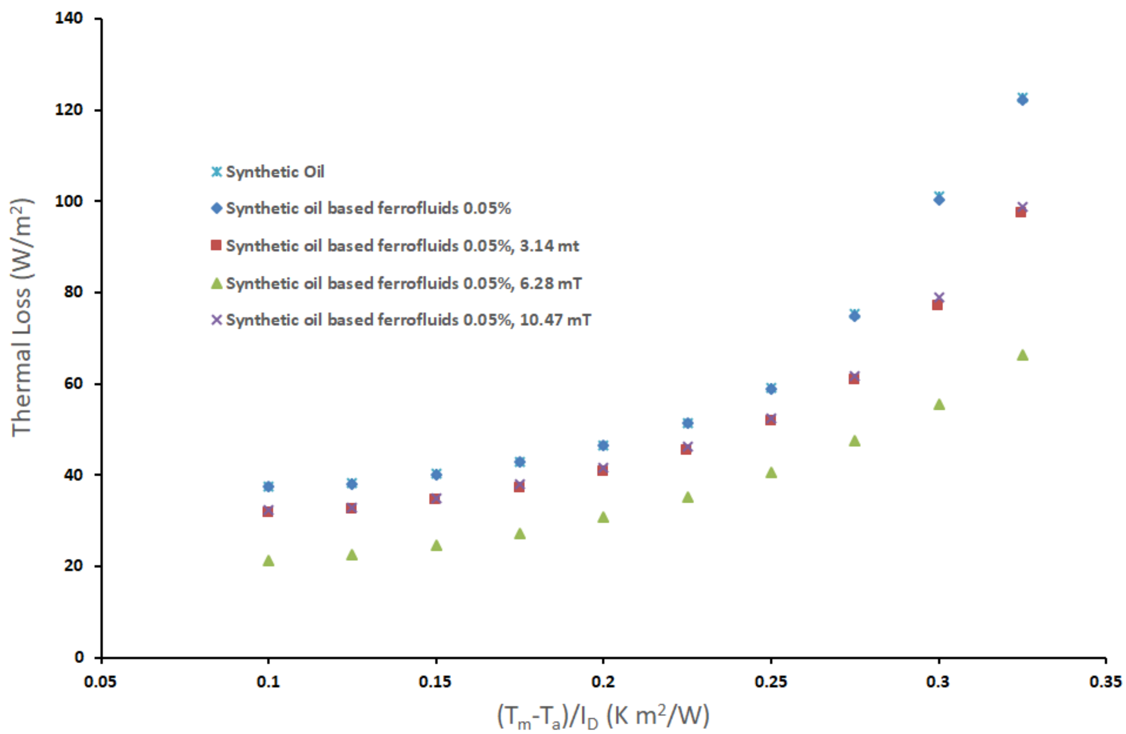

Figure 5-11: Heat loss of ferrofluids based parabolic trough collector AZTRAK design in the presence of an external magnetic field.

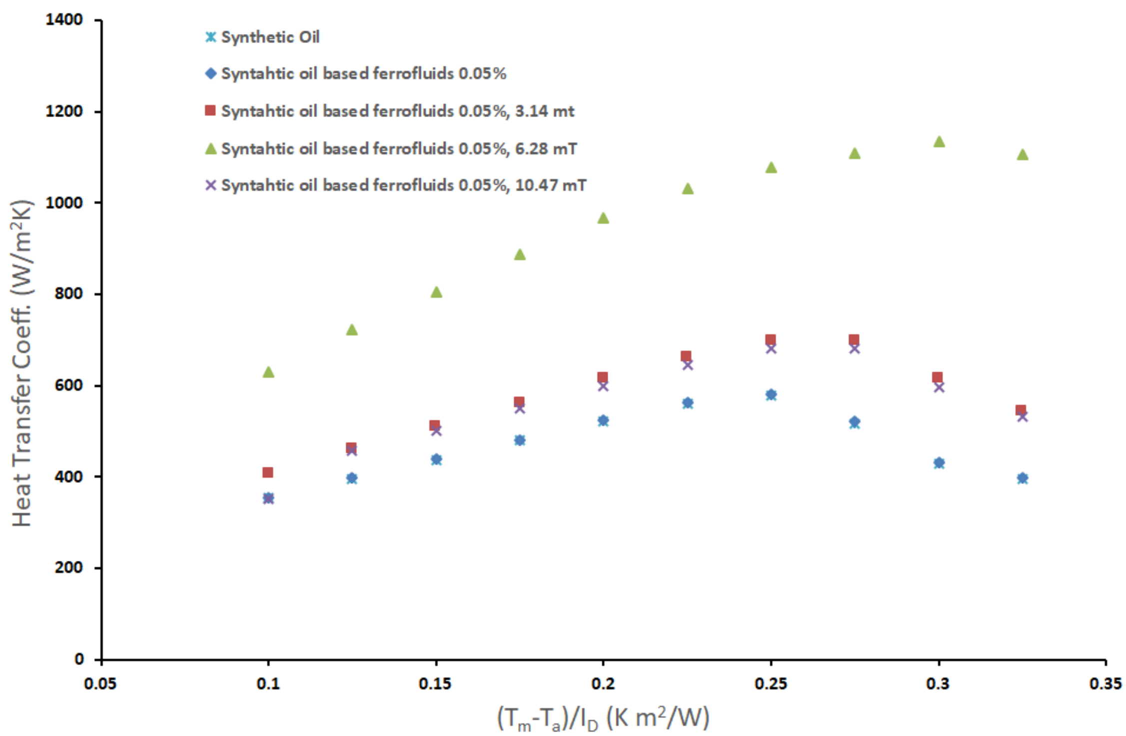

Figure 5-12: Convective heat transfer coefficient of different volume fraction vs. average temperature of ferrofluids above ambient.

5.6.1.3 Effect of glass envelope

Figure 5-13 illustrates the results of the heat transfer analysis of AZTRAK platform solar collector without glass envelope and with ferrofluids as heat transfer medium. The performance of the collector dropped significantly without glass envelope present. The efficiency was 20% lower than absorber with glass envelope at a reduced temperature of 100°C. The efficiency was much worst at higher operating temperatures where the efficiency of the solar collector with and without glass cover at a reduced temperature of 300°C was 62.9%, 30.7%, respectively. The results show how useful to use a glass envelope with vacuum in the annulus to reduce the thermal loss.

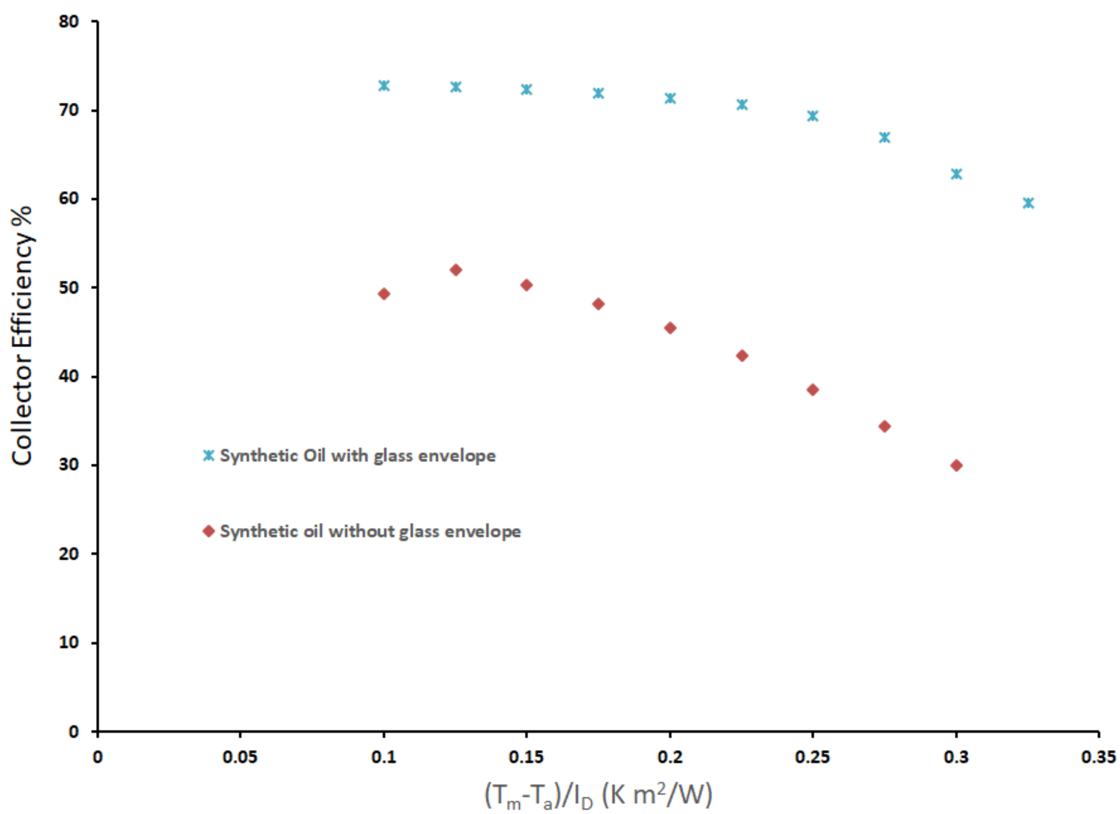

Figure 5-13: The efficiency of AZTRAK platform collector with and without glass envelope.

5.6.1.3 Effect of heat transfer fluid

The water showed high efficiencies when used as a heat transfer medium as parabolic trough Figure 5-14. The maximum efficiency was obtained was 78%, and the lowest was 74%. However, using water is limited due to the low boiling point of water and the high cost compared to flat plate collector.

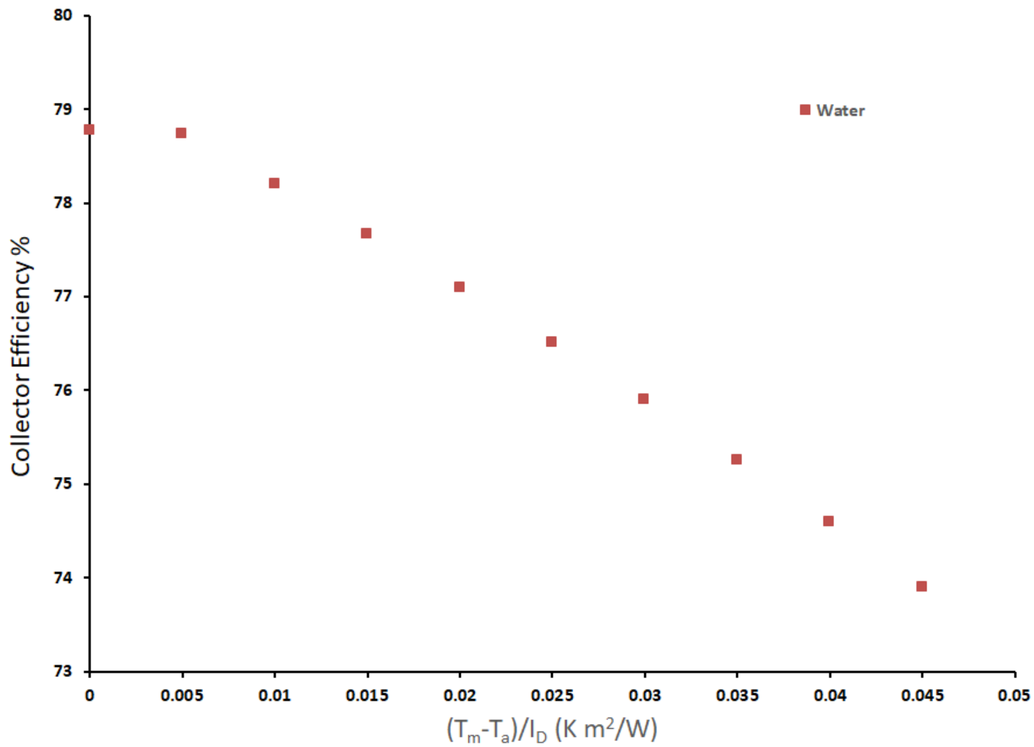

Figure 5-14: The efficiency of AZTRAK platform collector with water as heat transfer fluid.

5.6.2 Current study design (test rig)

The model was used to determine the performance of the test rig solar collector used in the present study (experiment design). The solar collector was first assumed to be a parabolic trough collector; then it was assumed to be a flat plate collector where the diameter of the solar absorber is replaced by the width of the collector. in both cases, no glass envelope was attached. The solar irradiance and the flow rate was equal to the ones used in the experiment in Chapter 4.

5.6.2.1 Performance of solar collector as concentrating collector

The performance of the collector of the experiment design with various concentration of nanoparticles is presented in Figure 5-15. Ferrofluids showed minimal improvement in the performance than the base fluid. With higher concentration, the performance enhanced further. The solar collector with 0.75% ferrofluids was greater than water by 0.28%. The difference of thermal loss of the ferrofluids based solar collector between various nanoparticles concentration is burly noticeable as shown in Figure 5-16. The maximum heat loss was 53.9 W with the volume fraction of 0.75%.

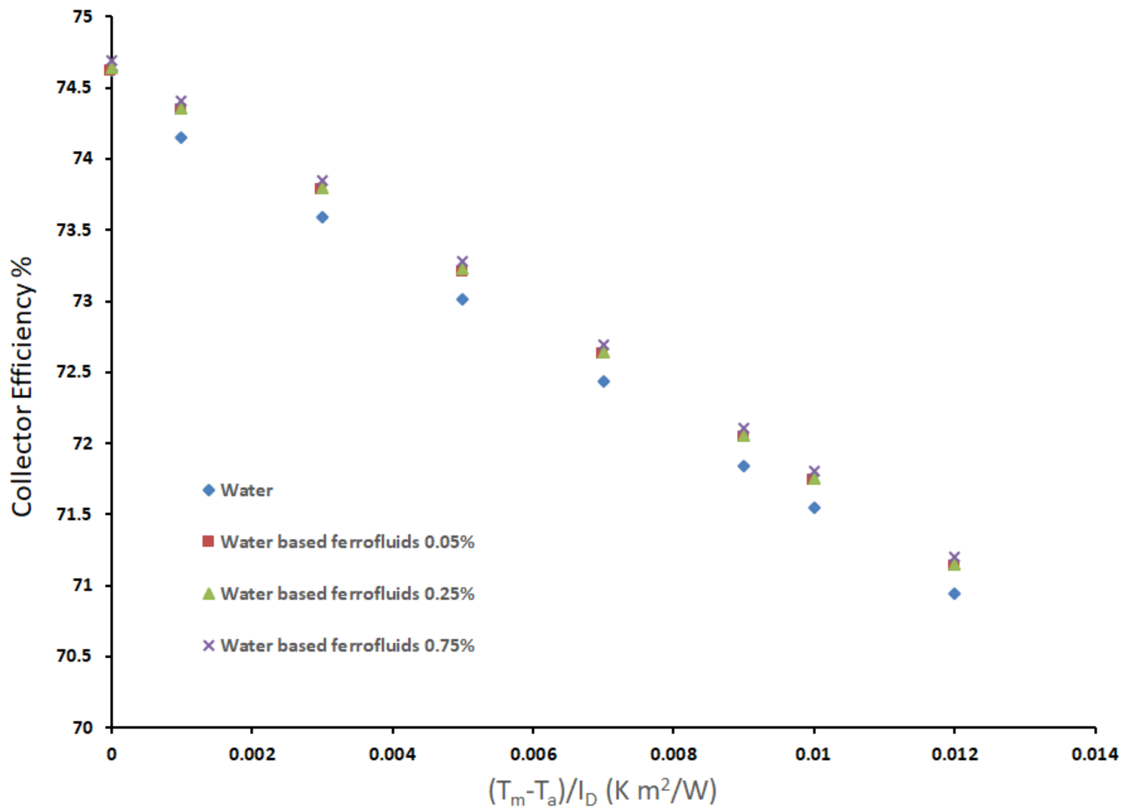

Figure 5-15: The efficiency of test rig ferrofluids based solar collector considered as concentrating collector with various nanoparticles volume concentration.

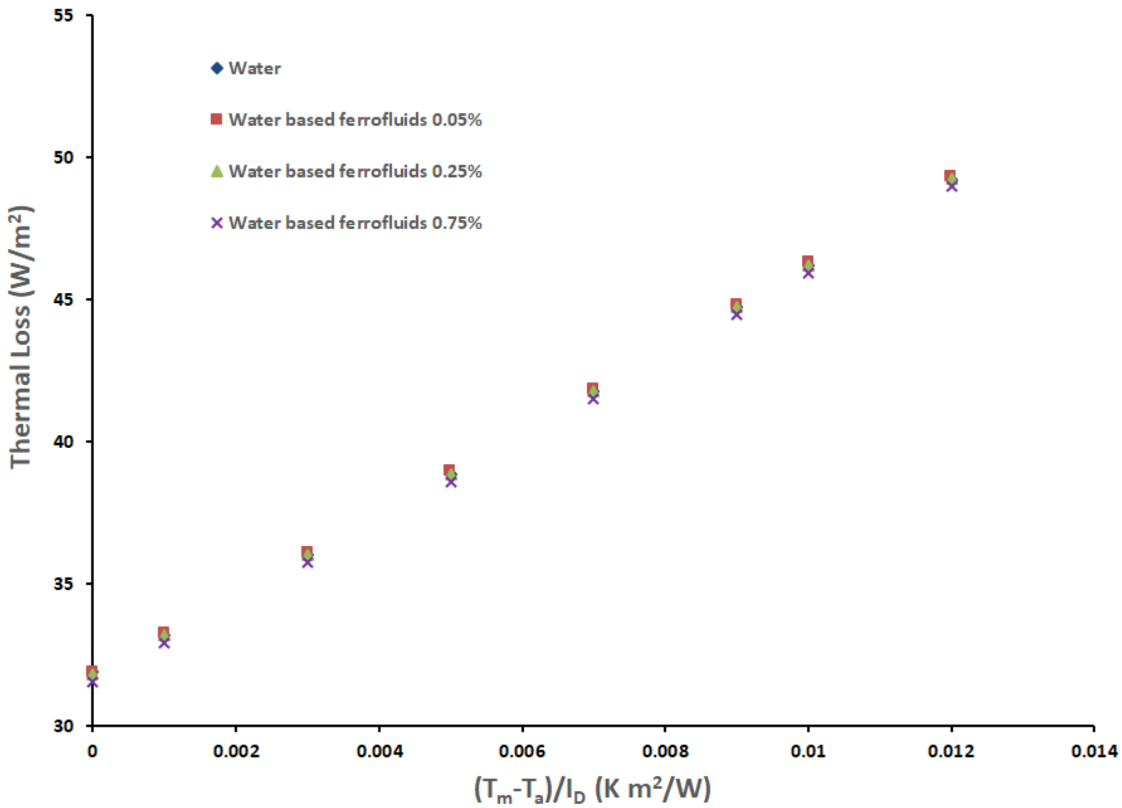

Figure 5-16: The thermal loss of test rig ferrofluids based solar collector considered as concentrating collector with different nanoparticles volume concentration.

5.6.2.2 Performance of solar collector as non-concentrating collector

The performance of the collector of the experiment design with various concentration of nanoparticles is presented in Figure 5-17. The performance of the collector was lower due to the assumption that heat loss occurs at the entire area of the collector and not only at the receiver cross area. Ferrofluids showed minimal improvement in the performance than the base fluid. With higher concentration, the performance enhanced further. The solar collector with 0.75% ferrofluids was greater than water by 0.28%.

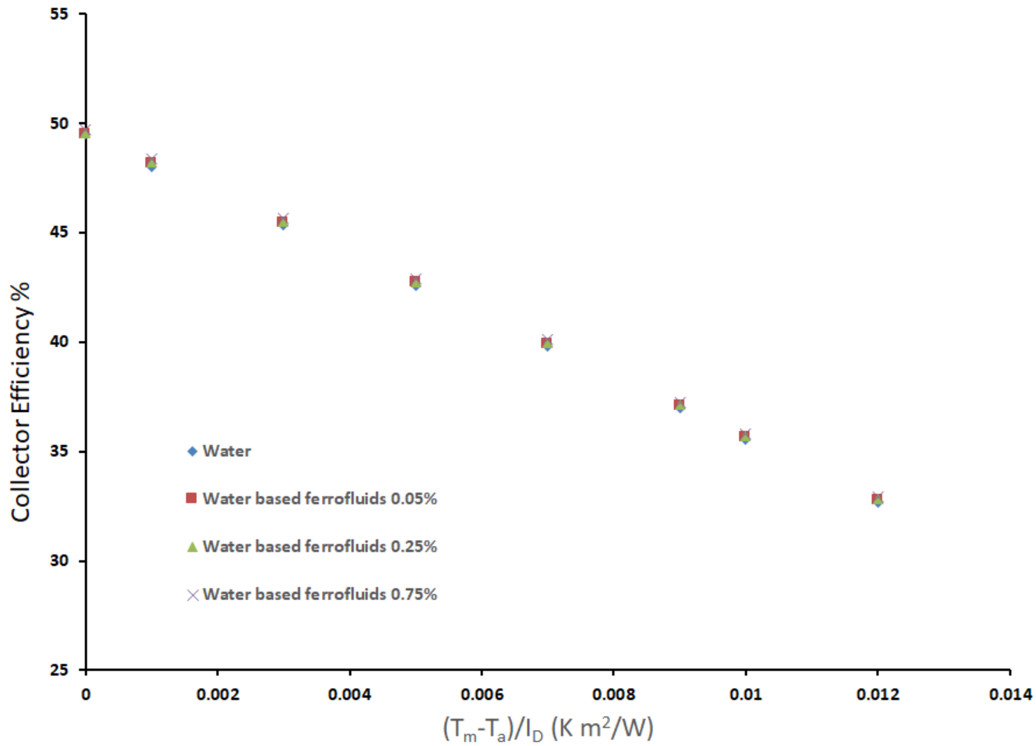

Figure 5-17: The efficiency of test rig ferrofluids based solar collector considered as non-concentrating collector with various nanoparticles volume concentration.

5.6.2.3 Performance of solar collector in the presence of magnetic field

The performance of the collector of the experiment design with different concentration of nanoparticles is presented in the presence of external magnetic field Figure 5-18. Ferrofluids showed better improvement than the base fluid in the performance of the collector in the presence of external magnetic field at 6.24 mT and higher. The efficiency enhanced maximum by 40% with 0.05% volume fraction and 10.47 mT. Figure 5-19 presents the thermal loss of the test rig ferrofluids based solar collector in the presence of magnetic field. The higher the magnetic field intensity, the lower the heat loss is. Compared to the experimental results the performance of the solar collector apparently acts as a flat plate collector due to the low concentration ratio, and no glass envelope was installed. The model is close to the experimental results at the small reduced temperature parameter, and at high reduced temperature, the experimental results are greater than the model. At higher reduced temperature, the solar collector cannot be considered as a non-concentrating collector. From the results, it's clear that the enhancement of the thermophysical properties can affect the performance of the collector significantly in the presence of magnetic field.

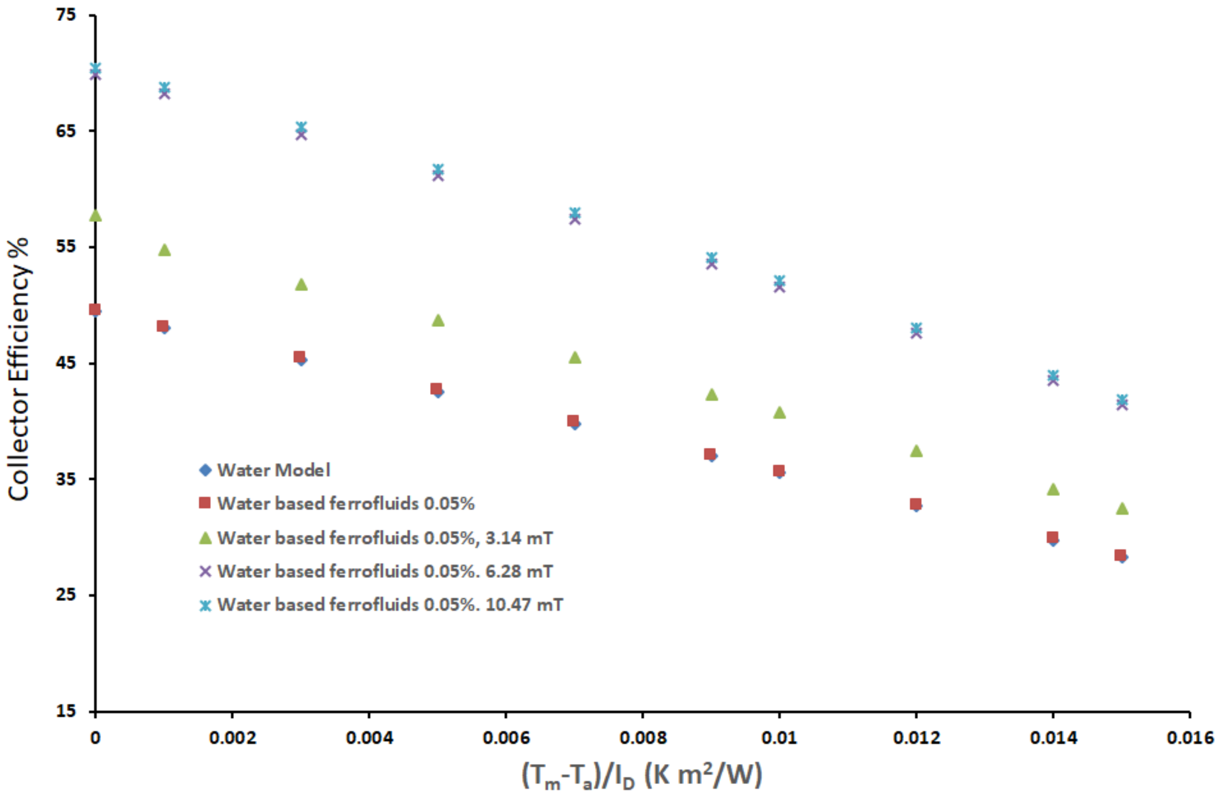

Figure 5-18: The efficiency of test rig ferrofluids based solar collector considered as non-concentrating collector with various nanoparticles volume concentration.

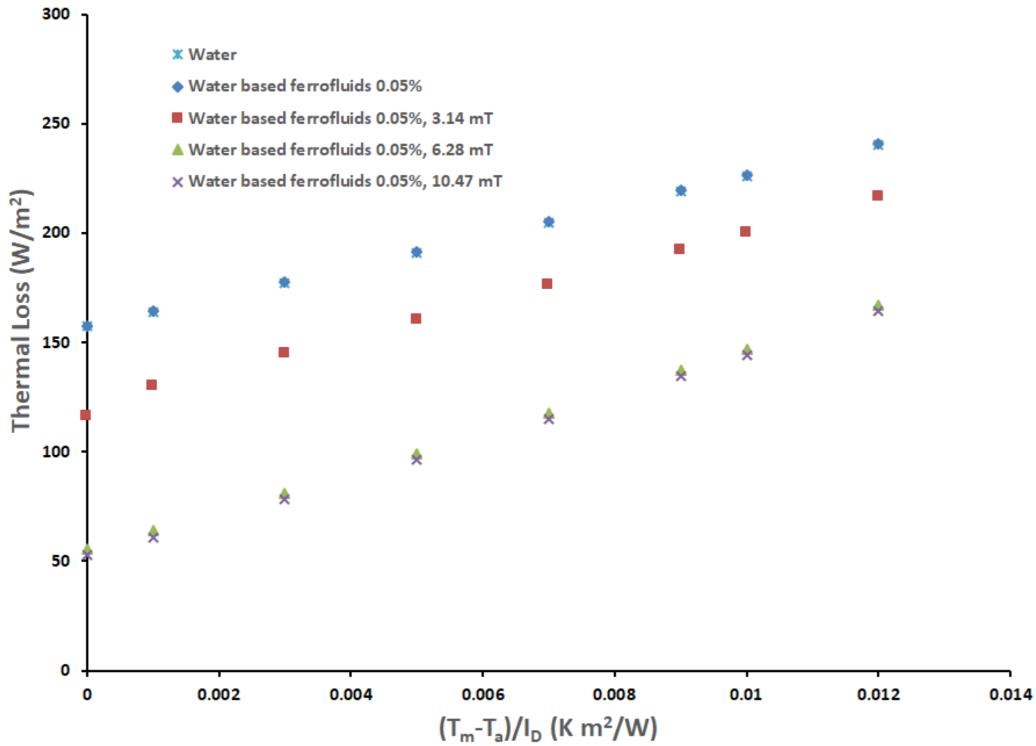

Figure 5-19: the thermal loss of test rig ferrofluids based solar collector regarded as not concentrating collector with different nanoparticles volume concentration.

5.7 Conclusion

The performance of ferrofluids based parabolic trough collector was theoretically investigated. The correlation, equations, and parameters used in the model were discussed in detail. The model was used to study two different parabolic trough designs. First, the parabolic trough was validated with the experimental results of AZTRAK platform. The results of the model showed a good agreement with the experimental data. Thereafter, nanoparticles were added to the heat transfer fluid, and the performance of the collector with and without the presence of external magnetic field was determined. The performance of the collector did not change a lot unless the external magnetic field was present. Moreover, the effect of the glass envelope on the performance was observed. A glass cover with vacuum in the annulus has higher performance and less thermal loss. Second, the model was used to study the performance of the test rig ferrofluids based parabolic trough. The performance of the parabolic trough was considered as concentrating collector and non-concentrating collector, due to the low concentration ratio and the absence of glass envelope. The performance of the collector as a non-concentrating solar collector is similar to the experimental results. The effect of ferrofluids in the absence and in the presence of magnetic with various nanoparticles concentration is determined. With the lack of an external magnetic field, the efficiency changed slightly, wherein the presence of the external magnetic field the performances of the collector enhanced and showed higher performances. In General, the presence of the magnetic field showed promising enhancement. However, computation fluids dynamics is needed to determine the change of thermophysical properties of ferrofluids across the length of the collector.

Chapter 6. Environmental and Economic Analysis

6.1 Introduction

As discussed in chapter 1 the electricity tariffs are increasing rapidly in Saudi Arabia, and it is expected to increase further in the next years. Therefore, using solar collectors is one of the methods that could be used to lower energy consumption. The improved efficiency of ferrofluids based solar collector compared to conventional solar collector makes it necessary to compare their economic and environmental impacts. Life cycle assessment has been used to determine the economic and environmental impacts of heating water utilising water solar thermal collector [155]. In this chapter, the environmental and economic analysis is carried out on the low concentration ratio ferrofluids parabolic trough collector presented in the previous chapters and compared to the conventional flat-plate collector. Both collectors are used as solar hot water collectors. Due to the simplicity of the parabolic trough design, the low concentration ratio of the parabolic mirror and the unglazed absorber, the parabolic trough collector applicable as solar hot water technology and its performance is equivalent to flat-plate collectors. The performances of direct and non-direct absorbers of the ferrofluids parabolic trough were investigated.

6.2 Analysis

The life cycle assessment is an adequate method to evaluate different components of a systems effects on the environment from its original resource distribution to its demolition/recycle after the system lifetime. The LCA used in the study is limited to focus on the main parts of manufacturing, and operation of the solar collector and their embodied energy. 70% of the embodied energy of the solar collector is caused by the manufacturing of the collector frame. Therefore, the distribution, maintenance, and disposal stages of the solar collectors have not been considered whereas the manufacturing was the focus of the embodied energy. The analysis was carried on with the solar collector area as the functional unit which is determined based on the thermal performance of the collector. The thermal performance of the collector was evaluated for Tabuk, Saudi Arabia region. The typical household in Tabuk is a 4-person family dwelling that utilises 300 L of hot water daily from electric water heaters. The averaged hot temperature delivered is 60°C.

6.2.1 Thermal analysis

The collector efficiency could determine the useful energy obtained from the solar collector.

$$\dot{Q}_u = \eta I_D A_C \qquad \text{Eq. 6-1}$$

The collector efficiency is based on the experimental data that is a function of solar irradiance and the ambient temperature. For a common flat-plate collector, which utilize moderate selective surface absorber, the efficiency of the collector given below is utilised [99].

$$\eta_{flat-plate} = 0.51 - 4.452\,(T_m - T_a)/I_D \qquad \text{Eq. 6-2}$$

Based on the experimental work shown in the previous chapters, the efficiencies of magnetic nanofluids parabolic trough collector for various magnetic intensity are the following:

$$\eta_{water} = 0.47 - 14.289\,(T_m - T_a)/I_D \qquad \text{Eq. 6-3}$$

$$\eta_{0.05\%,0\,mT} = 0.497 - 7.243\,(T_m - T_a)/I_D \qquad \text{Eq. 6-4}$$

$$\eta_{0.05\%,3.14\,mT} = 0.516 - 6.87\,(T_m - T_a)/I_D \qquad \text{Eq. 6-5}$$

$$\eta_{0.05\%,6.28\,mT} = 0.69 - 9.59\,(T_m - T_a)/I_D \qquad \text{Eq. 6-6}$$

$$\eta_{0.05\%,10.47\,mT} = 0.687 - 7.314\,(T_m - T_a)/I_D \qquad \text{Eq. 6-7}$$

For direct absorption absorber, the chosen efficiency was the following:

$$\eta_{0.25\%,10.47\,mT} = 0.69 - 13.99\,(T_m - T_a)/I_D \qquad \text{Eq. 6-8}$$

The efficiencies above were chosen based on their performances and their ferrofluids volume concentration. The lower the volume concentration, the lower the cost and the embodied energy.

The permeances of the collectors were used to determine the auxiliary energy needed that is provided by the conventional electric water heater:

$$\dot{Q}_{aux} = \dot{Q}_{Load} - \dot{Q}_u \qquad \text{Eq. 6-9}$$

where $\dot{Q}_{Load}$ is the energy required by the daily hot water load, theses parameters were all evaluated at ambient weather data and water temperature of Tabuk given in Table 6-1. From the auxiliary energy, percentage of saved energy due to the use of the solar collectors can be determined, this is known as solar fraction, from Eq. 6-9.

$$f = \frac{\dot{Q}_{Load} - \dot{Q}_{aux}}{\dot{Q}_{Load}} \qquad \text{Eq. 6-10}$$

The economic and the environmental analysis is based on the results of the thermal analysis.

Table 6-1: Environment weather data for Tabuk city [156].

Month	Solar Irradiance ($kWh/m^2/day$)	Ambient temperature (°C)	Water temperature (°C)
January	5.7	13	8.2
February	7	15.7	7.9
March	5.3	17.2	9.2
April	6.5	23.7	12.8
May	8	27.3	16.8
June	8	34	20
July	9	35.6	21.5
August	8.7	33.8	22.8
September	8.5	30.4	22.1
October	8.2	24.8	19.4
November	5.3	18	15.7
December	5.2	11.7	11

6.2.2 Economic analysis

To meet the hot water demand energy, additional energy needs to be provided by an electric hot water system. In this analysis, no financing for the solar collector is considered, and all capital costs are paid in the first year. The capital costs for solar collectors have generally defined as the integration of the area independent costs and the area based costs.

$$C_s = C_a A_c + C_f \qquad \text{Eq. 6-11}$$

where C_f is the area independent costs, and C_a is the area dependent costs. The design and the cost of the parabolic trough in the economic analysis was chosen to be based on NREL Sky Trough shown in Figure 6-1. The area independent cost for both collectors is considered to be £150 [155]. The area dependent costs for flat-plate solar collector and parabolic trough collector are estimated to be $140/m2, $132/m2 respectively [157, 158]. For the ferrofluids parabolic trough collector has additional area based cost which is the cost of magnetic nanoparticles, currently £1.88/g [159]. The maintenance cost C_m is 1% of the capital cost with a raise yearly by 1% for 15 years system life time. The ferrofluids parabolic trough collector is assumed to have the same lifetime as the common parabolic trough collector because it uses the same material as common collector. However, extra cost and embodied energy for using ferrofluids mixture is considered. The total cost is then:

$$C_t = C_s + C_m \qquad \text{Eq. 6.12}$$

To estimate the saved cost due to the operation of the solar collectors, the energy flow per day is used in combination with the local electricity tariffs based on pound per kWh [160].

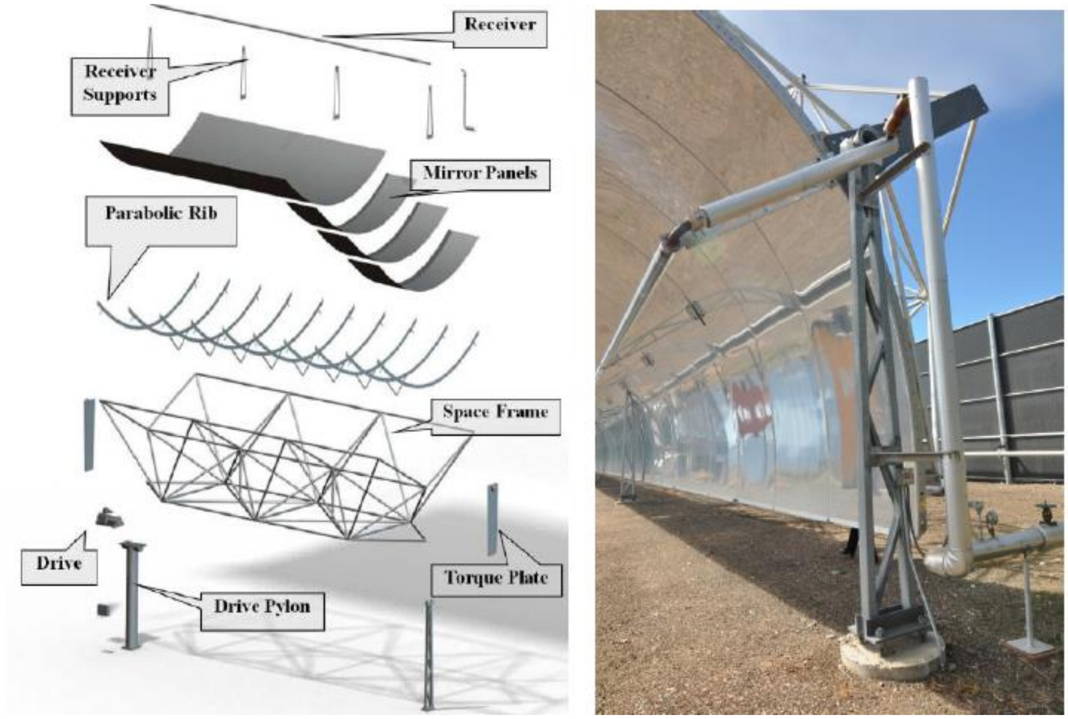

Figure 6-1: Main components of SkyTrough and picture of actual collector [161].

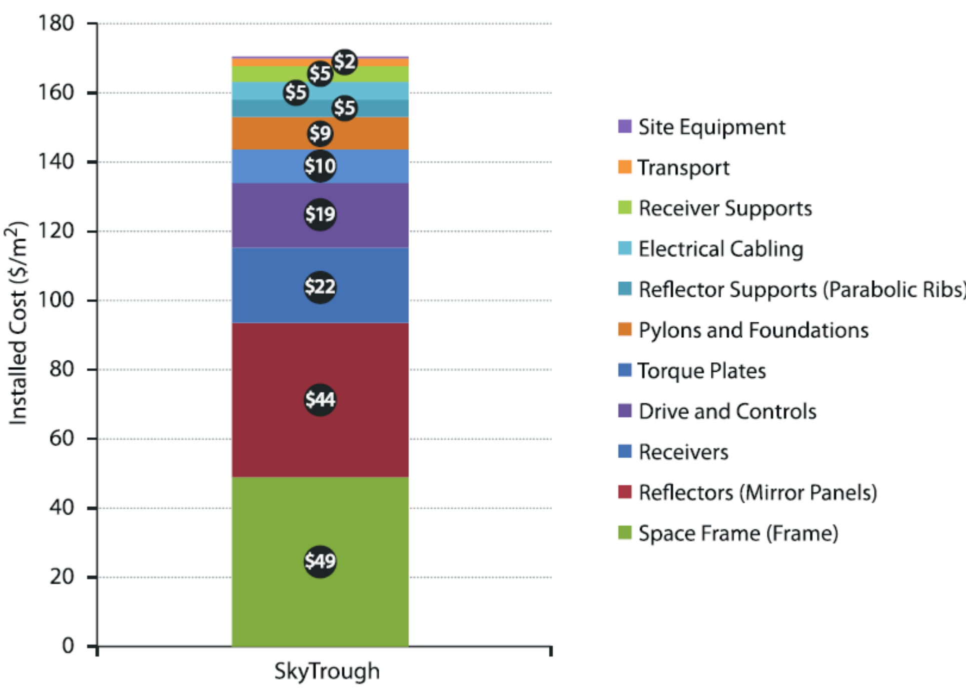

Figure 6-2: Installed cost of each component of SkyTrough [161].

6.2.3 Environmental analysis

The main reason for applying a solar collector to heat water is the reduction in emissions produced from burning fossil fuels to create energy to heat the water. The energy flows on daily and monthly base given by the results of the thermal analysis of the collector, the emissions offset can be estimated based on the energy offset $(\dot{Q}_{Load} - \dot{Q}_{aux})$ and the emissions profile for electricity generation for Tabuk.

$$P_{x,offset} = \sum_{j=1}^{N} A_{j,x} B_{j,x} (\dot{Q}_{Load} - \dot{Q}_{aux}) \quad \text{Eq. 6-14}$$

where A is the quantity of pollutant in kg per MJ of energy produced, B is the percentage of energy produced from a specific fuel type, and x is the pollutant type. The electricity distribution from different fuel types and the pollutants produced for the city of Tabuk is shown in Table 6-2.

Table 6-2: Electricity production by fuel type and elementary emissions mix for Tabuk.

Fuel	% of electricity generated	Carbon dioxide CO_2 (kg/MJ)	Nitrogen oxides, NO_x (kg/MJ)
Petroleum	65	0.220	0
Natural gas	35	0.113	0.00003

Additionally, a comprehensive environmental analysis should also contain the effect on different environment receptors from other phases such as allocation, maintenance, and post-consumer use. A recent study showed that most embodied energy for solar collector results from the manufacturing [162]. Therefore, only the manufacturing phase is considered in this embodied energy analysis and also other phases are discussed later. The type and mass of each material used in the manufacturing are needed to determine the embodied energy of each solar collector. This analysis uses the embodied energy index created by Alcorn [163] which estimates the embodied energy in different conventional construction materials, and these indexes contain the obtaining and transporting of the materials. SunEarth for the Empire collector provides the quantity of materials for common solar collectors. The embodied energy of the magnetic particles for ferrofluids based solar collector is considered based on the results for energy needed for magnetic nanoparticle production [164]. With the quantity of each component material determined and the embodied energy index, the embodied energy and thus the emissions from the manufacturing of the collectors (from Eq. 6-14, where $(Q_{load} - Q_{aux})$ is replaced with the embodied energy) can be estimated. The offset damage costs are calculated based on the damage cost factors for the three main pollutants studied: CO_2 and NO_x [165]. These offset damage costs are not factored into the economic analysis as they are not costs directly applicable to the collector owner.

6.3 Results and Discussion

The above analysis addressed the thermal performance, environmental effect, and economic effect for flat-plate and ferrofluids based solar collectors. The thermal performance is the groundwork for the remaining study as it provides the monthly energy needed to supply the solar collectors. The cost and pollutant reduction from the collector performance determined by the flow energy flow compared to base load. The results of the thermal analysis are shown in Figure 6-3 and Figure 6-4. From both figures, it can be seen that the ferrofluids based collector with the volume fraction of 0.05% and external magnetic field intensity of 10.47 mT provide the highest solar fraction and lowest auxiliary energy requirement. The parabolic trough collector with water as heat transfer medium had the lowest solar fraction and the highest auxiliary energy demand. Using ferrofluids as heat transfer fluids improved the performance of the parabolic trough collector, but it was lower than a conventional flat-plate collector. The performance of the parabolic trough collector improved further once an external magnetic field was a presence. The performance of the parabolic trough was higher than flat-plate collector with the external magnetic field of 6.28 mT. During the summer, the solar collectors generate all the energy required to meet the needed load. The needed load is extremely reduced in the summer due to the increased inlet temperatures of water. The annual solar fraction for the flat-plate collector and Ferrofluids based solar collector with 10.47 mT magnetic field intensity is 78% and 87%, respectively.

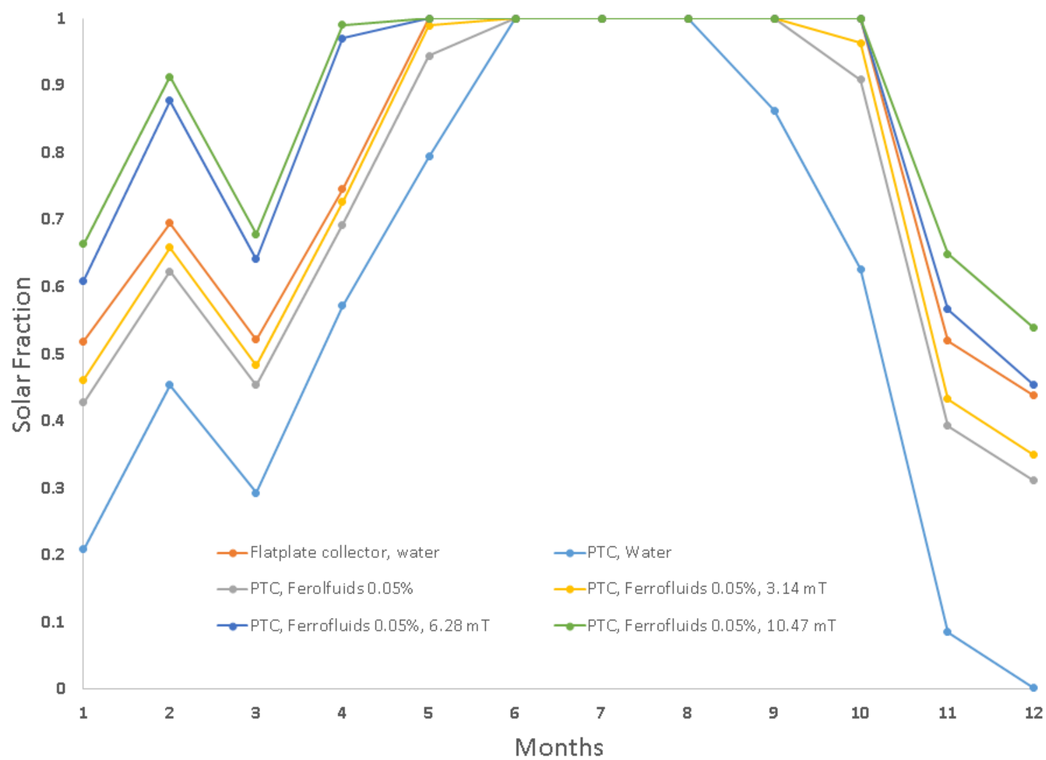

Figure 6-3: Solar fraction of flat plate collector and ferrofluids parabolic trough collector.

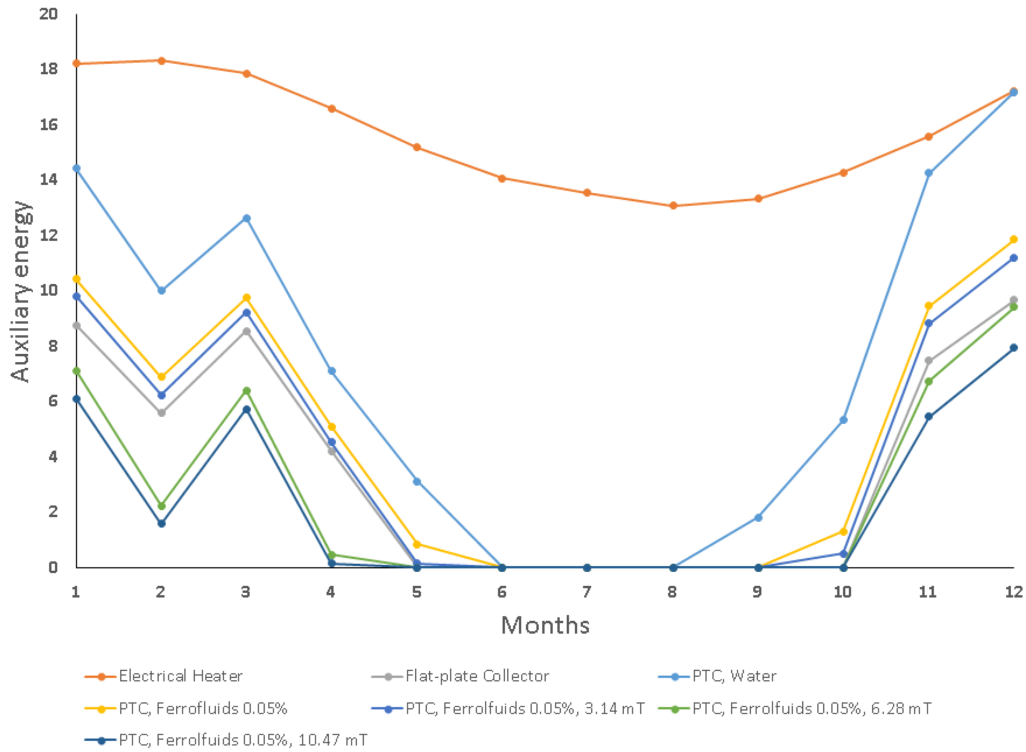

Figure 6-4: Auxiliary energy of flat plate collector and ferrofluids parabolic trough collector.

The saving in capital costs, maintenance costs, and offset fuel can be estimated based on the thermal analysis and the current price of electricity. The ferrofluids based solar collector has additional cost due to the cost of nanoparticles, permanent magnets, and higher maintenance costs. However, the ferrofluids based parabolic trough has greater electricity cost saving per year than flat-plate collector due to the higher efficiency and solar fraction. The payback period for the flat-plate collector is less than the ferrofluids based collector in the absence of magnetic field due to the higher capital cost of nanoparticles and lower thermal efficiency. In the presence of the external magnetic field, the capital cost is higher, however, the payback period is the lowest. In Saudi Arabia, the only electric water heater is used, due to the no existing natural gas infrastructure. The total life cycle saving is £1685 and £2369 for the flat-plate collector and ferrofluids based solar collector with permanent magnet respectively. The results show that from an economic perspective the use of the small scale ferrofluids based solar collector has an advantage over the commercial flat-plate collector. Both collectors give significant savings over the life of the collector. Additionally, it is expected that the price of nanoparticles decreases due to their expected increase in production and usage in the near which can further increase the saving with the ferrofluids based solar collector. Furthermore, an improvement on the small scale of the ferrofluids based solar collector could improve the thermal efficiency and increase the saving further.

Flat-plate collector and ferrofluids based parabolic trough collector differ in the materials used in their construction, which has an impact both on the collector weight and embodied energy. Table 6-3 presents the materials used in the ferrofluids parabolic trough collector as well as the embodied energy of each material and the collector total. The embodied energy for flat-plate collector when based on the area of the collector gives 1334.5 MJ/m^2 [93]. To reduce the embodied energy of parabolic trough collector, the traditional curved glass mirror is replaced by mirror film with aluminium sheet. This reduces the embodied energy for the mirror from 356 MJ/m^2 to 85MJ/m^2. The embodied energy of ferrofluids based parabolic trough collector is slightly higher than conventional parabolic trough due to the additional embodied energy form nanoparticles and a permanent magnet. Moreover, the embodied energy of the ferrofluids parabolic trough is 4845 MJ lower than a flat-plate collector.

The pollution created by manufacturing the solar collectors and the saving of pollution can be determined from the thermal analysis and the embodied energy assessment. The results of the analysis are presented in Table 6-3. The manufacturing of the ferrofluids based parabolic trough collector results in 31 kg more CO_2 emissions than water-based parabolic trough and 200 kg less CO_2 emissions than flat-plate collector while operational it saves 136 kg/year when compared to a flat-plate collector. Over 15 years expected a lifetime of the solar collectors; the ferrofluids collector would save more than 2040 kg of CO_2 in comparison to the flat-plate collector and 17,000 kg of CO2 when compared to an electric heater. The environmental impact of nanoparticles is not included in this study. few studies focused on the environmental impact of nanoparticles on ecological system and human health [166, 167]. Both studies focus on nanoparticles that are not suspended in the liquid, which considerably declines the risk for inhalation, but could present a potential problem if entered the water cycle.

Table 6-3: Embodied energy for ferrofluids based- and typical parabolic trough.

Description	Embodied energy index (MJ/m2)	Embodied energy content (MJ)	
		Conventional parabolic trough	Ferrofluids based parabolic trough
Aluminium for reflectors	65	260	260
Polymer film plus silver	20	80	80
Absorber Tube	75	300	300
Steel	20	80	80
Aluminium space frames	165	660	660
Concrete	30	120	120
Landfilling	20	80	80
Nanoparticles	1.8	0	7.20
Permanent magnet	28	0	168
Total		1580	1755.2

Table 6-4: Emissions from embodied energy of manufacturing and operational energy.

Emissions	Pollution from solar collector embodied energy		Saving of solar collector	
	Flat-plate (kg)	Ferrofluid-based (kg)	Flat-plate (kg/year)	Ferrofluid-based (kg/year)
Carbon dioxide (CO_2)	973.35	384.9	1127.9	1264
Nitrogen oxides (NOx)	0.06	0.02	0.06	0.07

6.4 Conclusion

Environmental and economic effects of using ferrofluids based solar collector compared to a flat-plate collector for domestic hot water systems. Results show that the ferrofluids based parabolic trough has lower payback period and higher economic saving at the end of its useful life than a flat-plate solar collector. The ferrofluids based collector has higher embodied energy and pollution offsets tan flat-plate collector. In addition, if 50% insertion of ferrofluids based parabolic trough for hot water heating could be reached in Tabuk over 83,750 metric ton of CO_2.

Chapter 7. Summary and Future Work

7.1 Summary of current work

Research works conducted by this thesis offer an innovative design on using magnetic nanofluids (ferrofluids) as a heat transfer fluid in parabolic trough collector. The ferrofluids based parabolic trough collectors enhance their thermal efficiency compared to conventional solar collectors. The design of ferrofluids based parabolic trough emphasis on the change of thermophysical and optical properties of ferrofluids in the presence of an external magnetic field. Comprehensive literature survey covered from early stage to up-to-date research works on ferrofluids, solar collector, and nanofluids based solar collector has been presented. Indoor experimental investigation on the performance of small scale ferrofluids based parabolic trough collector in laminar flow region was carried on. To compare the effect of ferrofluids on the performance of the collector and compare it to base fluid a steady state test condition was chosen. The solar collector test rig was assembled by the author with a collector area of 0.1125 m^2. The materials used in the test rig have been selected based on mimicking commercial parabolic trough considering availability, simplicity, and low-cost equipment. Low solar concentration ratio was picked to assure full reflection of solar irradiance from the mirror to absorber tube without escaping. Moreover, the absorber tube has no glass envelope due to the impermanent electromagnets installed on the absorber. The low concentration ratio and unglazed absorber cause the performance of the parabolic trough to act like non-concentrating solar collectors. Two absorber types were used non-direct absorber with selective surface copper tube and direct absorber tube with a transparent glass tube. The external magnetic field intensity was controlled by the current passing through the electromagnet. Three different intensity were chosen 3.14mT, 6.28mT, and 10.47mT. The ferromagnetic nanoparticles used in the experiment was prepared by a colleague using co-precipitation method. The average diameter of nanoparticles was 10 nm. Sodium dodecyl SDS absorbed onto the surface of the nanoparticle, and then the nanoparticles were suspended in water. SDS increase the stability of the suspension and avoid sedimentation of particles. Three different nanoparticle concentrations were used 0.05%, 0.25%, and 0.75% with an operational temperature between 19°C and 40°C. The experimental test showed that the use of ferrofluids can enhance the performance of the solar collector in the presence of external magnetic field. In the presence of the external magnetic field, the performance of the ferrofluids based parabolic trough improved when the magnetic field gradient was parallel to the flow direction and declined when the magnetic field gradient was opposite to the flow direction. Increasing the magnetic intensity improved the efficiency of the collector further. The enhancement in the performance is contributed to the chain-like structure and to the Kelvin force and auxiliary static pressure gradient. Ferrofluids also showed good results in direct absorber. The rising the volume concentration of the ferrofluids improve the absorption coefficient and increase the optical thickness of ferrofluids. In the presence of the external magnetic field, the performance of the ferrofluids based collector with direct absorber enhanced further. The use direct absorber showed promising results. However, the optimum optical thickness was not investigated where the optical thickness is a function of the absorption coefficient of the nanoparticles along a path. To achieve the highest efficiency of the system an optimum optical thickness of the receiver should be determined. In the study, the best performance of the ferrofluids based collector was with non-direct absorber with the volume fraction of 0.05% and magnetic intensity of 10.47 mT.

Heat transfer analysis model has been carried out to investigate the effect of utilizing ferrofluids as a heat transfer fluid in commercial parabolic trough design. In addition, the model was also carried out on the test rig design, and the results were compared with the above mentioned experimental results. The model was validated by comparing the results with experimental data obtained from Sandia National Laboratory. The model showed good agreement with the experimental data. When low concentration ferrofluids where used in the commercial parabolic trough design a slight increase in the efficiency was obtained. Marginally higher volume fractions make the convective heat transfer better and decrease the thermal loss by 24% at higher reduced temperature parameter. In the presence of magnetic field, the heat transfer showed higher efficiencies at lower particles concentration. In addition, the effect of galls envelope on the heat transfer was presented. Without glass envelope, the efficiency of the collector dropped significantly. For the test rig, the parabolic trough was first assumed to be a concentrating solar collector, and then it was assumed to be a non-concentrating solar collector. In both cases, ferrofluids showed minimal improvement in the performance compared to the base fluid. In the presence of the external magnetic field, the efficiency of the parabolic trough collector improved significantly. In the case of the non-concentrating solar collector, the results of the model for 0.05% agreed with the experimental data obtained in this study. Since the performance of the test rig is similar to the performance of flat-plate collector, the economic and environmental impacts of the test rig ferrofluids based collector is compared to a flat-plate collector for hot water systems. Comparing the payback period, the test rig ferrofluids based solar collector is lower than a flat-plate collector. In addition, the test rig had a higher economic saving at the end of its useful life. The ferrofluids based collector has higher embodied energy and pollution offsets tan flat-plate collector. In addition, if 50% insertion of ferrofluids based parabolic trough for hot water heating could be achieved in Tabuk over 83,750 metric Ton of CO_2.

The solar collector benefits from the magnetic and optical properties of ferrofluids which enhance the efficiency of the collector. Utilizing ferrofluids in solar collectors has environmental and economic benefits and causes improving in heat transfer, consequently reducing the needed area of collector and these advantages could be achieved with little change on the system.

7.2 Future work

Some future works are recommended based on current work.

- General improvement on the test rig is required.
    - Higher concentration ratio and glass envelope are needed to increase the efficiency of the collector and to treat it as concentrating collector.
    - Most of solar collector systems work in turbulent flow regime due to the higher heat transfer at higher flow rates. To achieve a steady flow rate with low fluctuation the pump needs to be replaced.
    - Higher optical properties of the selective surface are necessary.
    - Investigating the effect of absorber diameter on the performance of direct absorption absorber is required.
- Ferrofluids thermos-physical and optical properties in the absence and the presence of external magnetic field needs to be determined before conducting the experiment. Moreover, the thermophysical properties need to be determined at a wide range of temperatures and with different nanoparticles such as cobalt.
- Developing ferrofluids that behave as a Newtonian fluid and has low surfactant concentration is important to make ferrofluids efficient solution in heat transfer applications.

- Experiments need to be conducted at high operating temperatures considering the effect of Curie temperature on the performance of the collector.
- The effect of the location of the magnetic source and the distance between them on the performance of the collector needs to be investigated.
- The two-dimensional model needs to be developed using computational fluid dynamics to study the effect of nanoparticles distribution in the fluids, and hence its effects on the heat transfer fluids. Moreover, the effect of different forces such as magnetic force, Kelvin force on the nanoparticles and fluids can be determined by using the lattice-Boltzmann method.
- Further experimental and theoretical investigation on the direct solar absorber is needed. The optimum optical thickness needs to be determined.
- Outdoor experiment with larger prototype ferrofluids based solar collector considering all the improvement mentioned on the test rig is needed, and the experiment is planned to be installed in Saudi Arabia.
- Further economic and environmental study on the ferrofluids based parabolic trough when used in concentrating solar power to generate electricity is needed.

References

[1] Mobil, E., *The Outlook for Energy: A view to 2040.* ExxonMobil: Irving, TX, USA, 2013.

[2] Taher, N. and B. Al-Hajjar, *Energy and Environment in Saudi Arabia: Concerns & Opportunities*. 2013: Springer Science & Business Media.

[3] Group, W.B., *World Development Indicators 2016*. 2016: World Bank Publications.

[4] Technology, W.; Available from: http://www.water-technology.net/.

[5] Zell, E., et al., *Assessment of solar radiation resources in Saudi Arabia.* Solar Energy, 2015. **119**: p. 422-438.

[6] Twidell, J. and T. Weir, *Renewable energy resources*. 2015: Routledge.

[7] Lund, H., *Renewable energy systems: a smart energy systems approach to the choice and modeling of 100% renewable solutions*. 2014: Academic Press.

[8] Ellabban, O., H. Abu-Rub, and F. Blaabjerg, *Renewable energy resources: Current status, future prospects and their enabling technology.* Renewable and Sustainable Energy Reviews, 2014. **39**: p. 748-764.

[9] Brown, A., S. Müller, and Z. Dobrotkova, *Renewable energy: markets and prospects by technology.* IEA information paper, 2011.

[10] Birol, F., *World energy outlook 2010.* International Energy Agency, 2010. **1**.

[11] Duffie, J.A. and W.A. Beckman, *Solar engineering of thermal processes*. 2013: John Wiley & Sons.

[12] Quaschning, V., *Solar Thermal Power Plants—Technology Fundamentals.* Erneuerbare-Energien-und-Klimaschu. de. htp://www. volker-quaschning. de/articles/fundamentals2/index. php, 2003.

[13] Kalogirou, S., *The potential of solar industrial process heat applications.* Applied Energy, 2003. **76**(4): p. 337-361.

[14] Cowley, M. and R.E. Rosensweig, *The interfacial stability of a ferromagnetic fluid.* J. Fluid Mech, 1967. **30**(4): p. 671-688.

[15] Odenbach, S., *Recent progress in magnetic fluid research.* Journal of Physics: Condensed Matter, 2004. **16**(32): p. R1135.

[16] Odenbach, S. and S. Thurm, *Magnetoviscous effects in ferrofluids*. 2002: Springer.

[17] Charles, S.W., *The preparation of magnetic fluids*, in *Ferrofluids*. 2003, Springer. p. 3-18.

[18] Vékás, L., D. Bica, and M.V. Avdeev, *Magnetic nanoparticles and concentrated magnetic nanofluids: Synthesis, properties and some applications.* China Particuology, 2007. **5**(1-2): p. 43-49.

[19] Kuzubov, A. and O. Ivanova, *Magnetic liquids for heat exchange.* Journal de Physique III, 1994. **4**(1): p. 1-6.

[20] Wu, J.M. and J. Zhao, *A review of nanofluid heat transfer and critical heat flux enhancement—Research gap to engineering application.* Progress in Nuclear Energy, 2013. **66**: p. 13-24.

[21] Borbáth, T., et al. *Magnetic nanofluids and magnetic composite fluids in rotating seal systems*. in *IOP Conference Series: Earth and Environmental Science*. 2010. IOP Publishing.

[22] Stephen, P.S., *Low viscosity magnetic fluid obtained by the colloidal suspension of magnetic particles*. 1965, Google Patents.

[23] Bica, D., *Preparation of magnetic fluids for various applications.* Romanian Reports in Physics, 1995. **47**: p. 265-272.

[24] Pileni, M.P., *Structure and reactivity in reverse micelles.* 1989.

[25] Yu, W., et al., *Thermophysical property-related comparison criteria for nanofluid heat transfer enhancement in turbulent flow.* Applied Physics Letters, 2010. **96**(21): p. 213109.

[26] Kim, S.H., S.R. Choi, and D. KIM, *Thermal conductivity of metal-oxide nanofluids: particle size dependence and effect of laser irradiation.* Journal of heat transfer, 2007. **129**(3): p. 298-307.

[27] Nkurikiyimfura, I., Y. Wang, and Z. Pan, *Heat transfer enhancement by magnetic nanofluids—A review.* Renewable and Sustainable Energy Reviews, 2013. **21**: p. 548-561.

[28] Philip, J. and P.D. Shima, *Thermal properties of nanofluids.* Advances in Colloid and Interface Science, 2012. **183–184**(0): p. 30-45.

[29] Hong, K.S., T.-K. Hong, and H.-S. Yang, *Thermal conductivity of Fe nanofluids depending on the cluster size of nanoparticles.* Applied Physics Letters, 2006. **88**(3): p. 031901-031901-3.

[30] Philip, J., P.D. Shima, and B. Raj, *Enhancement of thermal conductivity in magnetite based nanofluid due to chainlike structures.* Applied Physics Letters, 2007. **91**(20): p. 203108.

[31] Gavili, A., et al., *The thermal conductivity of water base ferrofluids under magnetic field.* Experimental Thermal and Fluid Science, 2012. **41**(0): p. 94-98.

[32] Shahsavar, A., et al., *Effect of temperature and concentration on thermal conductivity and viscosity of ferrofluid loaded with carbon nanotubes.* Heat and Mass Transfer, 2016. **52**(10): p. 2293-2301.

[33] Sun, P., et al., *Magnetic graphite suspensions with reversible thermal conductivity.* Materials Letters, 2015. **149**: p. 92-94.

[34] Parekh, K., et al. *Experimental investigation of thermal conductivity of magnetic nanofluids*. in *AIP Conference Proceedings-American Institute of Physics*. 2012.

[35] Yu, W., et al., *Enhancement of thermal conductivity of kerosene-based Fe3O4 nanofluids prepared via phase-transfer method.* Colloids and Surfaces A: Physicochemical and Engineering Aspects, 2010. **355**(1–3): p. 109-113.

[36] Li, Q., Y. Xuan, and J. Wang, *Experimental investigations on transport properties of magnetic fluids.* Experimental Thermal and Fluid Science, 2005. **30**(2): p. 109-116.

[37] Zhu, H., et al., *Effects of nanoparticle clustering and alignment on thermal conductivities of <equation>Fe₃O₄</equation> aqueous nanofluids.* Applied Physics Letters, 2006. **89**(2): p. 023123-023123-3.

[38] Abareshi, M., et al., *Fabrication, characterization and measurement of thermal conductivity of Fe3O4 nanofluids.* Journal of Magnetism and Magnetic Materials, 2010. **322**(24): p. 3895-3901.

[39] Altan, C.L. and S. Bucak, *The effect of Fe3O4 nanoparticles on the thermal conductivities of various base fluids.* Nanotechnology, 2011. **22**(28): p. 285713.

[40] Syam Sundar, L., M.K. Singh, and A.C.M. Sousa, *Investigation of thermal conductivity and viscosity of Fe3O4 nanofluid for heat transfer applications.* International Communications in Heat and Mass Transfer, 2013. **44**: p. 7-14.

[41] Pastoriza-Gallego, M., et al., *Enhancement of thermal conductivity and volumetric behavior of FexOy nanofluids.* Journal of Applied Physics, 2011. **110**(1): p. 014309.

[42] Philip, J., P.D. Shima, and B. Raj, *Evidence for enhanced thermal conduction through percolating structures in nanofluids.* Nanotechnology, 2008. **19**(30): p. 305706.

[43] Gao, J., et al., *Experimental investigation of heat conduction mechanisms in nanofluids. Clue on clustering.* Nano letters, 2009. **9**(12): p. 4128-4132.

[44] Godson, L., et al., *Enhancement of heat transfer using nanofluids—An overview.* Renewable and Sustainable Energy Reviews, 2010. **14**(2): p. 629-641.

[45] Eapen, J., et al., *The classical nature of thermal conduction in nanofluids.* arXiv preprint arXiv:0901.0058, 2008.

[46] Fang, X., Y. Xuan, and Q. Li, *Anisotropic thermal conductivity of magnetic fluids.* Progress in Natural Science, 2009. **19**(2): p. 205-211.

[47] Fu, H.L. and L. Gao, *Theory for anisotropic thermal conductivity of magnetic nanofluids.* Physics Letters A, 2011. **375**(41): p. 3588-3592.

[48] Nkurikiyimfura, I., et al. *Enhancement of thermal conductivity of magnetic nanofluids in magnetic field*. in *Materials for Renewable Energy & Environment (ICMREE), 2011 International Conference on*. 2011. IEEE.
[49] Mahbubul, I., R. Saidur, and M. Amalina, *Latest developments on the viscosity of nanofluids.* International Journal of Heat and Mass Transfer, 2012. **55**(4): p. 874-885.
[50] Tsai, T.-H., et al., *Thermal conductivity of nanofluid with magnetic nanoparticles.* Piers Online, 2009. **5**(3): p. 231-234.
[51] Genc, S. and B. Derin, *Synthesis and rheology of ferrofluids: a review.* Current Opinion in Chemical Engineering, 2014. **3**: p. 118-124.
[52] Moeen, S.J., et al., *Synthesis and rheological properties of nickel-zinc ferrite polymer nanocomposites.* Journal of Applied Polymer Science, 2012. **123**(4): p. 2534-2539.
[53] Nowak, J., D. Wolf, and S. Odenbach, *A rheological and microscopical characterization of biocompatible ferrofluids.* Journal of Magnetism and Magnetic Materials, 2014. **354**(0): p. 98-104.
[54] Patel, R., *Effective viscosity of magnetic nanofluids through capillaries.* Physical Review E, 2012. **85**(2): p. 026316.
[55] Amani, M., et al., *Experimental study on viscosity of spinel-type manganese ferrite nanofluid in attendance of magnetic field.* Journal of Magnetism and Magnetic Materials, 2017. **428**: p. 457-463.
[56] Shima, P.D. and J. Philip, *Tuning of Thermal Conductivity and Rheology of Nanofluids Using an External Stimulus.* The Journal of Physical Chemistry C, 2011. **115**(41): p. 20097-20104.
[57] Zubarev, A.Y., J. Fleischer, and S. Odenbach, *Towards a theory of dynamical properties of polydisperse magnetic fluids: Effect of chain-like aggregates.* Physica A: Statistical Mechanics and its Applications, 2005. **358**(2–4): p. 475-491.
[58] Otanicar, T.P., P.E. Phelan, and J.S. Golden, *Optical properties of liquids for direct absorption solar thermal energy systems.* Solar Energy, 2009. **83**(7): p. 969-977.
[59] de Risi, A., M. Milanese, and D. Laforgia, *Modelling and optimization of transparent parabolic trough collector based on gas-phase nanofluids.* Renewable Energy, 2013. **58**: p. 134-139.
[60] Hordy, N., et al., *High temperature and long-term stability of carbon nanotube nanofluids for direct absorption solar thermal collectors.* Solar Energy, 2014. **105**: p. 82-90.
[61] Luo, Z., et al., *Performance improvement of a nanofluid solar collector based on direct absorption collection (DAC) concepts.* International Journal of Heat and Mass Transfer, 2014. **75**: p. 262-271.
[62] Zhang, L., et al., *Radiative properties of ionic liquid-based nanofluids for medium-to-high-temperature direct absorption solar collectors.* Solar Energy Materials and Solar Cells, 2014. **130**: p. 521-528.
[63] Chung, M.-F. and C.-M. Fu, *Optical Transmittance and Dynamic Properties of Ferrofluids (Fe $ _ {3} $ O $ _ {4} $) Under DC-Biased Magnetic Fields.* IEEE Transactions on Magnetics, 2011. **47**(10): p. 3170-3172.
[64] Taylor, R.A., et al., *Nanofluid optical property characterization: towards efficient direct absorption solar collectors.* Nanoscale research letters, 2011. **6**(1): p. 225.
[65] Lajvardi, M., et al., *Experimental investigation for enhanced ferrofluid heat transfer under magnetic field effect.* Journal of Magnetism and Magnetic Materials, 2010. **322**(21): p. 3508-3513.
[66] Goharkhah, M. and M. Ashjaee, *Effect of an alternating nonuniform magnetic field on ferrofluid flow and heat transfer in a channel.* Journal of Magnetism and Magnetic Materials, 2014. **362**: p. 80-89.

[67] Bahiraei, M. and M. Hangi, *Investigating the efficacy of magnetic nanofluid as a coolant in double-pipe heat exchanger in the presence of magnetic field.* Energy Conversion and Management, 2013. **76**: p. 1125-1133.

[68] Azizian, R., et al., *Effect of magnetic field on laminar convective heat transfer of magnetite nanofluids.* International Journal of Heat and Mass Transfer, 2014. **68**(0): p. 94-109.

[69] Sheikholeslami, M. and M. Gorji-Bandpy, *Free convection of ferrofluid in a cavity heated from below in the presence of an external magnetic field.* Powder Technology, 2014. **256**: p. 490-498.

[70] Kefayati, G., *Natural convection of ferrofluid in a linearly heated cavity utilizing LBM.* Journal of Molecular Liquids, 2014. **191**: p. 1-9.

[71] Calcagni, B., F. Marsili, and M. Paroncini, *Natural convective heat transfer in square enclosures heated from below.* Applied Thermal Engineering, 2005. **25**(16): p. 2522-2531.

[72] Nemati, H., et al., *Magnetic field effects on natural convection flow of nanofluid in a rectangular cavity using the Lattice Boltzmann model.* Scientia Iranica, 2012. **19**(2): p. 303-310.

[73] Hadavand, M. and A. Sousa, *Simulation of thermomagnetic convection in a cavity using the lattice Boltzmann model.* Journal of Applied Mathematics, 2011. **2011**.

[74] Aminfar, H., M. Mohammadpourfard, and Y. Narmani Kahnamouei, *A 3D numerical simulation of mixed convection of a magnetic nanofluid in the presence of non-uniform magnetic field in a vertical tube using two phase mixture model.* Journal of Magnetism and Magnetic Materials, 2011. **323**(15): p. 1963-1972.

[75] Aminfar, H., M. Mohammadpourfard, and Y.N. Kahnamouei, *Numerical study of magnetic field effects on the mixed convection of a magnetic nanofluid in a curved tube.* International Journal of Mechanical Sciences, 2014. **78**: p. 81-90.

[76] Shahsavar, A., et al., *Experimental investigation on laminar forced convective heat transfer of ferrofluid loaded with carbon nanotubes under constant and alternating magnetic fields.* Experimental Thermal and Fluid Science, 2016. **76**: p. 1-11.

[77] Sadeghinezhad, E., et al., *Experimental study on heat transfer augmentation of graphene based ferrofluids in presence of magnetic field.* Applied Thermal Engineering, 2017. **114**: p. 415-427.

[78] Sheikholeslami, M., K. Vajravelu, and M.M. Rashidi, *Forced convection heat transfer in a semi annulus under the influence of a variable magnetic field.* International Journal of Heat and Mass Transfer, 2016. **92**: p. 339-348.

[79] Scherer, C. and A.M.F. Neto, *Ferrofluid Properties and Applications.* Brazilian Journal of Physics, 2005. **35**.

[80] Shimada, K., *A heat conduction approach to a parallel duct-type energy conversion device utilizing a magnetic fluid.* International Journal of Applied Electromagnetics and Mechanics, 2007. **25**(1): p. 267-271.

[81] Lian, W., Y. Xuan, and Q. Li, *Design method of automatic energy transport devices based on the thermomagnetic effect of magnetic fluids.* International Journal of Heat and Mass Transfer, 2009. **52**(23): p. 5451-5458.

[82] Zablotsky, D., A. Mezulis, and E. Blums, *Surface cooling based on the thermomagnetic convection: Numerical simulation and experiment.* International Journal of Heat and Mass Transfer, 2009. **52**(23–24): p. 5302-5308.

[83] Xuan, Y. and W. Lian, *Electronic cooling using an automatic energy transport device based on thermomagnetic effect.* Applied Thermal Engineering, 2011. **31**(8–9): p. 1487-1494.

[84] Thirugnanasambandam, M., S. Iniyan, and R. Goic, *A review of solar thermal technologies.* Renewable and sustainable energy reviews, 2010. **14**(1): p. 312-322.

[85] Sharma, A., *A comprehensive study of solar power in India and World.* Renewable and Sustainable Energy Reviews, 2011. **15**(4): p. 1767-1776.

[86] Mekhilef, S., R. Saidur, and A. Safari, *A review on solar energy use in industries.* Renewable and Sustainable Energy Reviews, 2011. **15**(4): p. 1777-1790.

[87] Kalogirou, S.A., *Solar energy engineering: processes and systems*. 2013: Academic Press.

[88] Taylor, R.A., et al., *Nanofluid optical property characterization: towards efficient direct absorption solar collectors.* Nanoscale research letters, 2011. **6**(1): p. 1-11.

[89] Wang, X.-Q. and A.S. Mujumdar, *Heat transfer characteristics of nanofluids: a review.* International journal of thermal sciences, 2007. **46**(1): p. 1-19.

[90] Faizal, M., et al., *Energy, economic and environmental analysis of metal oxides nanofluid for flat-plate solar collector.* Energy Conversion and Management, 2013. **76**: p. 162-168.

[91] Goudarzi, K., E. Shojaeizadeh, and F. Nejati, *An experimental investigation on the simultaneous effect of CuO–H 2 O nanofluid and receiver helical pipe on the thermal efficiency of a cylindrical solar collector.* Applied Thermal Engineering, 2014. **73**(1): p. 1236-1243.

[92] Mahian, O., et al., *Performance analysis of a minichannel-based solar collector using different nanofluids.* Energy Conversion and Management, 2014. **88**: p. 129-138.

[93] Otanicar, T.P. and J.S. Golden, *Comparative environmental and economic analysis of conventional and nanofluid solar hot water technologies.* Environmental science & technology, 2009. **43**(15): p. 6082-6087.

[94] Said, Z., et al., *Analyses of exergy efficiency and pumping power for a conventional flat plate solar collector using SWCNTs based nanofluid.* Energy and Buildings, 2014. **78**: p. 1-9.

[95] Yousefi, T., et al., *An experimental investigation on the effect of pH variation of MWCNT–H< sub> 2</sub> O nanofluid on the efficiency of a flat-plate solar collector.* Solar Energy, 2012. **86**(2): p. 771-779.

[96] Yousefi, T., et al., *An experimental investigation on the effect of Al2O3–H2O nanofluid on the efficiency of flat-plate solar collectors.* Renewable Energy, 2012. **39**(1): p. 293-298.

[97] Zamzamian, A., et al., *An experimental study on the effect of Cu-synthesized/EG nanofluid on the efficiency of flat-plate solar collectors.* Renewable Energy, 2014. **71**: p. 658-664.

[98] Kasaeian, A., et al., *Performance evaluation and nanofluid using capability study of a solar parabolic trough collector.* Energy Conversion and Management, 2015. **89**: p. 368-375.

[99] Colangelo, G., et al., *A new solution for reduced sedimentation flat panel solar thermal collector using nanofluids.* Applied Energy, 2013. **111**: p. 80-93.

[100] Abdelrahman, M., P. Fumeaux, and P. Suter, *Study of solid-gas-suspensions used for direct absorption of concentrated solar radiation.* Solar Energy, 1979. **22**(1): p. 45-48.

[101] Otanicar, T.P., et al., *Nanofluid-based direct absorption solar collector.* Journal of Renewable and Sustainable Energy, 2010. **2**(3): p. 033102.

[102] Tyagi, H., P. Phelan, and R. Prasher, *Predicted efficiency of a low-temperature nanofluid-based direct absorption solar collector.* Journal of solar energy engineering, 2009. **131**(4): p. 041004.

[103] Taylor, R.A., et al. *Applicability of nanofluids in concentrated solar energy harvesting*. 2010. ASME.

[104] Hunt, A.J., *Small particle heat exchangers.* Lawrence Berkeley National Laboratory, 2011.

[105] Kumar, S. and C. Tien. *Analysis of combined radiation and convection in a particulate laden falling film*. in *Heat Transfer Phenomena in Radiation, Combustion, and Fires*. 1989. Publ by ASME.

[106] Lenert, A. and E.N. Wang, *Optimization of nanofluid volumetric receivers for solar thermal energy conversion.* Solar Energy, 2012. **86**(1): p. 253-265.

[107] Khullar, V. and H. Tyagi. *Application of nanofluids as the working fluid in concentrating parabolic solar collectors*. in *Proceedings of the 37th National and 4th International Conference on Fluid Mechanics and Fluid Power FMFP2010*. 2010.

[108] Khullar, V., et al., *Solar energy harvesting using nanofluids-based concentrating solar collector.* Journal of Nanotechnology in Engineering and Medicine, 2012. **3**(3): p. 031003-031003-9.

[109] Taylor, R.A., et al., *Applicability of nanofluids in high flux solar collectors.* Journal of Renewable and Sustainable Energy, 2011. **3**: p. 023104.

[110] Kumar, S. and C. Tien, *Analysis of combined radiation and convection in a particulate-laden liquid film.* Journal of solar energy engineering, 1990. **112**(4): p. 293-300.

[111] Turkyilmazoglu, M., *Performance of direct absorption solar collector with nanofluid mixture.* Energy Conversion and Management, 2016. **114**: p. 1-10.

[112] Khullar, V. and H. Tyagi, *A study on environmental impact of nanofluid-based concentrating solar water heating system.* International Journal of Environmental Studies, 2012. **69**(2): p. 220-232.

[113] He, Y., et al., *Experimental study on the light-heat conversion characteristics of nanofluids.* Nanoscience and Nanotechnology Letters, 2011. **3**(4): p. 494-496.

[114] Li, Y., et al. *Investigation on heat transfer performances of nanofluids in solar collector*. in *Materials Science Forum*. 2011. Trans Tech Publ.

[115] Vakili, M., et al., *Experimental investigation of graphene nanoplatelets nanofluid-based volumetric solar collector for domestic hot water systems.* Solar Energy, 2016. **131**: p. 119-130.

[116] Said, Z., et al., *Energy and exergy efficiency of a flat plate solar collector using pH treated Al 2 O 3 nanofluid.* Journal of Cleaner Production, 2016. **112**: p. 3915-3926.

[117] *BS EN ISO 9806, 2013. Solar Energy – Solar Thermal Collectors – Test Methods. British Standards Institute.*

[118] Fischer, S., E. Lüpfert, and H. Müller-Steinhagen. *Efficiency testing of parabolic trough collectors using the quasi-dynamic test procedure according to the European Standard EN 12975*. in *SolarPACES 13th Symposium on Concentrating Solar power and Chemical Energy Technologies. Sevilla*. 2006.

[119] Kohraku, S. and K. Kurokawa, *A fundamental experiment for discrete-wavelength LED solar simulator.* Solar energy materials and solar cells, 2006. **90**(18): p. 3364-3370.

[120] Grandi, G., A. Ienina, and M. Bardhi, *Effective low-cost hybrid LED-halogen solar simulator.* IEEE Transactions on Industry Applications, 2014. **50**(5): p. 3055-3064.

[121] Shatat, M., A. Mayere, and S. Riffat, *A standardized empirical method of testing solar simulator coupled with solar tube and concentrator collectors.* Internacional Journal of thermal & environmental engineering, 2013. **5**(1): p. 13-20.

[122] Altan, C.L., et al., *Enhancement of thermal conductivity upon application of magnetic field to Fe3O4 nanofluids.* Journal of Applied Physics, 2011. **110**(9): p. 093917.

[123] Nkurikiyimfura, I., Y. Wang, and Z. Pan, *Effect of chain-like magnetite nanoparticle aggregates on thermal conductivity of magnetic nanofluid in magnetic field.* Experimental Thermal and Fluid Science, 2013. **44**: p. 607-612.

[124] Beguš, S., et al., *Magnetic effects on thermocouples.* Measurement Science and Technology, 2014. **25**(3): p. 035006.

[125] Colangelo, G., et al., *Experimental test of an innovative high concentration nanofluid solar collector.* Applied Energy, 2015. **154**: p. 874-881.

[126] Dudley, V., et al., *SEGS LS2 solar collector—Test results.* Report of Sandia National Laboratories, Report No. SANDIA94-1884, 1994.

[127] Padilla, R.V., et al., *Heat transfer analysis of parabolic trough solar receiver.* Applied Energy, 2011. **88**(12): p. 5097-5110.

[128] Kumar, K.R. and K. Reddy, *Thermal analysis of solar parabolic trough with porous disc receiver.* Applied Energy, 2009. **86**(9): p. 1804-1812.

[129] Muñoz, J. and A. Abánades, *Analysis of internal helically finned tubes for parabolic trough design by CFD tools.* Applied energy, 2011. **88**(11): p. 4139-4149.

[130] Cheng, Z., Y. He, and F. Cui, *Numerical study of heat transfer enhancement by unilateral longitudinal vortex generators inside parabolic trough solar receivers.* International journal of heat and mass transfer, 2012. **55**(21): p. 5631-5641.
[131] Fuqiang, W., et al., *Parabolic trough receiver with corrugated tube for improving heat transfer and thermal deformation characteristics.* Applied Energy, 2016. **164**: p. 411-424.
[132] Zou, B., et al., *An experimental investigation on a small-sized parabolic trough solar collector for water heating in cold areas.* Applied Energy, 2016. **163**: p. 396-407.
[133] Wu, Y.-T., et al., *Experimental study on the heat transfer characteristics of a low melting point salt in a parabolic trough solar collector system.* Applied Thermal Engineering, 2015. **89**: p. 748-754.
[134] Lomascolo, M., et al., *Review of heat transfer in nanofluids: conductive, convective and radiative experimental results.* Renewable and Sustainable Energy Reviews, 2015. **43**: p. 1182-1198.
[135] Hussien, A.A., M.Z. Abdullah, and A.-N. Moh'd A, *Single-phase heat transfer enhancement in micro/minichannels using nanofluids: Theory and applications.* Applied Energy, 2016. **164**: p. 733-755.
[136] Bannerot, R., *Derivation of Universal Error Parameters for Comprehensive Optical Analysis of Parabolic Troughs1.* Journal of Solar Energy Engineering, 1986. **108**: p. 275.
[137] Coccia, G., G. Di Nicola, and M. Sotte, *Design, manufacture, and test of a prototype for a parabolic trough collector for industrial process heat.* Renewable Energy, 2015. **74**: p. 727-736.
[138] Jaramillo, O., et al., *Parabolic trough concentrators for low enthalpy processes.* Renewable energy, 2013. **60**: p. 529-539.
[139] Bakos, G., et al., *Design, optimisation and conversion-efficiency determination of a line-focus parabolic-trough solar-collector (PTC).* Applied energy, 2001. **68**(1): p. 43-50.
[140] Chen, H., et al., *Heat transfer and flow behaviour of aqueous suspensions of titanate nanotubes (nanofluids).* Powder Technology, 2008. **183**(1): p. 63-72.
[141] Ganguly, R., S. Sen, and I.K. Puri, *Heat transfer augmentation using a magnetic fluid under the influence of a line dipole.* Journal of Magnetism and Magnetic Materials, 2004. **271**(1): p. 63-73.
[142] Xuan, Y., Q. Li, and M. Ye, *Investigations of convective heat transfer in ferrofluid microflows using lattice-Boltzmann approach.* International Journal of Thermal Sciences, 2007. **46**(2): p. 105-111.
[143] Gnielinski, V., *New equation for heat and mass transfer in turbulent pipe and channel flow.* Int. Chem. Eng., 1976. **16**: p. 359-368.
[144] Petukhov, B. and L. Roizen, *Generalized relationships for heat transfer in a turbulent flow of gas in tubes of annular section(Heat transfer coefficients and adiabatic temperatures obtained for turbulent gas flow in tubes with annular section).* High Temperature, 1964. **2**: p. 65-68.
[145] Incropera, F.P., et al., *Fundamentals of heat and mass transfer*. 2007: Wiley.
[146] Churchill, S.W. and H.H. Chu, *Correlating equations for laminar and turbulent free convection from a vertical plate.* International journal of heat and mass transfer, 1975. **18**(11): p. 1323-1329.
[147] Price, H., *Concentrated solar power use in Africa.* NREL/TP. Golden, CO: National Renewable Energy Laboratory, 2001.
[148] Forristall, R., *Heat transfer analysis and modeling of a parabolic trough solar receiver implemented in engineering equation solver*. 2003: National Renewable Energy Laboratory.
[149] Love, J., *Paleomagnetic principles and practice.* Eos, Transactions American Geophysical Union, 2000. **81**(16): p. 172-172.
[150] Chandrasekar, M., S. Suresh, and A. Chandra Bose, *Experimental investigations and theoretical determination of thermal conductivity and viscosity of Al2O3/water nanofluid.* Experimental Thermal and Fluid Science, 2010. **34**(2): p. 210-216.

[151] Sokhansefat, T., A.B. Kasaeian, and F. Kowsary, *Heat transfer enhancement in parabolic trough collector tube using Al2O3/synthetic oil nanofluid.* Renewable and Sustainable Energy Reviews, 2014. **33**(0): p. 636-644.
[152] Zhou, S.-Q. and R. Ni, *Measurement of the specific heat capacity of water-based Al 2 O 3 nanofluid.* Applied Physics Letters, 2008. **92**(9): p. 093123-093123-3.
[153] Snow, C.L.M., *The Heat Capacity and Thermodynamic Properties of the Iron Oxides and Their Relation to the Mineral Core of the Iron Storage Protein Ferritin.* 2010.
[154] Alsaady, M., et al., *Thermo-physical properties and thermo-magnetic convection of ferrofluid.* Applied Thermal Engineering, 2014.
[155] Kalogirou, S., *Thermal performance, economic and environmental life cycle analysis of thermosiphon solar water heaters.* Solar energy, 2009. **83**(1): p. 39-48.
[156] Maghrabi, A., *Parameterization of a simple model to estimate monthly global solar radiation based on meteorological variables, and evaluation of existing solar radiation models for Tabouk, Saudi Arabia.* Energy conversion and management, 2009. **50**(11): p. 2754-2760.
[157] Administration, E.I., *Annual Energy Review 2011*. 2012: Government Printing Office.
[158] Kurup, P. and C.S. Turchi, *Parabolic trough collector cost update for the system advisor model (SAM)*. 2015, Technical Report.
[159] Corporation, S.A. http://www.sigmaaldrich.com. 2017].
[160] Company, S.E. https://www.se.com.sa/. [cited 2017 2017].
[161] Far, A. and R. Gee. *The SkyTrough Parabolic Trough Solar Collector*. in *Proceedings of the ASME 2009 3rd International Conference of Energy Sustainability, San Francisco, CA*. 2009.
[162] Tsilingiridis, G., G. Martinopoulos, and N. Kyriakis, *Life cycle environmental impact of a thermosyphonic domestic solar hot water system in comparison with electrical and gas water heating.* Renewable Energy, 2004. **29**(8): p. 1277-1288.
[163] Alcorn, A., *Embodied energy coefficients of building materials*. 1996: Centre for Building Performance Research, Victoria University of Wellington.
[164] Kushnir, D. and B.A. Sandén, *Energy requirements of carbon nanoparticle production.* Journal of Industrial Ecology, 2008. **12**(3): p. 360-375.
[165] Spadaro, J.V. and A. Rabl, *Estimates of real damage from air pollution: site dependence and simple impact indices for LCA.* The International Journal of Life Cycle Assessment, 1999. **4**(4): p. 229-243.
[166] Initiative, N.N., *Environmental, health and safety research needs for engineered nanoscale materials.* Nanoscale Science, Engineering, and Technology Subcommittee, Committee on Technology, National Science and Technology Council, 2006.
[167] Chen, Z., et al., *Age-related differences in pulmonary and cardiovascular responses to SiO2 nanoparticle inhalation: nanotoxicity has susceptible population.* Environmental science & technology, 2008. **42**(23): p. 8985-8992.

Appendix A

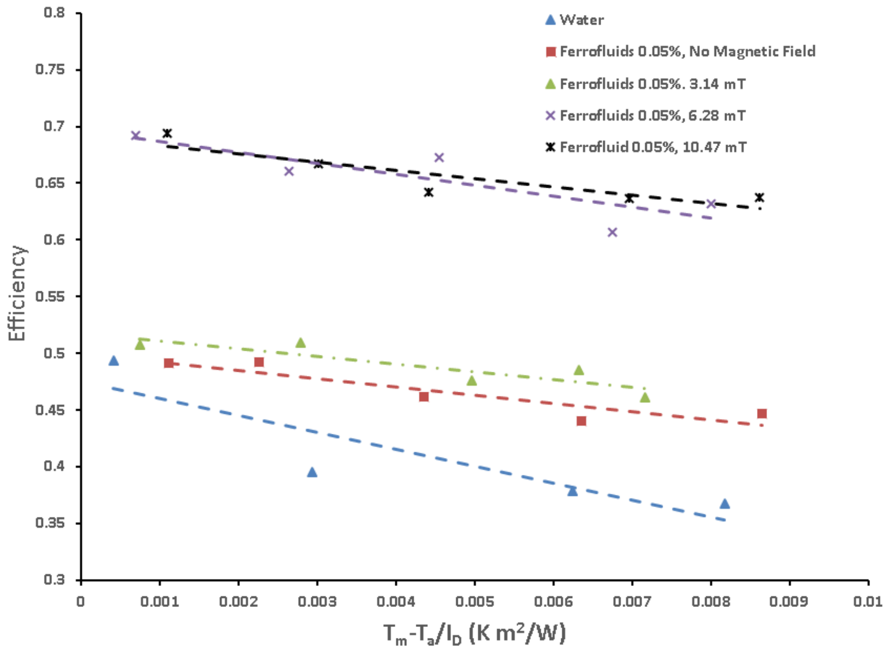

Figure 0-1: Ferrofluids based solar collector efficiency with selective surface absorber, 0.05% Ferrolfuids as heat transfer fluids and different mean fluids temperature.

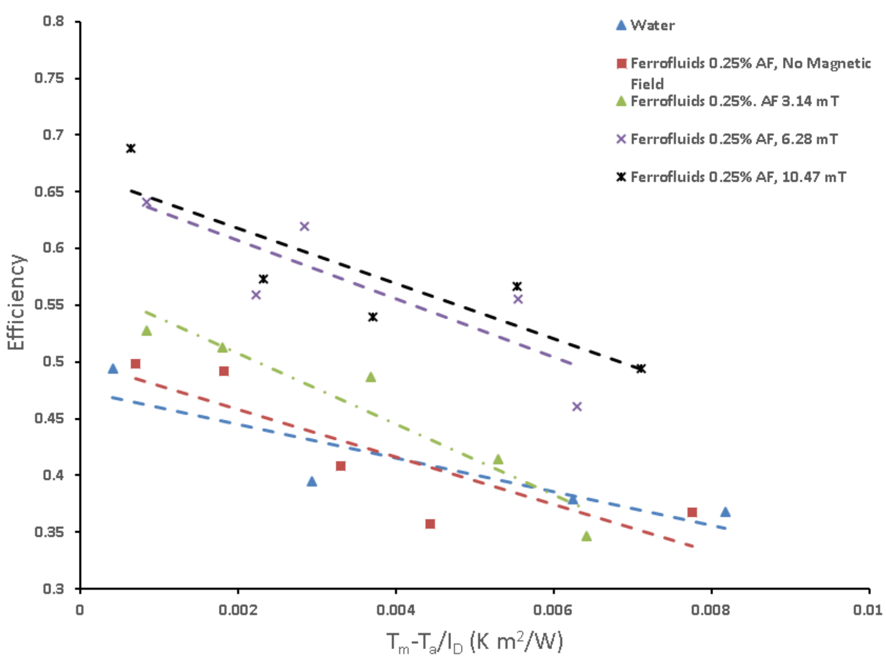

Figure 0-2: Ferrofluids based solar collector efficiency with selective surface absorber, 0.25% Ferrolfuids as heat transfer fluids and different mean fluids temperature.

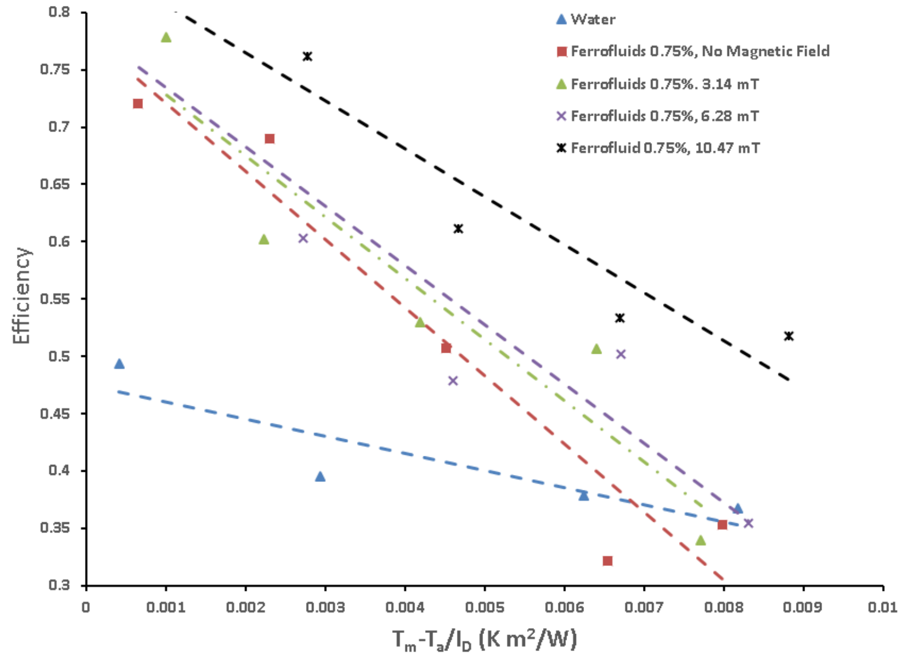

Figure 0-3: Ferrofluids based solar collector efficiency with selective surface absorber, 0.75% Ferrolfuids as heat transfer fluids and different mean fluids temperature.

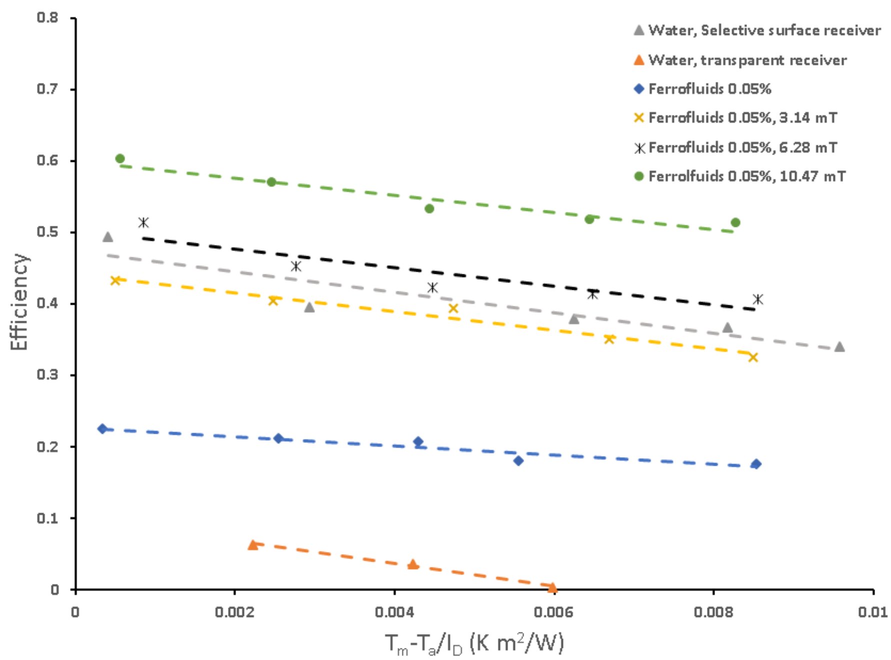

Figure 0-4: Ferrofluids based solar collector efficiency with direct absorber, 0.05% Ferrolfuids as heat transfer fluids and different mean fluids temperature.

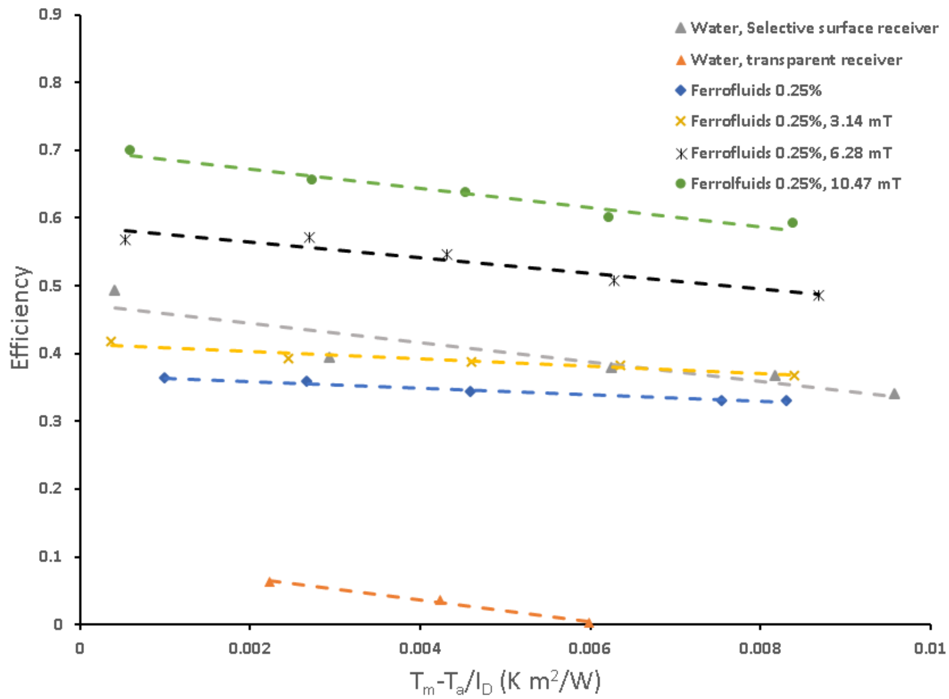

Figure 0-5: Ferrofluids based solar collector efficiency with direct absorber, 0.25% Ferrolfuids as heat transfer fluids and different mean fluids temperature.

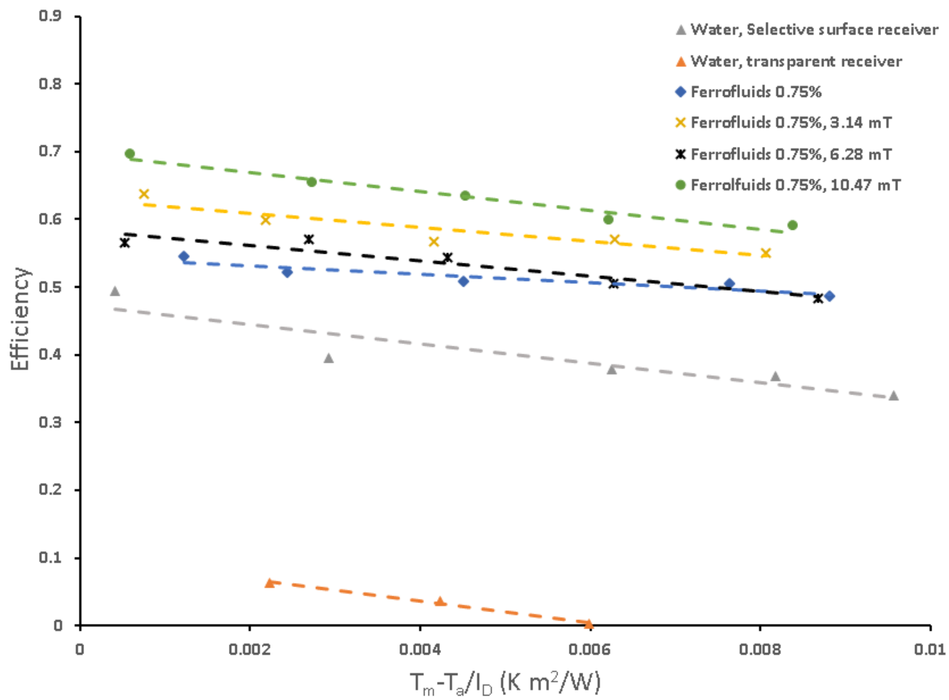

Figure 0-6: Ferrofluids based solar collector efficiency with direct absorber, 0.75% Ferrolfuids as heat transfer fluids and different mean fluids temperature.

Appendix B

Temperatures and energy of solar absorber from the heat transfer analysis presented in Chapter 5

Table 0-1: Temperatures and energy of AZTRAK design parabolic trough with synthetic oil.

T_1 °C	T_2 °C	T_3 °C	T_4 °C	T_5 °C	q_{12} W/m	q_{23} W/m	q_{34con} W/m	q_{34rad} W/m	q_{45cond} W/m	q_{56} W/m	q_{57} W/m	$q_{3SolAbs}$ W/m
113	343.0	310.0	55.6	53.6	3367.3	3367.3	0.0062	242.2	242.2	238.2	82.4	3609.6
162	347.6	313.4	53.1	51.0	3491.9	3491.9	0.0064	251.0	251.0	258.2	74.1	3742.9
208	360.2	326.1	63.3	61.0	3519.3	3519.3	0.0064	278.1	278.1	264.6	96.0	3797.4
259.5	368.7	337.8	63.3	60.8	3207.1	3207.1	0.0067	308.9	308.9	293.1	92.2	3516.0
306.5	416.6	386.9	104.6	100.9	3177.2	3177.2	0.0069	448.6	448.6	313.9	213.4	3625.8
308	406.9	379.0	78.4	74.8	2971.4	2971.4	0.0074	432.9	432.9	377.6	129.1	3404.3
364.5	480.6	456.2	102.5	96.1	2714.1	2714.1	0.0087	777.6	777.6	661.4	191.9	3491.7

Table 0-2: Temperatures and energy of AZTRAK design parabolic trough with 0.05% synthetic oil based ferrofluids.

T_1 °C	T_2 °C	T_3 °C	T_4 °C	T_5 °C	q_{12} W/m	q_{23} W/m	q_{34con} W/m	q_{34rad} W/m	q_{45cond} W/m	q_{56} W/m	q_{57} W/m	$q_{3SolAbs}$ W/m
125	330.1	293.9	56.5	54.8	3658.2	3658.2	0.0058	207.6	207.6	212.6	79.0	3865.9
150	332.9	296.8	57.1	55.4	3652.6	3652.6	0.0059	213.3	213.3	216.8	80.4	3865.9
175	340.2	304.4	58.8	56.9	3637.0	3637.0	0.0060	228.8	228.9	228.5	84.3	3865.9
200	349.7	314.3	61.1	59.1	3615.5	3615.5	0.0062	250.3	250.4	244.5	89.8	3865.9
225	361.1	326.3	64.1	61.8	3587.4	3587.4	0.0064	278.5	278.5	265.4	97.0	3865.9
250	375.4	341.3	68.1	65.6	3549.1	3549.1	0.0067	316.8	316.8	293.7	107.0	3865.9
275	394.5	361.4	74.1	71.0	3491.1	3491.1	0.0070	374.7	374.7	336.2	122.4	3865.9
300	428.7	397.4	86.5	82.5	3366.6	3366.6	0.0076	499.3	499.3	426.3	156.8	3865.9
325	471.2	442.5	105.4	99.7	3166.4	3166.4	0.0083	699.5	699.5	567.7	215.6	3865.9
350	500.0	473.3	120.6	113.4	2996.6	2996.6	0.0086	869.2	869.2	684.5	268.6	3865.9

Table 0-3: Temperatures and energy of AZTRAK design parabolic trough with 0.05% synthetic oil based ferrofluids and external magnetic field intensity of 10.47 mT.

T_1 °C	T_2 °C	T_3 °C	T_4 °C	T_5 °C	q_{12} W/m	q_{23} W/m	q_{34con} W/m	q_{34rad} W/m	q_{45cond} W/m	q_{56} W/m	q_{57} W/m	$q_{3SolAbs}$ W/m
125	244.4	204.8	42.5	41.8	3784.0	3784.0	0.0040	81.9	81.9	117.3	48.4	3865.9
150	254.1	214.7	43.6	42.9	3773.9	3773.9	0.0042	91.9	91.9	125.0	50.8	3865.9
175	267.8	229.0	45.4	44.5	3758.0	3758.0	0.0045	107.9	107.9	137.2	54.6	3865.9
200	283.7	245.5	47.8	46.7	3737.1	3737.1	0.0048	128.8	128.8	153.1	59.6	3865.9
225	301.4	264.0	50.8	49.5	3710.4	3710.4	0.0052	155.5	155.5	173.3	66.1	3865.9
250	321.0	284.3	54.6	53.0	3676.1	3676.1	0.0056	189.7	189.7	199.1	74.5	3865.9
275	342.1	306.4	59.3	57.4	3632.7	3632.7	0.0061	233.1	233.1	231.7	85.4	3865.9
300	364.2	329.5	64.9	62.6	3579.6	3579.6	0.0065	286.3	286.3	271.2	99.0	3865.9
325	386.7	353.1	71.6	68.7	3515.8	3515.8	0.0069	350.0	350.0	318.1	115.8	3865.9
350	411.7	379.5	80.1	76.5	3432.0	3432.0	0.0073	433.9	433.9	379.2	138.6	3865.9

Table 0-4: Temperatures and energy of AZTRAK design parabolic trough with 0.05% synthetic without glass envelope

T_1 °C	T_2 °C	T_3 °C	q_{12} W/m	q_{23} W/m	q_{36} W/m	q_{37} W/m	$q_{3SolAbs}$ W/m
125	267.54	242.08	2476.57	2476.57	1451.49	78.02	4006.08
150	253.11	225.93	2617.91	2617.91	1320.67	67.50	4006.08
175	262.08	235.97	2530.60	2530.60	1401.56	73.92	4006.08
200	273.14	248.36	2420.48	2420.48	1503.22	82.38	4006.08
225	286.18	262.97	2287.31	2287.31	1625.61	93.16	4006.08
250	301.39	280.04	2127.17	2127.17	1772.00	106.92	4006.08
275	318.67	299.43	1939.20	1939.20	1942.71	124.17	4006.08
300	337.21	320.26	1730.07	1730.07	2131.25	144.76	4006.08
325	355.88	341.26	1511.54	1511.54	2326.70	167.84	4006.08
350	374.08	361.75	1290.78	1290.78	2522.54	192.75	4006.08

Table 0-5: Temperatures and energy of laboratory design parabolic trough with water and the parabolic trough considered as concentrating solar collector

T_1 °C	T_2 °C	T_3 °C	q_{12} W/m	q_{23} W/m	q_{36} W/m	q_{37} W/m	$q_{3SolAbs}$ W/m
10.5	33.84	33.84	186.54	186.54	13.99	1.97	202.5
11.5	34.62	34.62	185.38	185.38	14.56	2.04	202.5
13.5	36.31	36.31	183.97	183.97	15.81	2.20	202.5
15.5	38.01	38.00	182.54	182.54	17.08	2.36	202.5
17.5	39.70	39.70	181.09	181.09	18.37	2.53	202.5
19.5	41.40	41.39	179.61	179.61	19.67	2.69	202.5
20.5	42.25	42.24	178.86	178.86	20.33	2.78	202.5
22.5	43.95	43.95	177.36	177.36	21.67	2.95	202.5
24.5	45.66	45.65	175.83	175.83	23.02	3.13	202.5
25.5	46.51	46.51	175.05	175.05	23.70	3.22	202.5

Table 0-6: Temperatures and energy of laboratory design parabolic trough with 0.05% water based ferrofluids and the parabolic trough considered as concentrating solar collector

T_1 °C	T_2 °C	T_3 °C	q_{12} W/m	q_{23} W/m	q_{36} W/m	q_{37} W/m	$q_{3SolAbs}$ W/m
10.5	33.83	33.82	186.55	186.55	13.98	1.97	202.5
11.5	34.67	34.67	185.86	185.86	14.60	2.04	202.5
13.5	36.36	36.36	184.45	184.45	15.84	2.20	202.5
15.5	38.05	38.05	183.02	183.02	17.11	2.37	202.5
17.5	39.75	39.74	181.57	181.57	18.40	2.53	202.5
19.5	41.45	41.44	180.09	180.09	19.71	2.70	202.5
20.5	42.30	42.29	179.35	179.35	20.37	2.78	202.5
22.5	44.00	43.99	177.84	177.84	21.70	2.96	202.5
24.5	45.70	45.70	176.31	176.31	23.06	3.13	202.5
25.5	46.56	46.55	175.54	175.54	23.74	3.22	202.5

Table 0-7: Temperatures and energy of laboratory design parabolic trough with water and the parabolic trough considered as non-concentrating solar collector

T_1 °C	T_2 °C	T_3 °C	q_{12} W/m	q_{23} W/m	q_{36} W/m	q_{37} W/m	$q_{3SolAbs}$ W/m
10.5	25.98	25.98	123.72	123.72	57.70	21.08	202.5
11.5	26.48	26.48	120.09	120.09	60.09	21.80	202.5
13.5	27.55	27.55	113.34	113.34	65.29	23.35	202.5
15.5	28.63	28.62	106.48	106.48	70.59	24.92	202.5
17.5	29.70	29.70	99.51	99.51	75.97	26.51	202.5
19.5	30.77	30.77	92.45	92.45	81.43	28.11	202.5
20.5	31.31	31.30	88.88	88.88	84.20	28.91	202.5
22.5	32.38	32.38	81.67	81.67	89.78	30.54	202.5
24.5	33.45	33.45	74.37	74.37	95.44	32.18	202.5
25.5	33.98	33.98	70.68	70.68	98.30	33.00	202.5

Table 0-8: Temperatures and energy of laboratory design parabolic trough with 0.05% water based ferrofluids and the parabolic trough considered as non-concentrating solar collector

T_1 °C	T_2 °C	T_3 °C	q_{12} W/m	q_{23} W/m	q_{36} W/m	q_{37} W/m	$q_{3SolAbs}$ W/m
10.5	25.97	25.97	123.75	123.75	57.68	21.08	202.5
11.5	26.51	26.51	120.41	120.41	60.24	21.85	202.5
13.5	27.59	27.58	113.65	113.65	65.45	23.40	202.5
15.5	28.66	28.66	106.79	106.79	70.74	24.97	202.5
17.5	29.73	29.73	99.82	99.82	76.13	26.55	202.5
19.5	30.80	30.80	92.76	92.76	81.59	28.15	202.5
20.5	31.34	31.34	89.18	89.18	84.36	28.96	202.5
22.5	32.41	32.41	81.97	81.97	89.94	30.58	202.5
24.5	33.48	33.48	74.67	74.67	95.61	32.22	202.5
25.5	34.02	34.01	70.98	70.98	98.47	33.05	202.5

Table 0-9: Temperatures and energy of laboratory design parabolic trough with 0.05% water based ferrofluids and external magnetic field intensity of 10.47 mT and the parabolic trough considered as non-concentrating solar collector

T_1 °C	T_2 °C	T_3 °C	q_{12} W/m	q_{23} W/m	q_{36} W/m	q_{37} W/m	$q_{3SolAbs}$ W/m
10.5	16.62	16.62	176.18	176.18	18.01	8.31	202.5
11.5	17.46	17.46	172.01	172.01	21.09	9.41	202.5
13.5	19.13	19.12	163.34	163.34	27.54	11.61	202.5
15.5	20.78	20.78	154.31	154.31	34.35	13.84	202.5
17.5	22.44	22.43	144.93	144.93	41.46	16.10	202.5
19.5	24.08	24.08	135.26	135.26	48.85	18.39	202.5
20.5	24.90	24.90	130.32	130.32	52.63	19.55	202.5
22.5	26.54	26.54	120.24	120.24	60.38	21.89	202.5
24.5	28.17	28.17	109.91	109.91	68.34	24.26	202.5
25.5	28.99	28.99	104.65	104.65	72.39	25.45	202.5

Table 0-10: Temperatures and energy of laboratory design parabolic trough with water in turbulent flow.

T_1 °C	T_2 °C	T_3 °C	q_{12} W/m	q_{23} W/m	q_{36} W/m	q_{37} W/m	$q_{3SolAbs}$ W/m
10.5	11.66	11.65	197.64	197.64	2.84	2.02	202.5
13.5	14.53	14.53	185.49	185.49	10.88	5.63	202.5
16.5	17.41	17.41	171.74	171.74	20.91	9.35	202.5
19.5	20.30	20.29	156.49	156.49	32.32	13.19	202.5
22.5	23.19	23.18	140.04	140.04	44.80	17.15	202.5
25.5	26.08	26.08	122.57	122.57	58.19	21.23	202.5
28.5	28.98	28.98	104.19	104.19	72.35	25.44	202.5
31.5	31.88	31.88	85.01	85.01	87.19	29.78	202.5
34.5	34.79	34.79	65.10	65.10	102.63	34.25	202.5
37.5	37.69	37.69	44.52	44.52	118.61	38.85	202.5